Optofluidics based fibre-optic variable optical attenuators

Anna Duduś

Department of Electronic and Electrical Engineering

Centre for Microsystems & Photonics

A thesis submitted to the Department of Electronic and Electrical Engineering

at the University of Strathclyde for the degree of Doctor of Philosophy

March 2015

I would like to dedicate my thesis to my parents,

Elżbieta and Józef Duduś,

Without whom none of my success would be possible

Declaration of Authenticity & Author's rights

This thesis is the result of the author's original research. It has been composed by the author and has not been previously submitted for examination which has led to the award of a degree.

The copyright of this thesis belongs to the author under the terms of the United Kingdom Copyright Acts as qualified by University of Strathclyde Regulation 3.50. Due acknowledgement must always be made of the use of any material contained in, or derived from, this thesis.

Signed:

Date:

Acknowledgements

First of all I want to express my huge gratitude to Professor Deepak Uttamchandani who trusted me and gave me the opportunity to start this PhD. I would not be able to successfully finish this project without his experience and guidance over these few last years. His ideas and knowledge were inspiring and he helped me discover a new research area for me – optofluidics. Professor Uttamchandani always found the time to discuss the problems that I faced with this project and helped to find the best solution for them.

Secondly I would like to thank my second supervisor Dr Michele Zagnoni for help with microfluidic part of my PhD project. His knowledge and assistance in some of parts of this project were vital. I am also very grateful for being given opportunity to take part in the weekly microfluidic group meetings where I could improve my presentation skills.

I would also like to express my huge thanks and gratitude to the person who worked with me side by side in the laboratory Doctor Robert Blue, who become my guidance in the optics part of research and all optics experiments. I admire his knowledge and engineering skills. I want also to thank Dr Blue for his help with proof reading of my writing in all papers and this thesis.

I would like to thank Professor George Stewart for his help with optical fibre theory which was one of critical parts of this thesis. I am also very grateful professor Stewart for the always open door for discussions about optics topics.

I would like to express my thanks to all the members of my research group (Centre for Microsystems and Photonics), especially to my best friends there: Barbara, Kay, Ian, Li Ran and Ralf, who made the working place very cheerful and made cloudy and rainy Glasgow more enjoyable. I will miss morning tea with talkative Kay and Friday afternoon conversations with Barbara. I would like also to thank Ian for his help with proof reading of parts of my thesis.

Finally I want to thank my parents who believed in me and helped me over all my studying years. Without their guidance and support in all my decisions I would not be where I am now.

Abstract

An important research topic in engineering and science is the miniaturization of systems and components, where small size and weight, low power consumption and low manufacturing cost can offer new functionalities. In recent years the fields of optics and fluidics have merged to create the area of research known as "optofluidics". The unique properties of fluids (compression, flow, and variable refractive index) can be combined with optical devices to create systems with advantages in optical measuring, communication and imaging areas.

Variable optical attenuators (VOAs) are components in optical communication networks for managing optical power levels. This thesis is focused on the design, fabrication and characterization of two novel optofluidics based single-mode fibre VOAs ("continuous fibre" type VOA and "fibre gap" type VOA).

The first VOA is constructed from a side-polished optical fibre which is characterized by a sloping shape profile of the external cladding thickness. The fibre is positioned on top of a platform which exploits electrowetting-on-dielectric (EWOD) techniques to move a liquid droplet. By moving a liquid droplet across EWOD platform (and along the polished region of the fibre), optical attenuation can be obtained. The droplet, whose refractive index is equal to or higher than the refractive index of the fibre core, is accessing and leaking radiation from the optical evanescent field of the polished fibre which then modifies the optical attenuation. The level of attenuation depends on the position of the droplet; the attenuation increases as the cladding thickness reduces and the droplet moves closer to the fibre core.

The second VOA is a fibre gap device, where a ferrofluid shutter/actuator is located in the gap between lensed single mode optical fibres. The ferrofluid shutter movement is controlled by a magnetic field and changes the light propagation between fibres. The level of attenuation is defined by the shutter position.

Table of Contents

List of Symbols

n	Refractive index
Λ	Grating period
m	Order of cladding mode
C	Capacitance of the dielectric layer
V	Electric potential
γ_{LG}	Liquid – gas interfacial tension
γ_{SG}	Solid – gas interfacial tension
θ_0	Zero-voltage contact angle
θ	Contact angle when a voltage is applied to the droplet.
B_0	Bond number
R_d	Droplet radius
g	Gravity
ρ	Density
ω_C	Frequency critical value
σ_L	Liquid conductivity
σ_D	Dielectric conductivity
ε_D	Liquid permittivity
ε_L	Dielectric permittivity,
k	Size ratio of the dielectric layer thickness and droplet radius
α	Value of angle hysteresis (between the non-actuated and actuated angle)
W_e	Weber number
v	Velocity of motion
l	Drop contact radius
η_e	Electrowetting number
f_{cap}	Capillary force
f_{EWOD}	Electrowetting on dielectric force
e	Width of electrode
μ	Liquid viscosity
h	Droplet height

d	Waveguide thickness
θ_m	Angle of propagation
λ	Wavelength
ϕ	Phase shift
$d_c(m)$	Mode cut-off waveguide thickness
θ_C	Critical angle
$\dfrac{1}{\gamma}$	Penetration depth
k_0	Propagation vector
R	Reflectivity of the ray
η	Number of reflections at the upper boundary per unit length
z	Propagation direction
d_e	Fibre effective thickness
d	Fibre core diameter
β_m	Propagation constant of a mode
s	Remaining cladding thickness
d_f	Distance along the fibre
a	Gradient
b	Intercept taken from the linear fit
σ	Standard deviation
A	Gaussian function
I	Intensity
L	Length of the light path

Chapter 1

Introduction and literature review of variable optical attenuators

1.1   Scope

This research has focused on the modelling, fabrication and testing of new types of variable optical attenuators (VOAs) created through a combination of fluidic technology and optical fibres. In general there are two different formats of VOA that can be identified, one that is called a "continuous fibre device" and the second called a "fibre-gap device". Common to these in the scope of this research is the introduction of a liquid medium that is manipulated to attenuate the light carried by an optical fibre. This emerging technology of combining fluids and optics is called optofluidics.

1.2   Optofluidics

One of the primary research goals in engineering and science is the miniaturization of systems and components, where small size and weight, low power consumption and low manufacturing cost are considered as advantages[1]. Optical measuring[2], communication[3],[4] and imaging devices[5] can benefit from these advantages. Traditionally, optics has been based on solid transparent materials such as glasses and plastics whose geometries and refractive indices are relatively fixed by manufacture. In more recent times the use of fluids to form optical components, that can subsequently be varied in shape and refractive index, allows the tuning of optical properties. This new area of research is called optofluidics[6] and the combination of fluidics with miniature optical systems[7] opens up the possibility of new devices and systems.

The term optofluidic[8] was used for the first time in 2003 to describe a combined system that contains optics and fluidics. Individually, optics is the study of light emission, propagation, interaction with matter, whilst fluidics is the science of fluid dynamics, for example moving, mixing, and separation. An optofluidic system is a combined system where the fluid manipulates the parameters of light.

In the literature, the term optofluidic system has been ascribed several definitions depending from which features (optic or fluidic) are most important. Psaltis *et al.*[9] described the optofluidic system as "(1) structured solid-liquid hybrids in which the optical properties of both media are relevant; (2) complete fluid-based systems in which only the optical properties of the fluids are relevant; and (3) colloid-based systems in which manipulation of solid particles in liquid, or using the unique optical properties of colloidal solution, form the basis of the optofluidic devices.". However Sinton *et al.*[10] described it as "(1) optofluidic light sources that employ fluidics as the gain medium; (2) optical devices that employ fluids to tune or configure optical response; and (3) fluidic sensors that employ integrated photonic structures." Such wide ranging capabilities are of interest for biological and chemical analysis such as lab-on-a-chip devices[11] and for medical applications such as optofluidic microscopes[12]–[14].

The combination of optics and fluidics can offer new flexibilities in optical systems. For example, simply by replacing one liquid with another can immediately change the refractive index of an otherwise fixed device and thus we now have an adaptive system[15]. Additionally, the refractive index could also be controlled by applying a magnetic field to a magnetic liquid (a so called ferrofluid[16]). The ability to modify the shape of a fluid body has gained popularity in the area of adaptive optofluidic lenses[17],[18]. The solid optics used in a general lens – based imaging system has mechanisms that allow the focal length of a lens system to be varied. The adjustment mechanism has remained constant over centuries and is usually based on moving mechanical parts actuated by hand or motor. The imaging system size cannot be significantly reduced because space is required for all mechanical parts and lenses[19]. Alternatively, a more easily reconfigurable system can be based on a liquid lens, where the liquid itself can change the focal length by the modification of its shape due to mechanical, electrical or magnetic actuation. An example of this is an imaging system comprising of only one fluidic lens where, by applying a voltage, the geometry of the lens surface is changed thereby adjusting its focal length[20]. Such a system lends itself to

miniaturisation and perhaps lower cost by mass production. Such optofluidic lenses are used in a variety of applications such as vision device[21], photography[22]'[23], bioengineering and medical devices and lab-on-a-chip devices[24].

The shape of a fluidic lens can be controlled mechanically as shown by De-Ying Zhang *et al.*[25] who demonstrated fluidic adaptive lenses with a variable focal length (range from 41 mm to 172 mm). The shape of the lens was controlled by a pressure system. The device consisted of a polydimethylsiloxane (PDMS) fluidic chamber covered by a thin membrane bonded to the glass slide. The main function of the chamber was to create the lens. The chamber was connected to a fluidic inlet and outlet by microchannels. Fluid (the authors did not provide information about fluid composition) was injected from a syringe and flowed into the chamber. The shape of the PDMS chamber depended on the applied fluidic pressure (range from 5865.2 P to 399.9 P) and thus changed the focal length of the lens. The diameter of the lens demonstrated by that research group was 20 mm.

A similar pressure induced focal change lens format was proposed by Pang *et al.*[26]. They demonstrated a device that consists of two adaptive cylindrical lenses. The structure was built from PDMS with two chambers separated by the membranes. The chambers are filled with the liquids of different refractive indices (Fig. 1.1). The different pressure in each chamber modifies the shape of the membrane, which creates an appropriate shape of the lens (for example a cylindrical shape). By using two different liquids (distilled water and immersion liquid (#5095, Cargille Laboratories Inc.)) of two different refractive indices (1.33 and 1.58) they could control the focal length of both lenses independently, regardless of the curvature of the membrane that create the lens (the focal length range was from -40 to 23 mm).
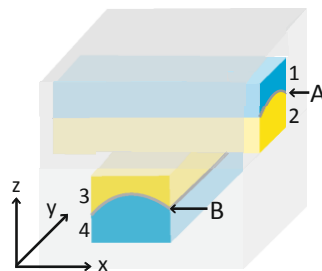
Fig. 1.1 Illustration of the lensing device containing four chambers 1-4, where chamber 1 and 4 contain the liquid of lower refractive index (1.33) and chamber 2 and 3 contain the liquid of higher refractive index (1.58) [26]

An interesting device that integrates optical fibres with a 2x2 switch was presented by Song *et al*[27]. The device was constructed from PDMS with fluidic channels and an air gap positioned between fibres in the light path (Fig. 1.2). A tunable lens was integrated into the structure to decrease the light divergence from the end of the fibre and focused the light beam into the output multimode fibre. The optical switching was achieved with a tunable air-gap mirror by which the light is deflected due to total internal reflection. The device had a switching speed of more than 5 Hz and an extinction ratio of 8 dB. The main disadvantage of the described device is the complicated design that involves fluidic and air channels, membranes and channels for fibres. A second disadvantage that can be found is that there is imperfection in the fibres alignment even when multimode fibre is used. The actual mechanical control of the switch operation required complex control systems such as a pressure system that is not compact and detracts from portability.
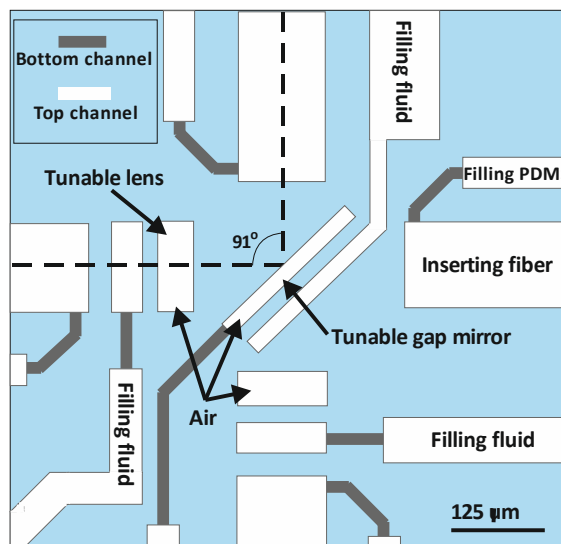
Fig. 1.2 Top view of the optofluidic switched with the lens and mirror integrated inside the device [27]

Besides mechanical control of the lens curvature, a more interesting case is when the liquid lens is controlled electrically by the phenomenon known as electrowetting[28]. Such a phenomenon is of interest here due to the connection to the main work presented in this thesis. A tunable liquid lens was described by Ren *et al.*[29], where an electric field was used

to change the lens shape. This device differs from the lenses discussed previously not only by the control system but also by the amount of the liquid used. The device presented by Ren *et al.* consisted of only one droplet of liquid immersed in a second fluid (Fig. 1.3). The two fluids (of refractive index 1.472 and 1.673) were immiscible so the droplet would retain its shape rather than disperse into the second medium. The device used a cell into which the droplet was placed. The top and bottom wall of the cell was made from the transparent indium tin oxide (ITO) coated glass. The ITO conductive glass was used to form electrodes. When a voltage is applied to the bottom and top electrodes the droplet experiences an electrowetting force and changes shape. Depending on the voltage level (range between 0 and 90 V_{rms}) the droplet can touch the top ITO surface so it can change shape from a convex into the concave shape. As the voltage increased the focal length of the lens decreased (from 620 μm to 500 μm). When the voltage was removed, the droplet relaxed and reverted back to its starting shape.
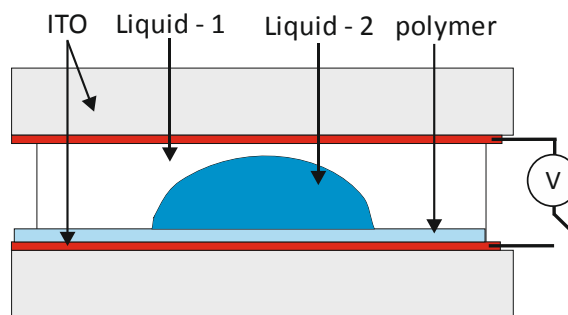
Fig. 1.3 Illustration of the electrowetting controlled liquid lens [29]

Another electrowetting actuated variable focus lens was discussed by the Kuiper *et al.*[22]. These researchers proposed a device that consisted of two liquids (lithium chloride of refractive index 1.38 and mixture of phenylmethylsiloxanes of refractive index 1.55) inside a transparent cell. The electrodes are located on the side of the cell and not on the top and bottom surface, as was proposed by Ren *et al.*[29]. By applying the voltage to the side walls the circular (droplet) shape of the conducting fluid (Fig. 1.4 a) is attracted to the walls and the droplet changes shape from convex to the concave (Fig. 1.4 b). The device can be controlled by an alternating or direct voltage of typically less than 50 V. The researchers

demonstrated direct application of their lens, where the lens was inserted into a camera and several pictures were taken using a different effective focal length (2.85 mm and 3.55 mm).
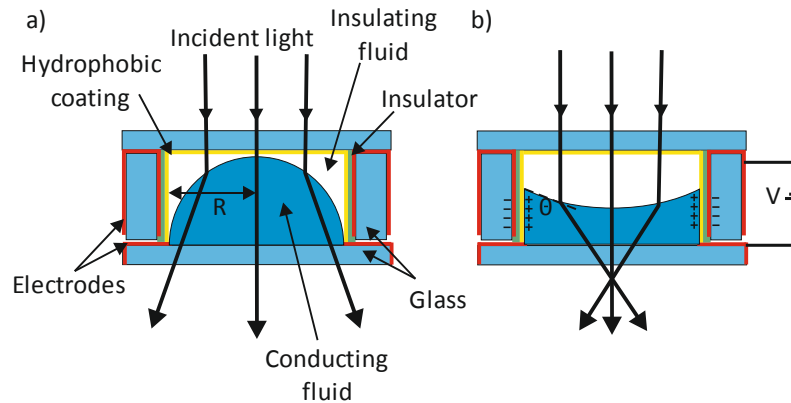
Fig. 1.4 Schematic of a lens device when a) the liquid lens is in the relaxation state, b) the liquid lens changed the shape when the voltage was applied to the side electrodes [22]

The advantage of using the electrowetting phenomenon to control the liquid lens shape is that the device does not require a mechanical system to control it. Therefore, such a device could be more amenable to miniaturisation.

The same research group of Ren *et al.* that built the liquid lens[29] controlled by electrowetting, also proposed a reconfigurable optical switch[30] which is an example of a two state optical attenuator. The structure of the device was very similar to that described above; the liquid lens is located between the two transparent electrodes inside a cell. In this case is that the liquid lens (glycerol) is immersed inside an opaque second liquid (dye-doped liquid crystal). When voltage (in range between 0 and 40 V_{rms}) is applied to the electrodes, the droplet is in contact at the same time with the bottom and top surface, pushing the opaque fluid to the sides (Fig. 1.5). The light (collimated He-Ne laser beam) that is fed into the system can travel with minimal absorption from one side of the device to the second, but when the voltage is removed and the transparent droplet forms a circular shape, it does not touch the top surface and the light is therefore absorbed by the opaque fluid and no light can travel to the opposite side. The switch was characterised by a 300 ms response time, the voltage was in the range from 0 to 40 V. The contrast ratio was measured to be 10:1 using 5 mW laser beam.
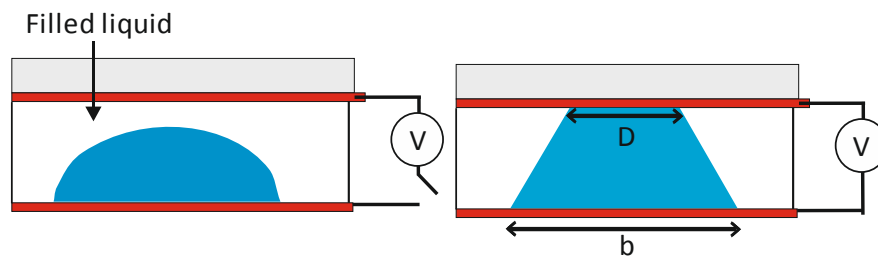
Fig. 1.5 Illustration of the device operation [30]

Similar to the above example, a switch based on electrowetting actuation was constructed by Li *et al.*[31], where a transparent droplet (salty water) surrounded by an opaque oil (silicone oil mixed with Sudan black dye) was encapsulated inside a cell. The main difference for both devices was the operation principle where in the Li *et al.* device the full transmission was achieved in the 0 V state where droplet was touching bottom and top surface in the same time (Fig. 1.6). When a voltage was applied to the bottom and side walls of the cell, the droplet stretched and the opaque oil reduced the light transmission. The measured responding time of 117 ms was shorter than the Ren et al. device response time but voltage increased of 20 V and reached a level of 60 V. The light power decreased to ~0.18 µW. Both Li *et al.*[31] and Ren *et al.* [29] devices are interesting from the electrowetting and light switching point of view, as the electrowetting technique and light switching are the basis of the operation principle of the VOA that is the main focus of this thesis.
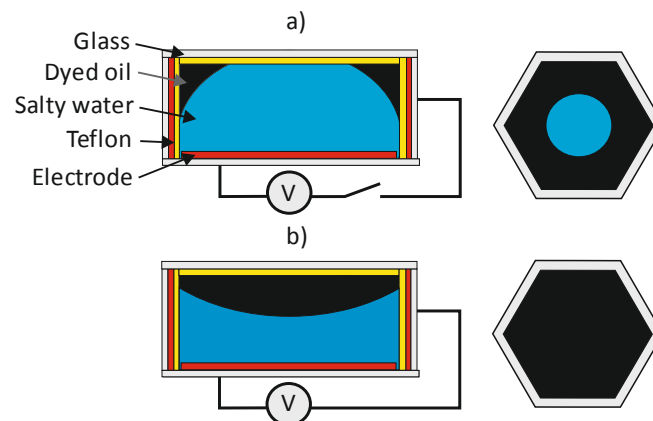
Fig. 1.6 Schematic of the switch based on the electrowetting movement of transparent droplet and opaque oil a) ON state, b) OFF state [31]

The same research group as above represented by Wang *et al.*[32] constructed another switch based on the electrowetting technique. This time the opaque droplet (ink doped with NaCl) was surrounded by a transparent oil (silicon oil). The droplet was moved either to the left or to the right side creating a free light path on the side of the cell (Fig. 1.7). The operating voltage compared to the previous switch device was reduced to 50 V but the switching time increased to 250 ms. In both switches, a laser He-Ne (632.8 nm) was used to illuminate the switch. In the previous example a CCD camera was used as the light detector and that is why there is no information about the level of optical attenuation. However, in the switch presented by Wang et al. the light was detected by a photodiode detector and the maximum attenuation that was measured reached -29 dB. Although both switches described use a laser light source to illuminate the device, it is possible to use single mode fibres with a broadband light source. The reason that it was not used in the above switches might be that researchers focused more on the design and fabrication of the device rather than on the optics applications aspect where the fibres alignment procedure is more complicated and difficult than usage of laser light to illuminate the switch.
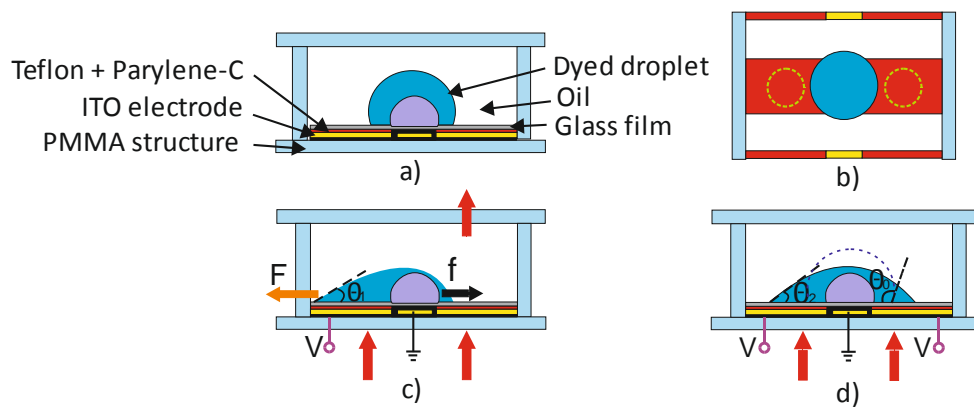
Fig. 1.7 Schematic of a droplet translation switch a) Initiate state, b) top view, c) movement of the droplet to the left side where voltage was applied, d) droplet stretching – voltage applied to both side of the device [32]

An optical switch with a tunable aperture, which used the electrowetting technique to switch light, was demonstrated by C. U. Murade *et al.*[33]. They presented a device which consisted of a bottom glass surface (covered with ITO, SU8 resist, Teflon AF), glass spacer, a

top surface (coated with teflon AF) with a hole and a rubber ring around a hole which acted as a water reservoir. Between the top and the bottom surfaces, a cell was created to store oil with a dye. The cell was larger than the hole (1.2 mm) on the top surface by about 0.6 mm. The SU8 resist in this case acted as the dielectric; the Teflon AF layer worked as the hydrophobic surface and ITO as a bottom electrode. The bottom surface, the glass spacer, the top surface, and the rubber ring were glued together with UV curable NVA 81.
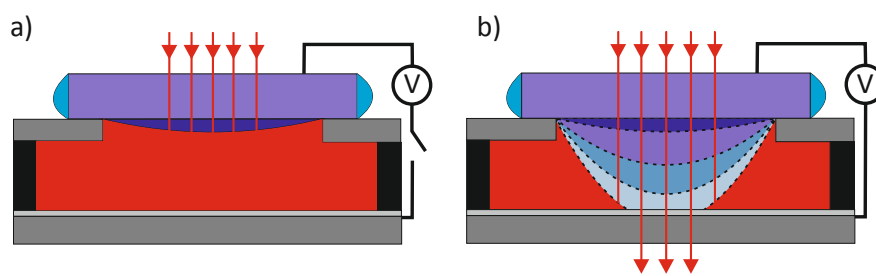
Fig. 1.8 Schematic of optical switch a) off state, b) on state [33]

A voltage was applied between the bottom surface and the water in the rubber reservoir, so that an electric field was created within the oil phase in the cell. The resulting electric stress pushed the water to the bottom surface and the oil and dye to the sides of the cell creating the transparent path for the light (changing from "off" to "on" state) (Fig. 1.8 a, b). Applying a voltage from 0 V to 50 V (rms) with modulation at 1 Hz achieved a response time of 2 ms for the "on" state and from 50 V to 0 V gave a response time of 120 ms for the "off" state. The voltage threshold for suddenly snapping water to the bottom surface was 42 V, creating a path for the light to reach the bottom with diameter of 1.2 mm. When the voltage was decreased the diameter of the path also decreased. The minimum diameter of the path was 0.2 mm for 20 V. The above device can be used in optical communication, displays and in lab-on-chip devices.

Another type of electrowetting device used for optical on/off switching was presented by Heikenfeld *et al.*[34]. This device consisted of a glass bottom surface covered with ITO electrodes, which were dip-coated with Teflon AF that acted as both dielectric and hydrophobic surface. Hydrophilic grid lines that defined the area of the cell, were placed on the top of the Teflon AF layer, limiting the size of the cell to 1x3 mm^2. The cell was filled with a few hundreds µL of deionised water and 100-300 µL of black oil (Fig. 1.9). In Heikenfeld's experiment, when a voltage was applied between the bottom surface and water, the water

meniscus was deflected downwards and pushed the oil to the side of the cell without electrodes. This created an open path for the light at the side of the cell where the water was located. The threshold voltage for downward deflection of the water was 8 V but 80 % light transmission was achieved at 24 V. The researchers also measured the switching response time, which was about 100 ms.
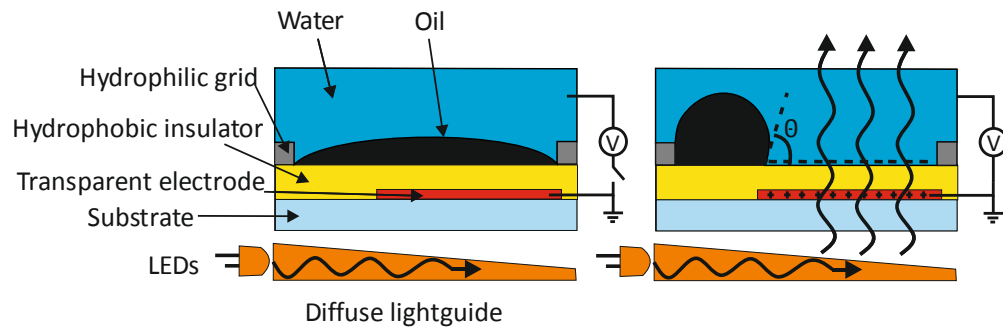
Fig. 1.9 Cross-section of optical switching device based on electrowetting actuation of liquid [34]

The above discussed examples of optofluidic devices have concentrated on systems that are the foundation for the variable optical attenuator. A common feature of these devices is a liquid in the form of a droplet is moved using the electrowetting technique and the main function of a droplet is to change the optical attenuation through the device.

1.3   Variable Optical Attenuators (VOA)

The field of optofluidics is aimed at creating new miniature tunable optical devices. Types of demonstrated tunable optofluidic devices have included examples of optical switches[27], [33]–[41] and also optical attenuators[40]–[43]. The development of the variable optical attenuator (VOA) based on optofluidics is an area of research that is examined in this thesis.

Fibre optical attenuators are important components used to manage power levels in modern WDM multi-channel single mode fibre networks[44]. At the optical source, VOAs are preferred to current modulation to dynamically control laser power. The disadvantage of diode current adjustment of the laser is that the power and wavelength change together during the operation, where the VOA changes only the power, keeping the wavelength

stable. VOAs are also used to equalise the unevenly amplified wavelength channels emitted from erbium doped amplifiers (EDFAs). At the end of optical fibre network, VOAs are employed in front of optical receivers to avoid saturation. Optical attenuators can either be fixed or variable, manually or electronically actuated. However, VOAs are preferred for dynamic regulation of optical power, and a desirable attenuation range is usually at least 20 dB attenuation combined with a broadband optical operation (desired wavelength range is between 1520 and 1560 nm). Linear operation and a low insertion loss of around 1 dB are preferred. In laboratory research, test, and measurement situations VOAs find applications for managing optical power levels.

1.3.1 Examples of variable optical attenuators

Based on a review of the literature there emerges (in general) two types of optical fibre VOA. Firstly, "fibre gap" devices, where the optical attenuation takes place in the free space between two optical fibres, and are often used in conjunction with MEMS (micro-electro-mechanic systems) devices and variable focus lenses. Secondly, "continuous fibre" devices, for example based on the long period grating (LPG) fibre where the optical fibre is unbroken and changing external parameters modifies the optical transmission of the fibre.

1.3.1.1   Fibre gap devices

A fibre-gap device configured as an optical fibre attenuator consists of either two well cleaved optical fibres with their end-faces very close together, or two optical fibres terminated by gradient index (GRIN) lenses aligned to face each other with a wider gap (Fig. 1.10). The GRIN lenses collimate the highly divergent light emitted by the first fibre and refocuses the collimated light into the second fibre. The gap between the fibres allows a controllable light attenuating element to be insert into the optical light path, such as an opaque shutter, movable mirror, or a deformable fluidic element[45],[46].
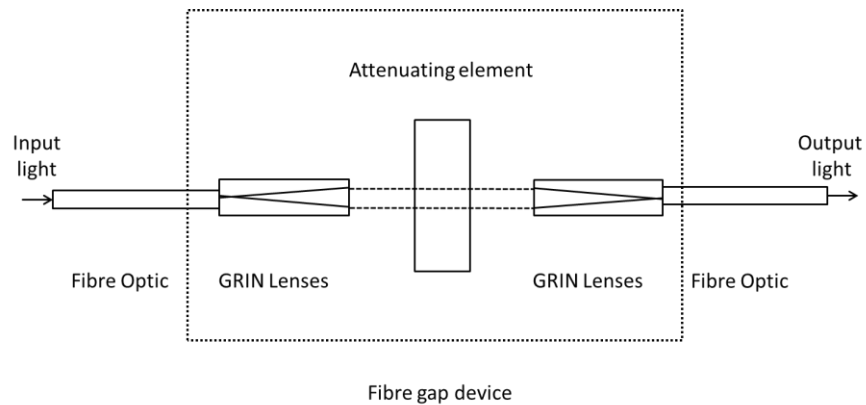
Fig. 1.10 Concept of the fibre-gap variable optical attenuator

A disadvantage of cleaved bare fibres is that the gap between them has to be very small (on the scale of microns) to avoid significant optical losses. Disadvantages of the GRIN lensed fibre-gap device is the requirement for time consuming alignment of the fibres (usually on multi-translational stages) and the associated optical loss (although this is usually less than 0.5 dB). Once assembled the fibre-gap device can also be sensitive to vibrations depending on the particular situation.

Another disadvantage arises from the fact that there is an air gap between two fibres therefore is a difference in the refractive index between the air and the medium that the GRIN lens or bare fibre is fabricated from. The light that travels from one fibre to the second can undergo Fresnel reflection (Fig. 1.11). For standard single mode fibres the loss from reflection from the boundary between the bare fibre and air can reach 4 % of the input power. Additionally, there will be losses due to diffraction and interference effects within the Fabry-Parot cavity. The reflected power loss can be calculated from[47]:

$$reflected\ power = (\frac{n_1 - n_2}{n_1 + n_2})^2 \qquad (1.1)$$

where n_1 is the refractive index of the first medium that light leaves (for example fibre core) and n_2 is the refractive index of the second medium that the light is entering (for example air). To overcome the losses related to the diffraction GRIN lensed fibre, antireflection coatings are often employed on the lenses, but this increases the costs further.
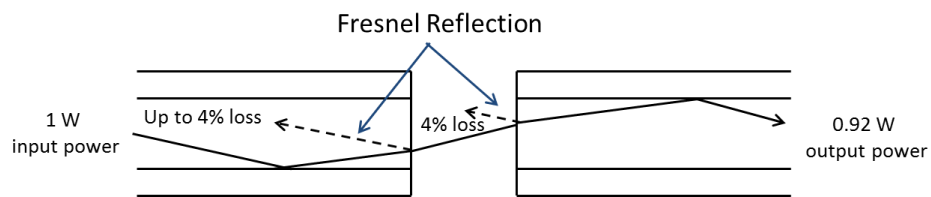
Fig. 1.11 Schematic of the Fresnel reflection occurring on each surface of the fibre-gap device.

One example of an early fibre-gap VOA was reported in 1990 by Benner *et al.*[48]. The device was built from two tapered fibres with bevelled end-faces. The tapers were placed inside ceramic sleeves (Fig. 1.12). In operation, when the axial separation increased the transmission between two fibres decreased. To reduce the loss associated with Fresnel reflection antireflection coatings were used on the end of the fibres. The maximum attenuation reached the level of 75 dB.
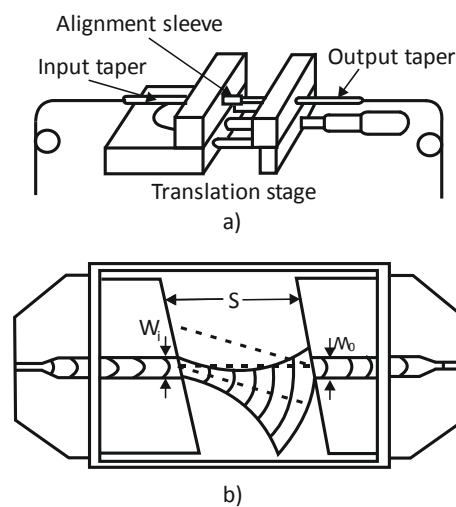
Fig. 1.12 a) Illustration of fibre-gap variable optical attenuator, b) the schematic presenting the physical parameters of the fibres alignment [48]

Modern VOA devices are dominated by MEMS structures. The advantages of MEMS devices are small size and easy integration[49]. In such systems, attenuation of the light is carried out by blocking the light path between the source and receiver fibres either by shutters[50]–[52], by misalignment of two facing fibres[53] or by changing the angle of a mirror[42], [54], [55] to deflect light away from a receiving fibre.

An example of a VOA based on a MEMS shutter structure was demonstrated by Uttamchandani *et al.*[56]. The device consisted of a micromechanical silicon double-bladed shutter actuated by a comb drive actuator and two optical fibres (Fig. 1.13). The movement of the shutter modulates the intensity of the light received by the second fibre. The separation between the two fibres was 70 μm to allow space for a micro shutter. The attenuation range achieved was from -1.4 dB to -29 dB, with an insertion loss of -1.4 dB, and a driving voltage between 0 and 34 V_{DC}. Fabrication required reactive ion etching and back-etching aperture for fibre positioning and gold coating. The weakness of fabrication was imperfection during etching of the shutter structure and in gold deposition which resulted in partial light transmission.
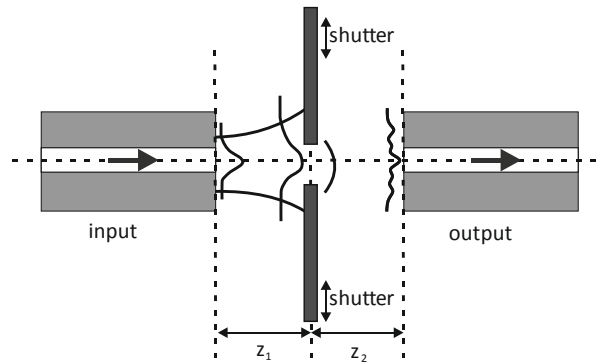
Fig. 1.13 Variable optical attenuator based on the shutter system [56]

A mirror-type MEMS VOA was described by Cai *et al.*[57]. The device (shown in Fig. 1.14) was based on the displacement of a mirror to modify the amount of light entering the output fibre. The device operated on 10.7 Volts, 44 dB attenuation, 0.8 dB polarization dependent loss and insertion loss level of 1 dB. The device manufacture involved micro-fabrication on a silicon wafer using deep reactive-ion etching and mirror coating with gold. A disadvantage of this device is the wavelength dependence loss increment with the increment of attenuation. It was found that for 20 dB attenuation, wavelength dependent loss (WDL) is below 1.3 dB but for the range 20 to 30 dB attenuation, WDL significantly increases to 4 dB. The authors blame the instability of the WDL due to an etched mirror imperfection which resulted in light scattering.
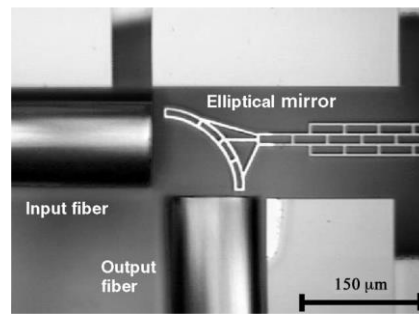
Fig. 1.14 VOA based on the mirror displacement[57]

An alternative to placing a displaceable device between two fibres is to displace one fibre relative to the other. The advantage of this is that the gap between the fibres can be reduced to a few tens of microns. Such a VOA was described by Unamuno *et al.*[58]. The VOA was constructed from two fibres and electrothermal microactuators. One fibre is held rigid within a fibre channel whilst the adjacent fibre is sandwiched between a microactuator and a restoring spring (Fig 1.15). A voltage applied to the device causes the thermo effect that results in a movement of the actuator and a displacement of the fibre. The change in the position of the fibre results in an attenuation of the light transmitted to the stationary fibre. The maximum attenuation that was achieved was 47 dB.
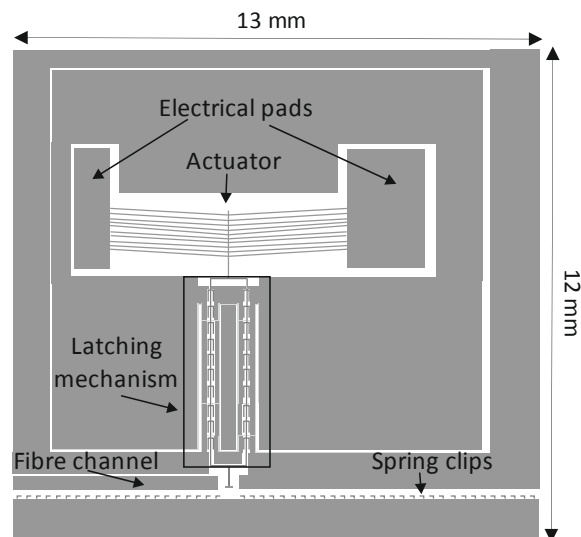
Fig. 1.15 Design of the Vernier latching MEMS VOA [58]

Although MEMS VOAs are the most common type of VOA, these devices can have reliability issues associated with movable micromechanical elements, as well as complicated

fabrication processes and careful alignment of the optical elements[55]. Optofluidic devices can offer the advantages of having no mechanical moving parts but to date there have been relatively few reported fibre optic VOAs using optofluidics.

Lapsley *et al.*[59] proposed an optofluidic VOA based on variable interfacial reflection from a water-based microfluidic channel between a fibre-lens system and achieved an optical attenuation up to 35 dB (Fig. 1.16). Light from a laser source (wavelength 532 nm) was injected into the fibre and a silicon detector was used to measure the output light power. Two reservoirs containing either water or a $CaCl_2$ solution fed into a common PDMS microchannel. By varying the concentration of $CaCl_2$ the refractive index of the solution could be controlled so as to alter the reflectivity of the liquid/PDMS surface and thus the light reflected into the second output fibre. A disadvantage of this system is that the fluidic system is an open loop system that means the fluid used once cannot be used again and depletes the reservoir. Additionally, for the device to operate required syringe pump systems to inject the liquids to channel and that increases the size of the final device setup.
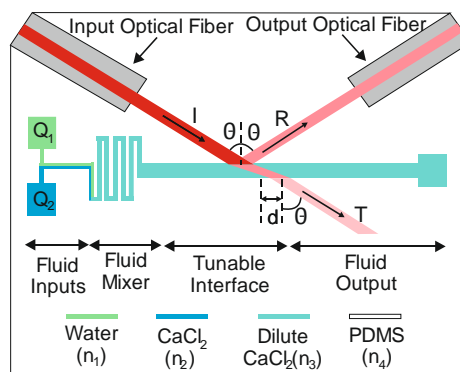
Fig. 1.16 Illustration of the VOA device based on variable interfacial reflection from a water-based microfluidic channel [59]

In contrast Xu *et al.*[46] used a voltage induced dielectric force to stretch a liquid crystal across an aperture between lensed single mode fibres (SMF). The liquid crystal was inserted into the transparent cell (Fig. 1.17 a) with patterned electrodes on the ITO glass slide (Fig. 1.17 c). When a voltage was applied to the electrodes the liquid crystal droplet was stretched and gradually deflected the beam that travelled from one single mode fibre to the other (Fig. 1.17 b). The light from a tunable laser source (1.52 μm – 1.62 μm) was injected to the input fibre, the light was collected via the SMF and measured by optical power meter.

This device could achieve broadband operation with a range of up to 32 dB with an insertion loss of 0.7 dB. Such an operation principle when light is deflected rather than absorbed is very interesting from the point of view of a fibre gap device, where usually the liquid is working as shutter that absorbs light and that phenomenon will be used to operate the VOA described in Chapter 5.
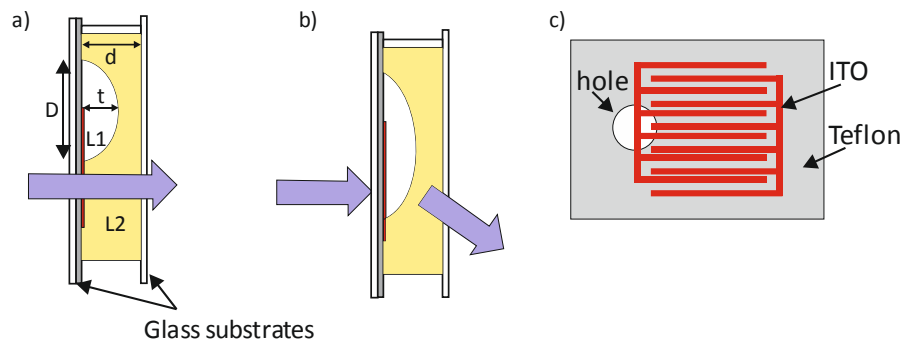
Fig. 1.17 Illustration of the VOA device a) cell with the liquid crystal droplet inside, b) droplet deflecting the light beam, c) electrode pattern on the ITO glass [46]

Similarly, Reza and Riza[60] created a VOA using a commercial liquid lens (Varioptic, France) situated in free space between two SMF coupled lenses. The liquid lens consisted of a combination of water and oil within a transparent cell and upon application of a voltage (range between 38 V up to 46 V) the meniscus of the liquid interface changed shape and altered the lens focussing properties. This electrowetting actuated device had broadband (1530 – 1560 nm) variable attenuation up to 40 dB and an insertion loss of 4.3 dB.

Another example of a device that uses the electrowetting phenomenon to create an optofluidic attenuator was reported by Muller *et al.*[45]. This research demonstrated a sandwich device design, which encapsulated two liquids inside a chamber (Fig. 1.18). One liquid was transparent and the second liquid was opaque. The chip consisted of a bottom glass surface, silicon spacer and top glass surface. Bottom and top surfaces were covered with a layer of ITO, which were then covered with a deposition of Parylene (2.5 µm thick). This Parylene layer was then covered with Cytop (1.0 µm thick) using a spun-sample deposition technique. In this design, Parylene acted as the dielectric and Cytop as the hydrophobic surface. Shaping of electrodes on the bottom and top surfaces was carried out by reactive ion etching (RIE). The bottom surface, silicon wafer and top surface were bonded together to create a microfluidic chamber with a height of 645 µm. The response time of the

droplet motion was 100 ms and the actuation speed of the liquids was 39 mm/s. The range of voltages used in the device was 45 - 160 V. Depending on the pigment or dye used and the input wavelength, different attenuation was achieved. The maximum attenuation varied between -17 dB up to -47 dB. The type of dye/pigment also influenced whether narowband or broadband wavelength operation was achieved. The main disadvantage is that device is working more as a switch rather than as varibale optical attenuator.
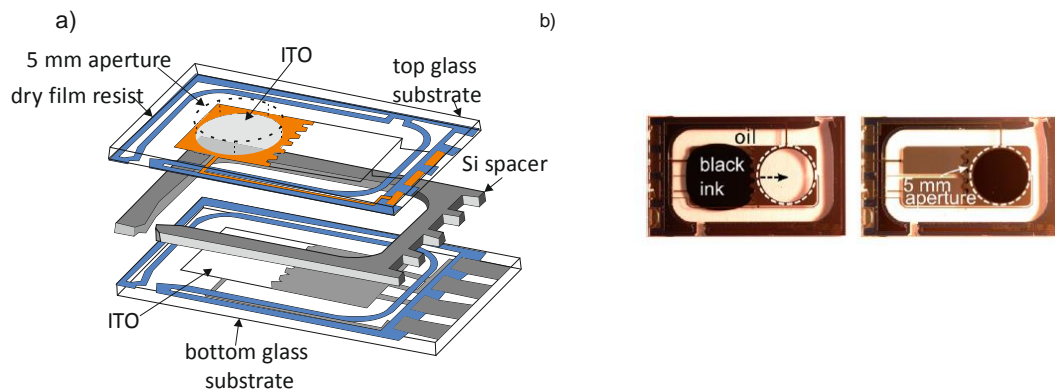
Fig. 1.18 a) Layered view of switching device, b) top view of switching device[61]

Another type of fibre gap device that is an example of an optofluidic attenuator was described by Hongbin *et al.*[62]. The device was a type of transmissive attenuator. The attenuator (shutter) was constructed from two transparent cells with a membrane positioned between them. Each layer of the shutter was constructed from PDMS. One cell was filled with the absorbing liquid and the second was filled with air. Different volumes of air in the second cell deformed the membrane. When the volume of air increased the membrane deflected pushing the liquid in the second cell creating a clear path for the light. Two types of attenuation were achieved by either decreasing the thickness of the liquid on the light path (Fig. 1.19 a) or by changing the aperture of the open light path by pushing liquid to the side of the cell (Fig. 1.19 b). The shutter was positioned between two fibres. There is no information about what types of fibres were used but from the experimental setup it should be possible to use single mode fibres for the input and output light paths. Optical attenuation reached a level of -38 dB within the wavelength range from 1520 nm to 1620 nm with a WDL of 1.8 dB.
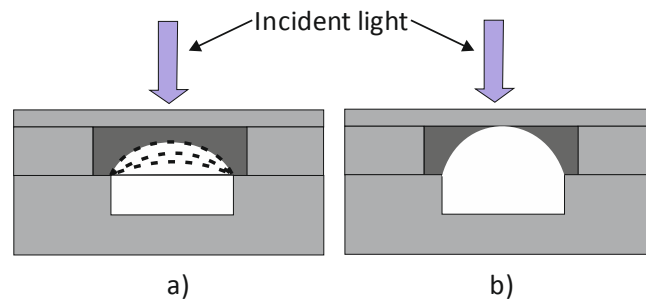
Fig. 1.19 Illustration of the device a) modulation of the liquid layer thickness, b) modulation of light path aperture [62]

Ranjini *et al.*[63] built a VOA that is an example of a gap device where a cell filled with a crystal liquid was located between the light source and a powermeter. The operation principle of this device is based on the refractive index change of the liquid crystal. The refractive index was varied due to flow that was introduced to the liquid. The normalized optical power changed from 0.8 to 0.0 when crystal liquid flow increased from 0 to 50 ml/hr. Although the light input that was used was delivered from a laser source (514 nm) the cell could also be inserted between two fibres and then device will be a standard example of fibre gap device.

Another interesting example of fibre gap device was presented by Zhu et al.[64]. The device was constructed from the microfluidic VOA inserted between a tapered fibre and multimode fibre. The tapered fibre was used to couple light into a PDMS waveguide and the multimode fibre collected light from the end of the PDMS waveguide. The PDMS waveguide had a rectangular cross-section. The waveguide top surface (top cladding) was replaced by the fluidic channel. The channel was filled with the liquids of different refractive indices. When the liquid refractive index was higher than the refractive index of the waveguide core then the light guided through the structure was attenuated. The maximum attenuation that was achieved was -28 dB. A disadvantage of such a device is that to change the refractive index of the fluidic cladding then the liquid had to be changed, and this introduces a power fluctuation after the change as well as adding to the complexity of the device. To switch between liquids required several different syringes with separate liquids. The described device has some similarity in device construction to the device that is going to be described in the following chapters, where the device principle of operation is based on the liquid interaction with the light that travels through an optical fibre via reduced cladding thickness.

In this subsection we have presented examples of optical devices whose operation principle form the basis of the design of VOAs that are developed and examined within this thesis. The main similarity to the first VOA that will be described in next three chapters is the use of the electrowetting technique that is used to manipulate a liquid droplet. Thereafter the form of a fibre gap device, where the shutter moves across the light path is the fundamental operation principle of the VOA designed, and characterised and described in chapter 5.

1.3.1.2   Continuous fibre devices

A continuous fibre device is a device that transmits an optical signal through a modulating device via an unbroken fibre. The light that travels through it can be modified from outside of the fibre. Researchers have demonstrated VOA formats in optical fibre other than SMF. An optical fibre Bragg grating (FBG) can be manufactured by exposing the core of an optical fibre to a high intensity optical pattern that imprints an area of periodically modified refractive index within the core of the fibre. One form of FBG is called the Long Period Grating (LPG). In this case the period of the grating is typically several hundred microns and the grating itself can extend over many millimetres. This extended grating creates the condition for the forward propagating modes (with a smaller difference in propagation constants) to couple power between themselves. Hence an optical mode carried by the core can couple into a number of lossy co-propagating cladding modes and results in periodic wavelength-dependent dips in the transmission spectrum. The cladding modes are confined due to the cladding-air boundary. In the case of the LPG the wavelength that resonantly couples to a cladding mode is given by[65]:

$$\lambda^m = \Lambda\big(n_{eff,core} - n_{eff,cladding}^m\big)$$

(1.2)

where Λ is the grating period, $n_{eff,core}$ and $n_{eff,cladding}^m$ are the effective index of the fundamental fibre core mode and mth cladding mode respectively.

The wavelength selective loss is sensitive to changes in the external refractive index surrounding the fibre as this modifies the phase-matched coupling conditions and causes a shift in the position of the resonance dips.

In 2003 Hsieh *et al.*[66] used electrowetting actuation of a conductive fluid in a circulating "racetrack" configuration to achieve dynamic tuning of an LPG fibre. The conductive fluid was in the form of a long liquid plug immersed within a lubricating fluid and was moved in stages along the LPG so that it increasingly overlapped with the entire grating section of the fibre (Fig. 1.20 a). The grating section was 15 mm long with a periodicity of 362 μm. This fluidic plug was composed of approximately 58 wt.% of sodium dichromate in water giving a refractive index close to that of silica. Increasing overlap with the LPG fibre grating section resulted in an observed change in the wavelength position of the optical transmission dip of the LPG fibre by a few nanometres (Fig. 1.20 b). The optical dynamic range of the LPG resonance peak (1538 nm and a full width half maximum (FWHM) – 10 nm) reached 20 dB. However, this VOA device is not a broadband device. Moreover, the sodium dichromate used to create the liquid solution is highly toxic.
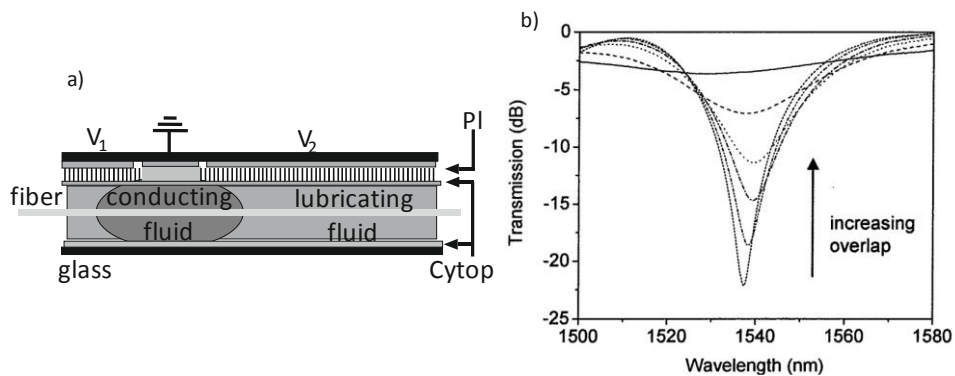
Fig. 1.20 a) Schematic of the VOA device, b) the LPG transmission spectrum change during the increase in the plug – fibre overlapping [66]

These researchers subsequently improved upon this concept by specifically engineering an LPG fibre so that the phase matching condition is met over a larger wavelength bandwidth (Acharya *et al.*[67]) achieving over 40 nm wavelength band and 20 dB attenuation (Fig. 1.21 b). The device design was also improved by creating the electrodes not only on the bottom plate but also on the cover ITO glass (Fig. 1.21 a).
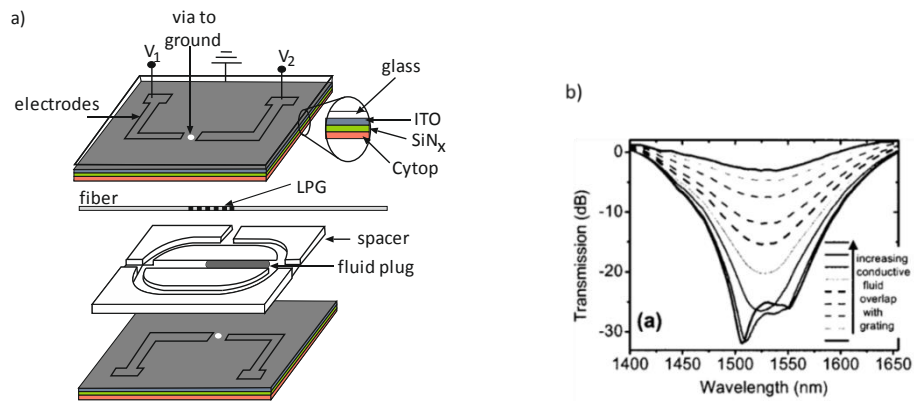
Fig. 1.21 a) VOA device layout, b) transmission spectrum during the plug movement along the LPG [67]

A different approach from the same research group was reported by Cattaneo *et al.*[68] This time the electrowetting platform was reconfigured to 8 "racetracks" to manipulate 8 independent smaller plugs (each approximately 2 mm in length) that transverse across (rather than along) a LPG fibre (Fig. 1.22 a). The device was a narrowband type with attenuation reaching only approximately 10 dB (Fig. 1.22 b).
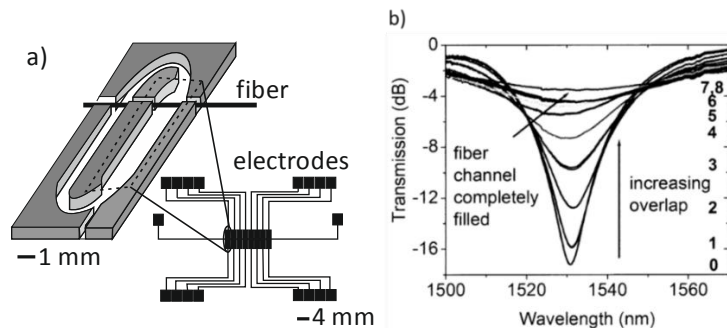
Fig. 1.22 a) Schematic of the electrowetting platform for movement of 8 plugs, b) transmission spectrum of LPG when the grating was subsequently covered with 8 plugs [68]

Another example of the continuous fibre VOA that does not use a standard optical fibre, was proposed by Mach *et al.*[69]. The fibre that was used in the device was a combination of standard single mode fibres fused with microstructured fibre (photonic band gap guidance fibre) with a long period grating that was written into the core. The microstructured fibre had six channels created in the cladding around fibre core (Fig. 1.23). The microfluidic plugs were injected into the channels and sealed inside, and by adjusting

their position within the fibre core, the optical propagation of the fibre was modulated. The microfluidic plugs manipulation was controlled by actuators and pumps formed on the fibre surface. The change in temperature provided by a heater on the fibre surface changed the pressure of the air that was trapped with the fluid plugs inside the channels. The change of the inside pressure moved the fluidic plugs into new position along the LPG part of the fibre. The fluid had a higher refractive index than the fibre core refractive index and disturbed the total internal reflection of the light propagation through the LPG part. The tuning of the fibre was modulated by the length of the plug overlapping the LPG. The device was characterised by 12 nm wavelength tunability and an attenuation range of 15 dB. The main disadvantage of this device is the complicated construction of different fibres types spliced together and a small attenuation range of device operation. The above examples made extensive use of special LPG fibres that are generally limited to narrowband operation. The main similarity to the device that is main part of the work presented in this thesis is the continuous fibre type of device and use of the liquid with special parameters that can change the light propagation inside the fibre.
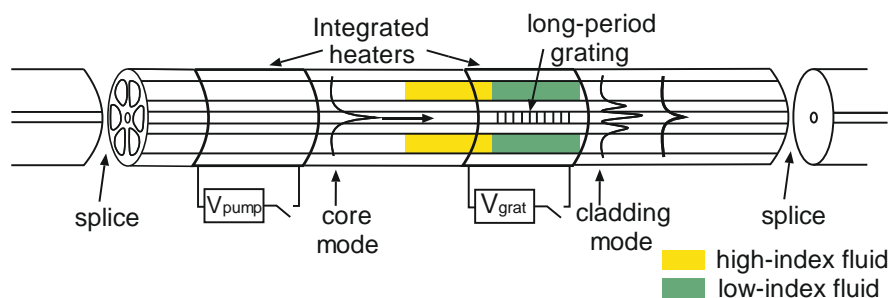
Fig. 1.23 Illustration of the fibre constructed with microstructured fibre and long period grating integrating together [69]

Mathews *et al.*[70] proposed a different approach to the VOA that uses a microstructured fibre (photonic crystal fibre) that was spliced between two single mode fibres. The construction of the device was not as complex as the example cited above. As it did not require a LPG written in the fibre core. As such the VOA was characterised by a broadband operation wavelength range between 1500 to 1600 nm. In the Mathews' device, seven holes located in the cladding along the fibre core were filled with nematic liquid crystal (NLC). The attenuation level of the VOA was controlled electrically, the voltage range applied

to the device varied from 170 to 310 Vpp. The application of an electric field to the liquid crystal molecules reoriented them and the refractive index of the LC changed causing change of the light propagation through the fibre as the light is coupled into the cladding and the optical transmission decreased. Attenuation changed linearly with the voltage increment. The maximum attenuation reached a level of 40 dB for 310 V. Despite the attenuation level reaching a level of 40 dB, the voltage level is very high comparing to the VOA that uses the electrowetting technique to move the liquid along the fibre and the voltage usually does not exceed 200 V.

Continuous fibre VOAs have also been demonstrated by modifying the geometry of standard optical fibre, either by tapering the diameter of the fibre or polishing one side of the fibre. A continuous fibre VOA based on a tapered fibre was reported in 2009 by Kim *et al.*[71] where a tapered fibre is bent (Fig. 1.24) and immersed into liquids of varied refractive indices. The tapered process involved flame brushing method, where the fibre is heated up from two torches and pulled along its length. Depending on different refractive index and bending of the fibre different optical losses were achieved. The maximum attenuation reached 35 dB for taper of diameter of 68.4 µm surrounded by liquid of 1.445 refractive index. This device suffers from the careful manufacturing processes required and the extreme fragility of the resultant tapered fibre.
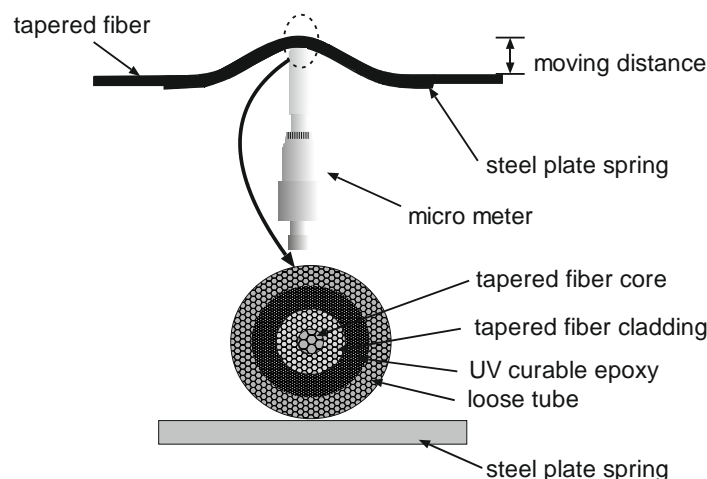
Fig. 1.24 Illustration of continuous tapered fibre VOA with schematic of fibre cross section [71]

To achieve a more robust VOA device format researchers have embedded SMFs into glass blocks. Such devices are term "half blocks" or "polished fibre couplers". A slot is cut into

a glass or quartz block using a diamond wire which creates a curved groove. The coating of an optical fibre is stripped over a length shorter than the length of the groove and is inserted into the groove under tension and fixed with glue (Fig. 1.25). The glass block is then mounted onto a polishing jig and undergoes continuous lapping and then polishing stages until the optical evanescent field of the fibre can be accessed externally[72]. The complete process can take several hours and usually one glass block is mounted onto one jig.
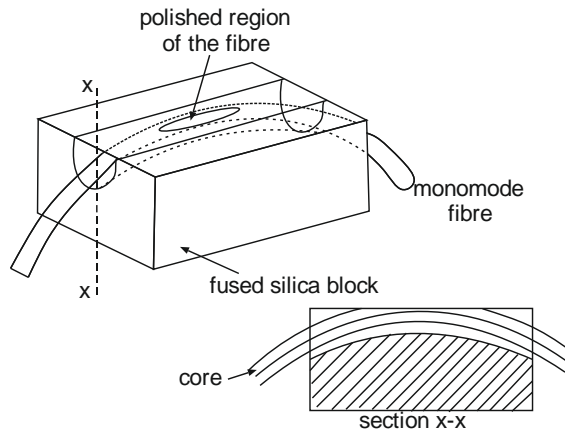
Fig. 1.25 Illustration of "half-block" with an embedded fibre polished to access the evanescent field [72]

An example of such device was presented by Kim et al.[73] where the evanescent field of the polished fibre is in contact with a sliding dielectric plate which is index matched to the fibre core (Fig. 1.26). Depending on the position of the plate the attenuation was variable and the maximum attenuation that was achieved was 49 dB.
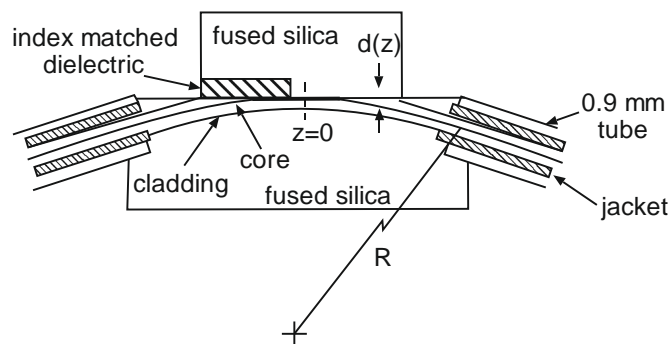
Fig. 1.26 Schematic of the half block type VOA [73]

The main advantage of the half block type of the continuous fibre device is that in contrast to the fibre-gap device there is no requirement for optical alignment of fibres with its associated losses, as well as the device not being sensitive to vibrations. This has to be balanced with the long processing time of device manufacture.

An alternative continuous fibre device is a side-polished fibre that is not embedded in a glass block (Fig. 1.27).
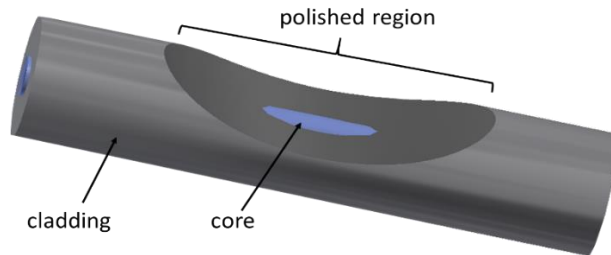
Fig. 1.27 Profile of a side-polished fibre (not to scale)

Standard SMF is polished on a grinding wheel (Fig. 1.28). With the use of appropriate fluids and/or abrasive powders the cladding of the fibre is reduced on one side leaving cladding on the opposite side of the fibre untouched[74]. The untouched cladding gives the fibre some robustness and allows general careful handling, but is less robust than the embedded polished half coupler. A major advantage of this fibre is the much reduced fabrication time.
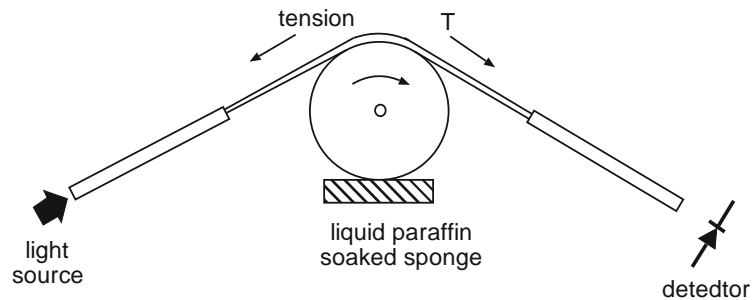
Fig. 1.28 Fibre polishing manufacture process, where fibre is positioned on the polishing wheel [74]

Gu *et al.*[75] demonstrated a VOA constructed from a side-polished fibre and a liquid crystal encapsulated inside a glass capillary upon the polished fibre section (Fig. 1.29). By applying a variable voltage the molecules of liquid crystal re-orientate and thus the refractive index of the liquid crystal was changed, modifying the optical transmission loss through the

fibre. The maximum attenuation achieved was approximately 25 dB for 20 V applied to the liquid crystal (refractive index 1.51).
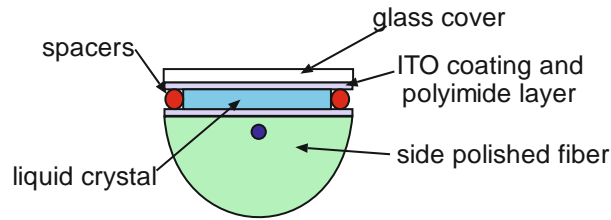
Fig. 1.29 Illustration of the VOA with description of the cell construction [75]

Based on the research on the side polished fibre topics, the idea of using this type of fibre in the VOA emerged. The main VOA that is examined and described in the following chapters has been constructed from a side polished fibre. The VOA operating principle is based on the interaction of the evanescent field of the fibre with a liquid.

1.4 Description of devices developed in this thesis

1.4.1 Objectives

The objective of this research work was to design novel optofluidic-based VOA devices that will meet the requirements of broadband operation (wavelength range between 1520 nm and 1560 nm), large attenuation range (at least 20 dB), easy handling, compactness and low cost of fabrication. These devices will be in a format of both continuous fibre and fibre-gap architectures. Experimental results will be compared to theoretical modelling of each device.

1.4.2 Overview of VOA devices to be developed

The different approaches to optofluidic and VOA devices were discussed above. To create an in-line optofluidic actuated VOA requires two main components: an optical fibre designed to allow access to the transmitted light and a platform that can control a liquid

medium to actuate the optical attenuation. The continuous fibre device has been implemented previously using LPG fibres[66]–[68] and therefore these devices do not have broadband operation. This research in this thesis aims to overcome this limitation to create an in-line VOA that is based on standard optical fibre with broadband operation. Desirable wavelengths of operation are in the telecommunication systems C-band from 1520 nm to 1560 nm[76]. One possible implementation of this could be via an embedded fibre in a "half block" (Fig. 1.21). However the small interaction region with the optical signal limits the desired gradual reduction in optical signal required for a viable variable attenuator, and also the embedded nature of the fibre restricts flexibility in fluidic platform design. Therefore the non-embedded side-polished fibre based on standard SMF was chosen as the in-line optical transmission medium.

The second consideration of the device is the method to manipulate a liquid medium. One method to implement this is through the use of an electrowetting on dielectric (EWOD) platform. Such a platform is investigated for the controlled translation of discrete liquid droplets of small volume in the range of 0.3 µL – 4 µL by application of a voltage. The combination of these two parts (side-polished fibre and electrowetting platform) created a VOA (Chapter 2 – 4).

The second format of an optofluidic VOA will be based upon a shutter type fibre-gap device using a magnetic liquid (ferrofluid) controlled by magnetic field actuation (Chapter 5). That type of device offers advantage of not using mechanical moving parts which improves reliability.

1.4.3 Operation principle of the continuous fibre device of this thesis

The continuous fibre VOA described above is constructed from a side-polished fibre that is located on an EWOD platform. The polished region of the fibre is in contact with a liquid droplet that is positioned on top of the EWOD platform. An electric field applied to the platform produces droplet movement across electrodes and along the polished region of the fibre. The polished region of the fibre is characterised by a sloping profile where the cladding thickness reduces to a few micrometres above the fibre core surface. Such cladding thickness reduction allows the optical evanescent field of fibre to increasingly penetrate the droplet as

the droplet moves along the polished region. When a droplet of refractive index close to the refractive index of the fibre core moves from position 1 to position 3, the radiative loss of optical power from the fibre increases (Fig. 1.30).
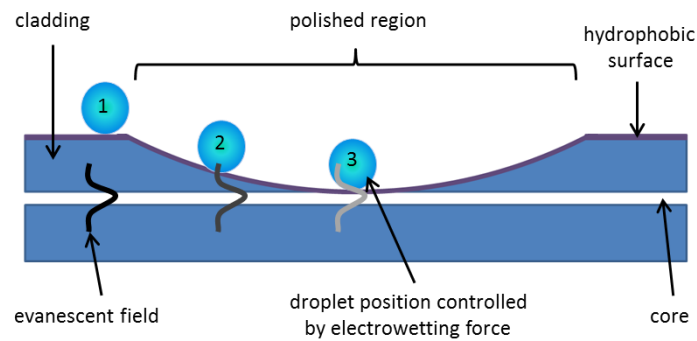
Fig. 1.30 The topology of a side polished fibre with a different position of the droplet along the polished region increasingly accessing the optical evanescent field

1.5   Novelty

The novelty of the research is first of all the development of a new, continuous-fibre, optofluidic VOA using the combination of side-polished fibre and a specifically designed EWOD platform. The complete system is shown to create an in-line VOA with broadband operation in the optical communications C-band.

Secondly an "all-fluidic" shutter type fibre-gap VOA device controlled with magnetic field is designed and evaluated. This fibre-gap device demonstrated broadband operation with large attenuation range.

Both devices are the integration of optics and fluidics to achieve two new optofluidic type devices not reported from any other research group.

1.6   Thesis organisation

The thesis organisation is as follows:

Chapter 1 briefly introduced the field of optofluidics with a short description of typical optofluidic devices reported by different research group. Next VOAs were described

starting from general description through examples of standard MEMS (micro-electro-mechanical-systems) type devices leading to the optofluidic VOAs and switches. Subsequently, the two formats of optical fibre mentioned (continuous fibre device and fibre-gap device) were presented. Finally a description of the concept of the proposed VOA devices was discussed and the novelty part of the research was emphasized.

Chapter 2 presents the electrowetting and electrowetting on dielectric (EWOD) phenomenon. The design process of an electrowetting platform with choice of the materials is discussed and the fabrication process of the platform is presented. Thereafter the fabricated platform is characterised with some basic electrowetting theory and analysis to evaluate its performance parameters.

The theoretical characterisation of light propagation inside a side-polished fibre is discussed in Chapter 3. The special case of light propagation through a side-polished fibre is considered in relation to the refractive index of the external medium and different contact lengths between the polished fibre and the outside medium.

Chapter 4 focuses on experimental results obtained and comparison with the theoretical model presented in the Chapter 3. The fabrication process of the side-polished fibre is described and different types of device operation will be described and linked to the predicted theoretical results.

Chapter 5 introduces a different type of the VOA, the fibre-gap device, where a fluid is used as a shutter to attenuate the light. The chapter starts with a short review of devices that use a magnetic liquid (ferrofluid) together with the design of the VOA demonstrated here. Theoretical analysis of the device operation is presented and compared with experimental results obtained.

The final chapter summarises the main results obtained from the two types of VOAs and a comparative discussion of the two devices. The performance of our devices is compared to the performance of the similar devices reported by other research groups.

1.7 References:

[1]   K. Gilleo, "MOEMS the Word," *Circuits Assem.*, no. November, pp. 28–34, 2000.

[2]   B. Lee, "Review of the present status of optical fiber sensors," *Opt. Fiber Technol.*, vol. 9, no. 2, pp. 57–79, Apr. 2003.

[3]   M. C. Wu, O. Solgaard, and J. E. Ford, "Optical MEMS for Lightwave Communication," *J. Light. Technol.*, vol. 24, no. 12, pp. 4433–4454, Dec. 2006.

[4]   E. R. Brown, "RF-MEMS switches for reconfigurable integrated circuits," *IEEE Trans. Microw. Theory Tech.*, vol. 46, no. 11, pp. 1868–1880, 1998.

[5]   L. Li, V. Stankovic, L. Stankovic, S. Cheng, and D. Uttamchandani, "Single pixel optical imaging using a scanning MEMS mirror," *J. Micromechanics Microengineering*, vol. 21, no. 2, p. 025022, Feb. 2011.

[6]   J. R. Adleman, D. a. Boyd, D. Goodwin, and D. Psaltis, "Optofluidic Technologies," in *2007 Digest of the IEEE/LEOS Summer Topical Meetings*, 2007, vol. 1, pp. 66–67.

[7]   C. Monat, P. Domachuk, and B. J. Eggleton, "Integrated optofluidics: A new river of light," *Nat. Photonics*, vol. 1, no. 2, pp. 106–114, Feb. 2007.

[8]   V. R. Horowitz, D. D. Awschalom, and S. Pennathur, "Optofluidics: field or technique?," *Lab Chip*, vol. 8, no. 11, pp. 1856–63, Nov. 2008.

[9]   D. Psaltis, S. R. Quake, and C. Yang, "Developing optofluidic technology through the fusion of microfluidics and optics.," *Nature*, vol. 442, no. 7101, pp. 381–6, Jul. 2006.

[10]   D. Sinton, R. Gordon, and A. G. Brolo, "Nanohole arrays in metal films as optofluidic elements: progress and potential," *Microfluid. Nanofluidics*, vol. 4, no. 1–2, pp. 107–116, Sep. 2007.

[11]   H. C. Hunt and J. S. Wilkinson, "Optofluidic integration for microanalysis," *Microfluid. Nanofluidics*, vol. 4, no. 1–2, pp. 53–79, Sep. 2007.

[12]   D. Erickson, L. R. Baugh, Z. Yaqoob, P. W. Sternberg, and D. Psaltis, "Optofluidic Microscope: A Novel High Resolution Microscope-on-a-Chip System," in *2006 Digest of the LEOS Summer Topical Meetings*, 2006, vol. 2, pp. 15–16.

[13]   X. Heng, D. Erickson, L. R. Baugh, Z. Yaqoob, P. W. Sternberg, D. Psaltis, and C. Yang, "Optofluidic microscopy--a method for implementing a high resolution optical microscope on a chip.," *Lab Chip*, vol. 6, no. 10, pp. 1274–6, Oct. 2006.

[14]   S. Yang, G. Zheng, S. A. Lee, and C. Yang, "Stereoscopic optofluidic on-chip microscope," in *IEEE Winter Topicals 2011*, 2011, vol. 2, pp. 91–92.

[15]   U. Levy and R. Shamai, "Tunable optofluidic devices," *Microfluid. Nanofluidics*, vol. 4, no. 1–2, pp. 97–105, Sep. 2007.

[16]   H. E. Horng, C.-Y. Hong, S. Y. Yang, and H. C. Yang, "Designing the refractive indices by using magnetic fluids," *Appl. Phys. Lett.*, vol. 82, no. 15, p. 2434, 2003.

[17]   Y. Fainman, L. Lee, D. Psaltis, and C. Yang, *Optofluidics: fundamentals, devices, and applications*. McGraw-Hill, Inc. New York, NY,, 2009, pp. 177–182,188, 193.

[18]   S. Xu, H. Ren, Y. Liu, and S.-T. Wu, "Dielectric Liquid Microlens With Switchable Negative and Positive Optical Power," *J. Microelectromechanical Syst.*, vol. 20, no. 1, pp. 297–301, Feb. 2011.

[19]   T. Bifano, "Adaptive imaging: MEMS deformable mirrors," *Nat. Photonics*, vol. 5, no. 1, pp. 21–23, Jan. 2011.

[20]   C.-C. Cheng, C. A. Chang, and J. A. Yeh, "Variable focus dielectric liquid droplet lens.," *Opt. Express*, vol. 14, no. 9, pp. 4101–6, May 2006.

[21]   T. liquid lens company Varioptic, "varioptic.com." .

[22]   S. Kuiper and B. H. W. Hendriks, "Variable-focus liquid lens for miniature cameras," *Appl. Phys. Lett.*, vol. 85, no. 7, p. 1128, 2004.

[23]   B. Berge and J. Peseux, "Variable focal lens controlled by an external voltage: An application of electrowetting," *Eur. Phys. J. E*, vol. 3, no. 2, pp. 159–163, Oct. 2000.

[24]   Y. Gambin, O. Legrand, and S. R. Quake, "Microfabricated rubber microscope using soft solid immersion lenses," *Appl. Phys. Lett.*, vol. 88, no. 17, p. 174102, 2006.

[25]   D.-Y. Zhang, V. Lien, Y. Berdichevsky, J. Choi, and Y.-H. Lo, "Fluidic adaptive lens with high focal length tunability," *Appl. Phys. Lett.*, vol. 82, no. 19, p. 3171, 2003.

[26]   L. Pang, U. Levy, K. Campbell, A. Groisman, and Y. Fainman, "Set of two orthogonal adaptive cylindrical lenses in a monolith elastomer device.," *Opt. Express*, vol. 13, no. 22, pp. 9003–13, Oct. 2005.

[27]   W. Song and D. Psaltis, "Pneumatically tunable optofluidic 2 × 2 switch for reconfigurable optical circuit.," *Lab Chip*, vol. 11, no. 14, pp. 2397–402, Jul. 2011.

[28]   J. Heikenfeld and A. Steckl, "Flat Electrowetting Optics," *IEEE LEOS Newsl.*, no. August, 2006.

[29]   H. Ren, H. Xianyu, S. Xu, and S.-T. Wu, "Adaptive dielectric liquid lens.," *Opt. Express*, vol. 16, no. 19, pp. 14954–60, Sep. 2008.

[30]   H. Ren, S. Xu, D. Ren, and S.-T. Wu, "Novel optical switch with a reconfigurable dielectric liquid droplet.," *Opt. Express*, vol. 19, no. 3, pp. 1985–90, Jan. 2011.

[31]   L. Li, Q.-H. Wang, C. Liu, and M.-H. Wang, "Adaptive liquid iris for optical switch," *Opt. Eng.*, vol. 53, no. 4, p. 047105, Apr. 2014.

[32]   M.-H. Wang, Q.-H. Wang, and C. Liu, "1×2 Optical Switch Based on Electrowetting," *Opt. Eng.*, vol. 53, no. 5, p. 055103, May 2014.

[33]   C. U. Murade, J. M. Oh, D. van den Ende, and F. Mugele, "Electrowetting driven optical switch and tunable aperture.," *Opt. Express*, vol. 19, no. 16, pp. 15525–31, Aug. 2011.

[34]   J. Heikenfeld and a. J. Steckl, "High-transmission electrowetting light valves," *Appl. Phys. Lett.*, vol. 86, no. 15, p. 151121, 2005.

[35]   J. L. Jackel, "Electrowetting optical switch," *Appl. Phys. Lett.*, vol. 40, no. 1, p. 4, 1982.

[36]   A. Groisman, S. Zamek, K. Campbell, L. Pang, U. Levy, and Y. Fainman, "Optofluidic 1x4 switch.," *Opt. Express*, vol. 16, no. 18, pp. 13499–508, Sep. 2008.

[37]   Q.-F. Dai, H.-D. Deng, W.-R. Zhao, J. Liu, L.-J. Wu, S. Lan, and A. V. Gopal, "All-optical switching mediated by magnetic nanoparticles.," *Opt. Lett.*, vol. 35, no. 2, pp. 97–9, Jan. 2010.

[38]   C. Hong, "Optical switch devices using the magnetic fluid thin films," *J. Magn. Magn. Mater.*, vol. 201, no. May 1998, pp. 178–181, 1999.

[39]   Y. Gu, G. Valentino, and E. Mongeau, "Ferrofluid-based reconfigurable optofluidic switches for integrated sensing and digital data storage," *Appl. Opt.*, vol. 53, no. 4, pp. 537–543, 2014.

[40]   H. E. Horng, C. S. Chen, K. L. Fang, S. Y. Yang, J. J. Chieh, C.-Y. Hong, and H. C. Yang, "Tunable optical switch using magnetic fluids," *Appl. Phys. Lett.*, vol. 85, no. 23, p. 5592, 2004.

[41]   H. Ren and S. Wu, "Optical switch using a deformable liquid droplet," *Opt. Lett.*, vol. 35, no. 22, pp. 3826–3828, 2010.

[42]   B.-T. Liao, H.-H. Shen, H.-H. Liao, and Y.-J. Yang, "A bi-stable 2x2 optical switch monolithically integrated with variable optical attenuators.," *Opt. Express*, vol. 17, no. 22, pp. 19919–25, Oct. 2009.

[43]   Y. Hongbin, Z. Guangya, C. F. Siong, and L. Feiwen, "A variable optical attenuator based on optofluidic technology," *J. Micromechanics Microengineering*, vol. 18, no. 11, p. 115016, Nov. 2008.

[44]   J. A. Yeh, "Development and evolution of MOEMS technology in variable optical attenuators," *J. Micro/Nanolithography, MEMS, MOEMS*, vol. 7, no. 2, p. 021003, Apr. 2008.

[45]   P. Müller, A. Kloss, P. Liebetraut, W. Mönch, and H. Zappe, "A fully integrated optofluidic attenuator," *J. Micromechanics Microengineering*, vol. 21, no. 12, p. 125027, Dec. 2011.

[46]   S. Xu, H. Ren, J. Sun, and S.-T. Wu, "Polarization independent VOA based on dielectrically stretched liquid crystal droplet," *Opt. Express*, vol. 20, no. 15, p. 17059, Jul. 2012.

[47]   J. Crisp, "Introduction to fiber optics," in *Introduction to fiber optics*, 2nd ed., Newnes, 2001, pp. 51–53.

[48]   a. Benner, H. M. Presby, and N. Amitay, "Low-reflectivity in-line variable attenuator utilizing optical fiber tapers," *J. Light. Technol.*, vol. 8, no. 1, pp. 7–10, 1990.

[49]   J. Dziuban, *Technologia i zastosowanie mikromechanicznych struktur krzemowych i krzemowo-szklanych w technice mikrosystemów*, 2nd ed. Oficyna Wydawnicza Politechniki Wrocławskiej, 2004, pp. 13–22,.

[50]   H. Toshiyoshi, H. Fujita, and T. Ueda, "A piezoelectrically operated optical chopper by quartz micromachining," *J. Microelectromechanical Syst.*, vol. 4, no. 1, pp. 3–9, Mar. 1995.

[51]   D. Uttamchandani, L. Li, and J. Zawadzka, "Characterisation of a nanostepper driven optical shutter for application in free-space microoptics," *IEE Proc. - Sci. Meas. Technol.*, vol. 151, no. 2, pp. 61–66, Mar. 2004.

[52]   R. R. a Syms, H. Zou, J. Stagg, and H. Veladi, "Sliding-blade MEMS iris and variable optical attenuator," *J. Micromechanics Microengineering*, vol. 14, no. 12, pp. 1700–1710, Dec. 2004.

[53]   A. Unamuno and D. Uttamchandani, "MEMS variable optical attenuator with vernier latching mechanism," *IEEE Photonics Technol. Lett.*, vol. 18, no. 1, pp. 88–90, Jan. 2006.

[54]   C. Lee, "Variable optical attenuator using planar light attenuation scheme based on rotational and translational misalignment," *Microsyst. Technol.*, vol. 13, no. 1, pp. 41–48, Oct. 2006.

[55]   K. H. Koh, Y. Qian, and C. Lee, "Design and characterization of a 3D MEMS VOA driven by hybrid electromagnetic and electrothermal actuation mechanisms," *J. Micromechanics Microengineering*, vol. 22, no. 10, p. 105031, Oct. 2012.

[56]   L. Li and D. Uttamchandani, "Design and evaluation of a MEMS optical chopper for fibre optic applications," *Sci. Meas. …*, vol. 151, pp. 77–84, 2004.

[57]   H. Cai, X. Zhang, C. Lu, A. Q. Liu, and E. H. Khoo, "Linear MEMS variable optical attenuator using reflective elliptical mirror," *IEEE Photonics Technol. Lett.*, vol. 17, no. 2, pp. 402–404, Feb. 2005.

[58]   A. Unamuno, R. Blue, and D. Uttamchandani, "Modeling and Characterization of a Vernier Latching MEMS Variable Optical Attenuator," *J. Microelectromechanical Syst.*, vol. 22, no. 5, pp. 1229–1241, Oct. 2013.

[59]   M. I. Lapsley, S.-C. S. Lin, X. Mao, and T. J. Huang, "An in-plane, variable optical attenuator using a fluid-based tunable reflective interface," *Appl. Phys. Lett.*, vol. 95, no. 8, p. 083507, 2009.

[60]   S. A. Reza and N. a. Riza, "A liquid lens-based broadband variable fiber optical attenuator," *Opt. Commun.*, vol. 282, no. 7, pp. 1298–1303, Apr. 2009.

[61]   P. Müller, A. Kloss, P. Liebetraut, W. Mönch, and H. Zappe, "A fully integrated optofluidic attenuator," *J. Micromechanics Microengineering*, vol. 21, no. 12, p. 125027, Dec. 2011.

[62]   Y. Hongbin, Z. Guangya, C. F. Siong, and L. Feiwen, "A variable optical attenuator based on optofluidic technology," *J. Micromechanics Microengineering*, vol. 18, no. 11, p. 115016, Nov. 2008.

[63]   R. Ranjini, A. K. Adiyodi, M. V. Matham, and N. Nam-Trung, "Optofluidic variable optical attenuator," in *2010 Photonics Global Conference*, 2010, pp. 1–3.

[64]   L. Zhu, Y. Huang, and A. Yariv, "Integrated microfluidic variable optical attenuator.," *Opt. Express*, vol. 13, no. 24, pp. 9916–21, Nov. 2005.

[65]   T. Erdogan, "Fiber grating spectra," *J. Light. Technol.*, vol. 15, no. 8, pp. 1277–1294, 1997.

[66]   J. Hsieh, P. Mach, F. Cattaneo, S. Yang, T. Krupenkine, K. Baldwin, and J. a. Rogers, "Tunable microfluidic optical-fiber devices based on electrowetting pumps and plastic microchannels," *IEEE Photonics Technol. Lett.*, vol. 15, no. 1, pp. 81–83, Jan. 2003.

[67]   B. R. Acharya, T. Krupenkin, S. Ramachandran, Z. Wang, C. C. Huang, and J. a. Rogers, "Tunable optical fiber devices based on broadband long-period gratings and pumped microfluidics," *Appl. Phys. Lett.*, vol. 83, no. 24, p. 4912, 2003.

[68]   F. Cattaneo, K. Baldwin, T. Krupenkine, S. Ramachandran, and J. a. Rogers, "Digitally Tunable Microfluidic Optical Fiber Devices," *J. Microelectromechanical Syst.*, vol. 12, no. 6, pp. 907–912, Dec. 2003.

[69]   P. Mach, M. Dolinski, K. W. Baldwin, J. a. Rogers, C. Kerbage, R. S. Windeler, and B. J. Eggleton, "Tunable microfluidic optical fiber," *Appl. Phys. Lett.*, vol. 80, no. 23, p. 4294, 2002.

[70]   S. Mathews, "Experimental demonstration of an all-fiber variable optical attenuator based on liquid crystal infiltrated photonic crystal fiber," *Microw. Opt. …*, vol. 53, no. 3, pp. 539–543, 2011.

[71]   K.-T. Kim, J.-H. Kang, S. HwangBo, and K.-G. Im, "In-line Variable Optical Attenuator Based on the Bending of the Tapered Single Mode Fiber," *J. Opt. Soc. Korea*, vol. 13, no. 3, pp. 349–353, Sep. 2009.

[72]   S. Nicholls, "Automatic manufacture of polished single-mode-fibre directional coupler," *Electron. Lett.*, vol. 21, no. 19, p. 825, 1985.

[73]   H. K. K. Kwang Taek Kim, "In-line variable attenuator based on the evanescent wave coupling between a side-polished single-mode fiber and an index matched dielectric plate," *J. Opt. Soc. Korea*, vol. 8, no. 1, pp. 17–20, 2004.

[74]   C. Hussey and J. Minelly, "Optical fibre polishing with a motor-driven polishing wheel," *Electron. Lett.*, vol. 24, no. 13, p. 805, 1988.

[75]   C. Gu, Y. Xu, Y. Liu, J.-J. Pan, F. Zhou, L. Dong, and H. He, "Fiber Based Devices for DWDM Optical Communication Systems," in *Proc. of SPIE Vol. 5642*, 2005, vol. 5642, no. 831, pp. 6–18.

[76]   "Optical Fiber Communications - wavelength bands." [Online]. Available: http://www.rp-photonics.com/optical_fiber_communications.html. [Accessed: 24-Sep-2015].

Chapter 2

Electrowetting on dielectric platform

2.1 Electrowetting on dielectric theory

Electrowetting on dielectric (EWOD) is a phenomenon that allows manipulation of a liquid droplet on a surface using the application of electric fields. In the static condition, EWOD can be used to change the contact angle of a liquid-solid interface [1] (Fig. 2.1), whilst using an array of electrodes EWOD can be used to transport, dispense, merge or split droplets on a surface. Typically, an electrically conductive droplet is placed on a hydrophobic insulated surface (to ensure that the droplet keeps a round shape on the surface) that has electrodes underneath (Fig. 2.1). An electric field applied between a bottom plate and a wire immersed into the droplet initiates the change of the droplet contact angle and increases the wettability of the surface[2].

2.1.1 Static condition of electrowetting on dielectric

Electrowetting on dielectric phenomena can be divided into those happening in either static condition (i.e. droplet remains in the same position) or dynamic condition (i.e. droplet translates between different electrodes). In the static condition, the steady state shape of a droplet is obtained when the surface tension forces are balanced by the electrowetting forces[3]. The change in contact angle is described by the Lippmann-Young equation[4]:

$$cos\theta = cos\theta_0 + \frac{C}{2\gamma_{LG}}V^2 \tag{2.1}$$

where C is the capacitance of the dielectric layer, V is the electric potential, γ_{LG} denotes liquid – gas interfacial tension, θ_0 is the zero-voltage contact angle (defined as the angle between

the droplet interface and the flat microelectrode surface) and θ is the contact angle when a voltage is applied to the droplet.
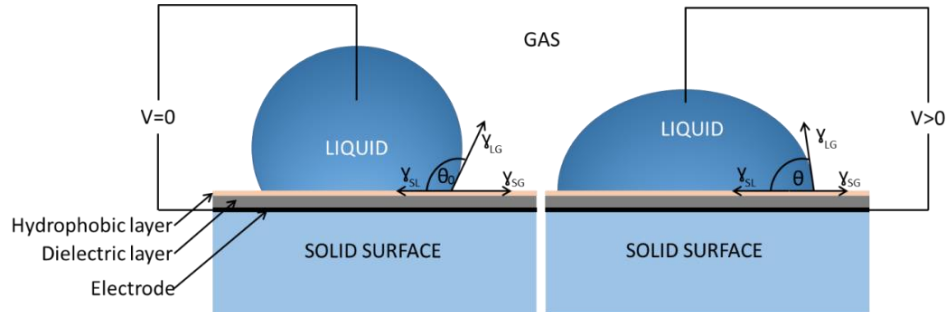
Fig. 2.1 Change in droplet contact angle due to applied electric potential between droplet and electrode

The Lippmann classic model describes electrowetting when an electric field is applied between a droplet and an electrode resulting in an electric double layer building up on the interface between the liquid and solid surface. This causes the charges of opposite polarity being repelled from the interface. When this phenomenon occurs the liquid solid interfacial energy decreases causing the droplet contact angle to change and at the same time the surface to becomes more hydrophilic[2]. Hydrophobicity is a property of a material that determines the wetting extent of water on the surface of a material. For a hydrophobic material a droplet of water forms a contact angle of ≥90° when is in contact with the surface[5].

In EWOD the thickness of the dielectric layer is larger than the size of the electric double layer and therefore the stored dielectric electrostatic energy is the source of the liquid solid interfacial energy decrement[2].

In electrowetting, in static condition a droplet tries to retain a spherical shape. The Bond number is a dimensionless number that implies that a droplet of known size located on a surface has a spherical shape. The number expresses the balance between the gravitational force and surface tension forces, so that a droplet remains spherical and does not easily spread on a surface. The Bond number can be calculated from[4]:

$$B_o = \frac{\rho g R_d^2}{\gamma_{LG}} \tag{2.2}$$

where R_d is a droplet radius, g is acceleration due to gravity, ρ is droplet density.

It is noted that with increasing droplet size, a droplet on a horizontal surface will lose its spherical shape, becoming a flattened structure as a consequence of the increasing effect due to gravity. Therefore, it is important to choose the right size of droplet to maintain the spherical shape on a horizontal surface. To demonstrate that the droplet has the spherical shape, the Bond number is typically accepted to be less than 1.

When an electric field is applied to the droplet, the droplet changes contact angle. In the perfect condition, the droplet is placed on a perfect surface without any defects. However perfect conditions are difficult to achieve and the surface where the droplet is placed can have defects or roughness (for example the droplet can experience adherence to the surface due to the microparticles located on the surface). Such imperfections cause emergence of droplet contact angle hysteresis where the contact angle is not fully reversible. When an electric field is no longer applied between the droplet and electrode, the droplet returns to the first state (spherical shape) but the contact angle is not the same as before[4].

2.1.1.1 DC and AC electrowetting

An AC voltage is used more often than DC voltage for electrowetting experiments because of the following advantages:

- The contact angle hysteresis which exists in DC electrowetting is reduced because the pinning effect is overcome[2]. In other words, during electrowetting, the droplet contact line (see Fig. 2.4) is de-pinned from the surface when the balance of forces is disturbed during the AC oscillation cycle[6].
- During AC electrowetting it is less likely that the droplet contact angle will saturate. Contact angle saturation appears less for smaller contact angles and a higher voltage for AC than for DC electrowetting[2].

When AC voltage is applied to a droplet, the shape and the contact angle of a droplet follows the change of AC electric fields[7]. It can be assumed that a droplet is a perfect conductor when the AC frequency does not exceed the critical frequency (typically of 10-100 kHz)[2]. In the real world, a droplet does not behave like a perfect conductor when the frequency of the applied voltage exceeds the critical value ω_c. When the frequency is higher than ω_c a droplet

behaves like a dielectric[7] (the forces that act on the liquid droplet are the dielectric body forces) which leads to the breakdown of electrowetting[2]. When the frequency is higher than the critical frequency the dissolved ions in the liquid droplet cannot follow the applied electric field and screen the electric filed from the inside of the liquid droplet. The equivalent electric circuit can describe the AC electrowetting. In that model, the resistor and capacitor can represent the droplet and another capacitor represents the dielectric layer (Fig. 2.2). In that model, the double layer is not taken into account.
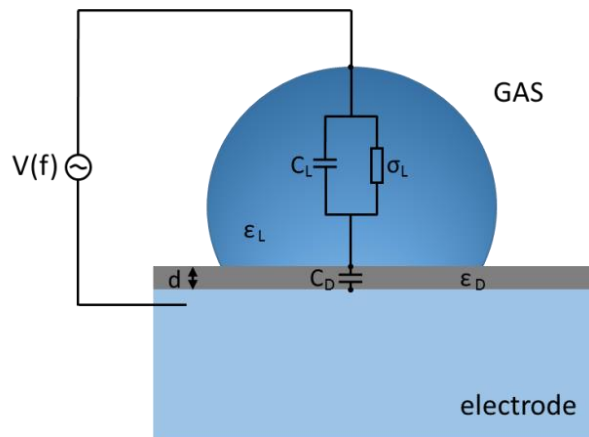
Fig. 2.2 Representation of the equivalent electric circuit for AC electrowetting

This critical value ω_C can be calculated from the equation[2]:

$$\omega_C = \frac{\sigma_D + \sigma_L k}{\varepsilon_0(\varepsilon_D + \varepsilon_L k)} \tag{2.3}$$

where σ_L, σ_D are liquid and dielectric conductivity, ε_D, ε_L are liquid and dielectric permittivity, k ~ d_D/R_d is the ratio of the dielectric layer thickness and droplet radius.
Both conductivity of the liquid and frequency of the applied voltage affect the intensity of the electric field created inside the droplet[8] .

To initiate the movement of the contact line, the electrostatic force needs to exceed the pinning force. The balance of those two forces can be expressed by the minimum voltage. The minimum voltage can be expressed as[4]:

$$V_{min} = 2\sqrt{\frac{\gamma_{LG}\alpha sin\theta_0}{C}}$$ (2.4)

where α is value of angle hysteresis (between the non-actuated and actuated angle), C is capacitance of the hydrophobic and dielectric layer separating the bottom electrode from the liquid.

2.1.1.2 Contact angle saturation

According to the Young-Lippmann Equation 2.1, the droplet contact angle changes with voltage. As voltage increases, the contact angle decreases. However, there is a threshold level and when the voltage exceeds that level, the contact angle will saturate. Therefore, the saturation voltage is the upper limit that can be used to move a droplet. As described above, using AC electrowetting is a method that can delay the contact angle saturation. Depending upon the system, saturation of the contact angle typically varies from 30° to 80° [9]–[12]. There are many studies concerning contact angle saturation for example[2]:

- Zero interfacial tension – the change of contact angle can be described as a reduction of the liquid/solid interfacial tension, therefore to retain the thermodynamic stability the interfacial tension should not decrease below zero. However, when the liquid/solid interfacial tension reaches zero value saturation of the contact angle occurs.

- Dielectric breakdown – when voltage is applied between a droplet and an electrode, the electric field can break the dielectric due to its strength. The charges that are transferred to the dielectric layer reduce the electrostatic input and cause contact angle saturation.

- Contact line instability – when voltage reaches the saturation voltage, the contact line becomes instable and the liquid droplet extrudes small satellite droplets due to an increment of Maxwell forces that become larger than the capillary forces. The contact line instability can be identified as the reason for contact angle saturation.

There are a few other studies concerning contact angle saturation (for example gas ionization or insulating fluid charge or minimization of the electrostatic energy etc.). However, they require more evidence to confirm if they strongly contribute to contact angle saturation.

The maximum electrowetting effect occurs due to saturation of the droplet contact angle. The maximum voltage that can be applied to the system so that the electrowetting effect will still occur can be calculated by[4]:

$$V_{max} = \sqrt{\frac{2(\gamma_{SG} - \gamma_{LG}cos\theta_0)}{C}} \qquad (2.5)$$

where γ_{SG} is solid – gas interfacial tension, C is capacitance of the hydrophobic and dielectric layer separating the bottom electrode from the liquid, θ_0 is the non-actuated contact angle.

From the Equation 2.5 above it can be seen that the maximum voltage depends on the structure of the device through the total capacitance of the platform, which is based on the thickness of the dielectric layer and its surface tension. It should be noted that the properties of the liquid (interfacial tension between the liquid and gas) also affect the maximum voltage.

2.1.2 Dynamic condition of electrowetting on dielectric

The dynamic condition of electrowetting concerns the droplet transient behaviour under the effect of a voltage input that induces motion of a droplet across electrodes. This phenomenon strongly depends on the dynamic change of contact angle through a force balance at the contact line[3]. In dynamic condition not only the contact angle change is of interest but also the movement of the entire droplet where the translation of droplet centre of the mass is happening[7].

In order to move a droplet from one electrode to the next, across an electrode array, the droplet needs to fulfil the static spherical shape condition (B_o<1) and then fulfil condition that require balance between the electrowetting inertial forces and surface tension forces. These requirements[4] are achieved when the Weber number is less than 1.1 so that the

droplet does not breakup and the electrowetting number is more than 1. Under these conditions, the droplet motion can initiated. The Weber number is described by the ratio between inertial and surface tension forces[4]:

$$We = \frac{\rho v^2 l}{\gamma_{LG}}$$

(2.6)

where ρ is the density, *v* is the velocity of motion, *l* is the drop contact radius.

The electrowetting number is expressed by the ratio between the electric and surface tension forces[4]:

$$\eta_e = \frac{CV^2}{2\gamma_{LG}}$$

(2.7)

where *C* is the capacitance per unit area of the dielectric layer (F/m^2).

2.1.2.1 Droplet movement

The driving force created by the interfacial tension gradient between the droplet and an insulator surface initiates droplet transport. Interfacial tension between the droplet and the insulator is modified by the charges created on the insulator surface when an electrical potential is applied between the droplet and an electrode. A change in the droplet interfacial tension affects the contact angle of the droplet[13].

The EWOD actuation is a multi-stage process (Fig. 2.3) that involves the following steps to perform droplet movement under an electric field[14]:

- An electric field is formed during reorientation and/or migration of electric charges in response to the applied voltage
- The droplet elongates in the direction of motion before the contact line moves
- The entire droplet moves to a new position.
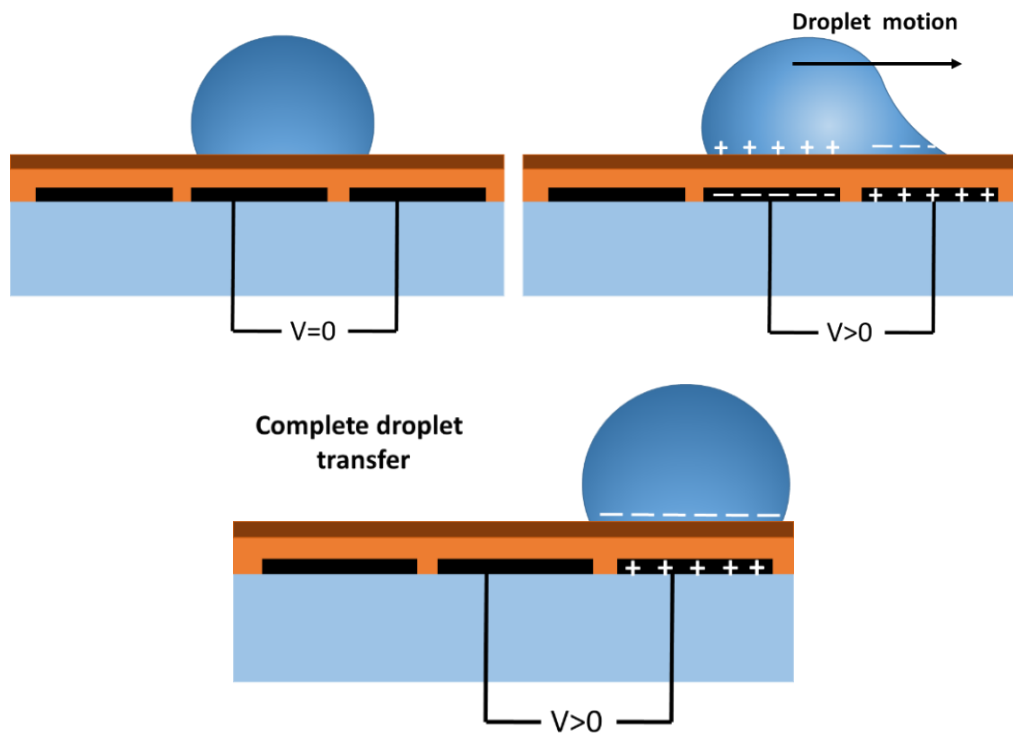
Fig. 2.3 Droplet's multi-stage droplet transport process across electrodes array

A gradient in the interfacial tension is formed between the droplet and the insulator surface under the electric field at the point of contact between the liquid-air-insulator. The interfacial tension is modified by the charges formed on the insulator surface when the electric field is applied between the droplet and electrodes. The interfacial tension gradient produces the driving force for droplet transport which leads to the net force of the wetting[13]. Under the wetting force a droplet moves between a non-actuated electrode (ground electrode) and an actuated electrode (active electrode). After that motion the droplet adapt new contact angle and become stationary again. Above the actuated electrode is located the three phase contact line on which the electrowetting line force acts. The three phase contact line describes the place where three phases meet together: the solid surface (S), the liquid droplet (L) and the ambient phase (vapour) (G)[7] (Fig. 2.4).
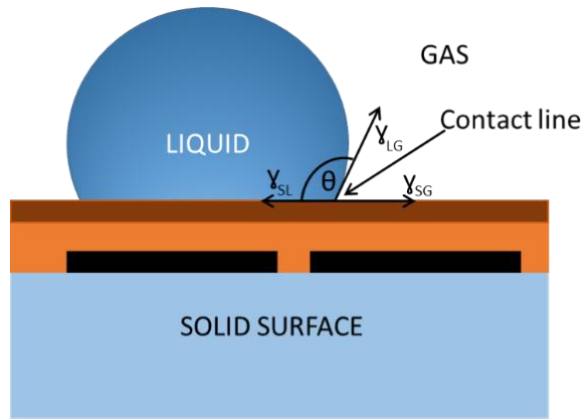
Fig. 2.4 Force balance at the three phase contact line located between liquid droplet and EWOD platform

The capillary force emergences on the three phase contact line.

$$f_{cap} = \gamma_{LG} cos\theta_0 \qquad (2.8)$$

where θ is the droplet contact angle related to interfacial tension.

The capillary line forces represent the part of the three phase contact line, which is positioned under the non-actuated electrode (Fig. 2.5). The insulation surface is covered with a hydrophobic material so that the capillary forces are facing the same direction as the electrowetting forces. If the surface were perfect the droplet would move at the instant when the electric field was applied to the next electrode, but because the surface is not ideal there is the minimum voltage that is required to cause a droplet to move[4]. Electrowetting on dielectric force:

$$f_{EWOD} = \frac{C}{2}V^2 = \gamma_{LG}(cos\theta - cos\theta_0) \qquad (2.9)$$

where C is capacitance of the hydrophobic and dielectric layer separating the bottom electrode from the liquid., V is electric potential, γ_{LG} is liquid – gas interfacial tension, θ is contact angle related to interfacial tension.
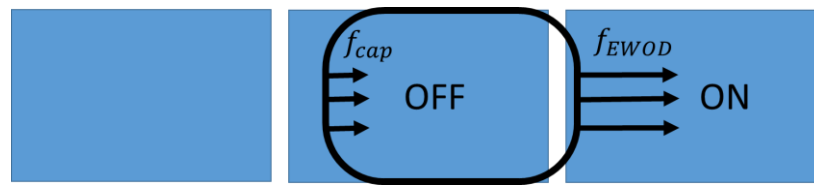
Fig. 2.5 Electrowetting on dielectric forces during droplet translation between two neighbouring electrodes

The two forces attempt to balance each other at the liquid-air-solid phases contact region. When the forces are balanced the contact between the three phases is minimized. Therefore, the minimization of the contact between the phases is due to balance of the forces between the molecules inside the liquid. However, the force between the liquid molecules and the gas molecules is not balanced anymore and the liquid molecules on the liquid surface are pulled towards the liquid interior. The force acting between the liquid molecules is larger than the force between the liquid and gas molecules which results in keeping the spherical shape of the droplet (smaller surface area is leading to the smaller energy)[1].

Even small changes of the electrode shape can change the voltage distribution along the droplet transport path, which translates into droplet deformation or movement parameters. The square electrode is a geometry (Fig. 2.5) that is commonly used in electrowetting applications because of its uncomplicated fabrication process. In other reports, different shapes of electrodes are presented (for example "zig-zag" shapes or "crescent" shapes)[15] that enable the droplet overlap with the next electrode (Fig. 2.6). Such configurations allows the use of a larger droplet for easier position change in the array of electrodes[15].

a)   b)

Fig. 2.6 Schematic of the electrodes geometries a) "zig-zag", b) "crescent"

There are a few considerations that should be followed to optimize the droplet translation on the electrode array[16]:

- Droplets should be always in contact with a ground electrode, which will results in an electric field increment on the front side of a droplet. This increment of the electric field translates into charge accumulation and finally the increment of the electrowetting force.

- A droplet should overlap onto the next electrode so the width of each electrode should be smaller than the droplet diameter. When a droplet overlaps onto the next electrode, the arising force is generated on the larger part of the triplet line.

- The electrodes should be shaped such that a droplet will increase the contact line with the actuated electrode. This will result in an electrowetting force increment from the start of the droplet's motion.

When these rules are followed, the electrowetting force is maximised and droplet transport will be more effective.

If "zig-zag" shaped electrodes are considered (Fig. 2.7), the magnitude of the electrowetting force differs from the electrowetting force magnitude of the square electrodes considered above.
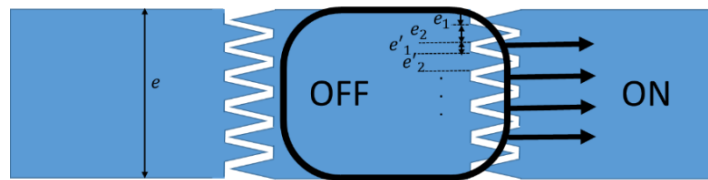
Fig. 2.7 Schematic of "zigzag" electrodes geometry with the description of the cross dimension of the zigzag spike

The magnitude of the electrowetting force, produced on a "zig-zag" shape electrode array, during the droplet motion depends on the width of the spike [4]:

$$F_{e,motion} = e\gamma_{LG}(cos\theta - cos\theta_0) \qquad (2.10)$$

where e is the width of an electrode.

To begin, the droplet is in contact with the next electrode only via the spikes of the zig-zag pattern and the electrowetting force becomes:

$$F_{e,start} = e_1\gamma_{LG}cos\theta + e_2\gamma_{LG}cos\theta_0 - e\gamma_{LG}cos\theta_0 \qquad (2.11)$$

The first part in the equation 2.11 is the pulling force applied on the liquid droplet by the active electrode and the second term is the force located on the non-active electrode.

$$e = e_1 + e_2 \qquad (2.12)$$

$$e_1 = e_1 + e_1' + \cdots \qquad (2.13)$$

$$e_2 = e_2 + e_2' + \cdots \qquad (2.14)$$

Substituting Eq. 2.12 into Eq. 2.11 gives:

$$F_{e,start} = e_1\gamma_{LG}(cos\theta - cos\theta_0) \qquad (2.15)$$

$$F_{e,start} = \frac{e_1}{e} F_{e,motion} \qquad (2.16)$$

where e_1 and e_2 are total cross dimension widths of a "zig-zag" spike, θ is the actuated contact angle, θ_0 is the non-actuated contact angle.

If e_1 is equal to 0 then the droplet does not overlap with the next electrode and there is no electrowetting force acting on it, therefore the droplet will not translate to the next electrode.

From the equations above it can be seen that the shape of electrodes influence the electrowetting force that acts upon the droplet. If the electrowetting force equations are compared it can be seen that there is an increment in force value for the zig-zag shaped electrodes and the size of the increment depends on the dimensions of the electrode's spikes.

The description above indicates that a droplet can only move between electrodes when there is an electrowetting force acting on it. When an electrowetting force acts on a droplet, the droplet moves from one position to the next with a defined velocity. In the beginning of the translation, the droplet accelerates and achieves a nearly constant velocity due to the small inertia forces. When the electrowetting forces are equal to the friction forces then velocity becomes constant[4]. The strength of the electrowetting force affects the

velocity value. However, the velocity also depends on the parameters of the system such as the surface tension between droplet and platform, contact angle of the droplet, viscosity of the fluid and internal fluid motion.

Constant velocity of a droplet is given by:

$$v = \frac{2h}{5\pi\mu l} CV^2$$

(2.17)

where μ is liquid viscosity, h is droplet height, l is contact radius, V is electric potential, C is capacitance of the hydrophobic and dielectric layer separating the bottom electrode from the liquid.

As a conclusion, the sections above have described the parameters having an impact on the strength of the electrowetting phenomenon (i.e. the materials used to fabricate the platform, the fabrication processes, type of liquids, the electrode patterns and the voltage magnitude). All of these factors strongly influence the performance of the EWOD system.

2.2 Design and validation of electrowetting on dielectric platform

The first step towards fabricating an electrowetting on dielectric platform (Fig. 2.8) to digitally move a liquid droplet across electrodes, was to design the shape of the electrodes. The platform would consist of aluminium microelectrodes, a dielectric layer and a hydrophobic layer, constructed on a glass substrate.
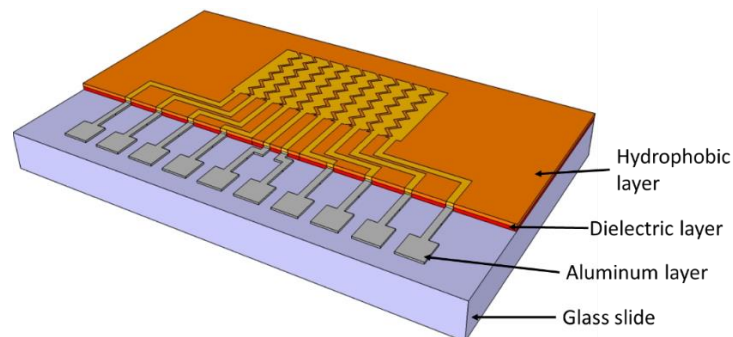

Fig. 2.8 Schematic of electrowetting on dielectric platform (not in scale)

The second step in designing the EWOD platform was choosing the right materials for fabrication. A glass substrate was patterned either with ITO (Indium Tin Oxide)[17] or with aluminium for creating the conductive surface.

ITO is a conductive material, which can be patterned onto the glass slide and form transparent electrodes[18]. The main disadvantage of using ITO electrodes is the difficulty in visualising where the electrodes are placed.

If transparency is not required, there are different materials that can be used to create electrodes (i.e. aluminium). Aluminium is a conductive material that can be easily evaporated onto any substrate[19]. Aluminium was chosen for the electrode material to construct the device.

Electrodes in EWOD devices were covered with a film of dielectric. As was described above, this dielectric is needed to prevent spontaneous charging of the system, which leads to current flow. A photoresist (AZ4562) was used to create the dielectric surface via photolithography. When transparency is not required to build the EWOD chip, both aluminium and AZ4562 resist (semi-transparent)[20] are good choices of material.

A hydrophobic layer is the last surface to be fabricated on top of the dielectric layer this allowing a water droplet to have a contact angle > 90 degrees and facilitate its movement on the surface.

One example of a hydrophobic material that can be used in industry is Teflon AF (Fig. 2.9). Teflon is characterized as a hydrophobic material with weak van der Waals forces and as a good electrical insulator[21]. Teflon AF is an amorphous fluoropolymer with high optical transparency.
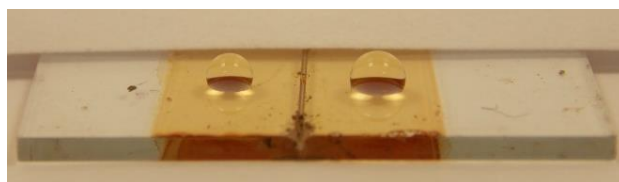

Fig. 2.9 Photograph of water droplet positioned on Teflon AF layer

Electrowetting on dielectric can be characterised by calculating different parameters. It was stated previously that a droplet changes its surface contact angle under the influence of an applied voltage (Equation 2.1).

Table. 2.1 Parameters of materials used to fabricate EWOD platform:

Dielectric thickness	1.5 µm
Dielectric permittivity (relative)	3
Teflon thickness (relative)	0.100 µm
Teflon permittivity	2.1
Teflon/gas surface tension	0.047 N/m

Table. 2.2 Parameters of liquid droplets[22]:

	Water	**Glycerine (water solution 93% wt.)**
Volume	2 µL	2 µL
Density	1000 kg/m^3	1243 kg/m^3
Viscosity	0.0894 kg/ms	0.367 kg/ms
Surface tension liquid/gas	0.07197 N/m	0.06463 N/m
Dielectric constant (relative)	80.4	45.24
Conductivity	5.5 µS	120 µS
Contact angle on Teflon	115°	111.43°

For a droplet to translate upon the EWOD platform, it must be spherical and have an appropriate Bond number[4]. For a 93% glycerine solution droplet of the chosen dimensions, the Bond number was calculated (using Eq. 2.2) to be 0.1154, which is much lower than the critical value of 1. For comparison, a water droplet has a Bond number of 0.08335. The difference in the Bond number for water and glycerine droplets is caused by the differences in density and surface tension; where the density of the glycerine solution is higher than the density of water and the surface tension of the glycerine is lower than water surface tension (Table 2.2).

Another condition, that implies a droplet will not break-up during movement across the electrode array, characterised by the Weber number, needs to be lower than 1 and the electrowetting number higher than 1. Both the Weber number (We ~ 0.3) and electrowetting number (η_e ~ 2) for a 93% glycerine solution droplet satisfy the required conditions.

2.2.1 Fabrication procedure of the platform

The electrowetting on dielectric platform consists of a linear pattern of zig-zag electrodes. The process used to fabricate EWOD platform is based on photolithography.

Device generation starts with designing the photolithography mask in Corel Draw software, which allows design templates, suitable for printing onto an acetate mask for photolithography, to be created.

Different shapes and spaces between the electrodes were designed including different electrode sizes, gap distances between the electrodes and the electrodes shape. The electrode size varied from 1 mm to 0.15 mm and electrodes gap from 0.1 to 0.05 mm (for the electrode size of 0.6 mm with 0.7 mm gap the e_1 is 0.5 mm and e_2 is 0.4 mm) (Fig. 2.10). Several different designs of the electrode masks were fabricated to provide multiple parameters to investigate in relation to the dependence on the size of a droplet and voltage needed to move the droplet.
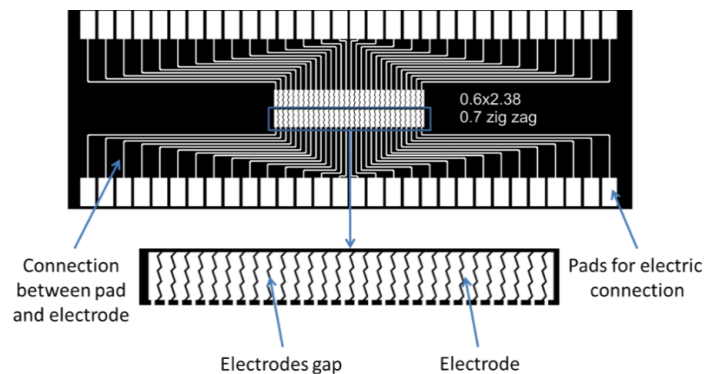

Fig. 2.10 Example of electrodes mask geometry designed in graphic program (Corel draw) that was used to fabricate EWOD platform

The acetate masks are high-resolution (<15 µm resolution[23]) and allow designed structures to include features in the micrometre range. These masks are used in a photolithography process (Fig. 2.14) to transfer the patterned shapes from the mask onto the resist surface. There are two types of resists: positive and negative (Fig. 2.11)[24]. In the following fabrication processes, positive resist was used in the manufacture of the EWOD devices.
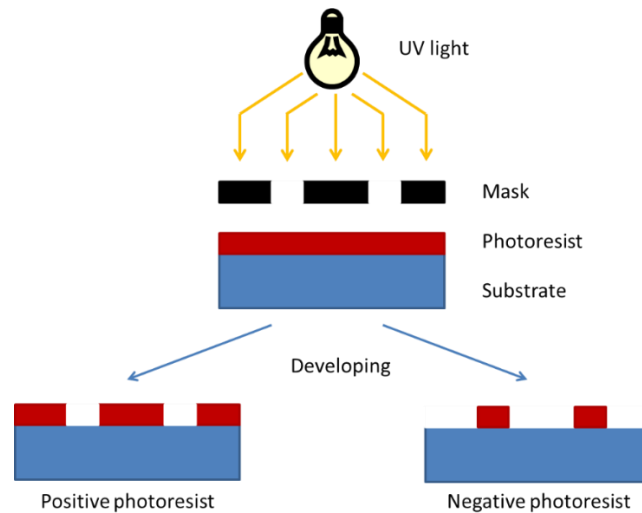
Fig. 2.11 Photolithography process describing transfer the patterned shapes from the mask onto the resist surface

Fabrication starts with preparation of a glass slide, which has dimensions 25.8 x 75.8 x 1.0 mm. Firstly, the slide is cleaned in acetone (Fisher Chemical) for 3 min, then 3 min in methanol (Fisher Chemical), and 3 min in isopropanol (Fisher Chemical). Then the glass slide is dried on a hotplate at 200°C for 15 min and allowed to cool. Subsequently, a Hexamethyldislazane primer (HMDS, Technic, France) is spun (4000 rpm, 5 sec.) on top of the glass. On the top of the HDMS layer, resist (AZ 4562, MicroChemicals GmbH) is spun (4000 rpm, 30 sec) (6 µm thick layer). This procedure covers the whole slide with resist and avoids leaving any corners exposed. The glass substrate was soft baked for 5 min on a hotplate at 100°C and then exposed to UV light via the designed photomask (JD Photo-Tools, UK) for 30 sec. Next, the glass slide was developed in AZ 400K developer (MicroChemicals GmbH) (DI water in ratio 1:2) for 10-15 min. Developing times depend on the thickness of the resist layer, with thicker layers taking longer to remove redundant areas of resist. After developing,

the glass slide required another cleaning step with DI (deionized) water and was blown dry with nitrogen.
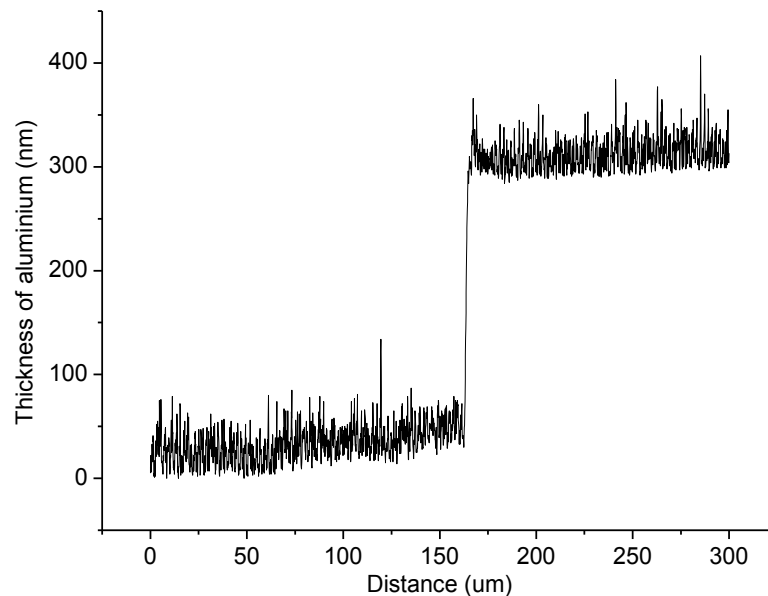
Fig. 2.12 Measured thickness of aluminium electrodes layer on top of the glass slide.

The next stage in device fabrication was evaporation of aluminium onto the prepared glass slide. Before evaporation of the metal, the glass slide was cleaned with oxygen plasma for 3 min at 100% power (Diener electronics Plasma-Surface-Technology, Pico). Evaporation took 2.5 h, and covered the glass slide with a 300 nm layer of aluminium (measured with KLA Tencor Alpha-Step IQ Surface Profiler) (Fig. 2.12).

Because the whole glass slide was covered with aluminium, the redundant areas of this material needed to be removed. To achieve this, the glass slide was washed with Acetone for 10 mins, obtaining lift-off of the undesired metal.

Next in the process was the creation of the dielectric layer. Again, the processed samples were cleaned in Acetone, Methanol and Isopropanol (3 min each). AZ 4562 resist diluted by PGMEA (Methoxy propyl acetate solvent, Microposit™ EC, Belgium) in a 5:2 ratio behaves as a dielectric and was spun at 5000 rpm to create 1.5 µm thick layer. As can be seen in Figure 2.13, the layer of resist is not starting with uniform surface but there is a large spike, which was created from resist accumulation at the edge of the layer. The resists on the rest of the glass slides covered with aluminium formed uniform surface without any other

accumulation spots. Using a diluted solution achieves a thinner layer of dielectric on the platform, which allows the use of lower switching voltages during operation of the final device.
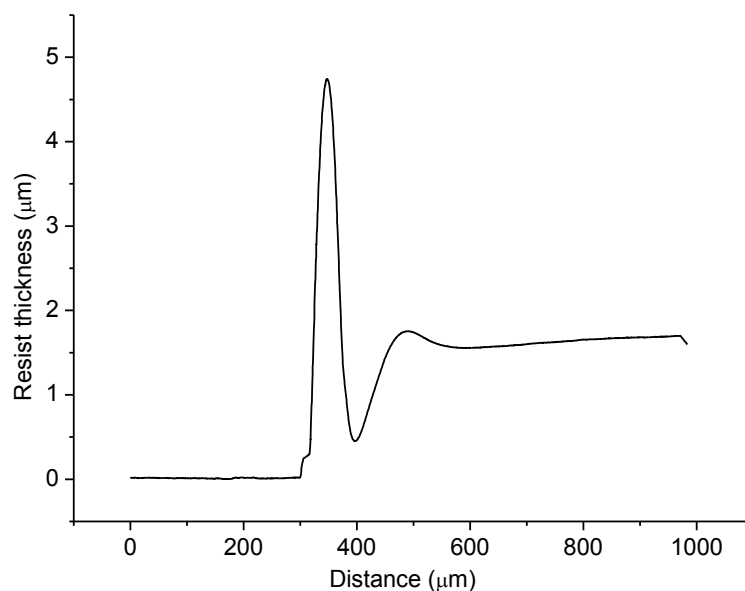
Fig. 2.13 Thickness of diluted AZ4562 resist in PGMEA (spinning velocity 5000 rpm)

Then, the sample was baked at 125°C for 25 min on a hotplate to harden the layer. The hydrophobic material (Teflon AF, DuPont, USA) was spun onto the surface and was baked to form a layer of hydrophobic material. To create a solution of Teflon AF that can be used to produce thin films, grains of Teflon AF were dissolved in perfluorinated solvent, FC-40 oil (Fluorinert, Sigma-Aldrich, Belgium). Depending on the type of Teflon AF, different concentrations of FC-40 is needed to dissolve the grains. For 3 % solution of Teflon AF 1600 and FC-40, 4 days of shaking was required. For 1 % solution of Teflon AF 2400 and FC-40, 7 days of shaking was required to achieve a solution that can be used in the coating procedure. Such prepared solutions can be spun on the surface and then baked. Different speeds of spinning translate to different thicknesses of Teflon film. To achieve a 1000 nm thick film, 1000 rpm spin coating followed by 10 minutes baking at 160°C are needed. For a 50 nm thick film, 2000 rpm and 10 min at 160°C are required[25].

Contact angles of water droplets that lie on the surfaces covered with Teflon AF are 105°, in the case of the 2400 type polymer, and 104°, in the case of the 1600 type

polymer[25]. These contact angles translate to low surface energies of 15.7 dynes/cm for the 2400 type and 15.6 dynes/cm in the case of the 1600 type Teflon coating[25].

Teflon AF is spun on the top of the sample with the speed of 1000 rpm for 60 s to achieve a 100 nm thick layer. Finally, the sample is baked at 240°C for 2 min and then in 160°C for 8 min to harden the Teflon layer. Figure 2.14 shows the simple methodology of device construction.

Glass slide

Formation of mask layer

Electrode mask photolithography

Aluminium evaporation

Removal of masking layer

Dielectric layer deposition

Hydrophobic layer deposition
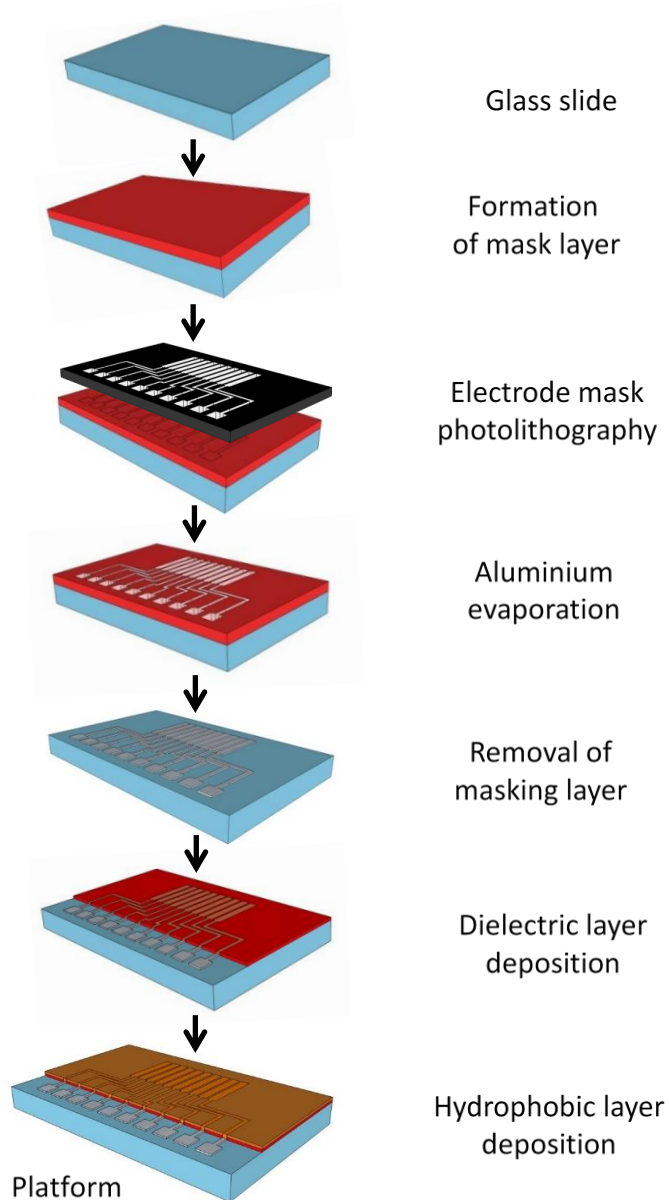
Platform

Fig. 2.14 Device fabrication process presenting each step of fabrication

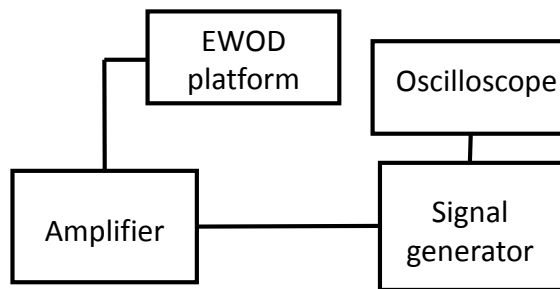## 2.3   Testing of the electrowetting platform

Fig. 2.15 Experimental setup for EWOD platform testing

Testing an electrowetting on dielectric platform required preparation of the device. On top of the electrodes was placed a droplet of specified volume (dispensed with a pipette). The width of the droplet needed to be larger than the width of the electrode, so that the droplet overlaps onto the next electrode and can be transported across electrodes.

Investigations included measurements of the voltage that was required to move a droplet, observations on how long a device worked before breaking down, how droplets moved, if it was possible to move a droplet forward and backward, and confirmation that the droplet did not split thus leaving satellite microdroplets.

A signal generator was used to generate a square signal from 0 to 10 V with a variety of frequencies. This signal was sent to the amplifier, which amplified the signal 20 times. It needs to be noted that too large frequency can decrease the efficiency of the electrowetting on dielectric effect[26]. It can be noted that different types of EWOD platform, depending on the structure and materials used to fabricate them, can operate with different frequencies starting with 20 Hz[27] via 1 kHz [28],[29] to 18 kHz[30],[31]. The lower frequency of operation was demonstrated with lower voltages around 30-40 V, while the 18 kHz device operation was used with high voltage 400-500 V.

The signal was monitored using an oscilloscope during the experiment and was sequentially applied to individual electrodes on the platform (Fig. 2.15). As the signal was applied, the droplet followed the higher potential when it moved from one electrode to another.

The electrowetting experiments also included comparison of a water droplet and a mix of glycerine and water (93% glycerine and 7% water) droplet behaviour on different electrode designs. Use of a glycerine droplet is related to the refractive index of the liquid, which will be important in improving the performance of the final device, which will have an optical fibre attached to it. Deeper explanation of the influence of the liquid refractive index on the properties of the fibre will be presented in Chapter 3.

The tested designs are:

a) 1 mm width electrodes with 0.1 mm gap between,

b) 0.6 mm width electrodes with 0.1 and 0.07 mm gap between,

c) 0.4 mm width electrodes with 0.1 mm and 0.07 mm gap between,

d) 0.3 mm width electrodes with 0.05 mm gap between,

e) 0.2 mm width electrodes with 0.05 mm gap between.

Based on the investigations, the gap between the electrodes was found to be a very important part in EWOD platform performance. If the gap is small enough, the droplet can easily and smoothly move to the next electrode. If the electrode width is bigger, the droplet needs to have greater volume. For example, for 1 mm width electrode with 0.1 mm gap the droplet volume needs to be 5 µL (~2 mm diameter), but for 0.6 mm wide electrodes with 0.07 mm gaps a droplet volume of 2 µL (~1.6 mm diameter) (Fig. 2.16) is required to enable movement.
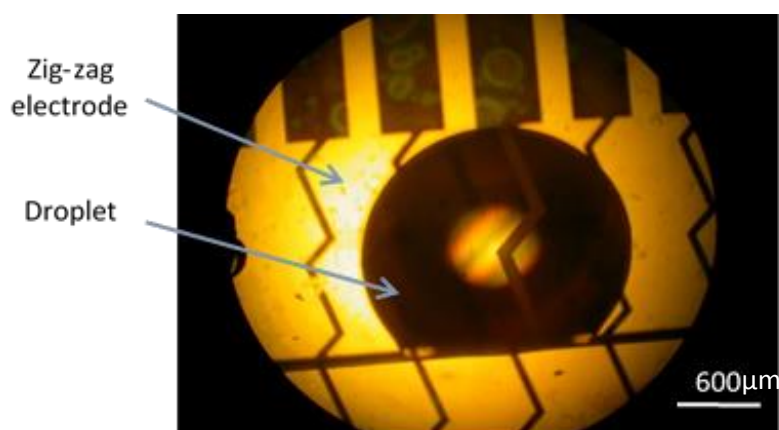

Fig. 2.16 Photography presenting droplet placed on the zig-zag electrodes

The shape of the electrodes influenced the performance of the EWOD platform, requiring that a droplet overlaps onto the next electrode to execute movement. Both square and zig-zag electrode types were tested to verify their efficiency in transferring the droplet. By design, a zig-zag shape increases the overlapping space and the movement of the droplet is carried out smoothly (without droplet pausing during movement or droplet leaving satellite small droplets).

Two tests were undertaken: the first test involved only an EWOD platform and a droplet of water or glycerine; the second test involved a droplet, an EWOD platform with a piece of fibre attached to it. This second test was used to investigate how the fibre influenced the droplet transport. During both tests, different levels of voltage and frequency were applied to the electrowetting on dielectric platform to find smooth droplet movement and no dielectric and droplet breakdowns. The voltage varied from 50 V to 200 V (square wave) and the frequency varied from 10 Hz to 20 kHz. Different voltages were required for different sizes of electrodes and droplet volumes. The best results were achieved with 0.6 mm wide zig-zag electrodes and a 2 µL glycerine droplet.

It was observed that there are differences in performance between water and a glycerine droplet. There were also differences in required voltage levels between an EWOD platform with fibre attached to it and an EWOD platform without fibre. It was noticeable that to move a droplet on the EWOD platform with fibre the required voltage was higher, particularly for the glycerine droplet. When an EWOD platform without fibre was tested, the required voltage to move a water droplet was 80 V and for glycerine was 120 V. 180 V was required to perform the movement of the glycerine droplet along the fibre. The water droplet did not need so high voltage to make a move on the electrodes; 100 V was enough to move a water droplet. From the testing phase, it was decided that 180 V was the optimal voltage to perform transfer of the droplet. When a glycerine droplet is subjected to 180 V at 1 kHz, it moves smoothly across the electrodes, and there is no visible vibration of the droplet. When the voltage and frequency is below 180 V and 1 kHz, the water droplet shakes and then jumps from one electrode to the next.

2.3.1 Measurements of droplet contact angle change

A crucial piece of knowledge to obtain is information about the contact angle of the droplet with the surface without an applied voltage. The contact angle was measured with "Kruss easy drop"[32] equipment. The Kruss equipment can measure the contact angle of a droplet placed on the hydrophobic surface and the surface tension of the liquids using drop methods. The device was equipped with a high zoom camera that enables taking pictures with high resolution, which increases the measurement accuracy. The Kruss device was interfaced to a computer with dedicated software that automatically analyses the picture of the droplet and calculates the contact angle. The contact angle was measured using the "drop shape analysis software". This uses an algorithm that measures the contact angle using an image of the sessile droplet at points of contact between the face of the droplet and the surface where the droplet is placed. Each droplet was placed on the platform, which was levelled, and lit by a light source. The high-resolution camera is located on the opposite side of the droplet to the light source and requires the strength of the light to be optimised so that the picture will not be blurred and the software can calculate the contact angle accurately.

Measurements were performed for water and glycerine droplets (93% glycerine in water solution) over the voltage range from 0 V to 180 V. Both droplets had volumes of 2 µL and were placed on the electrowetting on dielectric platform where the software analysed the contact angles. After the first picture (Table 2.3, 2.4 voltage: 0 V) a wire was inserted into the droplet from above and voltages were applied between the wire and the bottom electrodes of the EWOD platform. When the droplet shape changed under the voltage influence, a picture was taken again (for example Table 2.3, 2.4 voltage: 100 V) and the software used to calculate the new contact angle. The last stage of the measurements involves the measurements of the reverse contact angle, after switching off the voltage.

These measurements were carried out in air, so during the procedure some problems arose. It was noticed that water droplets of this size very quickly evaporate and it is difficult to accurately measure the contact angle of a droplet. However, water droplets are of less interest because the refractive index is less useful to the application so the measurements were focused on glycerine droplets. The glycerine droplet did not evaporate as quickly as

water droplet because of the low concentration of water. The standard deviation of the glycerine droplet contact angle varied from 0.44 to 4.77 (Fig. 2.17). This large variation may be due to the wire immersed into the droplet. Because the experiment needed to be completed quickly to minimise the influence of evaporation, the wire was immersed in each test in a different position of the droplet. This situation could enter uncertainty into the results due to the deformation of the droplet surface near to the wire causing the software to have difficulty with interpretation of the counter of the droplet that is base for the measurements. Another problem met during the measurements was that glycerine droplets left residue on the surface and caused the contact angle of the new droplet to differ from the previous droplet contact angle. The new glycerine droplet needed to be located the new place on the surface to prevent this occurring.

The results for both water and glycerine solution droplets are presented in Table 2.3 and Figure 2.17. It can be seen from the pictures that the shape of the droplet changes when voltage is applied and the droplet contact angle is decreasing as voltage increases. From the measurements, it can also be observed that the contact angle changed under the voltage influence from 111° (without voltage) to 76° (180 V) for the glycerine droplet and from 115° (without voltage) to 84.5° (180 V) for the water droplet. The reversibility of contact angle for glycerine droplets was 7.5° and for water droplets was 4.2°. Reversibility is defined here as the difference between the droplet contact angle before an applied voltage to it and the new droplet contact angle when the applied voltage to the droplet is removed and droplet reverts to its original geometry.

Table 2.3 Contact angle of glycerine and water droplets under voltage influence:

Glycerine droplet:

Voltage	Picture
0 V	

20 V	
60 V	
100 V	
140 V	
180 V	

Water droplet:

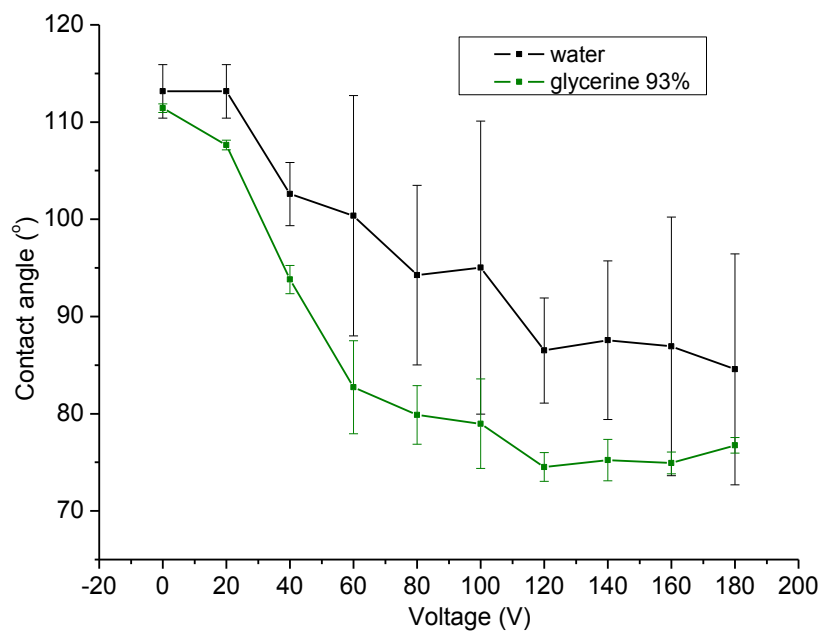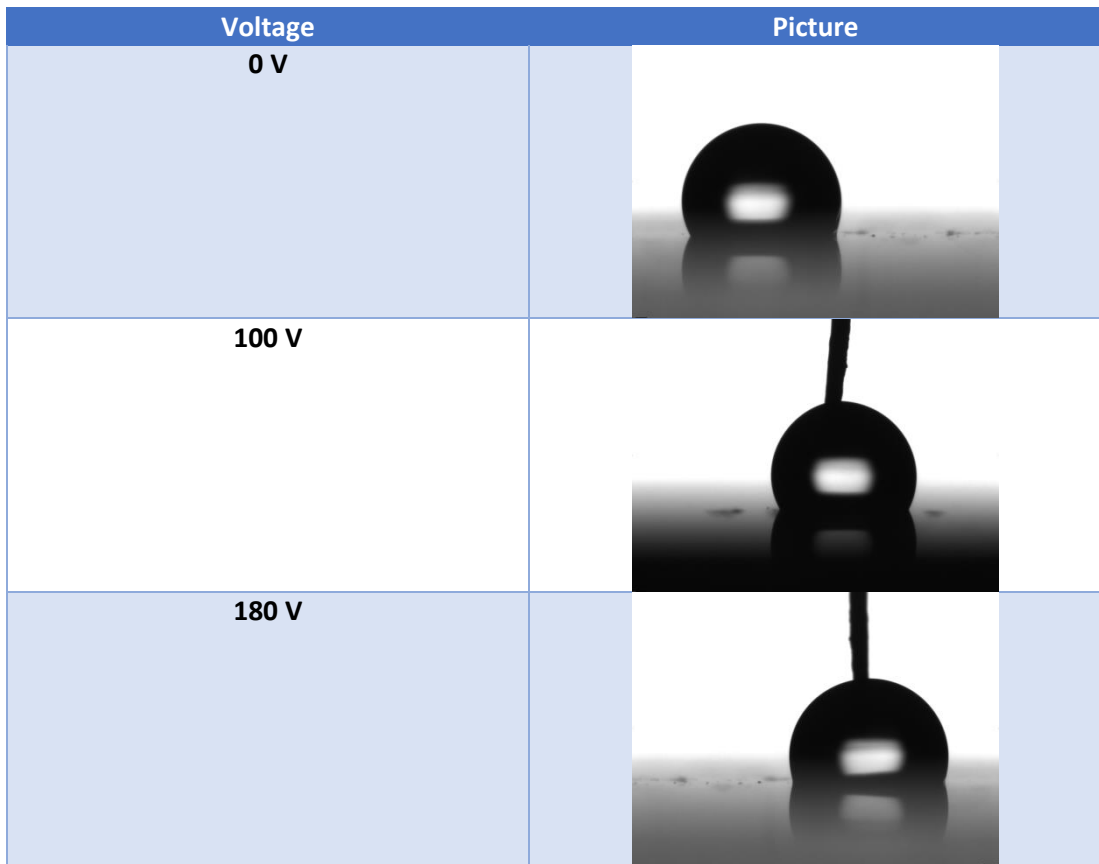| Voltage	Picture
0 V	
100 V	
180 V	
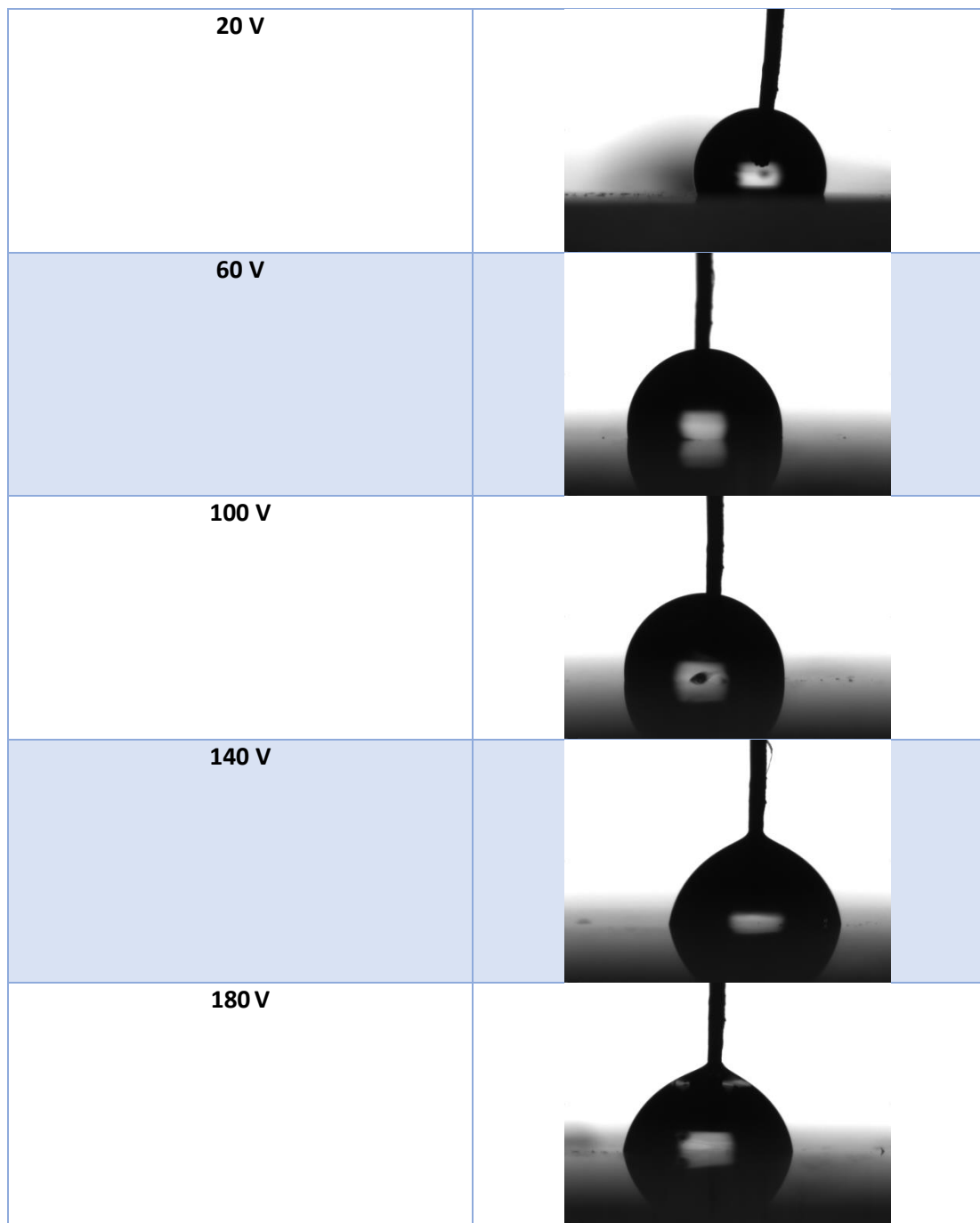
Fig. 2.17 Change of the contact angle of water and glycerine droplets under the influence of voltage

From Figure 2.17 it can be seen that the difference in contact angle between the glycerine droplet and water droplet is less than 15°. The largest change in contact angles, from 115° to 100° for water and from 111° to 82° for glycerine, occurs between 0 and 60 V. The rate of change of the contact angle decreases and the change in contact angle is less than 15° for both water, glycerine droplet over the remainder of the voltage range therefore illustrating that in the higher voltage regime saturation occurs, and the contact angle does not change with voltage. For the glycerine droplet, it can be noticed that the contact angle is not changing significantly when the voltage exceed 120 V.

2.4   Comparison of droplet behaviour with theory

Figure 2.18 presents the Lippmann-Young equation description of how contact angle should change in perfect conditions for the electrowetting on dielectric platform, using parameters from Table 2.1 and Table 2.2. It can be seen that the contact angle for a water droplet will change from 115° (0 V) to 4° (159 V) and the contact angle for a glycerine droplet will change from 111° (0 V) to 10° (147 V). For the voltages higher than 159 V and 147 V, the contact angle cannot be calculated. This is characteristic of a change from hydrophobic to hydrophilic features of the EWOD platform.
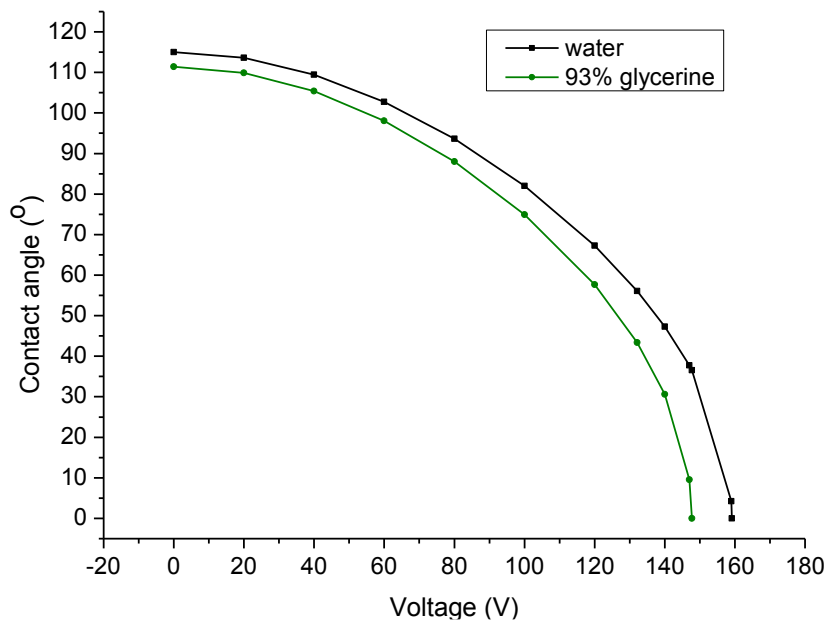
Fig. 2.18 Change of contact angle for water and glycerine droplet calculated from Lippmann-Young equation

This contact angle saturation phenomenon occurs when the voltage applied to the EWOD platform exceeds the device maximum voltage. It is possible to calculate the maximum voltage that identifies the threshold for saturation (Equation 2.5).

From Figure 2.19, it can be seen that the saturation of contact angle takes place when the applied voltage exceeds 132 V for the glycerine droplet and 138 V for the water droplet. The saturation contact angle for the glycerine droplet is 43° and for the water droplet saturation occurs at 49°. These values are significantly lower than those measured with the Kruss equipment, which was around 75° for the glycerine solution and 85° for the water droplet.
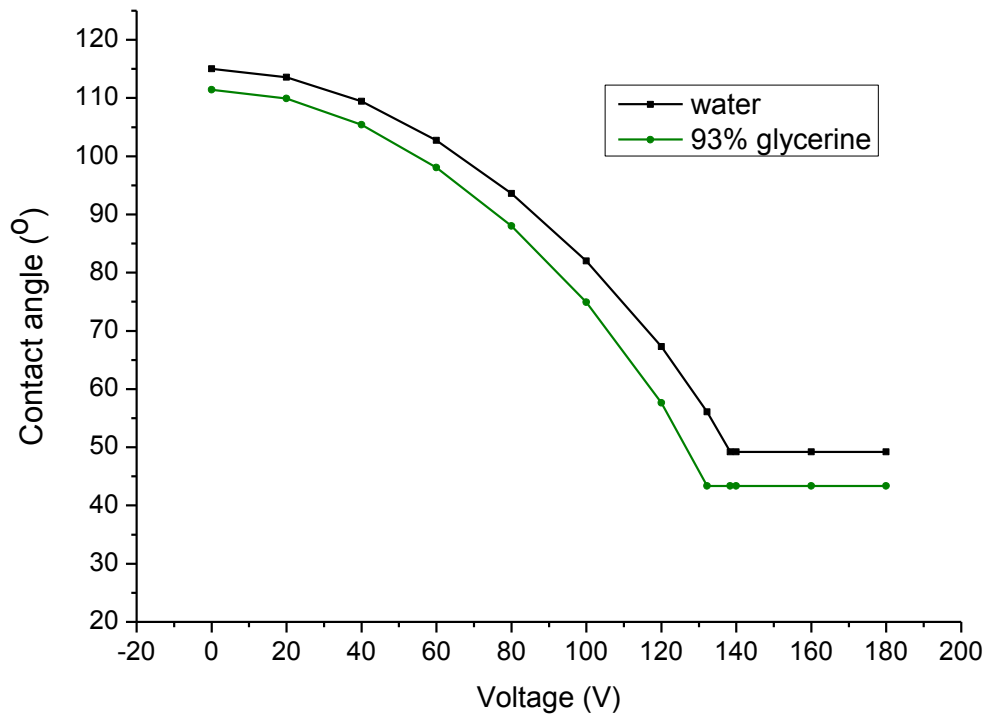
Fig. 2.19 Change of contact angle included contact angle saturation for water and glycerine droplet calculated from Lippmann-Young equation

In contrast, the measured saturation voltages are comparable to the calculated values. Measurement showed that for the glycerine droplet, the voltage when saturation takes place is 120 V and for the water droplet it was approximately 120 V, with the difference between calculation and measurement voltage values around 10 V. The possibility of the contact angle discrepancy is the inaccuracy in measuring the thickness of each platform layer.

These mismatches could arise in the fabrication process of the platform and can be linked to the conditions in the laboratory during fabrication, so that every platform may be different from each other.

An AC voltage was used with a square wave-shape and frequency chosen to be 1 kHz. It is known that when the applied voltage signal frequency exceeds a critical value ω_c (Equation 2.3) the droplet starts to behave as a dielectric instead of as a conductor[7]. It was calculated that the critical frequency for the water droplet was 7.76 kHz and for the 93% glycerine droplet 300 kHz. The used frequency of 1 kHz is well below the critical value so both droplets behave as conductors during the experiment. The difference in the critical frequency between water and glycerine droplets is determined mainly by the high conductivity difference of the liquids (Table 2.2).

The theoretical minimum voltage, which is the threshold for the electrowetting phenomenon to occur and allow droplet translation from one electrode to another, can also be calculated (Equation 2.4). The minimum voltage for the water droplet was approximately 45 V and for the glycerine droplet, it was calculated to be approximately 62 V. These values are theoretical for perfect conditions. In addition, the platform is operated in an unconditioned air environment and particles of dust on the device surface, liquid evaporation, airflow, platform defects (imperfect surface smoothness) or defects in the dielectric/hydrophobic surface can all disrupt the electrowetting phenomenon.

Droplet velocity of the droplet can also be calculated (Equation 2.17). The velocity of the 93% glycerine droplet, when 180 V is applied to the system, is of the level of 0.13 m/s. In comparison, the speed of the water droplet for this voltage is calculated to be 58 m/s. This difference between water and 93% glycerine droplet velocities is caused mostly by the difference in viscosity between these two liquids.

2.5   Conclusion

In this chapter, the electrowetting on dielectric phenomenon and platform construction were presented. The fabrication process and materials used to manufacture the electrowetting platform were described. It was shown that a 93% glycerine droplet changed

its contact angle when a voltage was applied to it and was moved by the electrowetting force when placed on the designed platform. Different designs of the platform were tested. It was experimentally verified that bigger electrodes with a larger gap between electrodes required a larger droplet and higher voltage to move the droplet across the platform. It was verified also that a water droplet did not need as much voltage as a glycerine droplet to be moved across the electrodes pattern. The shape of the electrodes also had an impact on the EWOD performance, with the zig-zag electrode shape ensuring smoother droplet movement.

2.6   Reference:

[1]   D. Li, *Encyclopedia of microfluidics and nanofluidics*. Springer, 2008, pp. 192–193,600–602.

[2]   L. Chen and E. Bonaccurso, "Electrowetting - From statics to dynamics.," *Adv. Colloid Interface Sci.*, pp. 1–11, Oct. 2013.

[3]   S. Annapragada, S. Dash, S. Garimella, and J. Murthy, "Dynamics of droplet motion under electrowetting actuation," *Langmuir*, vol. 27, pp. 8198–8204, 2011.

[4]   J. Berthier, *Microdrops and digital microfluidics*. William Andrew Inc., 2008, pp. 161–178, 206–213, 232–243.

[5]   L. Feng, S. Li, Y. Li, H. Li, L. Zhang, J. Zhai, Y. Song, B. Liu, L. Jiang, and D. Zhu, "Super-Hydrophobic Surfaces: From Natural to Artificial," *Adv. Mater.*, vol. 14, no. 24, pp. 1857–1860, Dec. 2002.

[6]   F. Li and F. Mugele, "How to make sticky surfaces slippery: Contact angle hysteresis in electrowetting with alternating voltage," *Appl. Phys. Lett.*, vol. 92, no. 24, p. 244108, 2008.

[7]   F. Mugele and J.-C. Baret, "Electrowetting: from basics to applications," *J. Phys. Condens. Matter*, vol. 17, no. 28, pp. R705–R774, Jul. 2005.

[8]   T. B. Jones, "An electromechanical interpretation of electrowetting," *J. Micromechanics Microengineering*, vol. 15, no. 6, pp. 1184–1187, Jun. 2005.

[9]   W. J. J. Welters and L. G. J. Fokkink, "Fast Electrically Switchable Capillary Effects," *Langmuir*, vol. 14, no. 7, pp. 1535–1538, Mar. 1998.

[10]   H. J. J. Verheijen and M. W. J. Prins, "Reversible Electrowetting and Trapping of Charge: Model and Experiments," *Langmuir*, vol. 15, no. 20, pp. 6616–6620, Sep. 1999.

[11]   V. Peykov, A. Quinn, and J. Ralston, "Electrowetting: a model for contact-angle saturation," *Colloid Polym. Sci.*, vol. 278, no. 8, pp. 789–793, Aug. 2000.

[12]   H. Moon, S. K. Cho, R. L. Garrell, and C.-J. "Cj" Kim, "Low voltage electrowetting-on-dielectric," *J. Appl. Phys.*, vol. 92, no. 7, p. 4080, 2002.

[13]   J. H. Song, R. Evans, Y. Lin, B. Hsu, and R. B. Fair, "A scaling model for electrowetting-on-dielectric microfluidic actuators," *Microfluid. Nanofluidics*, vol. 7, no. 1, pp. 75–89, Nov. 2008.

[14] W. C. Nelson and C.-J. "CJ" Kim, "Droplet Actuation by Electrowetting-on-Dielectric (EWOD): A Review," *J. Adhes. Sci. Technol.*, vol. 26, pp. 1747–1771, Jan. 2012.

[15] N. Rajabi and A. Dolatabadi, "A novel electrode shape for electrowetting-based microfluidics," *Colloids Surfaces A Physicochem. Eng. Asp.*, vol. 365, no. 1–3, pp. 230–236, Aug. 2010.

[16] M. Abdelgawad, P. Park, and A. R. Wheeler, "Optimization of device geometry in single-plate digital microfluidics," *J. Appl. Phys.*, vol. 105, no. 9, p. 094506, 2009.

[17] A. Stadler, "Transparent Conducting Oxides—An Up-To-Date Overview," *Materials (Basel).*, vol. 5, no. 12, pp. 661–683, Apr. 2012.

[18] "Indium-Tin Oxide (ITO)." [Online]. Available: http://www.indium.com/technical-documents/product-data-sheets/. [Accessed: 15-May-2012].

[19] "Aluminium properties." [Online]. Available: http://www.rsc.org/periodic-table/element/13/aluminium. [Accessed: 05-Aug-2012].

[20] "AZ 4500 Series Thick Film." [Online]. Available: http://www.first.ethz.ch/infrastructure/Chemicals/Photolithography/Data_AZ4500.pdf. [Accessed: 10-Sep-2012].

[21] H. Zhang and S. G. Weber, "Teflon AF Materials.," *Top. Curr. Chem.*, vol. 308, no. September 2011, pp. 307–337, Jan. 2012.

[22] *Physical properties of glycerol and its solutions*. New York : Glycerine Producers' Association, 1963, p. 27.

[23] "JD Photo-Tools." [Online]. Available: ttp://www.jdphoto.co.uk/. [Accessed: 26-Nov-2014].

[24] S. A. Campbell, *The science and engineering of microelectronic fabrication*, Second. New York: Oxford University Press, 2001, pp. 183–184.

[25] P. D. Sheet, "DuPont Teflon AF ™ ®," 2012.

[26] R. Dufour, A. Dibao-Dina, M. Harnois, X. Tao, C. Dufour, R. Boukherroub, V. Senez, and V. Thomy, "Electrowetting on functional fibers," *Soft Matter*, vol. 9, pp. 492–497, 2013.

[27] M. Pollack, "Electrowetting-based actuation of liquid droplets for microfluidic applications," *Appl. Phys. Lett.*, vol. 1725, no. 2000, pp. 10–12, 2000.

[28]   U.-C. Yi and C.-J. Kim, "Characterization of electrowetting actuation on addressable single-side coplanar electrodes," *J. Micromechanics Microengineering*, vol. 16, no. 10, pp. 2053–2059, Oct. 2006.

[29]   J. Jenkins and C. Kim, "Generation of pressure by ewod-actuated droplets," *Solid-State Sensors, Actuators, Microsystems Work.*, vol. 2, pp. 145–148, 2012.

[30]   M. Abdelgawad and A. R. Wheeler, "Low-cost, rapid-prototyping of digital microfluidics devices," *Microfluid. Nanofluidics*, vol. 4, no. 4, pp. 349–355, Jul. 2007.

[31]   M. Abdelgawad and a. R. Wheeler, "Rapid Prototyping in Copper Substrates for Digital Microfluidics," *Adv. Mater.*, vol. 19, no. 1, pp. 133–137, Jan. 2007.

[32]   "Kruss easy drop." [Online]. Available: http://www.kruss.de/products/contact-angle/dsa25/drop-shape-analyzer-dsa25e/. [Accessed: 09-Mar-2014].

Chapter 3

Fundamental principles of light propagation in optical fibre waveguides

3.1   Light propagation theory

The variable optical attenuator presented in this thesis operates through a combination of an electrowetting-on-dielectric platform and a side polished optical fibre. It is a continuous fibre type device, as the fibre is unbroken and the light is attenuated via interaction with the evanescent field, from the side of the structure. The liquid droplet, translated by the electrowetting phenomenon, attenuates the light which travels through the fibre. Therefore, one of the most important aspects of the operation of this device is the light interaction with the liquid droplet with specific droplet optical parameters (refractive index and dimensions). To aid this understanding, the theory of light propagation in optical waveguides is briefly reviewed.

3.1.1 Ray propagation on the boundary of media of different refractive indices

Using the ray propagation phenomenon to describe how light travels inside a waveguide, it is first required to understand how light behaves at the boundary of two media of different refractive indices.

Depending on the refractive indices of the two media, light can be transmitted, reflected or refracted at the boundary. Light is transmitted, unaltered, through the boundary when the media have the same refractive index. The more interesting case is when the two

media have different refractive indices. In this case, when light crosses the boundary, a part of the incident ray is reflected and a part travels into the second medium.

Light can be reflected on the boundary of two media and gives the possibility to guide light in a high index medium surrounded by two other lower index media. "Guiding" describes a situation when light is confined to a medium through reflections from bounding interfaces. In the simplest case, the requirement for light to be guided in a middle medium is that the first and third media need to have lower refractive indices than the "guiding" middle medium. The total internal reflection phenomenon should therefore be satisfied at two confining boundaries. The structure of this three layer model is known as a waveguide (Fig. 3.1).

The following analysis is based on the well-known description of planar waveguides. However it represents an approximate description which can be used for a simple analytical model of optical fibres where the geometry has circular cross section. In this thesis, the waveguide that is of interest is single mode optical fibre. In comparison to a multimode fibre the advantages of using the evanescent field of single mode fibre to form a variable optical attenuator[1] are:

- it is possible to design a device with the maximum sensitivity using only the fundamental waveguiding mode,

- sensitivity does not depend on the modal distribution (no influence of the source and fibre launching condition),

- Less influence from external disturbances, which affects the modal distribution in multimode fibres. So overall the single mode fibre is more stable than multimode fibre.
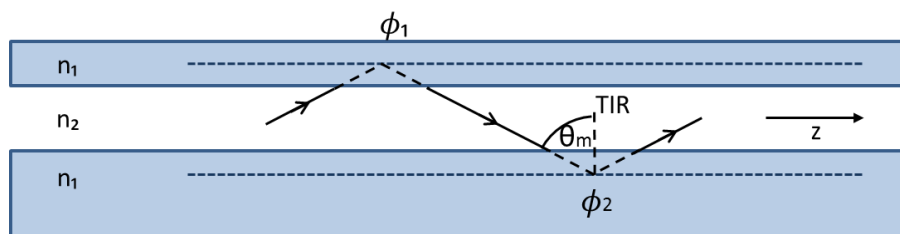

Fig. 3.1 Waveguide structure of three layer with different refractive indices (not to scale)

Light inside a waveguide travels by multiple internal reflections, so the incident angle of the reflected rays needs to be greater than the critical angle. There is also another condition that needs to be satisfied to guide the light inside a waveguide: the formation of a standing wave in the transverse direction[2], which leads to the planar waveguide equation:

$$\frac{4\pi d n_2 cos\theta_m}{\lambda_0} = 2m\pi + \phi_1 + \phi_2 \tag{3.1}$$

where n_2 is the refractive index of the guiding medium, d is the waveguide thickness, θ_m is the angle of propagation and λ_0 is the wavelength, m is the order of the guide mode and ϕ is the phase shift. In above equation the part of $\frac{4\pi d n_2 cos\theta_m}{\lambda_0}$ define phase change in transverse direction of propagating wave, ϕ_1 and ϕ_2 phase change on TIR (total internal reflection) and $2m\pi$ is a condition for standing wave in transverse direction.

From equation 3.1, it can be seen that for fixed values of refractive index and waveguide thickness it is only possible for certain angles of propagation to guide light. These angles correspond to waveguide modes. In conclusion there is a finite number of modes that can be supported by a particular waveguide.

Equation 3.1 shows that only a finite number of modes can be supported, so by manipulating the thickness of the waveguide it is possible to change the number of modes supported by the waveguide. Reduction of the waveguide thickness can lead to a design that will support only one mode. Such a structure is known as a single mode waveguide and has a guiding section. Equation 3.1 can be rearranged to calculate the mode cut-off thicknesses. A cut-off thickness is in physical meaning of minimal thickness that allows a particular mode to be guided. A mode is cut-off when $\theta_m = \theta_c$ (critical angle) and $\phi=0$ for this condition. Hence the mode cut-off waveguide thickness is[2]:

$$\frac{m\lambda_0}{2n_2 cos\theta_C} = d_c(m) \tag{3.2}$$

The Equation 3.2 defines the cut-off thicknesses for planar waveguide and cannot give an accurate value of thickness for single mode fibre with circular cross section. The difference comes down to the geometry of the cross section of waveguide and cross section

of fibre. For planar waveguide the number V_{pl} defined by $V_{pl} = k_0 a \sqrt{n_2^2 - n_1^2}$ must be less than $\frac{\pi}{2} \sim 1.5$ for a single mode operation, where as for a single mode fibre V number $V = k_0 a \sqrt{n_2^2 - n_1^2}$ (fibre parameter)[3] must be less than 2.4; where a is the core radius. Therefore the fibre optic operates as single mode waveguide when V<2.4 and the planar waveguide operates as single mode waveguide when V_{pl}< 1.5.

As described above, in a waveguide light cannot propagate into the lower refractive index medium when the incident angle of the rays is higher than the critical angle, and as a result is completely reflected from the medium boundary. However, part of the light wave penetrates into the lower index medium and is known as an evanescent field (Fig. 3.2)[4].
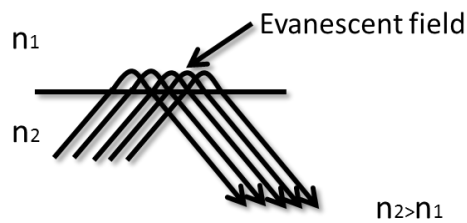

Fig. 3.2 Pictorial representation of the evanescent field established when light reflects from a boundary

The evanescent field exist when total internal reflection occurs between two media and is created at the boundary between a higher and lower index media[1]. The principal optical features arising from total internal reflection are[2]:

- light penetrates the second medium by a small distance (usually less than a micron from optical wavelengths) defined by the penetration depth ($\frac{1}{\gamma}$) of the evanescent field,

- as result of the short penetration depth into the second medium, a small phase shift (the Goos-Hanchen shift[4]) is added to the reflected beam.

The amplitude of the evanescent field in the medium of the lower refractive index decreases exponentially with the distance from the boundary. The evanescent field contains and transports energy and therefore the light guided an optical fibre core does not travel only in the core of the fibre but also partially in the cladding as an evanescent field (Fig. 3.3).

There is no significant loss of the energy in the cladding unless the cladding is made from material that absorbs the light[5].
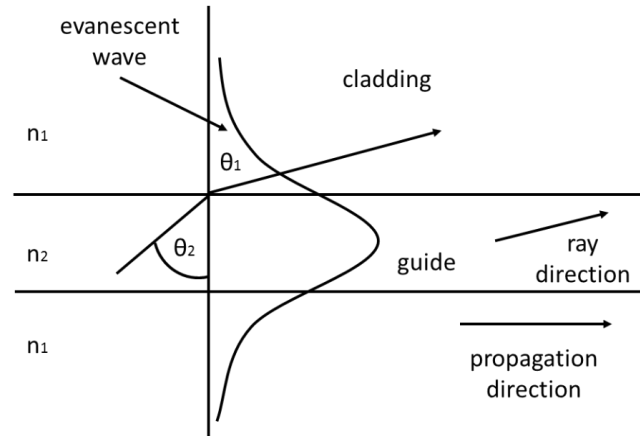

Fig. 3.3 The illustration of the electric field penetration into the cladding in the waveguide

In order to calculate the penetration depth of the evanescent wave, it has to be considered that the angle of the incident ray θ_2 (Fig. 3.4) is larger than the critical angle. The amplitude of the evanescent wave exponentially disappears in the direction y into the cladding. The penetration depth $(\frac{1}{\gamma})$ of the evanescent wave and can be described as:

$$\frac{1}{\gamma} = \frac{1}{k_0\sqrt{n_e^2 - n_1^2}}$$

(3.3)

where k_0 is the propagation vector, which gives the direction of propagation and the rate of change of phase with distance ($k_0 = 2\pi/\lambda_0$).
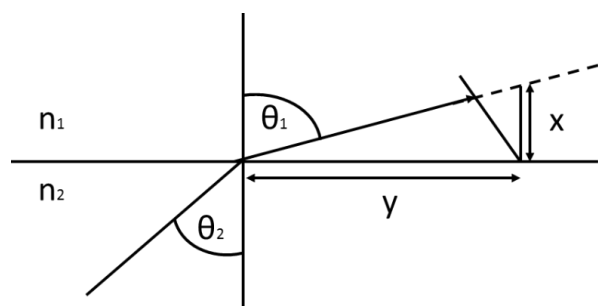

Fig. 3.4 Illustration of the geometry of a refracted wave

In a standard waveguide the cladding thickness is thick enough (thicker than the penetration depth) so that the amplitude of evanescent field vanishes to zero[5] away from the interface. In addition, the cladding is a solid material that is transparent for the guiding wavelength to minimize losses.

In this research, the main operation principle of device is based on accessing the evanescent field to change the light propagation inside waveguide. To access the evanescent field the cladding thickness needs to be reduced; and therefore it is important to estimate the penetration depth of the evanescent field. Figure 3.5 shows how the penetration depth varies with wavelength for the given parameters.

cladding refractive index 1.4547
core refractive index 1.46
ray propagation angle θ_1=88.5°
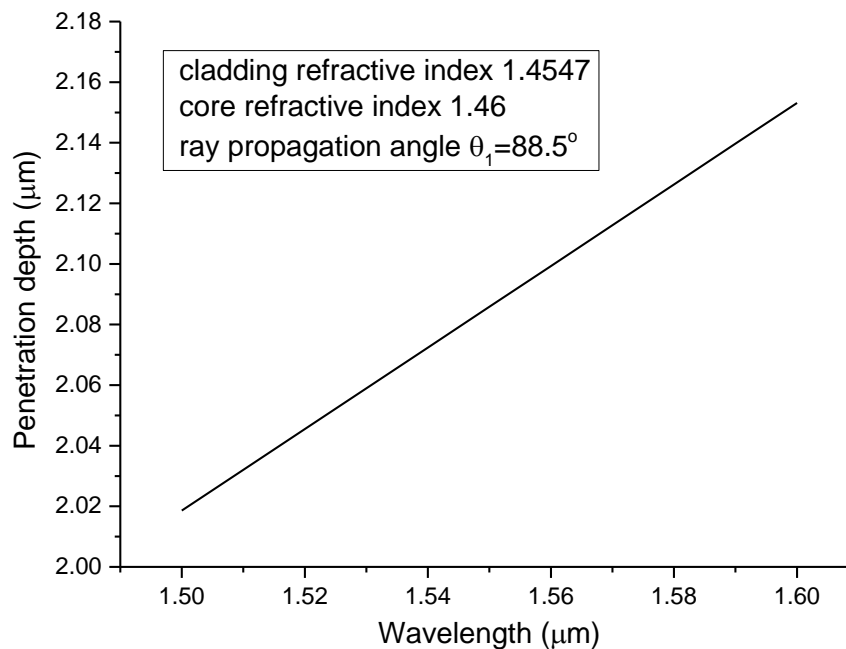
Fig. 3.5 Penetration depth change against the wavelength range for fixed value of cladding, core refractive index and ray propagation angle

From Figure 3.5 it can be seen that the penetration depth increases with an incremental increase of the wavelength. The difference of the penetration depth reaches 0.135 μm over a 100 nm wavelength range, which is relatively small difference when the penetration depth is more than 2 μm. The ray propagation angle (θ_1) needs to be larger than the critical angle

which was calculated to be 85°. For consistency, the chosen angle (θ_1) was 88.5°, that angle was based on the effective index and core refractive index (table 3.1 in section 3.2.2). The angle was calculated from:

$$\theta_1 = sin^{-1}\frac{n_e}{n_1}$$

(3.4)

where n_e is the effective index and n_1 is the core refractive index.

The calculated value of the penetration depth indicates that the cladding thickness needs to be reduced below 2.2 μm before the evanescent field can be affected by the external medium and the light propagation of the waveguide will change.

3.2   Theoretical Analysis of a Side Polished Fibre

In this research a single mode optical fibre is modified by reducing the thickness of the cladding on one side of the fibre using a polishing technique. The fibre's cladding was reduced to access the evanescent field at the optical fibre core-cladding boundary. The cladding thickness was reduced in a graded form with the middle region of the polished area exhibiting the minimum thickness (Fig. 3.6).
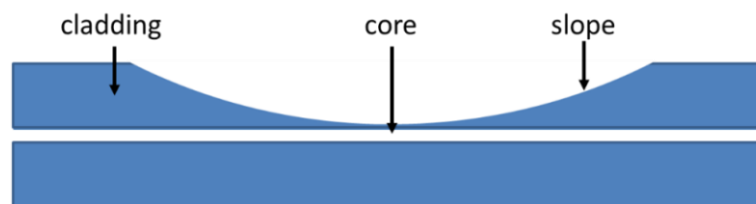

Fig. 3.6 Schematic of cladding reduction (not to scale)

3.2.1 Theoretical model

A theoretical analysis was carried out to calculate how the optical attenuation would change when a discrete droplet came in contact with the reduced cladding region. By

reducing the cladding, the discrete droplet can be placed within the evanescent field and so can exert an influence on it. The theoretical analysis was carried out to determine the optical transmission for different cases, as follows:

- different polished cladding thicknesses,
- different interaction lengths between the droplet and the polished region,
- different refractive indices of the discrete droplet.

The numerical analysis was based on the ray optics approach illustrated in Figure 3.7.
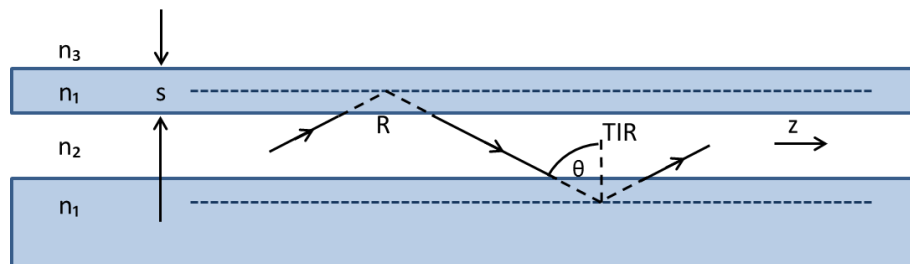

Fig. 3.7 Schematic of the ray optics approach applied to a side-polished optical fibre

(not to scale)

If the thickness of the cladding (s) is less than the penetration depth the external medium can influence the evanescent field, and the ray will be disturbed. The perturbation will arise as a consequence of an unsatisfied condition of total internal reflection. If the external medium has higher or equal refractive index to the guided mode effective index then an evanescent field no longer exists and energy will be lost to the external medium[4]. The external medium is represented by the discrete droplet that can be created from the liquids of varied refractive index.

The insertion losses will become higher with a cladding thickness reduction[4]. If we consider an evanescent field in the electromagnetic approach, as in Figure 3.8, the outside environment (droplet) will interact more strongly with the evanescent field when it is closer to the core.
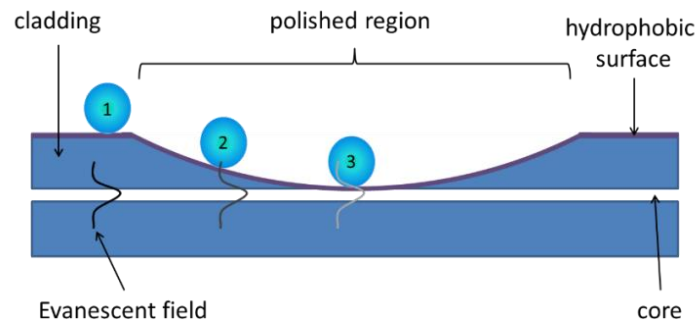
Fig. 3.8 Droplet interaction with the evanescent field according to the droplet position along the side-polished fibre (not to scale)

The theoretical analysis considers the position of the droplet as a specified length of fibre overlay (called the interaction length), where the droplet is moving towards the middle of the polished area in discrete steps (Fig. 3.8 & Fig. 3.9).
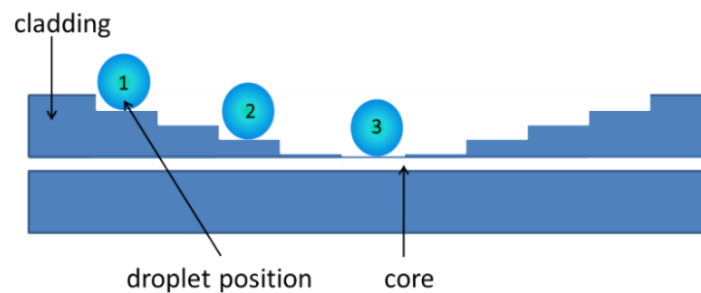
Fig. 3.9 Discrete movement of the droplet along the fibre polishing side (not to scale)

The output power P_{out} (neglecting all other losses) is related to the input power P_{in} by[1]:

$$\frac{P_{out}}{P_{in}} = R^{\eta z} \tag{3.5}$$

R is reflectivity of the ray, η is the number of reflections at the upper boundary per unit length, and z is the propagation direction (as shown in Fig. 3.8). The number of reflections can be calculated from[1]:

$$\eta = \frac{1}{2d_e tan\theta} = \frac{\alpha}{\beta} \cdot \frac{1}{2d_e} \tag{3.6}$$

where d_e is the effective thickness ($d_e = d + \frac{2}{\gamma}$), d is the fibre core diameter and $\alpha = k_0\sqrt{n_2^2 - n_e^2}$, $\gamma = k_0\sqrt{n_e^2 - n_1^2}$, $\beta_m = k_0 n_e$, $k_0 = \frac{2\pi}{\lambda}$, β_m is propagation constant of a mode and n_e is its effective refractive index, $\frac{1}{\gamma}$ is the penetration depth of the evanescent field. The reflectivity for frustrated total internal reflection can be calculated from[6]:

$$R = \frac{e^{2\gamma s} + e^{-2\gamma s} + 2\cos(\varphi_{21} - \varphi_{13})}{e^{2\gamma s} + e^{-2\gamma s} + 2\cos(\varphi_{21} + \varphi_{13})} \tag{3.7}$$

where s is the remaining cladding thickness and φ_{21} and φ_{13} are the phase shifts for the reflection coefficients at the n_2/n_1 boundary and the n_1/n_3 boundary respectively, given by[6]:

$$\varphi_{21} = -2tan^{-1}(\frac{\gamma}{\alpha}) \tag{3.8}$$

$$\varphi_{13} = \pi - 2tan^{-1}(\frac{\gamma}{\rho}) \tag{3.9}$$

Where $\rho = k_0\sqrt{n_3^2 - n_e^2}$, n_1, n_2, n_3 are the refractive indices of the fibre cladding, fibre core, and the external medium, respectively, or $n_e = n_2 sin\theta$, where θ is the propagation angle (Fig. 3.7).

The reflection coefficient therefore depends on the refractive index of the core, cladding and surrounding medium, and critically on the remaining cladding thickness *s*. If the reflection coefficient is 1 there is no change in light propagation due to the presence of the droplet, total internal reflection occurs and 100% of light is reflected back into the core and transferred through the fibre. Where R<1 the droplet has an influence on the reflection of the light and power is coupled out of the waveguide mode. That phenomenon indicates that it is possible to reduce the transmitted power, in steps, by reducing the cladding thickness and placing a medium of equal (or higher) refractive index than that of the waveguide core on the polished area.

3.2.2   Numerical Analysis

The theoretical results presented in the following subsections show how the output optical power will change when cladding thickness is reduced, and the interaction length (size of a droplet) and refractive index of the external medium vary. Calculations were performed with the listed parameters below:

Table 3.1 Typical parameters used in theoretical analysis[7]:

Parameter	Symbol	Value
Core refractive index	n_2	1.46
Cladding refractive index	n_1	1.4547
External medium refractive index	n_3	variable range: $1.4596 - 1.464$
Effective index of the guided mode	n_e	1.4595
Core diameter	d	8.12 µm
One side cladding thickness	s	variable from 22 µm to 0 µm
Wavelength	λ	1.55 µm
Interaction length	z	variable range: 0.2 mm - 2.4 mm

3.2.2.1   Refractive index impact

The first calculation that was completed studied how the refractive index of the external medium of refractive index n_3 influenced the transmitted power of guided light at a wavelength of 1550 nm. In this analysis the interaction length is not variable and 1.2 mm has been selected, as it is the standard interaction length between the droplet and fibre that will be used in the final device. The refractive index of the external medium was varied between a value below, equal to and above the value of the core refractive index. From these studies it was ascertained what the best value of external medium refractive index should be in order to accomplish the highest attenuation in the fibre.
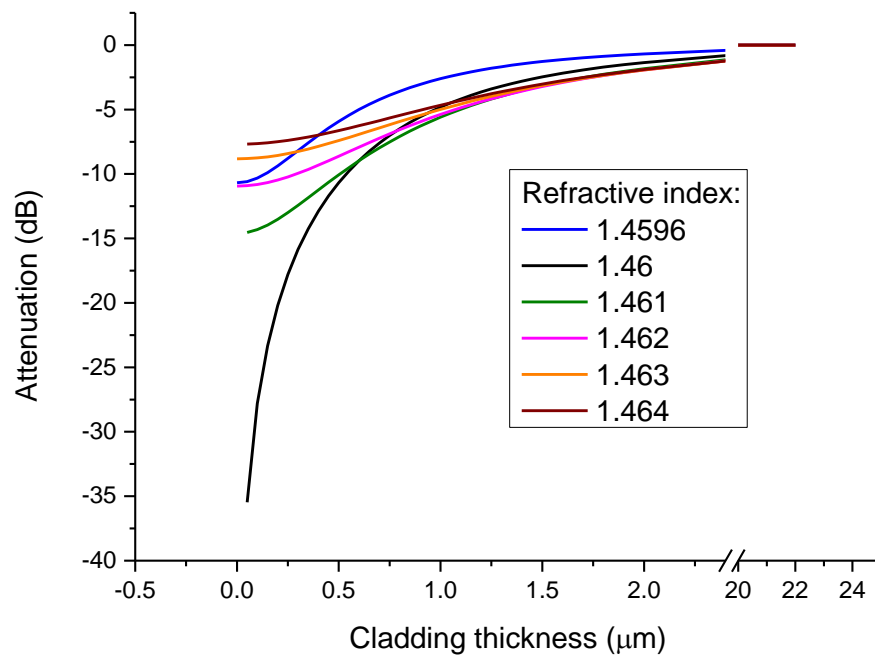
Fig. 3.10 Attenuation change against cladding thickness for different refractive indices

From Figure 3.10 it can be seen that the highest attenuation can be achieved for a droplet refractive index equal to the refractive index of the core (1.46). When the refractive index of the external medium is higher than that of the core, the attenuation becomes smaller than for the case of a medium of equal refractive index. Moving away from the optimal refractive index, the change in attenuation is high; changing from -37 dB to -15 dB with a single third decimal place increment in index. With further increments of the refractive index of the external medium the attenuation reduces to -7 dB. When the refractive index of the external medium is smaller than the core refractive index the attenuation can be achieved is -11 dB, which is small compared to -37 dB under optimal conditions when the refractive index of the external medium is equal to the core refractive index.

Figure 3.10 also illustrates the change in attenuation when the remaining cladding thickness changes. It can be seen that there is no significant impact on the performance when the cladding thickness is above 20 µm. At this thickness there is no influence on the attenuation from the external medium, because the external medium is located too far away from the evanescent field. When the cladding thickness reduces from 20 µm to 1 µm the

change in attenuation is in the range of 5 dB and it can be seen that the refractive index of the external medium begins to have an impact on the attenuation.

The stronger effect of the cladding thickness can be observed when the layer decreases from 1 µm. The refractive index of the external medium starts playing a stronger role and the attenuation behaviour changes in different ways for the various values of the refractive index. The highest attenuation can be achieved when there is no remaining cladding and the core is exposed to the external medium. A small remaining cladding, of the order of 100 nm, can reduce the attenuation from -37 dB to about -30 dB (for external medium refractive index of 1.46). It is therefore very important to reduce the cladding thickness as much as possible to fabricate a device of the best performance.

Finally, Figure 3.10 showed the effect of differing refractive index of the external medium with changes at the third decimal place. Figure 3.11 illustrates the case when the refractive index of the external medium is very close to the refractive index of the core and when the difference between the refractive indices is of the order of the fourth decimal place.
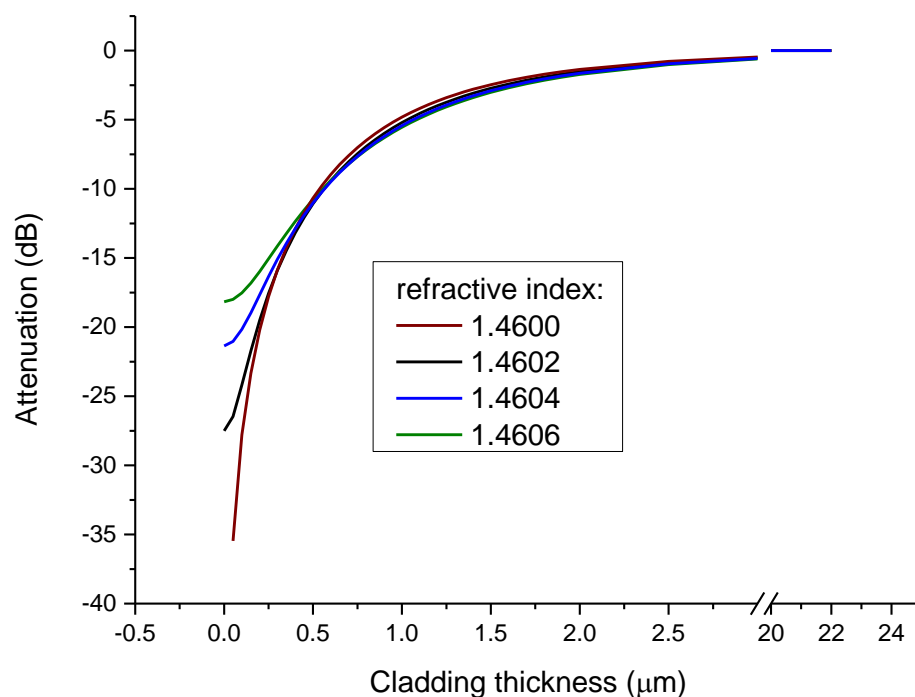
Fig. 3.11 Attenuation change for external media n_3 of refractive indices close to the refractive index of the core (1.46)

Figure 3.11 shows that these very small (fourth decimal place) differences from 1.4600 have great influence on the attenuation. It can be seen that with higher refractive index the attenuation becomes smaller; changing from -37 dB for 1.4600 to -18 dB for 1.4606. -28 dB can be achieved when the refractive index of external medium is 1.4602, but the attenuation is 9 dB smaller than the optimum case. When the refractive index increases to 1.4604 the attenuation is -21 dB and the performance degradation from optimum conditions becomes 16 dB. Therefore very small deviations of refractive index around the value of the core have a great influence on the performance. It can also be seen that the results for these different external medium refractive indices do not differ much for cladding thicknesses above 0.4 μm. The impact of the cladding thickness is noticeable when the remaining material is less than 0.4 μm thick. The cladding thickness influence on the attenuation was stronger when the refractive index of the external medium was further away from the core refractive index (Fig. 3.10). It was shown, above, that the impact of the cladding thickness on system performance starts when the thickness was approximately 1 μm. There is significant difference of impact of the cladding thickness on the device efficiency between various refractive indices of the external medium.

The presented theoretical results indicate that, to reach the highest attenuation, the refractive index of the external medium has to be very close to the refractive index of the waveguide core. Even a small difference from the core refractive index value of 1.46 has a strong impact on the achieved attenuation. When refractive index of the external medium is equal to refractive index of the core it is very important to reduce the cladding thickness as much as possible to obtain the best performance of the device.

3.2.2.2 Effect of wavelength on device operation

Theoretical analysis was also conducted for different wavelengths to check if there is any change in performance. It is very important to have a stable system for various wavelengths and to have the possibility to design a broadband variable optical attenuator with the same attenuation behaviour for a spectrum of wavelengths. In telecommunication systems variable optical attenuator devices work from 1520 nm up to 1560 nm.

The theoretical attenuation calculated from equations (3.5), (3.6), (3.7) are wavelength dependent through the k_0 term. However $\frac{\Delta k_0}{k_0} = \frac{\Delta \lambda}{\lambda}$ <3% over the 1520 - 1560 nm range so the effect of wavelength on device attenuation is small and is shown in the theoretical results of figure 3.12.
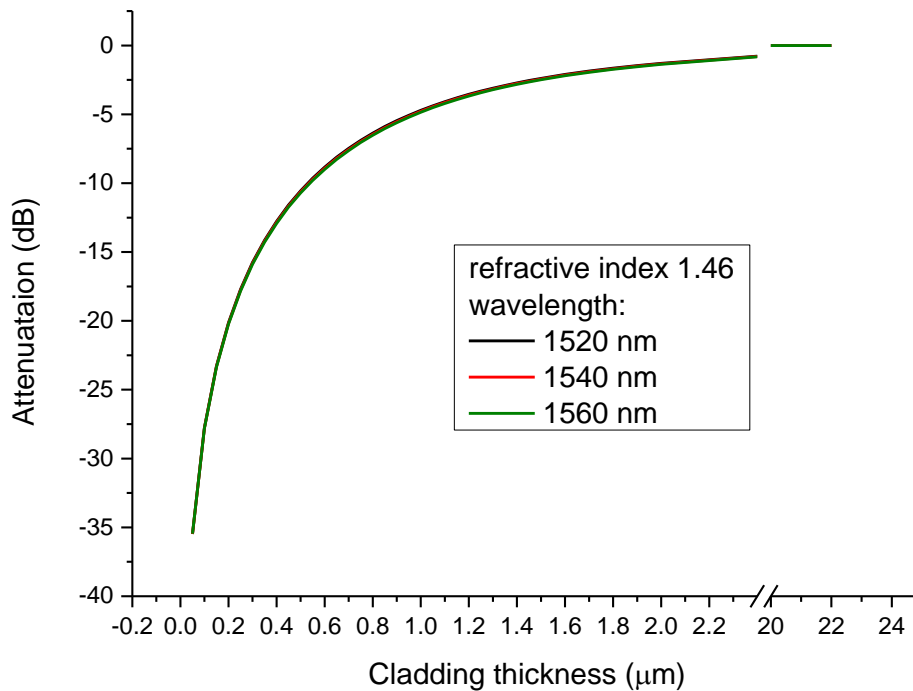
Fig. 3.12 Attenuation change for different wavelengths

Figure 3.12 shows theoretical results for one external medium refractive index of 1.46 at three different wavelengths: 1520 nm, 1540 nm and 1560 nm. The refractive index was chosen because of its strongest impact on the achievable attenuation level. It can be seen that over the range of different cladding thicknesses there is no significant change between the results for these three wavelengths. In the graph above (Fig. 3.12), it is hard to distinguish between the lines that identify three wavelengths, so Figure 3.13 below shows a zoomed-in area of the results around the highest attenuation.
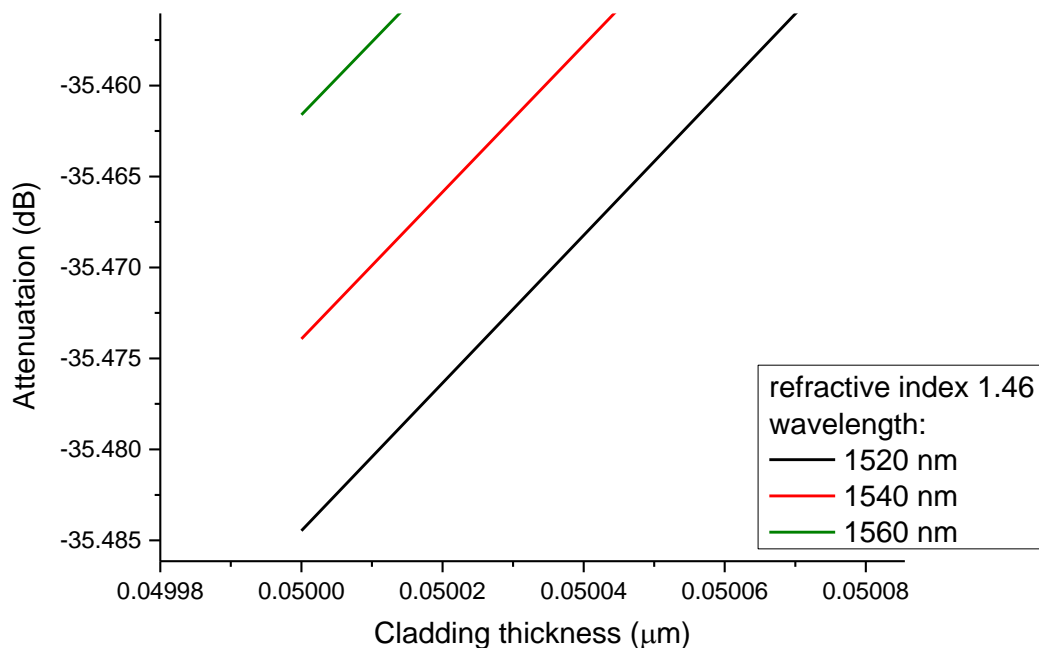
Fig. 3.13 Zoom in on the results for the three wavelengths for the highest attenuation

Figure 3.13 presents an enlarged area from the previous graph (Fig. 3.12). Differences in performance of the three wavelengths can be seen in this area of the highest attenuation. Attenuation increases with wavelength; providing -35.462 dB, -35.475 dB and -35.485 dB attenuations at 1520 nm, 1540 nm and 1560 nm, respectively. The increase in attenuation between 1520 nm and 1560 nm is in the range of 0.023 dB (~0.5 %). Such a small difference can be neglected, as it will not have a great impact on the performance of the device. Hence, theoretical results have proven that there is potential to design a variable optical attenuator for a range of different wavelengths. Therefore, such a VOA has the advantage that it can be used as a broadband device.

3.2.2.3 Effect of interaction length

Theoretical analysis also considers the attenuation change for different interaction lengths between the reduced cladding fibre and external medium. The calculations were performed for an external medium refractive index of 1.46 which is equal to the refractive

index of the core. The wavelength used in the analysis was chosen to be 1550 nm which lies in the standard telecommunication wavelength band.
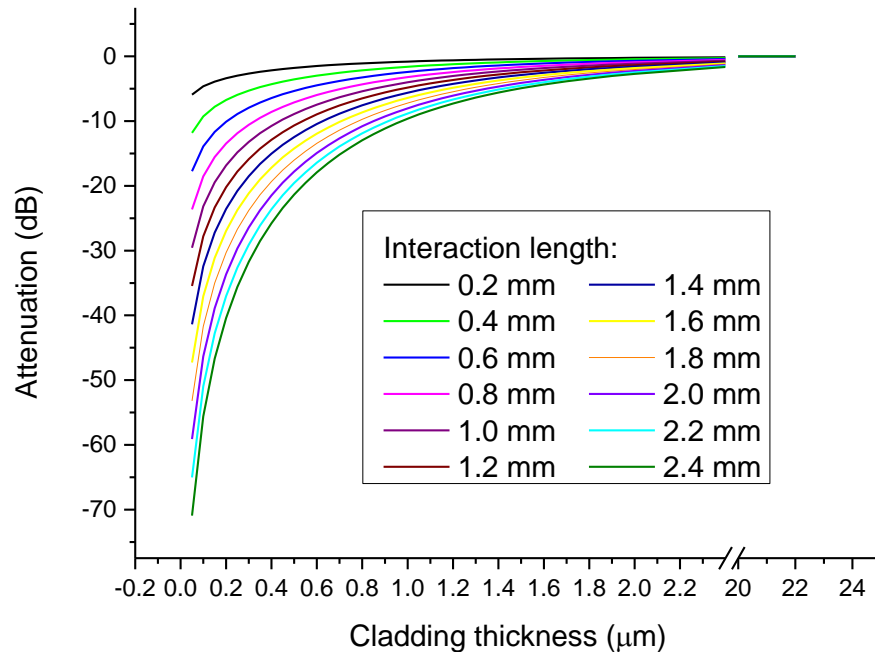

Fig. 3.14 Attenuation change for different interaction lengths for an external medium index of 1.46 and operating wavelength of 1550 nm

Interaction length was used as a variable in the theoretical analysis and was varied over the range from 0.2 mm to 2.4 mm. For a shorter interaction length of 0.2 mm the highest attenuation that can be achieved is -4.5 dB and for the longest interaction length of 2.4 mm that was used in the calculations the attenuation reached -70 dB. It can also be seen in Figure 3.14 that when the interaction length increases by 0.2 mm the maximum attenuation increases by approximately 5 dB. The difference in attenuation between the shortest and longest interaction lengths is ~65 dB. This shows that the interaction length has a great impact on the performance of the system.

It can also be seen that cladding thickness has no impact on the performance until it is reduced below 20 μm. Below this thickness, the attenuation differs for different interaction lengths. A stronger impact of the reduction of the cladding begins when the thickness reduces below 2 μm.
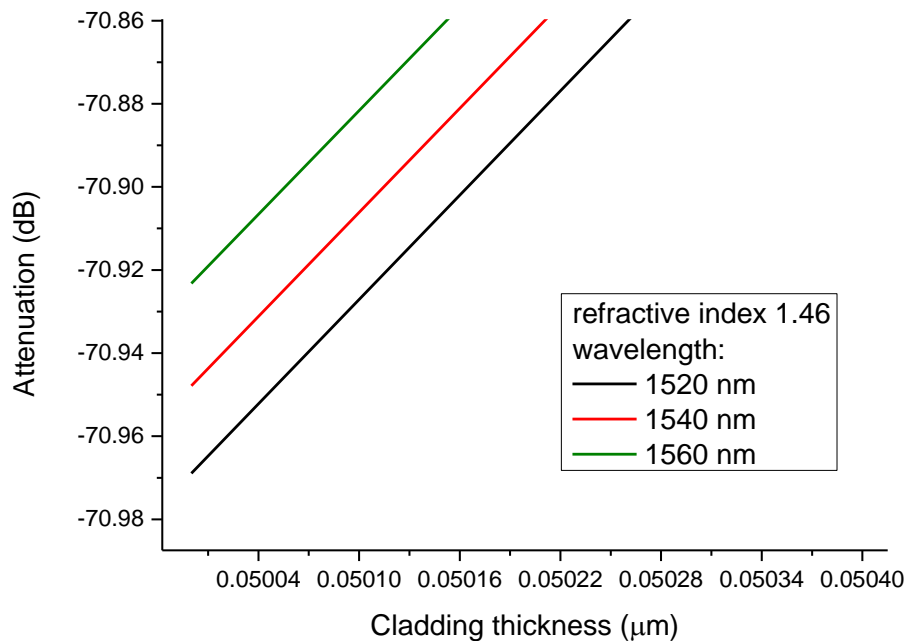
Fig. 3.15 Zoom in on the data for an interaction length of 2.4 mm, with an external medium
index of 1.46, showing the wavelength dependence

Figure 3.15 verifies that the different wavelengths have negligible impact on the achievable attenuation. From the presented results it can be seen that the attenuation changes insignificantly from -70.92 dB (1520 nm) through -70.95 dB (1540 nm) to -70.97 dB (1560 nm). The change in attenuation across the band of wavelengths from 1520 nm to 1560 nm is 0.05 dB for a 2.4 mm interaction length between a medium of 1.46 refractive index and the polished fibre region. For the wavelength band (1520 nm - 1560 nm) the attenuation change (0.05 dB) for a 2.4 mm interaction length is larger than the change for a 1.2 mm interaction length (0.023 dB), but is still in a range that will not perturb the performance of a broadband operation device; as was predicted from k_0 factor from theoretical study.

The above theoretical analysis presented the operating principle for a variable optical attenuator that can be constructed from a side polished fibre in contact with a medium (liquid droplet) of refractive index equal to or higher than the fibre core refractive index. The study focused on the use of media with different refractive indices and varying interaction lengths of the polished side of the fibre. Analysis also considered the range of wavelengths which can be used for operation. Examination proved that the VOA's performance depends

on the interaction length between the external medium and optical fibre and refractive index of the medium, but does not depend on the wavelength. The device can therefore be used as a broadband device.

3.2.3 Numerical Analysis – Lossy medium

Separately, another theoretical analysis was carried out to calculate how the optical attenuation will change when a discrete droplet is in contact with the reduced cladding region for the case where the liquid introduces absorption of light. The basic analysis principles are the same as when the liquid does not absorb the light. The droplet is translated sequentially along the fibre in steps creating fixed interaction lengths between the external medium and the fibre.

The description of the reflectivity for frustrated total internal reflection, when the medium (liquid) is described by a complex refractive index (n+jk), can be seen in Appendix 1. Using this description, the theoretical analysis now shows how the non-ideal optical transmission will change for various refractive indices of the external medium and various interaction lengths between a medium and a fibre.

3.2.3.1 Absorption of the external medium

The first requirement for this new analysis is to have knowledge about the absorption of the external liquid medium. An in-house glass cell was manufactured for the purpose of an absorption measurement experiment.

Figure 3.16 shows the design of the cell and the light path transmission through the liquid. The transmission loss was measured using a Bentham monochromator and can be expressed by the relationship:

$$I = I_0 e^{-2kk_0} \qquad (3.10)$$

where I_0 is light intensity at the input, $k_0 = \frac{2\pi}{\lambda}$, λ is the wavelength and $k = \frac{loss\left(\frac{dB}{m}\right)}{8.686k_0}$

where k is imaginary part and 8.686 is related to the change from Np/m to dB/m
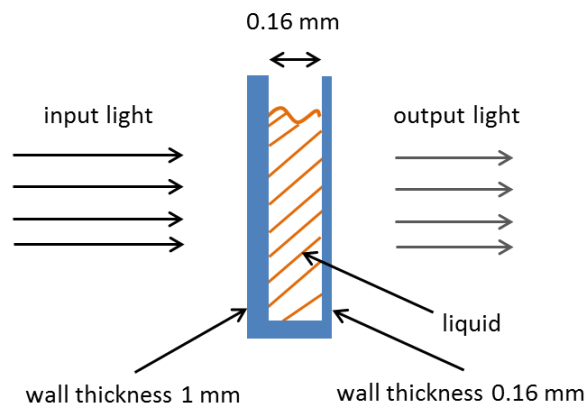
Fig. 3.16 Cell design for absorption measurements (not to scale)

Measurements were made for no cell, the empty cell and for the cell filled with water and three different glycerine-water solutions of refractive indices 1.425, 1.442 and 1.461. The wavelength band of the light that was used in measurements started at 1300 nm up to 1700 nm. The light travelled through the cell glass wall of thickness 1 mm then through the 0.16 mm of the test liquid and through a second glass wall of thickness 0.16 mm. An optical detector converted the received optical power to volts.

Fig. 3.17 Detected optical power for different wavelength and different liquids

The Figure 3.17 shows the raw measured results of the optical power for different cases. It is seen that the glycerine-water solutions does not have strong absorption compared to the measurement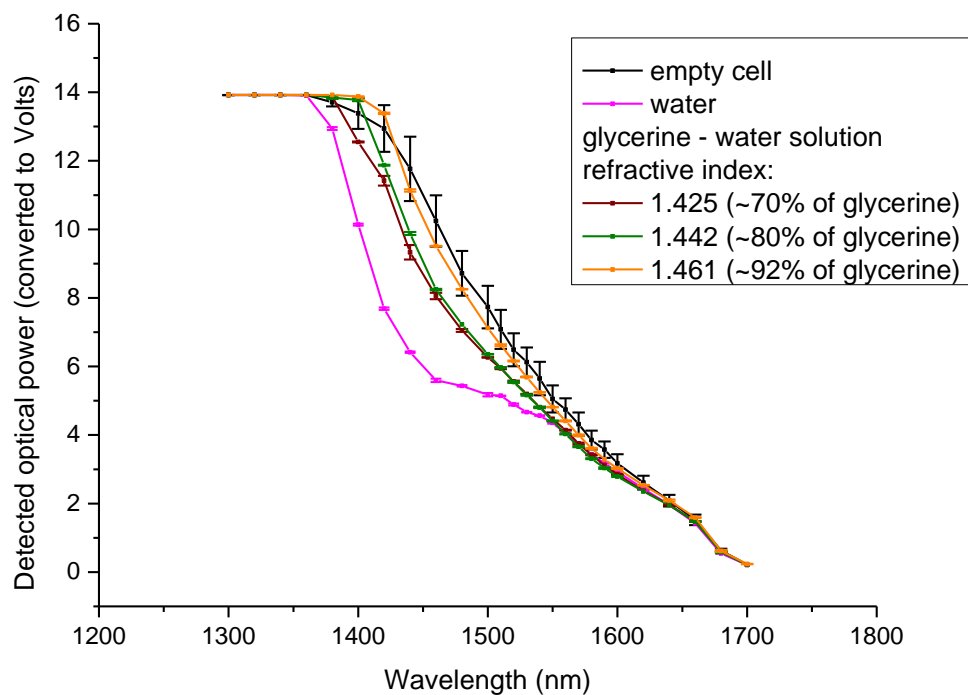s on the empty cell. Glycerine solutions absorb less light than water in some wavelength bands. For example, at 1420 nm the detected signal was 11.8 V (for 1.442 refractive index glycerine solution) but for water of the signal was 7.7 V. It was confirmed with the calculation (www.spectralcalc.com) that water has higher absorption between 1400 nm and 1500 nm.

The region of interest for the VOA design is between 1520 nm and 1560 nm and the graph below (Fig. 3.18) presents a polynomial fit of normalized results for wavelengths over that range.
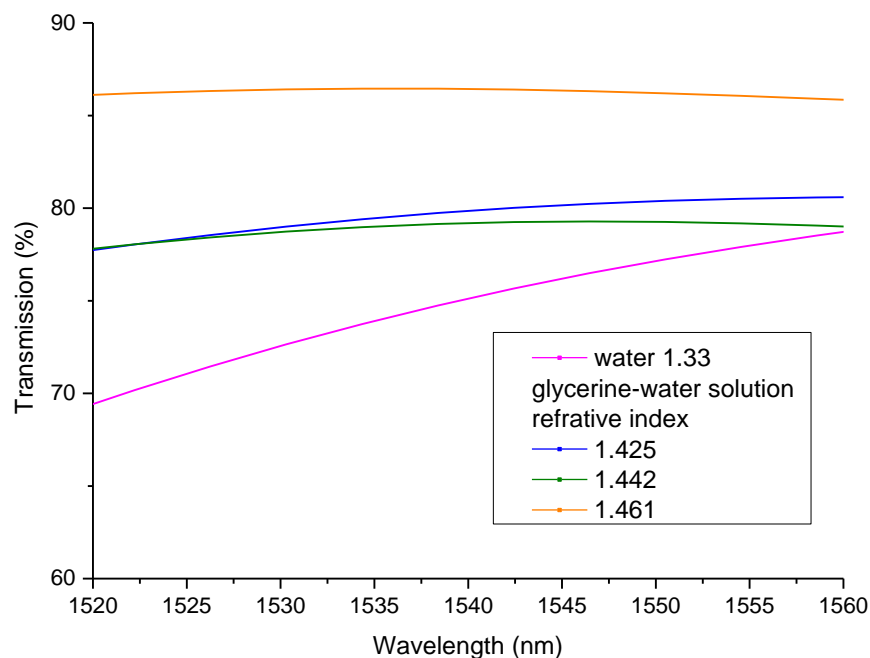
Fig. 3.18 Polynomial fit for normalized results of transmission for different liquids

Figure 3.18 presents the normalized results of light transmission through the cell filled with different liquids. The results were normalized to the results obtained for the empty cell, then converted to percentages. It can be seen that the transmission for a glycerine-water solution with 1.461 refractive index is in the order of 86 %. When the refractive index of the glycerine-water solution decreases the transmission decreases to 78 %. The light transmission through water is on the range of 68 % to 78 %.

3.2.3.2 Numerical theoretical analysis taking into account absorption of the external medium

To verify the impact of the absorption of glycerine-water solution on the transmission, a numerical theoretical analysis of the case will be presented below. The study focuses on one external medium refractive index of 1.461 to show that there is no significant difference between the theoretical results that do and do not consider a lossy external medium.
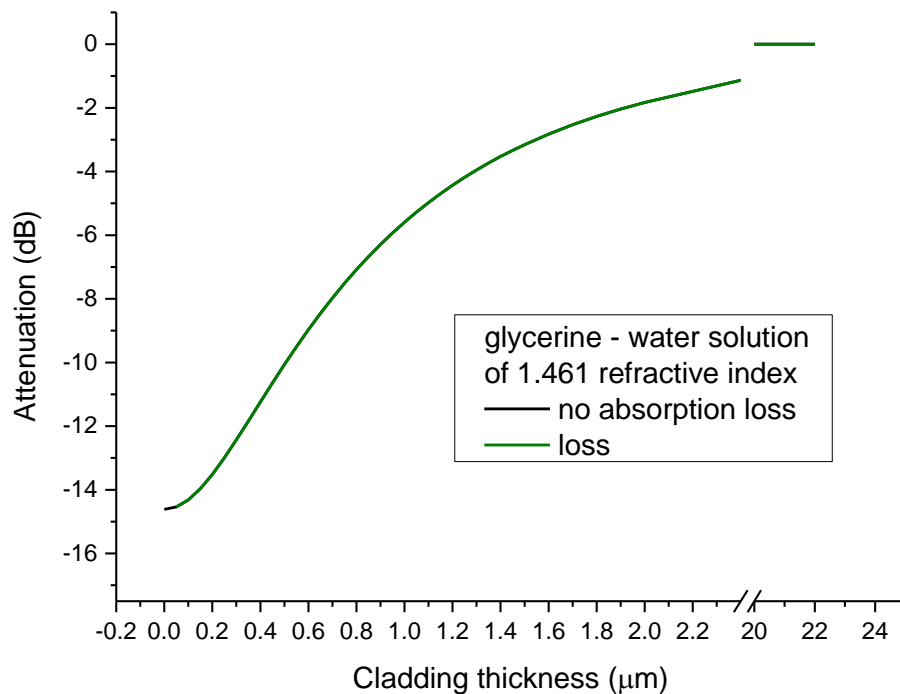
Fig. 3.19 Attenuation change for a 1.461 refractive index medium with and without absorption loss

From Figure 3.19 it can be seen that there is no change in performance for an external medium without the optical loss and for a medium that absorbs light. For Figure 3.19, a measured absorption loss of $k=1.84 \times 10^{-4}$ or 0.0065 dB at 1550 nm for the external liquid medium was used in the theoretical analysis. The loss of 0.0065 dB has no significant impact on the operation of the device and can be neglected in the future theoretical analysis.

3.3 Summary

Both theoretical analyses presented above have one aim, which is to support the preliminary idea of using a droplet, of fixed size and refractive index, in contact with the polished side of an optical fibre to attenuate the transmitted light. The above numerical analysis provided various results that approached the problem from different directions. It was shown that there are three significant design parameters that can influence the light transmitted through the fibre:

- refractive index of external medium

- cladding thickness

- droplet size

Each of the listed parameters can change the performance of the device and need to be considered in the design process of the side polished VOA. The size of droplet used (defining the interaction length between the core and external medium) with refractive index equal to index of the guide core can vary the level of attenuation from -4.5 dB (0.2 mm interaction length) to -70 dB (2.4 mm interaction length). The theoretical analysis revealed that the larger the index difference between external medium and core the more light is transmitted. The highest attenuation of -70 dB was obtained using a 2.4 mm interaction length between fibre and external medium and equal refractive indices (1.46) of core and external liquid. It was also shown that the glycerine-water solution which will be used to attenuate the transmitted light has no additional loss impact on the device performance.

The next chapter will introduce fibre optic fabrication process and the experimental results of the designed variable optical attenuator where a droplet of given refractive index and size will be "digitally" moved along the tapered side of the optical fibre.

3.4   References:

[1]   G. Stewart and B. Culshaw, "Optical waveguide modelling and design for evanescent field chemical sensors," *Opt. Quantum Electron.*, vol. 26, pp. 249–259, 1994.

[2]   G. Flockhart, W. Johnstone, M. Lengden, and C. Michie, "Photonic Systems," 2012.

[3]   M. Teich and B. Saleh, "Fundamentals of photonics," in *Fundamentals of photonics*, Canada, Wiley Interscience, 1991, pp. 279–283.

[4]   F. de Fornel, "Evanescent waves: from Newtonian optics to atomic optics," in *Evanescent waves: from Newtonian optics to atomic optics*, Springer Berlin Heidelberg, 2001, pp. 3–7, 12–18, 54–60.

[5]   F. Smith, T. King, and D. Wilkins, "Optics and photonics: an introduction," in *Optics and photonics: an introduction*, Second., Wiley, 2008, pp. 141–143.

[6]   M. Born and E. Wolf, "Principles of optics: electromagnetic theory of propagation, interference and diffraction of light," in *Principles of optics: electromagnetic theory of propagation, interference and diffraction of light*, 7th ed., NY: Cambridge University Press, 1999, p. Chapter 1.

[7]   G. Keiser, "Optical Fiber Communications," in *Optical Fiber Communications*, Third., Mc Graw Hi, 2000, p. 123.

Chapter 4

Experimental evaluation of electrowetting on dielectric variable optical attenuator

4.1 Device operation principle

4.1.1 Fibre geometry for electrowetting on dielectric variable optical attenuator

The two previous chapters described the electrowetting on dielectric phenomenon and light propagation through optical fibres. The principle of the VOA operation is the influence on the evanescent field of the fibre by an external fluid of appropriate physical parameters (refractive index, interaction length).

The selection of fibre geometry to form the heart of the VOA was considered. Accessing the evanescent field of the fibre is generally done using two methods: fibre tapering or side polishing the fibre.

Side polishing standard fibres was introduced in the early 1980s to access the evanescent field of a half block coupler for single mode fibre[1],[2]. One disadvantage of using a polished half block is the short interaction length of a few millimetres and another is that the fabrication process is very slow. In the late 1980s a new technique using a polishing wheel was reported, allowing longer interaction lengths to be achieved[3] and enabling larger scale production. The polishing process usually stopped a few micrometres above surface of the core.

4.1.2 Side polished fibre fabrication

As well as acquiring commercial side polished fibres, in-house side polished fibres were also produced by a developed polishing technique that allowed us flexibility to specify our own parameters. This side-polished fibre (with a polished region of approximately 10 mm) was fabricated using a 75 mm diameter polishing wheel (Silverline Tools Ltd., UK) in conjunction with 9 µm particulate aluminium oxide and 0.5 µm particulate cerium oxide powders in water. The outer polymer jacket was removed over a short region of the fibre and this section was placed upon the polishing wheel. Weights were placed on both sides of the fibre to apply tension while the polishing wheel rotated at less 100 rpm and the polishing powders were sequentially applied to the wheel. The optical power transmitted through the fibre was continuously monitored during the polishing process (Fig. 4.1) and the speed of the wheel was adjusted, during the fabrication process, depending on changes in the received optical power. The fibre cladding thickness was gradually decreased until the optical transmission changed, indicating that the evanescent field could be accessed externally[4]. This occurred when the cladding was reduced to a few microns above the core of the fibre and the remaining cladding provides the fibre with sufficient robustness for general handling. A last test was carried out using an oil of refractive index higher than the refractive index of the core. When the optical power decreased dramatically to around -40 dB, or less, the fibre was deemed to be ready for experimental testing with the EWOD platform.
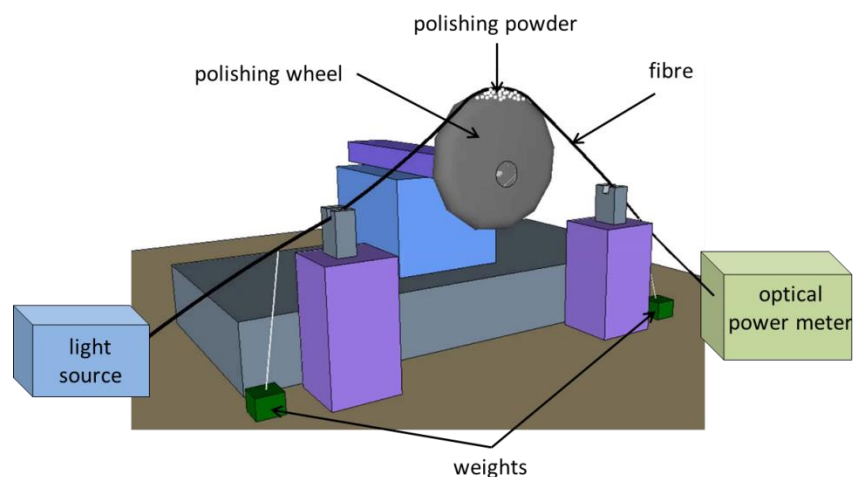

Fig. 4.1 Illustration of side polished fibre fabrication process

Due to the geometry of the polishing wheel, the polished section of fibre attains a non-uniform profile with the outer cladding tapering down to a minimum depth in the centre of this region. Figure 4.2 illustrates the topology of the side-polished fibre where the cladding is reduced, to create the evanescent field access region.
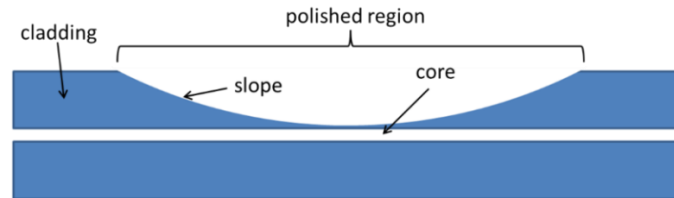

Fig. 4.2 Longitudinal section of the fibre with polishing region (not in scale)

A cross-section image of a fibre cleaved across the polished region is presented in Figure 4.3, showing the proximity between the light guiding core and the remaining cladding. It can be seen that the core was not exposed to the external environment and there remains a thin layer of cladding above the core.
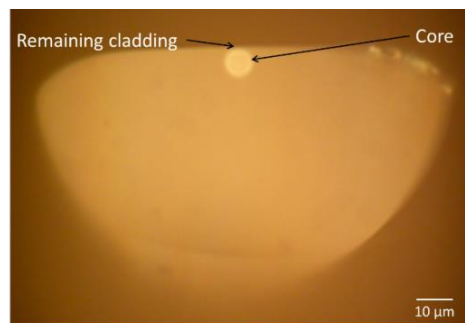
Fig. 4.3 Microscope image of end of cleaved side polished fibre section

After the fabrication process, some images were taken of a side polished fibre using a scanning electron microscope (SEM). Figure 4.4 presents a cross-section of the middle point of the polished region. From the picture, it can be seen that the cladding thickness was reduced such that no cladding surface remained on top of the core (standard cladding dimension 125 µm, remaining thickness ~ 62.5 µm – Fig. 4.4). The fibre in Figure 4.4 retained its outside plastic cover to enable easier handling during the SEM picture session; however, during experiments each fibre had this layer removed to reduce the chances of glycerine-water droplets sticking to the non-uniform surface of the fibre coating.
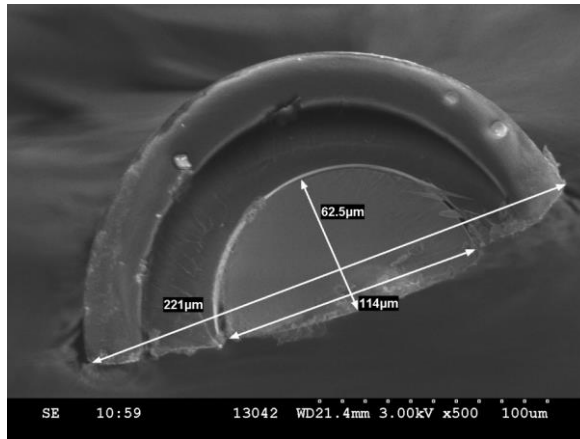
Fig. 4.4 SEM picture of cross section of the fibre polished region

Figure 4.5 a), b) shows SEM pictures of the surface of the polished fibre region. Figure 4.5 a) documents the surface finish achievable using the polishing process. The surface looks relatively smooth; there are no noticeable holes or bulges, but it is possible that micropores, that are not visible on the SEM picture, are present. In Figure 4.5 b, the start of the polishing region is shown. The surface of this region is rough and non-uniform; containing some pores and bulges. The start of the polished region has a triangular shape which is consistent with the manufacturing process where the fibre is aligned on the top of the round polishing wheel.
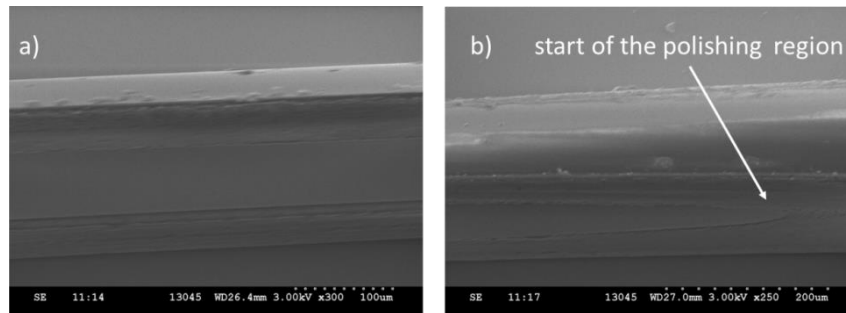
Fig. 4.5 a) SEM image of the central surface finish achieved after polishing, b) SEM picture of the start of the polished fibre region

The pictures taken with the scanning electron microscope do not show the surface quality in high detail. Therefore, an optical white light interferometer (Veeco NT1100) was used to check the surface quality.
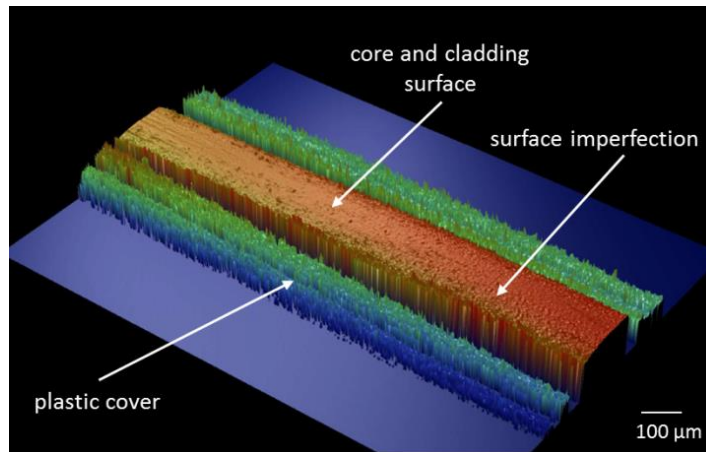
Fig. 4.6 Optical profile of polished fibre surface captured using an optical white light interferometer

Figure 4.6 shows the surface quality of the polished region of the fibre. From this picture it is more obvious that the surface is not completely smooth, as was suggested by the SEM pictures of Figure 4.6.
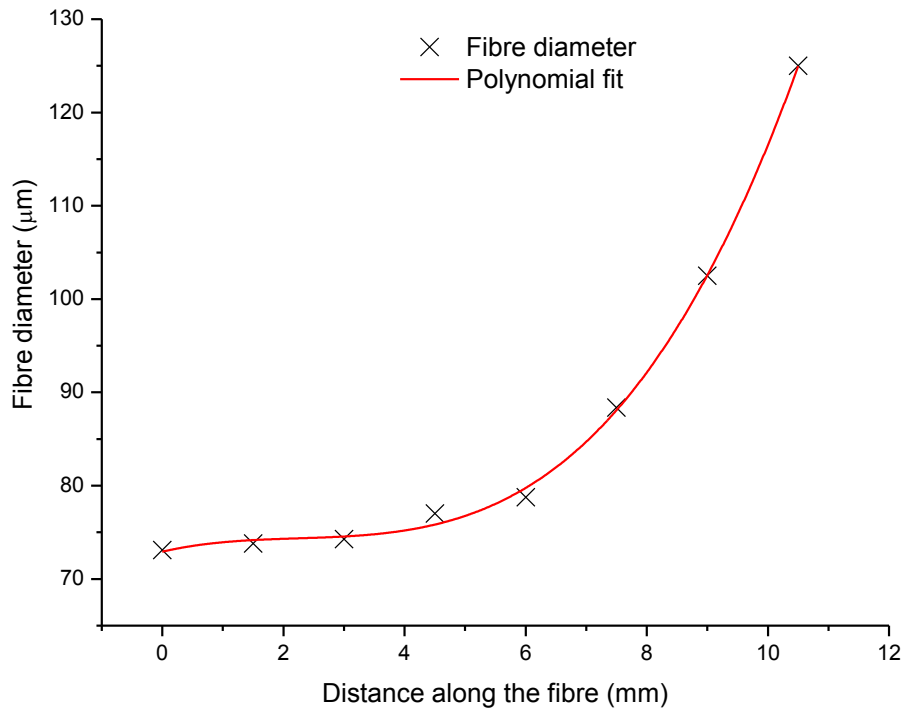
Fig. 4.7 Effect of polishing on the fibre diameter measured directly using an optical microscope (third order of polynomial)

Another in-house fabricated fibre was investigated to ascertain if the profile of this fibre matched the slope profile. The investigation focused on taking series of pictures of several sections of the polished region of the fibre with the use of a microscope. The pictures can be found in Appendix 2. The Figure 4.7 presents a plot of the fibre diameter along the polished region taken from these photographs showing the reducing diameter towards the centre of the fibre.

4.1.3 External fluid refractive index specification

The variable optical attenuator (VOA) is combined from two parts; an electrowetting on dielectric platform and a side polished fibre (Fig. 4.8). The EWOD platform is used to digitally control the movement of a microliter droplet across the electrodes. The side polished fibre is placed on top of the EWOD platform with its interaction region facing towards the droplet. When the droplet translates between electrodes while touching the polished region of the fibre, the optical transmission through the fibre changes.
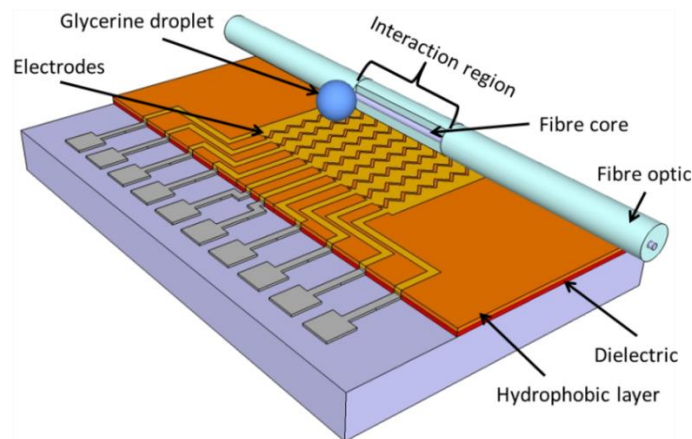
Fig. 4.8 Schematic of the EWOD platform with side polished fibre (not to scale)

As described in Chapter 3, the maximum attenuation of the light carried by a fibre can be achieved if an external liquid has a refractive index close to the core refractive index. A challenge in creating the EWOD-VOA was finding the appropriate liquid to be used for droplet creation. There are several liquids with a refractive index equal or greater than the fibre core index (1.46) but most of these are oils which cannot create a droplet that can be

moved by the electrowetting phenomenon. Oil also spreads immediately along the surface of the fibre surface losing a compact droplet geometry. Yet another problem is that oil is very hard to remove from the device surfaces and cleaning the fibre is more difficult due to the fragility of the fibre. The liquid selection process focused on finding a liquid that has a base of water with a mix of a second liquid. Water has been presented in several articles[5]–[7] as a liquid that can form a droplet and can be moved by electrowetting. The second liquid that may have been suitable was glucose, but it was found that to create a refractive index higher than 1.46, the concentration of glucose in the water solution would be too high to form a droplet aqueous enough to move by electrowetting. For example, the glucose concentration, in water, by weight, to achieve a refractive index of 1.439 is 66 %[8] and would be higher to achieve an index of 1.46. However, another liquid that can mix with water and can give an appropriate refractive index is glycerine. The maximum refractive index that 100 % glycerine can achieve is 1.47399 (Tab. 4.1)[8].

Tab. 4.1 Examples of glycerine water solution of different refractive index at 20°C:

Glycerine % by weight	Refractive index [8]	Refractive index measured
10	1.34481	1.3528
20	1.35749	1.3577
30	1.37070	1.3785
40	1.38413	1.3890
50	1.39809	1.4081
60	1.41299	1.4180
70	1.42789	1.4258
80	1.44290	1.4425
91	1.45989	1.4518
92	1.46139	1.4596
93	1.46290	1.4602
94	1.4644	1.4606

Appropriate concentrations of glycerine-water solutions were prepared for a series of experiments. It was assumed that the values in Table 4.1 were correct at the time of preparation. It was also noted that the refractive index can change as a droplet absorbs water from the outside environment[9], so the refractive index could decrease over time. Small errors could also be made during the solution preparation. In fact, only a 1 % (by weight) difference of glycerine could change the refractive index from residing above 1.46 to falling below 1.46. Such an error could result from the fact that glycerine is highly viscous (1.410 kg/ms – 100% glycerine; 0.0894 kg/ms – water[10]) and could adhere to the preparation equipment and not be included in the aqueous solution. The refractive indices of the prepared solutions were measured with an Abbe Refractometer at the wavelength of 589 nm. The measurements (shown in Table 4.1) were made to quantify the index of the specific solutions and to ascertain the similarity between theoretical refractive indices and the actual refractive index of the solution.

4.2 Influence of liquid refractive index on the device performance

In the initial device experiments, an electrical potential difference was sequentially applied to the array of electrodes on the EWOD platform, causing a droplet to translate along the side polished fibre. A square waveform of 10 V at a frequency of 1 kHz was produced by a waveform generator (Agilent 3228A) and amplified (A400, FLC Electronics) to 180 V. Broadband light from an erbium doped amplifier (EDFA) was used to inject optical power into the fibre. A photoreceiver (LNP-2, Optosci Ltd, UK) was used to monitor the level of the optical power at the fibre output. Next, the signal from the photoreceiver was sent to a PicoScope (Pico Techology Ltd, UK) data logger which recorded the photodiode output voltage in real time during motion of the droplet along the interaction region of the fibre (Fig. 4.9). Finally the signal was sent to a computer to store the data.
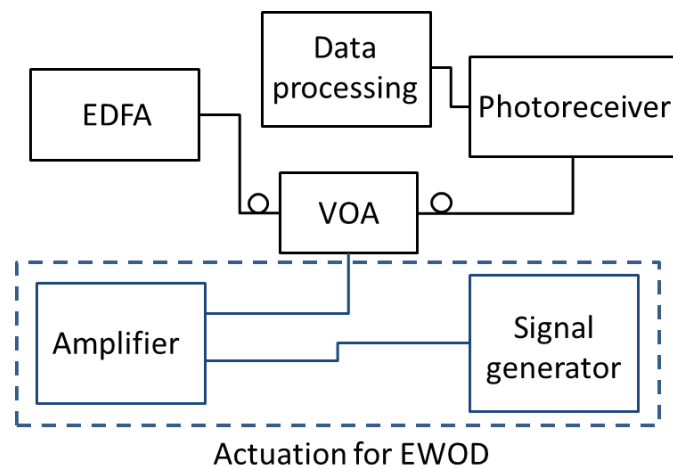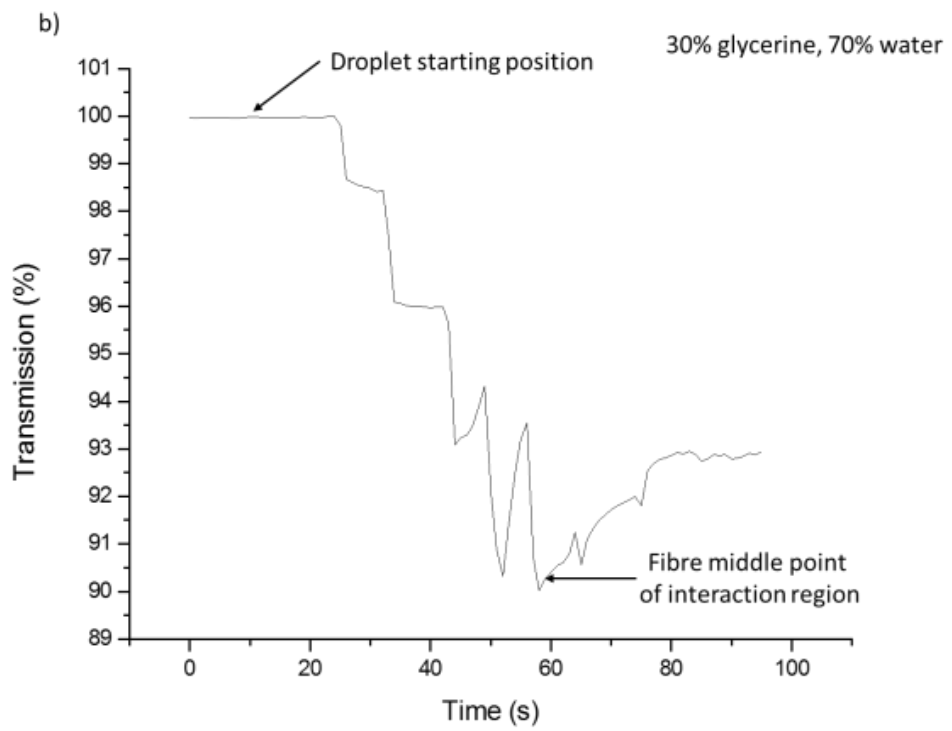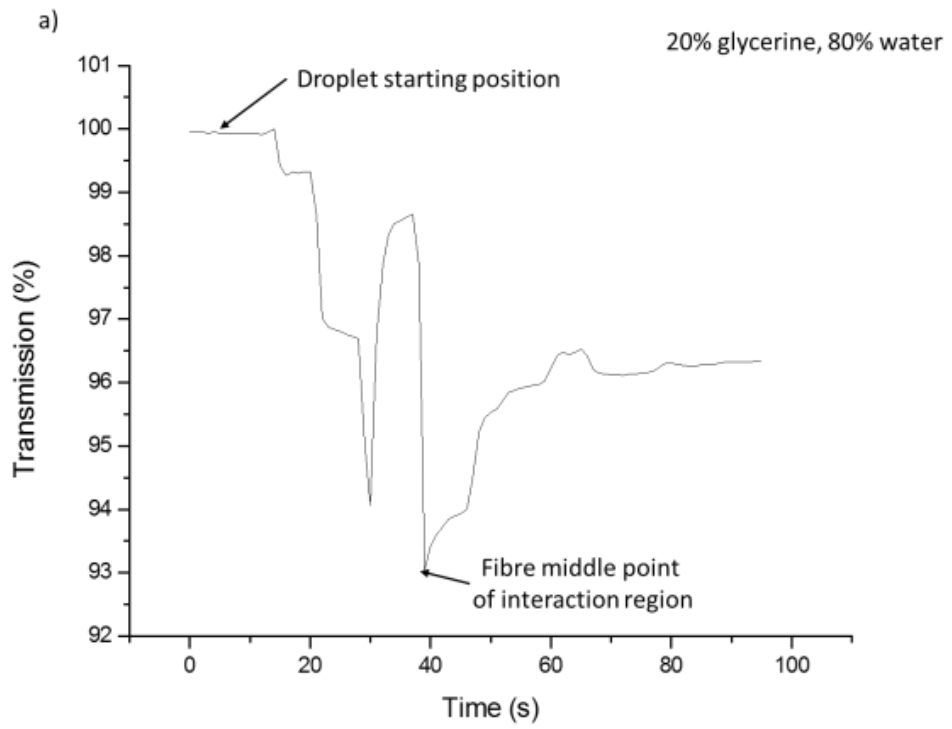
Fig. 4.9 Components of experimental setup to evaluate side-polished fibre VOA

The voltage and frequency settings were chosen after the results of tests that were performed with differently sized electrodes (see Section 2.4). The most efficient voltage signal for the 600 μm wide electrodes with a 2 μL glycerine-water droplet was found to be 180 V at 1 kHz. The voltage was applied to individual electrodes sequentially and the droplet would move to the electrode with the higher potential.

Investigation of the complete EWOD-VOA platform enabled investigation of how different glycerine-water solutions influenced the optical transmission inside the fibre. The most important part of these investigations was to show that only appropriate concentrations of glycerine in the glycerine-water solution will have a refractive index that can assert an influence on the light transmission of the side polished fibre. In these initial experiments the side polished fibre used was the commercial type (Phoenix Photonics Ltd (UK)). In order to correctly mount the polished face of the fibre on the EWOD platform it was placed on a micro-stage which could be also be rotated around the propagation axis of the fibre. The droplet was positioned in the middle of the polished region. During the investigation, the fibre was rotated and the optical power was measured after a droplet was placed in the middle point of the marked region. When the lowest optical power was measured, the polished region was correctly oriented, maximising access of the droplet to the evanescent field. After finding the appropriate fibre orientation, the fibre was fixed in place.

a)

20% glycerine, 80% water

Droplet starting position

Fibre middle point
of interaction region

Transmission (%)

Time (s)

b)

30% glycerine, 70% water

Droplet starting position

Fibre middle point
of interaction region

Transmission (%)

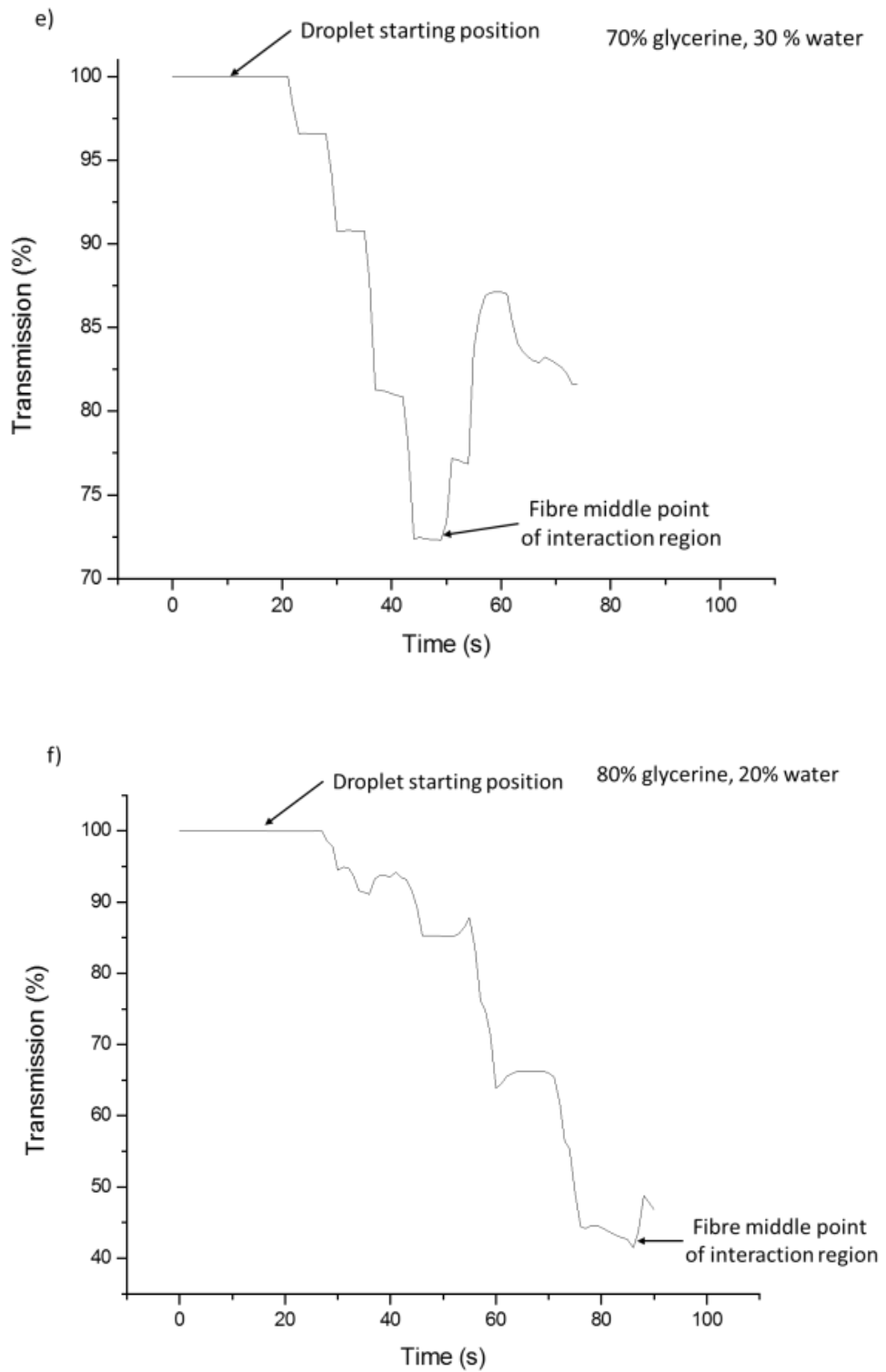Time (s)

c)

d)
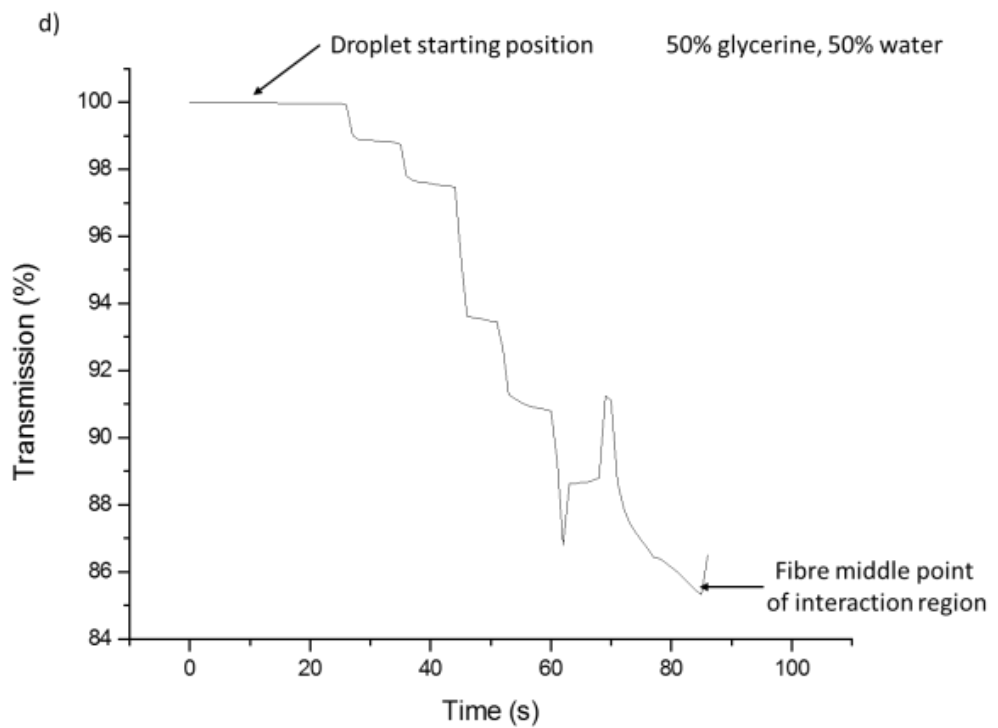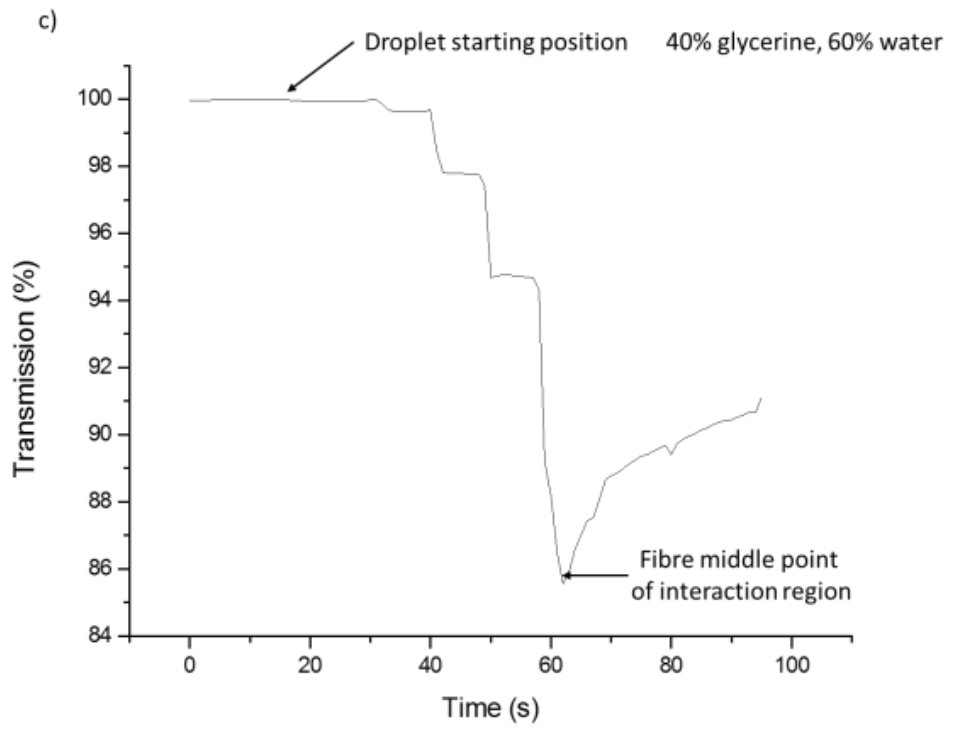
Fig. 4.10 The fibre transmission change during droplet motion for different glycerine concentrations in glycerine-water solutions

A 2 µL droplet was then placed at the start of the interaction region and moved digitally along it by applying the voltage signal to the sequence of electrodes. Optical transmission was recorded as the droplet translated across the polished region of fibre, and is shown in Figure 4.10. On each graph it is marked where the droplet was on the edge of the interaction region and when it reaches the mid-point, where the cladding thickness of the fibre is the lowest. More importantly, Figure 4.10 shows how the fibre transmission behaves as a function of droplet glycerine concentration.

It can be seen that with an increment of glycerine concentration, the transmission decreases. As the glycerine concentration of the solution increases, the refractive index also increases, becoming closer to the refractive index of the fibre's core, causing more light to be coupled out of the fibre. The 20% glycerine solution, provides only a 7% decrease in optical transmission when the droplet is in the position where the cladding thickness is the lowest (Fig. 4.10 a). When the concentration of glycerine increase to 30%, the transmission decreases more and the pattern repeats with every increment of the glycerine concentration in water until the 80% glycerine solution provides ~40% transmission (Fig. 4.10 f).

From the obtained results it can be seen that some fluctuations in transmission are present and it is assumed they are caused by motion of the droplet. As the transmission was recorded constantly as a function of time, there was no time to stabilize the level of transmission, and the optical transmission variations (that can be caused by unstable movement of droplet, vibration of the platform, and the laboratory temperature change) were also captured. The stronger fluctuations are more visible for lower glycerine concentrations (20 % to 30% of glycerine) in the water solution, and the readings are more stable for higher glycerine concentrations (40 % to 80 % of glycerine). Such example of the unstable movement of the droplet is clearly visible on the Figure 4.10 a, between 30 s and 40 s. The transmission increases by 5 % when the droplet was translated into the region of thinner cladding thickness. In the region of the thinner cladding thickness transmission should decrease rather than increase. The reason for these responses can be caused by lower refractive index (20 % of glycerine) of the droplet where transmission changes only by a few percentage (from 100 % to 93 % for the smallest cladding thickness). Since the scale of the change is up to 7 %, the noise is more noticeable than the noise produced by the droplet of higher refractive index where the transmission change is up to 60 % for 80 % glycerine solution.

These experiments have shown that as the refractive index of the droplet gets closer to that of the fibre core the achievable attenuation through the fibre will be higher. The next series of experiments will utilise a liquid droplet that has the refractive index much closer to the core index and will also present how the droplet motion influences the optical transmission in more detail.

4.3 Device switching time between different levels of attenuation

One of the important properties of the device is how quickly the motion of the droplet will affect the optical transmission through the fibre. This is essentially the switching time between each droplet step and how much time is needed for the transmission to stabilize. For performing this experiment it was not vital if the fibre was polished as close as possible to the core. Timing measurements examined changes in the transmission when a droplet was moved along the interaction region of the fibre. Using a polished fibre produced in-house (as described in the previous section) and a PicoScope (analog to digital converter) sampling the photodetector output at 0.1 s intervals, the optical transmission was monitored to characterise the switching time of the device.
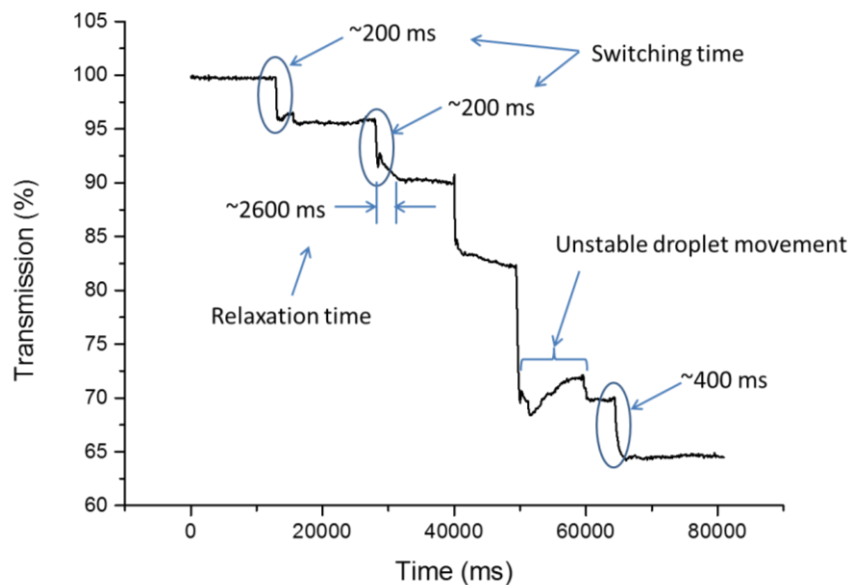

Fig. 4.11 Switching times during droplet motion along the fibre

Figure 4.11 illustrates the switching characteristics during droplet movements along the electrode array. A 2 µL droplet (92 % glycerine in water solution) was moved by applying 180 V with 1 kHz frequency to the EWOD platform. The droplet formed a 1.2 mm interaction length with the fibre (Fig. 4.12) which translates a distance equal to 600 µm with 0.07 mm gap between electrodes. During these motions the reading from the photoreceiver was captured. Transmission decreases with each of the droplet steps as can be seen on the graph (Fig. 4.11). The transmission decreases with each new droplet position along the fibre polished region due to reducing fibre cladding thickness along the polished region.

Transmission switching times vary from 200 to 400 ms as shows in Fig. 4.11. The switching time differences were an effect of the disturbed motion of the droplet, caused by higher resistance from the fibre surface, due to the polishing quality, or defects in the EWOD platform. The experimental result presented in Figure 4.11 are shown to give a general indication of switching time, which is less than 500 ms. The average speed of the droplet, translating over 600 µm in average time of 300 ms, was 0.03 m/s. This is smaller than the droplet velocity (0.13 m/s) calculated in Chapter 2.5, and the reasons of that difference are not fully understood. The theoretical calculation was based on the conditions where a surface of the EWOD platform does not have any contamination or defects and additionally in the calculation fibre resistance was not taken into account. During the experiment, the droplet was subjected to fibre resistance and additional resistance from the EWOD platform which was exposed to the outside environment where dust and moisture could settle on the surface.

The relaxation time (time needed to stabilize the level of transmission after droplet movement) for optical transmission was measured to be less than 2600 ms (Fig. 4.11). One step, between 50k ms and 60k ms of Figure 4.11, shows how the unstable droplet movement can influence the transmission. The viscosity of the 92 % glycerine droplet affected the motion, causing a perturbation during the translation, and caused the relaxation time to be longer than during other movements. Such conditions do not occur often but these events clearly impact the device performance negatively. Such situations can be avoided if the fibre polishing region is smoother and no defects are present on the surface of the EWOD platform. The settling time is an effect of the movement of the droplet; as it elongates and moves towards the next electrode and then resumes its round shape. The measured light transmission stabilizes as the droplet, once again, covers 1.2 mm of the fibre interaction

region. Despite the fact that the droplet (with a high concentration (92 %) of glycerine) has a higher viscosity (0.367 kg/ms) in comparison to water (0.0894 kg/ms), a switching time of approximately 200 ms is achievable.
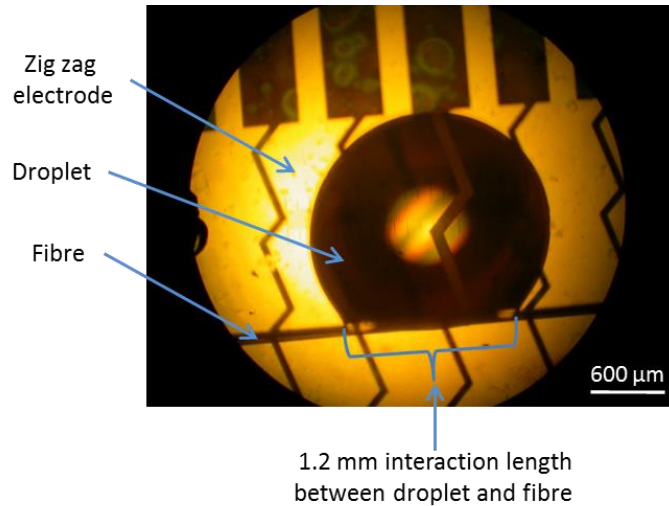
Fig. 4.12 Droplet placed on the EWOD platform and positioned along the fibre

4.4 Refractive index impact on the VOA performance

As was shown in the theoretical analysis of Chapter 3.2, the fibre transmission, the refractive index and the size of the droplet play important roles in achieving high attenuation. The refractive indices of droplets used in these experiments were in the range between 1.3538 and 1.4425; not very close to the core refractive index. Here we will focus on the refractive indices closer to the core refractive index to reach a higher attenuation and different droplet sizes to investigate the impact of the size on the device performance.

4.4.1 EWOD-VOA with commercial side polished fibre

A study of the refractive index's influence on the device performance focussed on the 2 µL droplet of glycerine solution (with a refractive index in the range of 1.4600 +/- 0.0006) in contact with the side polished fibre that was acquired from Phoenix Photonics Ltd (UK). The system was set up as discussed in Section 4.2 (Fig. 4.9) to assess the performance

of the working device. A droplet was placed at the start of the polished fibre region and then moved digitally across the electrodes and, consequently, along the fibre. The voltage was applied between two adjacent electrodes, causing the droplet to move to the live electrode, with each step of the droplet 0.6 mm.

4.4.1.1 Performance using droplet refractive index less than fibre core refractive index

Initial investigation of the refractive index of the droplet on the VOA performance was focussed on use of a glycerine solution droplet with a refractive index of 1.4596, which is slightly lower than refractive index of the fibre core (1.4600).
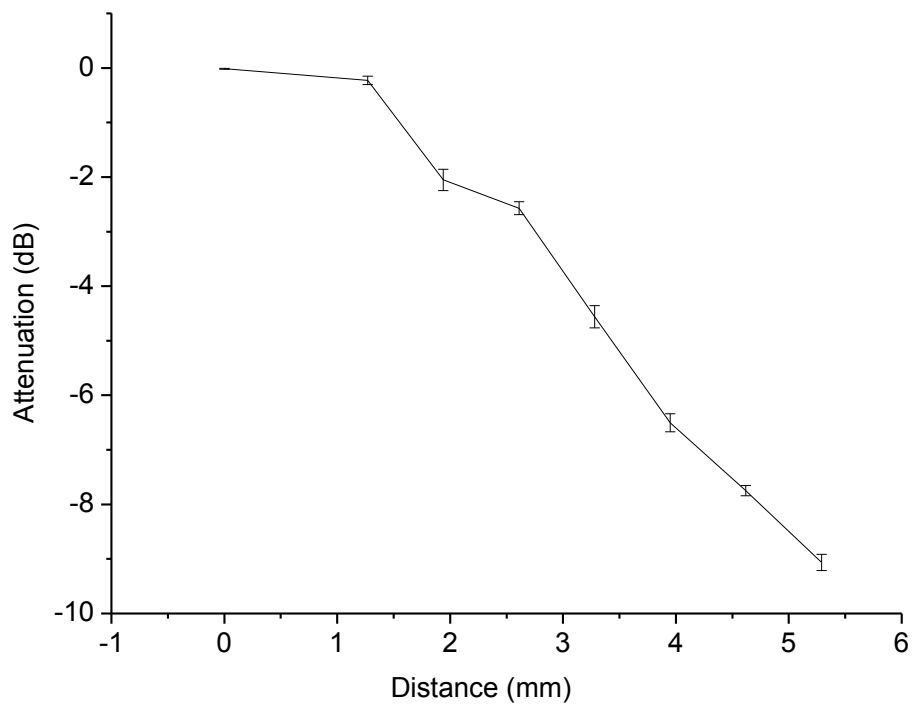
Fig. 4.13 Attenuation versus distance along the interaction length for droplet of 1.4596 refractive index

Figure 4.13 shows the change in optical attenuation as the droplet traverses the polished interaction region. The data was recorded in the time domain and then calibrated to distance. A maximum attenuation of -9 dB was achieved. The droplet moved from a region (distance = 0 mm) where the evanescent field does not interact the droplet due to full

cladding thickness to a region (at a distance = 5.5 mm - the middle point of the fibre polishing region) where the cladding thickness is reduced and the evanescent field interacts with the droplet. In comparison the maximum predicted attenuation, for this droplet refractive index and interaction length between droplet and fibre, that could be achieved was -10.6 dB, according to theoretical analysis (Section 3.2.2.1). From the achieved maximum attenuation, the conclusion can be made that the fibre cladding was not polished to the core and that some remaining cladding was left on the top of the core. It can be estimated that for an attenuation of -9 dB the remaining cladding thickness is around 0.3 μm for a 1.4596 droplet refractive index. For the data shown in Figure 4.13 the standard deviation is in the range between ~ ± 0.1 dB to ~ ± 0.2 dB. This indicates that the results are repeatable and that similar results in each test were obtained. The differences in each test could arise from differing droplet positions during translation, instability of the external environment in the laboratory, such as temperature changes causing droplet evaporation (which would decrease the size of the droplet and change the glycerine concentration and refractive index).

4.4.1.2 Performance using droplet refractive index close to the core refractive index

If the droplet refractive index exactly equals the core refractive index (1.46) the attenuation according to the theoretical results will significantly increase from -10 dB to around -37 dB. The experimental setup of Fig. 4.9 was now used in conjunction with an external medium (droplet) of 1.4602 refractive index. Again, the droplet was moved across the EWOD platform digitally by applying electric potential to the individual electrodes.
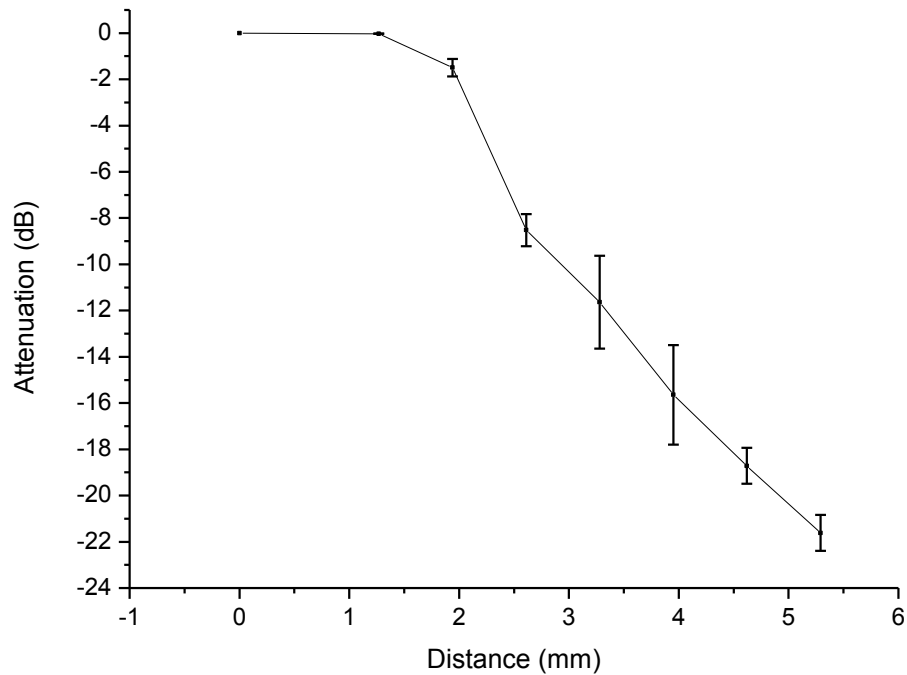
Fig. 4.14 Attenuation versus distance along the interaction length for droplet of 1.4602 refractive index

During droplet translation along the fibre the optical attenuation increased as shown on Fig. 4.14. The attenuation reaches a maximum of around -22 dB. From the theoretical analysis the maximum attenuation that can be achieved for this refractive index is -28 dB. As stated previously it is theorized that the fibre was not polished down to the surface of the core and some remaining cladding was left on the top of the core. The remaining cladding had an estimating thickness of around 0.2 μm for the -22 dB. From Figure 4.14 it can be seen that for the last point (-22 dB) of the attenuation slope the error bar is around ± 1 dB. When the cladding thickness is reduced below 3 μm and the droplet refractive index is close to the core refractive index (fourth decimal place differences from 1.4600), the fibre is more sensitive and any disturbance can influence the transmission (theoretical analysis confirmed that in Section 3.2.2). In this experiment it can be seen that the standard deviation for any of the attenuation results are bigger than in the previous experiment. For a droplet refractive index of 1.4596 it falls in the range ~ ± 0.5 dB to ~ ± 1 dB. The larger standard deviation could be the result of more sensitive behaviour of the fibre due to the external refractive index being closer to the core refractive index.

4.4.1.3 Performance using droplet refractive index higher than core refractive index

For completeness the refractive index of the external liquid was changed towards a higher refractive index than 1.4602 (from previous subchapter 4.4.1.2). The refractive index that was chosen for the following experiment was 1.4606.

Figure 4.15 shows the change in attenuation when the droplet alters position along polished region of the fibre. As can be seen, the maximum attenuation achieved was approximately -12.5 dB and the standard deviation is in the range between ± 0.1 dB to ± 0.5 dB. The maximum attenuation that was achieved is lower than the attenuation of ~-17 dB that was achieved using ideal conditions, as was presented in theoretical calculations (Section 3.2.2.1). As noted previously, the fibre was not polished to the surface of the core and therefore the attenuation is not as high as was predicted for the ideal conditions. Again, calculation of the remaining core cladding which yields an attenuation of -12.5 dB results in an estimated value around 0.3 µm, which is similar to the previous results for external refractive indices of 1.4596 and 1.4602. The three sets of measurements show consistency in the estimate of cladding thickness.
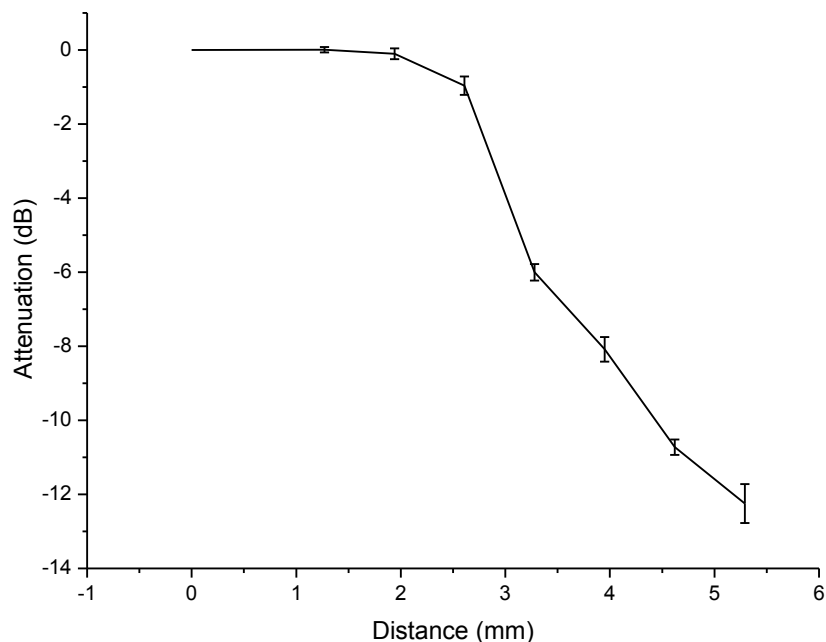

Fig. 4.15 Attenuation versus distance along the interaction length for droplet of 1.4606 refractive index

4.4.1.4 Comparison of three refractive indices

To provide a visible comparison between the refractive index variations, Figure 4.16 shows the three results of the three experiments presented together. As can be seen, the highest attenuation was achieved for the 1.4602 refractive index then for the 1.4606 refractive index and the smallest achieved attenuation for the refractive index of 1.4596 (all refractive index of the droplets were measured at the wavelength of 589 nm). The conclusion can be made that the external refractive index required to achieve the highest attenuation, as was described in Chapter 3.2.2.1, needs to be very close to the refractive index of the core (1.46 for the wavelength of 1550 nm).

The variations (0.2 μm to 0.3 μm) in the cladding thickness calculated from the achieved maximum attenuation for each of the experiments of different refractive indices (for the same fibre), suggests that there is an error that could be caused by potentially differing experimental conditions. The experimental condition could be sensitive to laboratorial temperature that could be different when experiments were performed (the temperature difference between the summer and winter time in laboratory was about 6°C).
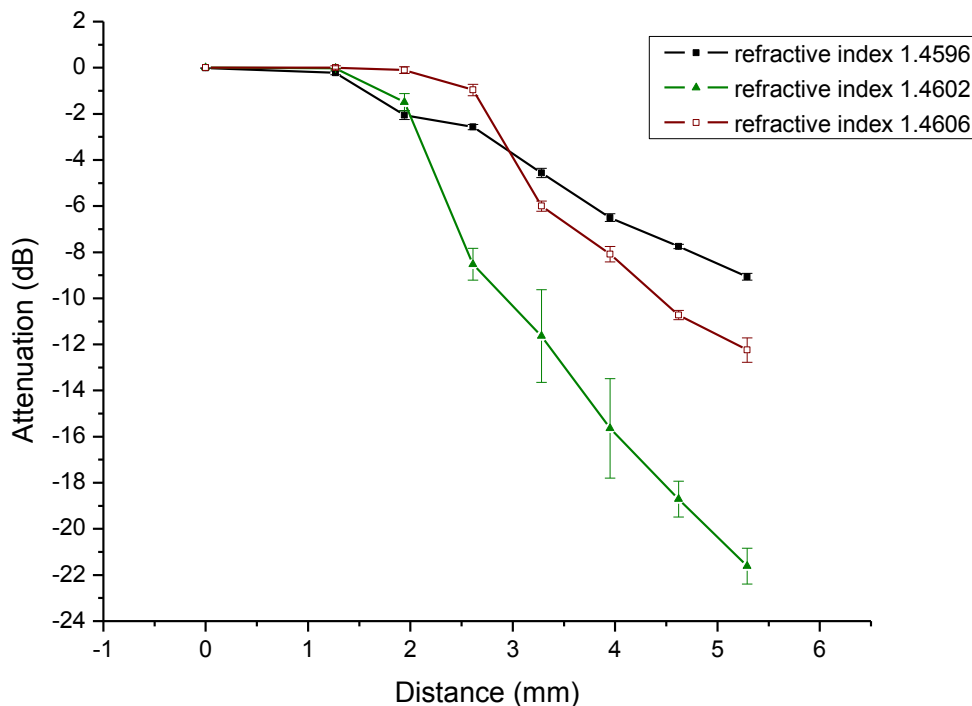

Fig. 4.16 Comparison between the results for three different refractive indices of external liquid

4.4.1.5 VOA broadband operation

One of the goals for this VOA design was that the device needs to operate as a broadband attenuator. To achieve this goal the attenuation levels for a range of wavelengths should be constant, as quantified by a wavelength dependent loss (WDL) close to zero. Wavelength dependent loss describes the variation of the insertion loss over a wavelength range[11].

An experimental system shown in Fig. 4.17 was designed to measure the spectrum of wavelengths between 1520 to 1560 nm. An EDFA was used as a light source to supply light of the desired wavelength range to one end of the fibre, while the other end of the fibre was connected to the OSA. A 180V (1 kHz) square wave signal was supplied to the array of electrodes on the EWOD platform by a waveform generator (Agilent 3228A) and subsequently amplified (A400, FLC Electronics). The spectrum received by the OSA for each droplet position was displayed and recorded on the computer.
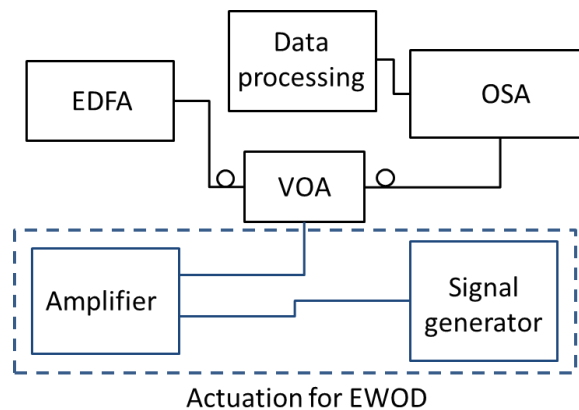
Fig. 4.17 Setup of experiment for recording VOA broadband operation

A 2 µL glycerine water solution droplet, of refractive index 1.4602, was placed on the EWOD platform and sequentially moved in 0.6 mm steps by the electric field from one end of the polished fibre region to the centre of this region. The droplet made contact with a 1.2 mm length of the fibre in each of the positions.

Figure 4.18 shows the broadband nature of the VOA device. Each line of different colour characterises a different position of the droplet, resulting in steps of attenuation from around 0 dB towards to -22 dB.
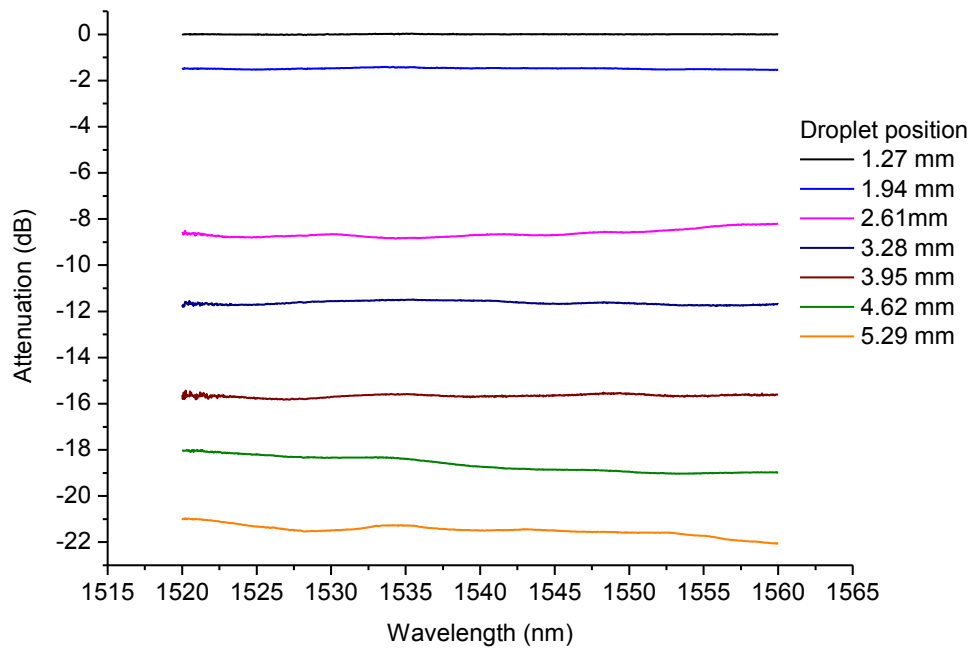
Fig. 4.18 Broadband spectrum for the external liquid of 1.4602 refractive index measured with optical spectrum analyser
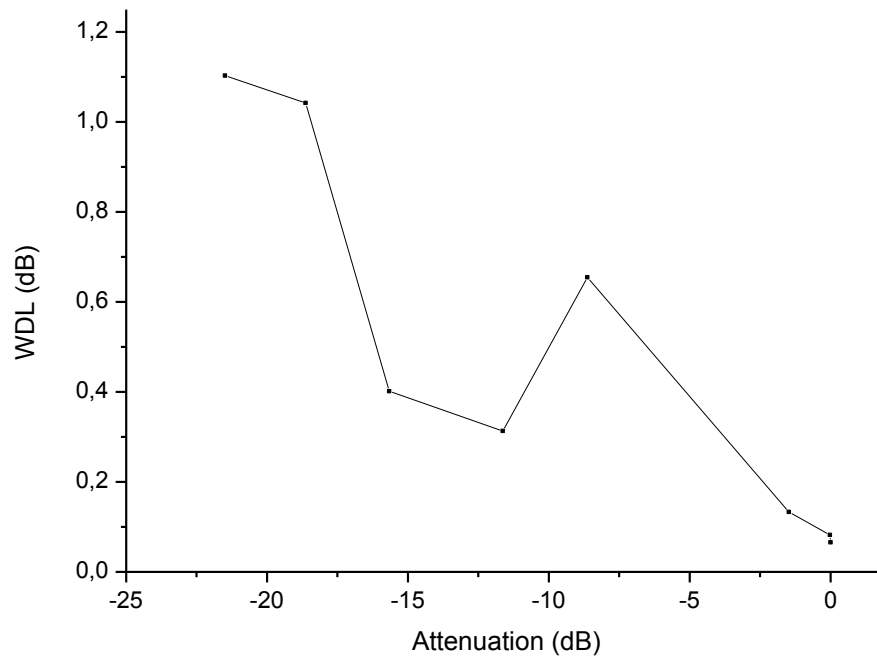
Fig. 4.19 Wavelength dependent loss for different attenuation for droplet of refractive index 1.4602

At the highest attenuation of around -22 dB the WDL reaches a value of 1.1 dB, while for a lower attenuation of approximately -11 dB the WDL is reduced to only 0.3 dB (Fig. 4.19). This level of WDL is comparable to other published research on VOAs where the WDL is noted to vary from 0.04 dB[12] to 1.2 dB[13]. Typical values cited for commercial VOAs can vary between 0.3 dB to 1.4 dB[14].

A further experiment using this equipment was focused on the wavelength dependence of the device due to a different refractive index of the external liquid. The second refractive index that was used (1.4606) was higher than the previous refractive index (1.4602), placing it further away from the refractive index of the core (1.4600) and reducing the expected attenuation levels which could be achieved.
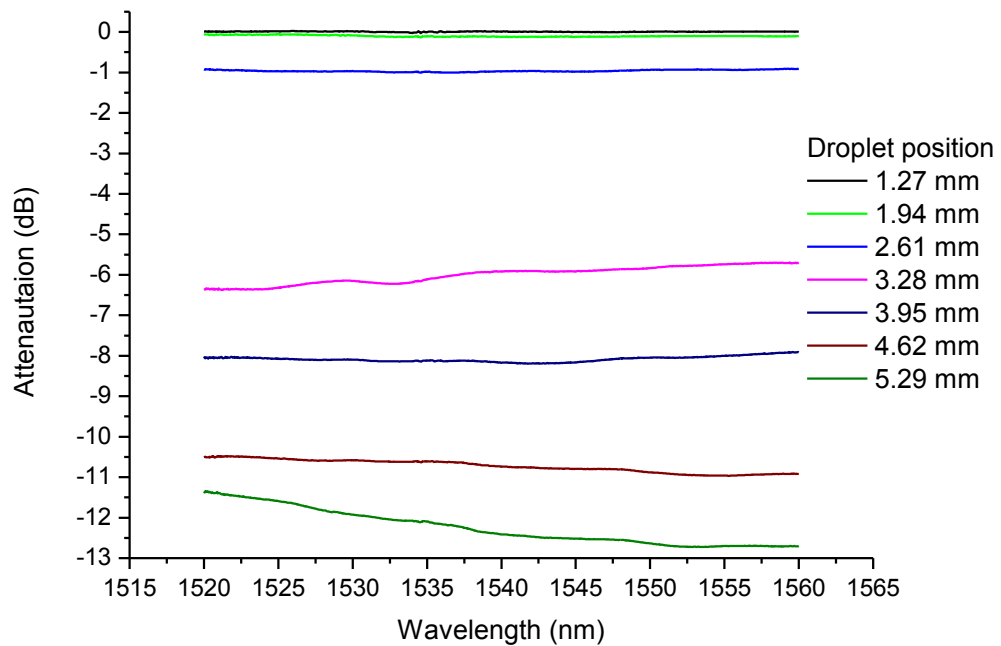
Fig. 4.20 Broadband spectrum for the external liquid of 1.4606 refractive index measured with optical spectrum analyser

As can be seen from Figure 4.20 the highest attenuation that was achieved for this refractive index is in the range of – 11.5 dB to -13 dB.

WDL for the maximum attenuation (-12 dB) reaches 1.4 dB and for the rest of the droplet positions the WDL varies between ~0.1 dB to ~0.7 dB (Fig. 4.21). Once more a higher WDL is seen for the maximum attenuation, where the fibre has the thinner cladding thickness

and is strongly sensitive to the external environment with any disruption in this area influencing on the achieved results. As can be seen in Figures 4.18 & 4.20, higher WDL is visible when the attenuation is bigger for example for the 1.4602 refractive index when the attenuation reaches -22 dB and for 1.4606 refractive index when attenuation reaches -12 dB. The higher value of WDL in this point can be a result of the drastic change of the remaining cladding thickness and in that position fibre is facing higher sensitive for any disturbance.
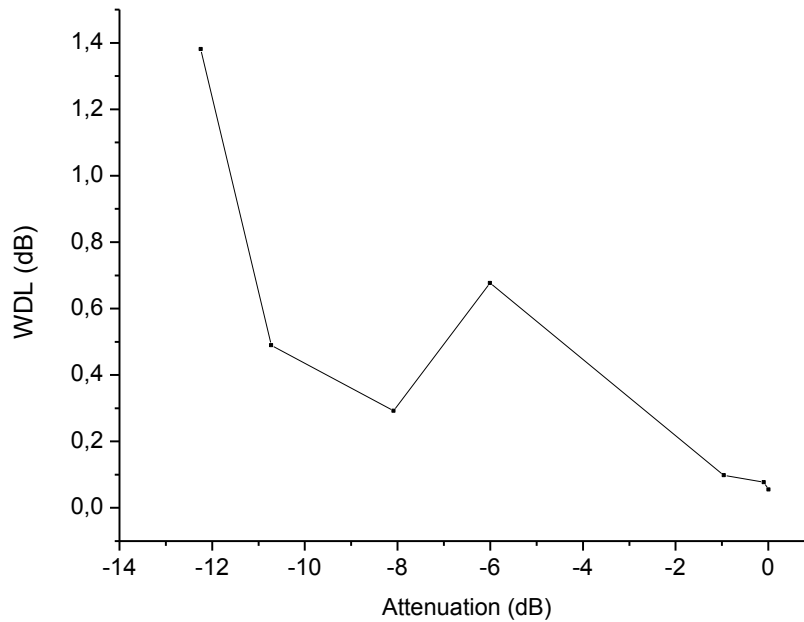
Fig. 4.21 Wavelength dependent loss for different attenuation for droplet of refractive index 1.4606

4.4.2 Polished fibre produced in-house

It was stated earlier that the polished fibre to be used in the VOA can also be fabricated in-house. The main reason for in-house fibre fabrication was to gain control of the polishing depth, at the expense of the poorer quality of the polished surface, when compared to commercial fibres. As presented above, the maximum attenuation that can be achieved with fibre acquired from the company Phoenix Photonics Ltd (UK) was -22 dB but theory predicts that the attenuation should reach a maximum of -28 dB when the core of the fibre

is completely exposed to the outside environment. Several fibres were produced in-house and tested to investigate the attenuation levels and the polishing depth of the fibre.

4.4.2.1 Impact of the polishing depth of the fibre

Two in-house side polished fibres were tested: placed on the EWOD platform, with the polished side facing toward the droplet which was positioned on the start of the electrodes array. Light was injected into the fibre from the broadband EDFA source and the optical power emitted from the other end of the fibre was monitored with the photoreceiver (Fig. 4.9). The droplet was moved electrically across the electrodes of 600 μm width.

The following results were obtained from the two different fibres using a 2 μL glycerine-water droplet of refractive index of 1.4596. The attenuation of the fibres was recorded in real time as the droplet moved step by step, along the electrode array. Fibre 1 was polished deeper and the attenuation increased from ~ 0 dB to a maximum of around -13 dB. Fibre 2 had more cladding remaining in the polished region of the fibre and attenuation increases to only -5 dB (Fig. 4.22)[15]. The obtained maximum attenuation according to the theoretical analysis (Chapter 3.2.2.1) translates to a cladding of 0.6 μm for fibre 2 and to around 0.01 μm for fibre 1.
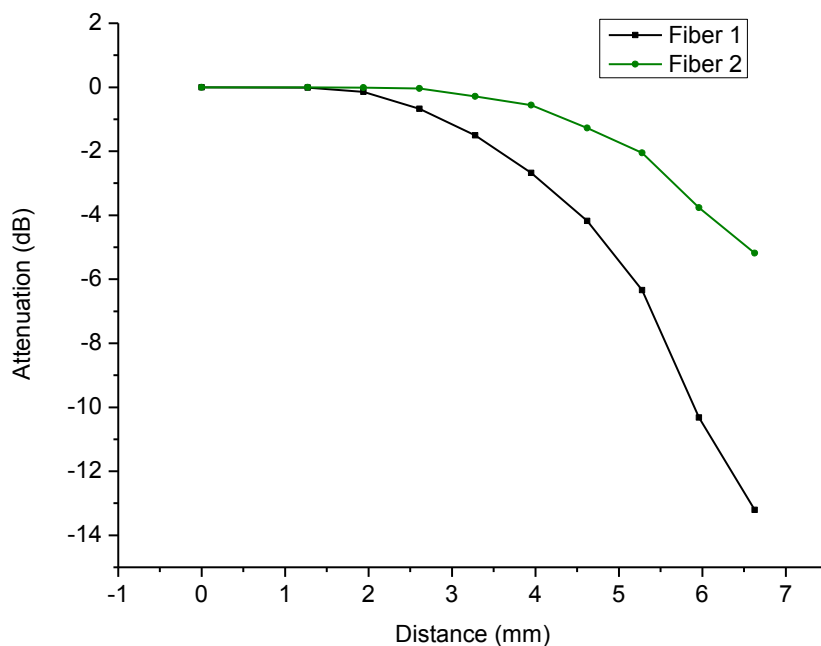
Fig. 4.22 Attenuation through two fibres of different polished depth

From Figure 4.22, it can be concluded that the polishing depth is very critical in reducing the transmission and achieving high attenuations. A difference of 0.6 μm results in 8 dB difference of the attenuation for this refractive index of the droplet.

As the fibres are manufactured in-house there is no dedicated equipment to measure the polishing depth. The polishing depth was monitored only by the power change recorded by a powermeter (FiberHome Technologies Group) during the fabrication process. The reproducibility varied from fibre to fibre and the following results will focus on the VOA using the fibre whose cladding was polished closest to the core and achieved the highest attenuation.

4.4.2.2 Impact of higher refractive indices than core refractive index on the performance of the device with in-house fabricated fibre

Light from an EDFA was launched into the in-house fabricated fibre and monitored at the output end by an optical spectrum analyser (OSA) (Fig. 4.17). Using the same fibre, performance of the VOA was measured for two droplet concentrations: one droplet had a refractive index of 1.4602 and the second had a refractive index of 1.4606.
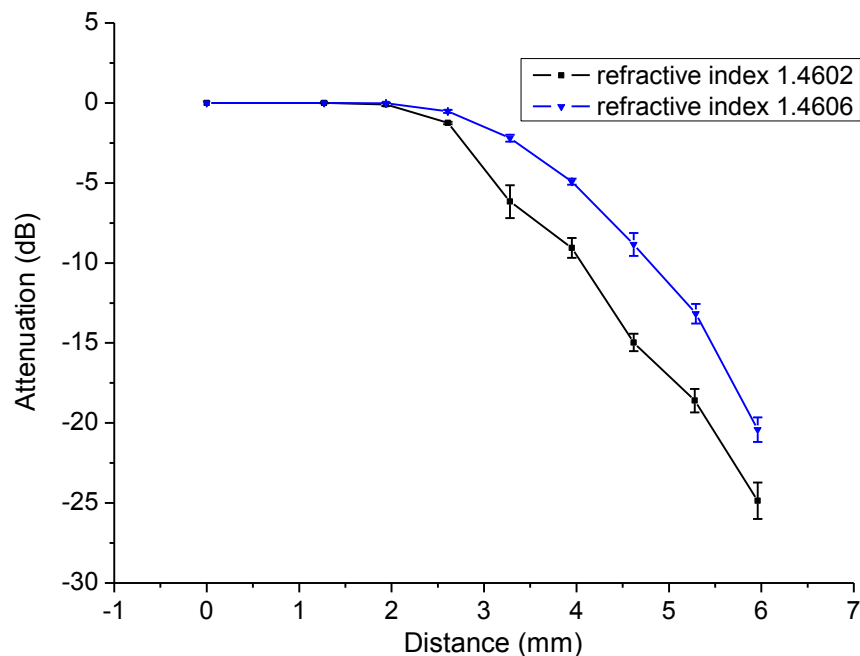
Fig. 4.23 Attenuation change over the interaction distance of the fibre for two refractive indices of external liquid

As can be seen above in Figure 4.23, a higher attenuation was achieved for a droplet with a refractive index of 1.4602, where the attenuation level reached a value of -25 dB. In comparison, the 1.4606 refractive index droplet achieved only a -20 dB attenuation. According to theory, the highest attenuation expected for the 1.4602 refractive index droplet (2 μL, 1.2 mm interaction length) is around -28 dB. Using the theoretical analysis presented in Chapter 3 (Section 3.2.1) the remaining cladding on the fibre is estimated to have a thickness of 0.13 μm. This is less than the remaining cladding thickness of the commercially polished fibre (0.3 μm) that was used in the previous experiments (Chapter 4.4.1.4).

4.4.2.3 VOA broadband operation

The wavelength dependent loss of the in-house fibre was measured over the optical band from 1520 nm to 1560 nm. As before the optical spectrum of the fibre was monitored by the OSA in experimental setup defined as on the Figure 4.17.
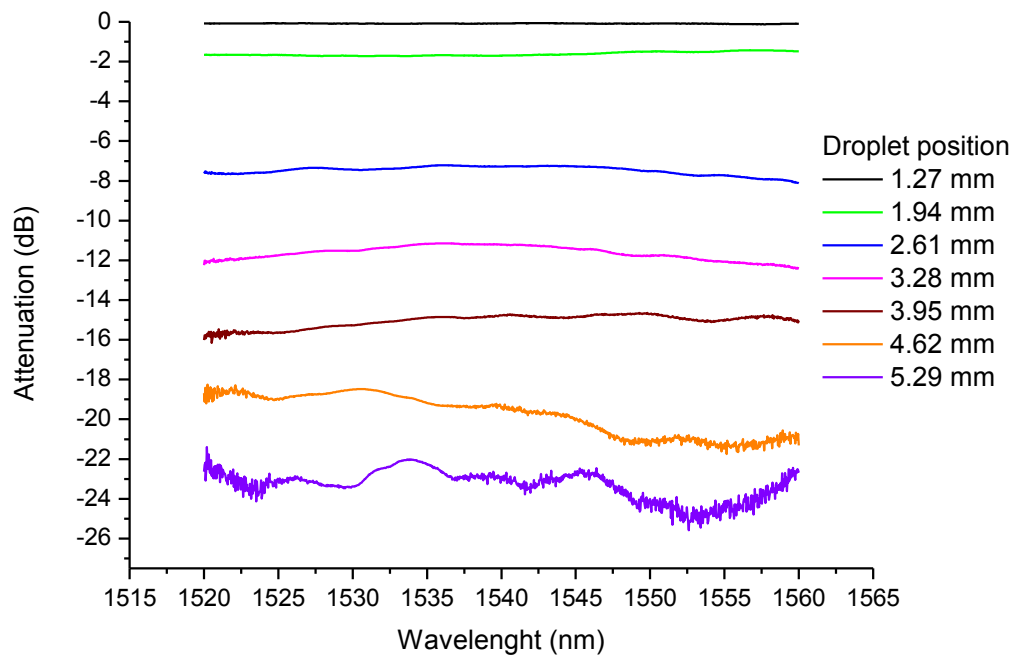
Fig. 4.24 Wavelength dependent loss of EWOD-VOA for the droplet of the refractive index of 1.4602

The presented graph (Fig. 4.24) above shows the wavelength dependent loss (WDL) for the droplet of refractive index 1.4602. As the droplet was moved closer to the core the attenuation increased, but the fibre also became more sensitive to changes in the outside environment, causing the addition of noise. The noise is visible on the spectrum especially at the highest attenuation location of the droplet.
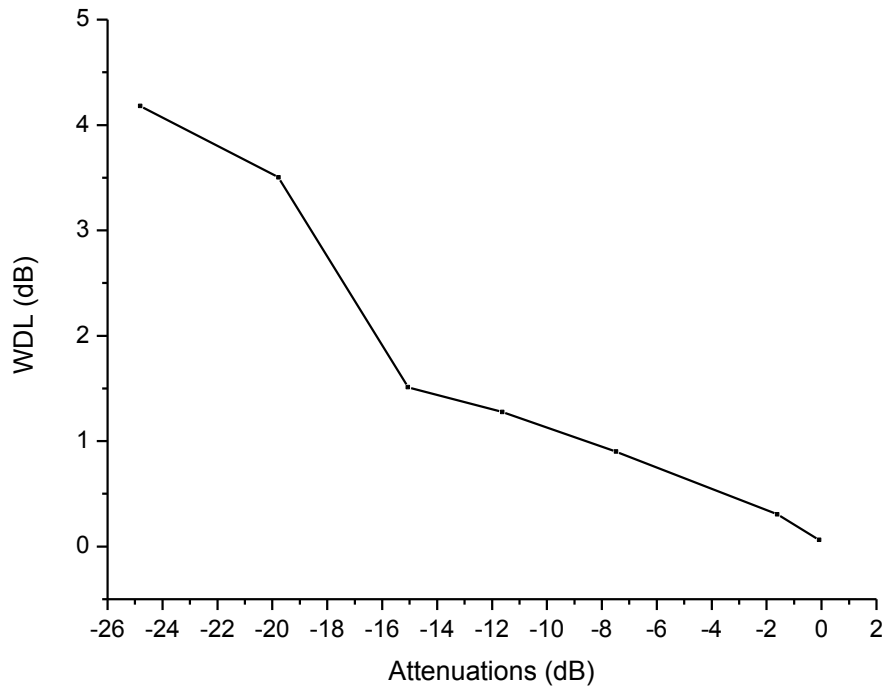
Fig. 4.25 WDL for different attenuations achieved by the EWOD-VOA that used liquid of 1.4602 refractive index

Figure 4.25 shows how the WDL changed as the attenuation changed. As before, the highest attenuation exhibits the highest WDL. For -25 dB attenuation, WDL reaches 4.2 dB, which is higher than that recorded for the commercial Phoenix fibre, where the highest achieved attenuation -22 dB resulted in 1.1 dB WDL. The variation could be a result of the improved polished surface quality of the commercial fibre.

The polished surface quality is also an important factor when the surface has micropores or bulges. When the surface is of poor quality, a droplet can leave a residue behind causing the attenuation steps to reduce and measurement errors to occur. Another problem associated with a poor surface quality is the droplet velocity has a reduced consistency and is more prone to adhere to the surface as it translates along the fibre.

In conclusion, it was proved that remaining cladding thicknesses on the core surface have negative impacts on the achievable attenuation performance of the VOA design. As the residual cladding of the fibre becomes thinner the attenuation approaches the theoretical results. Changes of the refractive index of the external liquid also have an impact on the attenuation and this was verified by the VOA using the commercial Phoenix fibre. As theory predicted, the closer the refractive index of the droplet is to the refractive index of the core of the fibre the higher an attenuation can be achieved by the VOA. However, the quality of the polished fibre surface can influence the results and it is important to take this into consideration during the design of the VOA. Work for future VOA designs will need to include improvement of the in-house production process to obtain a smoother surface with the desired cladding thickness on the top of the fibre.

4.5 Profile of the polished region of the fibre

During fabrication of the polished region, a fibre is placed in contact with a rotating polishing wheel, and weighted to applying tension and to maintain contact with the polishing wheel. The polishing procedure leads to the creation of a slope on the polished cladding surface of the fibre. It is difficult to directly measure the profile of the polished region of the fibre where the thickness changes by only a few microns over a length of several millimetres. In fact the measured attenuation as a function of droplet position is one way of performing such a measurement. In order to demonstrate the effect and the importance of the cladding thickness profile on the characteristics of the VOA, the theoretical curves for the attenuation as a function of droplet position for linear and quadratic profiles have been computed in order to compare them with the experimental results. The profile which gives a best linear fit to the experimental data has also been derived.

The best linear fit has been calculated from the results that were obtained for the VOA with commercial Phoenix fibre and glycerine droplet of refractive index 1.4602. The linear fit was proposed for the region where the attenuation significantly decreased (Fig. 4.26).
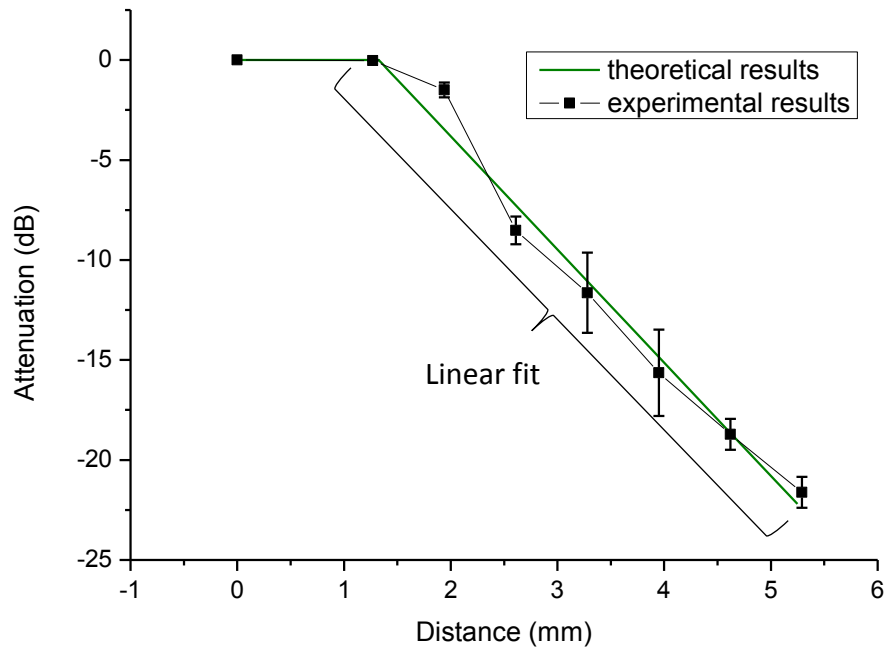
Fig. 4.26 Linear best fit to the experimental results for the VOA with Phoenix fibre and droplet of 1.4602 refractive index

From the linear fit it was possible to calculate the profile of the polished region of the fibre according to the theoretical analysis discussed in Chapter 3.2.1. From equations 3.6 and 3.7, in Chapter 3.2.1 the attenuation is a function of the remaining cladding thickness and can be written as:

$$Attenuation = f(s) \tag{4.1}$$

and from the experimental data with a linear fit, we also know that:

$$Attenuation = a * d_f + b \tag{4.2}$$

where d_f is the distance along the fibre, a is the gradient and b is the intercept taken from the linear fit. Rearranging (4.2) to find the thickness profile for the experimental data gives:

$$d_f = \frac{f(s) - b}{a} \tag{4.3}$$

From the above equations it is possible to derive how the cladding thickness changes over the distance where the fibre is sensitive for an external medium and hence to find the profile of the interaction region.
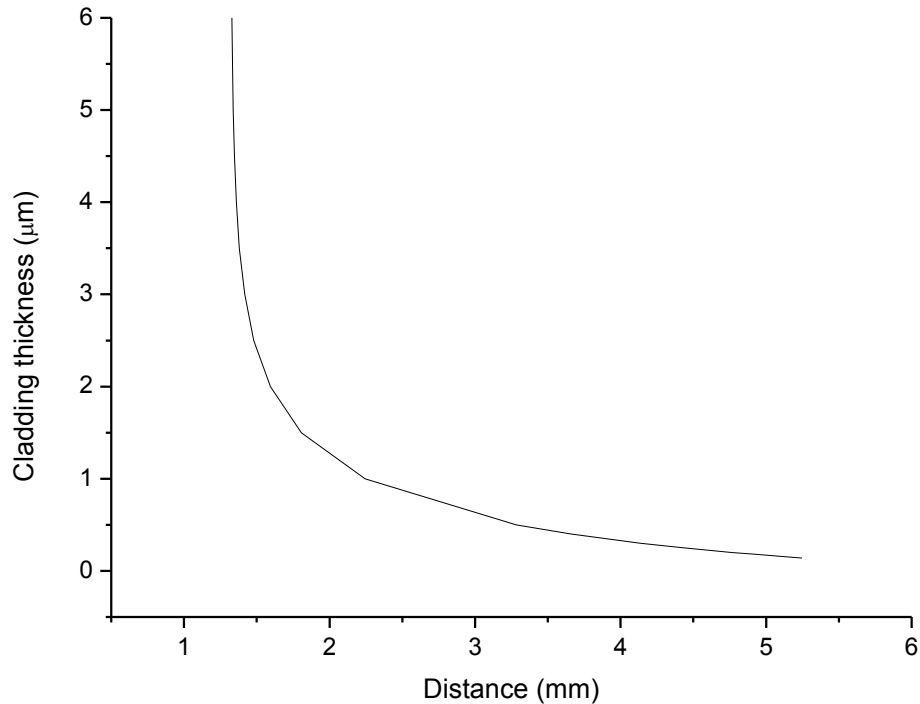
Fig. 4.27 Profile of the polished region of the Pheonix Ltd fibre

From the figure above (Fig. 4.27), it can be seen that the cladding surface does not change linearly and has a non-uniform decrease of thickness along the interaction region. The maximum cladding thickness where the attenuation change can be measured is 6 µm. Above that value the attenuation is not changing significantly as the cladding thickness is too thick for the evanescent field to be exposed to the outside environment, therefore the droplet of higher refractive index than refractive index of the core does not affect the evanescent field and hence the attenuation. The conclusion from this analysis is that the VOA effect can only be exploited when the cladding surface is between 6 µm and 0 µm.

A similar analysis of the fibre polishing profile can be done with the fibre fabricated in the laboratory. Additionally, the graphical representation of the calculated polishing profile of that fibre can be compared with the profile of that measured from the microscope photography fibre diameter (fibre photograph from Appendix 2).
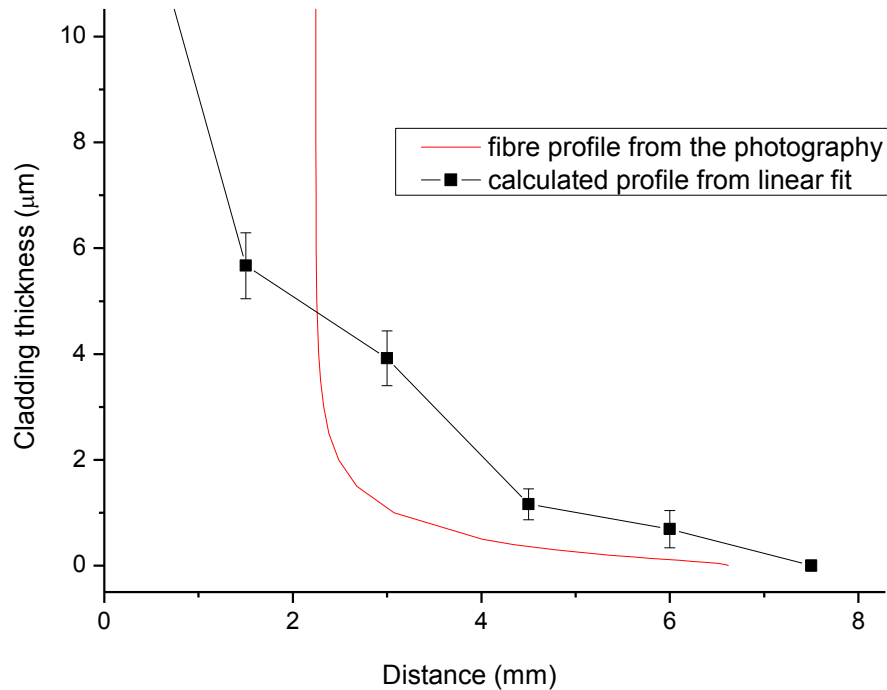
Fig. 4.28 Profile of the polished region of the fibre manufactured in the laboratory

From Figure 4.28 it can be seen that the measured profile from the microscope photograph does not diverge much from the calculated profile for the linear fit. The linear fit was calculated from the results presented on Figure 4.23, droplet of refractive index 1.4602. Both obtained profiles follow the same shape. It needs to be noted that the most accurate obtained values for linear fit are when the cladding thickness is less than 3 µm (the most sensitive region) where for the profile obtained from the fibre photography is more precise than for measurement above 3 µm.

Every fibre can differ and therefore the shape of the polished region can vary. For completeness, linear and quadratic shapes of the cladding profile will be presented.

The linear decrease of the cladding considers an axial distance of around 5.5 mm where the cladding changes between 6 µm and 0 µm (Fig. 4.29). The production of this shape will not be possible with a polishing wheel but some special process and equipment would be needed to implement the design. Another approximation that can be made is that the cladding profile exhibits a quadratic shape, where the cladding thickness will decrease accordingly with the quadratic curve (Fig. 4.29).
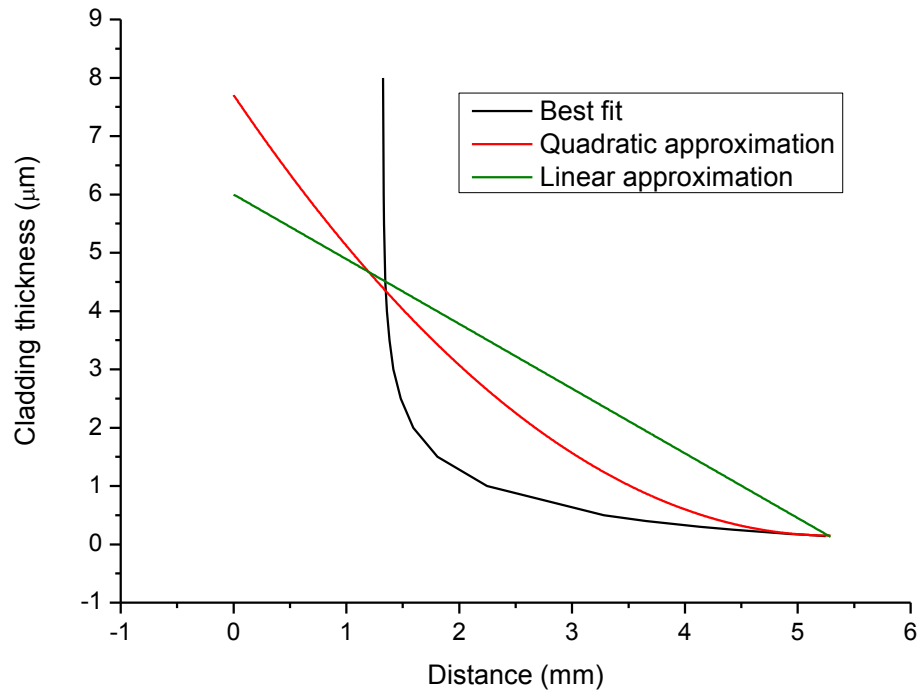
Fig. 4.29 Different approximations of the cladding decrease over the polished fibre region

It is possible, using these polished surface profiles to theoretically derive the change in the attenuation along the interaction region. The three different cladding profiles show how a small change in the polished profile can influence the attenuation characteristics of the VOA device. Figure 4.30 presents how different shapes of polishing region differ in their effects of the signal attenuation. Theoretical attenuation results for the linear and quadratic cladding thickness profiles diverge significantly from the experimental results. It is clear that neither of these two shapes are demonstrating a match to the shape of the Phoenix fibre's profile. Only the linear attenuation approximation derived from the experimental results, giving a polynomial shape for the cladding profile, accurately models the slope shape of the polishing region of the fibre. These results clearly prove the impact and the significance of the remaining cladding thickness profile on the operational characteristics of the VOA.
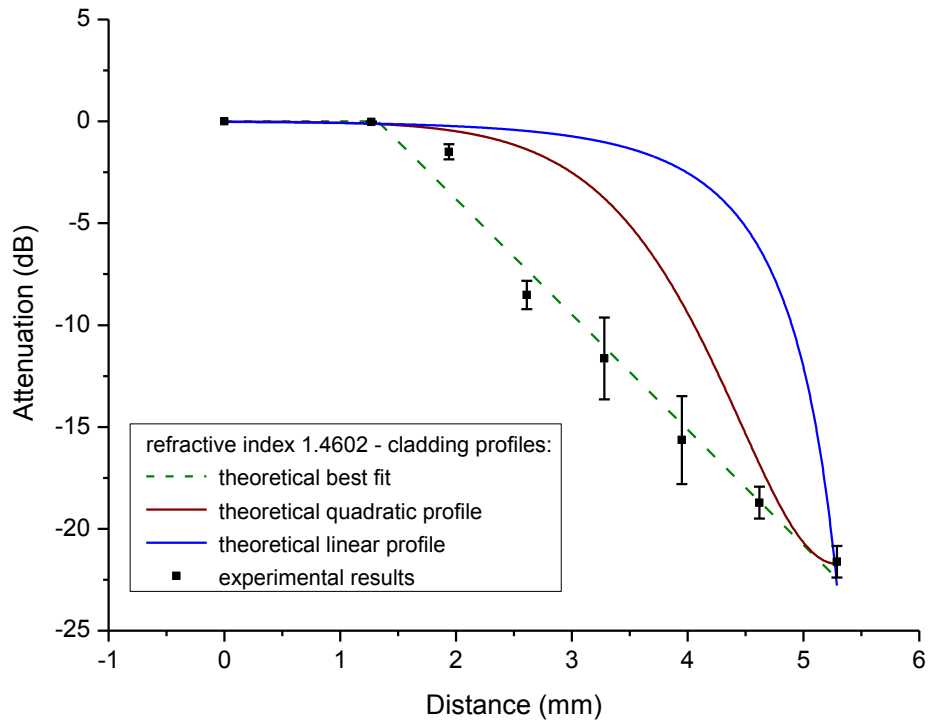
Fig. 4.30 Theoretical and experimental results of the optical attenuation through a polished single mode fibre according to the 2 µL droplet of 1.4602 refractive index position

4.6 Effect of droplet size on EWOD-VOA

Previously, the impact of fibre polishing depth and the refractive index of the droplet of the VOA performance was discussed. In this section the discussion will focus on the size of the droplet and its influence on the maximum attenuation achieved by the VOA. It should be noted that for simplicity here the "droplet size" will be taken as the interaction length between the droplet and the polished surface of the fibre. It has been shown in Chapter 3.2.2.3 that the size of the droplet has an impact on the maximum attenuation that can be achieved. Comparing different sizes of droplets shows that the attenuation achieved for the bigger droplet (1.2 mm to 2.4 mm interaction length) will reach higher attenuation than the droplet of much smaller size (0.6 mm to 1.0 mm interaction length).

Six different sizes of droplet were used in the VOA with each volume of droplet exhibiting a different interaction length along the fibre. In each case the EWOD platform had

different electrodes and gaps size (Tab. 4.3) to accommodate the different droplet dimensions.

Table 4.3. Relationship between droplet size and electrowetting on dielectric platform size

Droplet size	Interaction length between droplet and fibre	Electrode size	Gap size
0.3 μL	0.6 mm	300 μm	50 μm
0.7 μL	0.8 mm	400 μm	50 μm
1 μm	1.0 mm	600 μm	70 μm
2 μL	1.2 mm	600 μm	70 μm
3 μL	1.6 mm	1000 μm	70 μm
4 μL	2.4 mm	1000 μm	70 μm

The interaction length between droplet and fibre was measured using a microscope. Firstly, a droplet was placed on the electrowetting platform, in contact with the fibre. Next, the VOA was placed under the microscope, where an image was taken. The image was transferred to a CAD program (Autodesk AutoCad) where the interaction length could be measured using the known reference value of the electrode width. Some examples of the different interaction lengths are presented below in Figure 4.31.

a) 300 μm — 0.6 mm interaction length between droplet and fibre
b) 400 μm — 0.8 mm interaction length between droplet and fibre
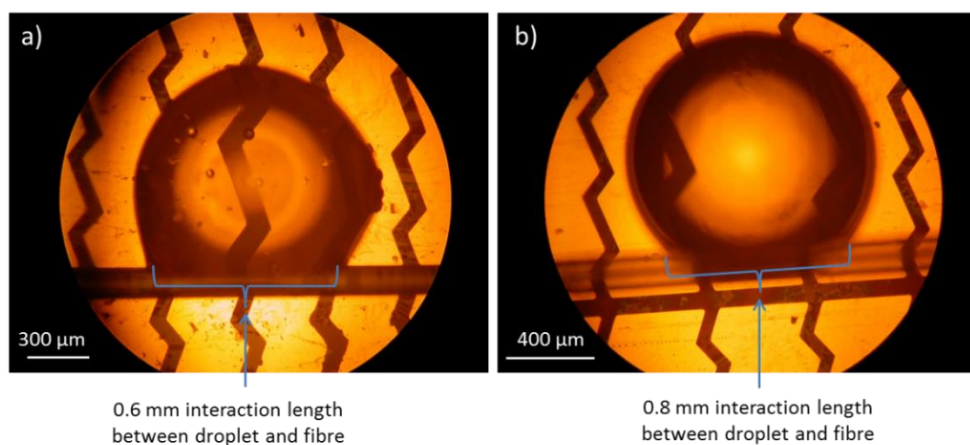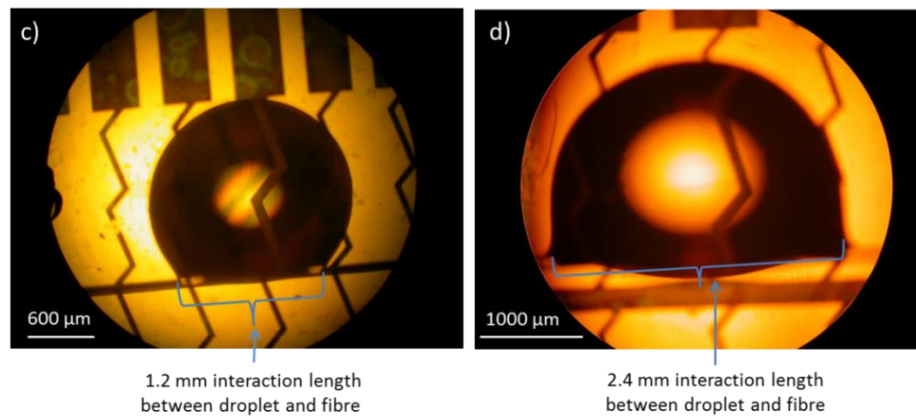
Fig. 4.31 Examples of the different interaction length for droplet of volumes a) 0.3 μL, b) 0.7 μL , c) 2 μL and d) 4 μL

In each of the experiments a droplet of the appropriate size was placed at the start of the interaction region of a fibre and moved by electric field application along the polished region. The voltage applied to the electrodes varied according to the size of a droplet. For the smaller droplets (0.6 mm to 0.8 mm interaction length), the voltage used was 160 V (1 kHz square wave), for the middle sized droplets (1.0 mm to 1.2 mm interaction length) 180 V was used (1 kHz square wave) and for the biggest droplets (1.6 mm to 2.4 mm interaction length) 200 V (1 kHz square wave) was required. Light from an EDFA was launched into the fibre and received at the other end by the photoreceiver (LNP-2, Optosci Ltd, UK).

4.6.1 Commercial polished fibre with 0.6 mm and 1.2 mm droplets

In a comparative experiment a commercial Phoenix fibre with a superior polished surface quality was employed to try and achieve a more consistent droplet motion (using a 0.3 μL droplet). The refractive index of the droplet was 1.4596 and as the droplet was translated along the polishing region of the fibre, it was found that the attenuation did not increase significantly until 4 mm of the polished region had been traversed (Fig. 4.32). Clearly the size of the droplet has a significant impact on the change of the attenuation. The attenuation change for a 0.6 mm droplet becomes apparent from the 4 mm point onwards whereas a 1.2 mm droplet of the same refractive index causes change of the attenuation at

1.27 mm from the start of the polished region. The 0.6 mm droplet caused the attenuation to increase to -3.5 dB where the 1.2 mm droplet caused attenuation of -9 dB (Fig. 4.32).
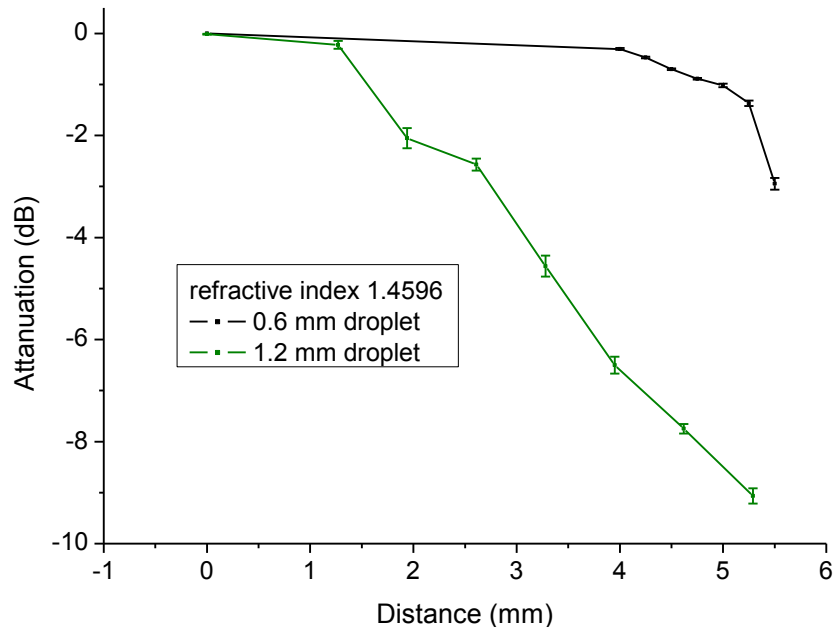
Fig. 4.32 Attenuation changes over the fibre polishing region for 0.6 mm and 1.2 mm droplets

For comparison, theoretical analysis of an ideal VOA indicates that the maximum attenuation for a 1.4596 refractive index, 1.2 mm droplet is -11 dB while for 0.6 mm droplet is -5 dB. The remaining cladding thickness, estimated using the 1.2 mm droplet's maximum attenuation of -9 dB, is around 0.3 µm and using the 0.6 mm droplet results, is 0.4 µm. Experimental and theoretical results therefore agree that if a droplet has a shorter interaction length with fibre, the attenuation will be smaller.

4.6.2 In-house polished fibre with 0.8 mm – 2.4 mm droplets

The theoretical analysis also indicates that the attenuation should increase further when the droplet size increases beyond 1.2 mm. Experiments for different sizes of droplet larger than 1.2 mm were conducted to confirm that this was the case in a real device. The size of the droplet was increased from 0.7 µL (0.8 mm interaction length), through 1 µL (1 mm interaction length), 2 µL (1.2 mm interaction length) and 3 µL (1.6 mm interaction length) to 4 µL (2.4 mm interaction length). The VOA was built with the fibre produced in-house using

droplets of 1.4602 refractive index. The maximum predicted attenuations should increase from -18 dB (for the 0.8 mm droplet) to -55 dB (for the 2.4 mm droplet).

The light from a broadband EDFA source was injected into the fibre and was detected using the OSA. Five sets of experiments with the same fibre were performed for different droplet sizes, each with a refractive index of 1.4602. The 0.8 mm droplet was moved on a 0.4 mm wide electrode array, 1.0 mm and 1.2 mm droplets were moved on 0.6 mm wide electrodes, and 1.6 mm and 2.4 mm droplets were moved on 1.0 mm wide electrodes. As was predicted by theory, attenuation will increase for larger droplets but only until an interaction length of 1.2 mm is reached; beyond that size it was discovered that attenuation did not increased further. The attenuation for the droplet of sizes from 0.8 mm to 1.2 mm reached values that do not differ very much from the values predicted by the theoretical calculations. Droplets of 0.8 mm reached maximum attenuation values of -16 dB and theory claims that attenuation should reach -18 dB. In comparison, the attenuation for 1.6 mm droplets was equal to the 1.2 mm droplet results and 2.4 mm droplets reduced attenuation by 4 dB compared to the 1.2 mm droplet results. (Fig. 4.33). Inaccuracies in the results could be due to experimental error, especially for the smaller droplet (1.2 mm) where the maximum attenuation exceeds the maximum predicted theoretical attenuation of -28 dB.
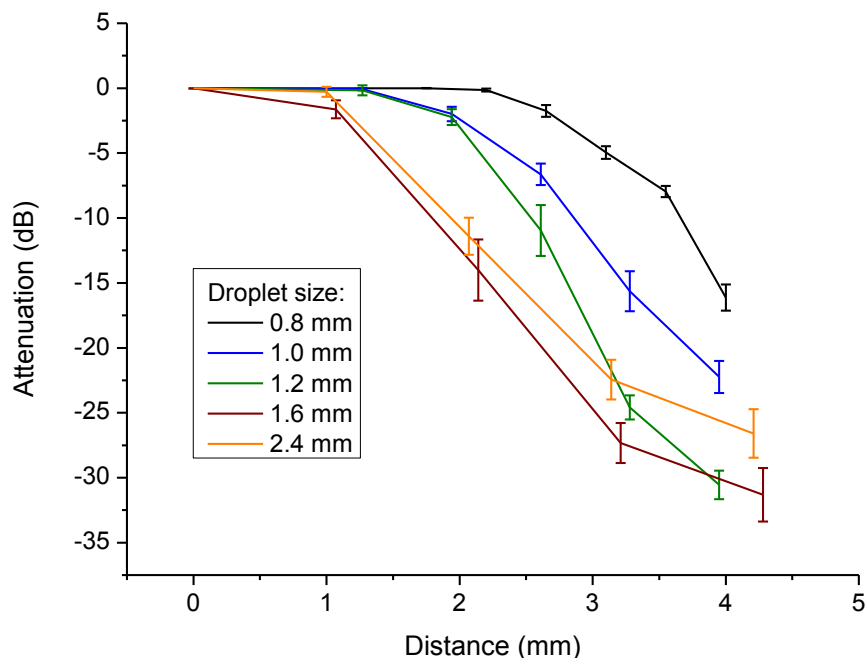

Fig. 4.33 Attenuation change over the distance of the polished fibre length for 0.8 mm, 1 mm, 1.2 mm, 1.6mm and 2.4 mm droplets

Key to this investigation is the fact that the attenuation for droplets larger than 1.2 mm did not reach the attenuations predicted by theoretical calculation. Such unusual results could arise from the production process of the polished fibre. Small changes of hundreds of nanometres in the cladding thickness profile can significantly alter the achievable attenuation. The profile shape does not provide uniform cladding changes and over a selected distance of the polished region will not change for hundreds of nanometres. Indeed, the smallest cladding thickness (estimated at 0.3 μm previously in Chapter 3, section 3.2.2.3) is likely to cover a length smaller than 1.2 mm. The increment of droplet size will therefore not influence the achievable attenuation of the fibre as strongly as the theory of Chapter 3 predicts. Despite the droplet covering more of the fibre, the cladding over that particular distance will have a range of thicknesses. The thinnest cladding residue might have a shorter length than the interaction length with the external liquid and will not achieve the predicted maximum attenuation for the droplet size. The fact that attenuation was not seen to increase significantly for larger droplets suggests that the optimum droplet size for the presented fibre is 1.2 mm.

4.7 Cleaning the fibre and potential solution to adhesion problems.

All the results which have been presented for the different types of VOA do not illustrate how the device works when the droplet leaves the interaction region. The reason for this is that the VOA transmission does not recover in the same step pattern, as could be assumed from the transmission steps decrease pattern. The droplets that were used were glycerine-water solutions of concentration from 92% to 94%. Such high concentrations of glycerine have high viscosities of ~0.367 kg/ms; compared to viscosity of water (0.0894 kg/ms)[10]. During motion along the fibre, the glycerine-water droplet leaves some residue that adheres to the surface of the polished fibre. This residue ensures that the light transmission does not return to 100 % when the droplet moves out of the polished fibre region. A possible solution for preventing glycerine-fibre adhesion is to cover the fibre with some long-lasting hydrophobic surface that will prevent the glycerine sticking. The requirement for such a layer is a very small thickness of the order of maximum 50 nm or less

so it will not disturb the performance of the VOA. If the thickness of the hydrophobic layer exceeds 50 nm then the overall cladding will increase and the maximum attenuation that could be achieved will reduce. One available option was Aquapel (Aquapel Glass Treatment, PPG Industries Inc., USA), which is a liquid solution that creates a hydrophobic layer. Aquapel was used to coat the polished fibre but it did not permanently help with preventing the glycerine adhering to the glass. Another solution for creating a hydrophobic surface was to evaporate a layer of Silan[16] (1H,1H,2H,2H-perfluorooctyl-trichlorosilane, Sigma-Aldrich Company Ltd., UK) onto the interaction region of the fibre. However, the Silan layer acted as an additional layer and when the droplet moved along the polished region of the fibre the optical transmission did not decrease. Currently we have not found any surface solution that can help with preventing glycerine adhesion to the surface of the fibre.
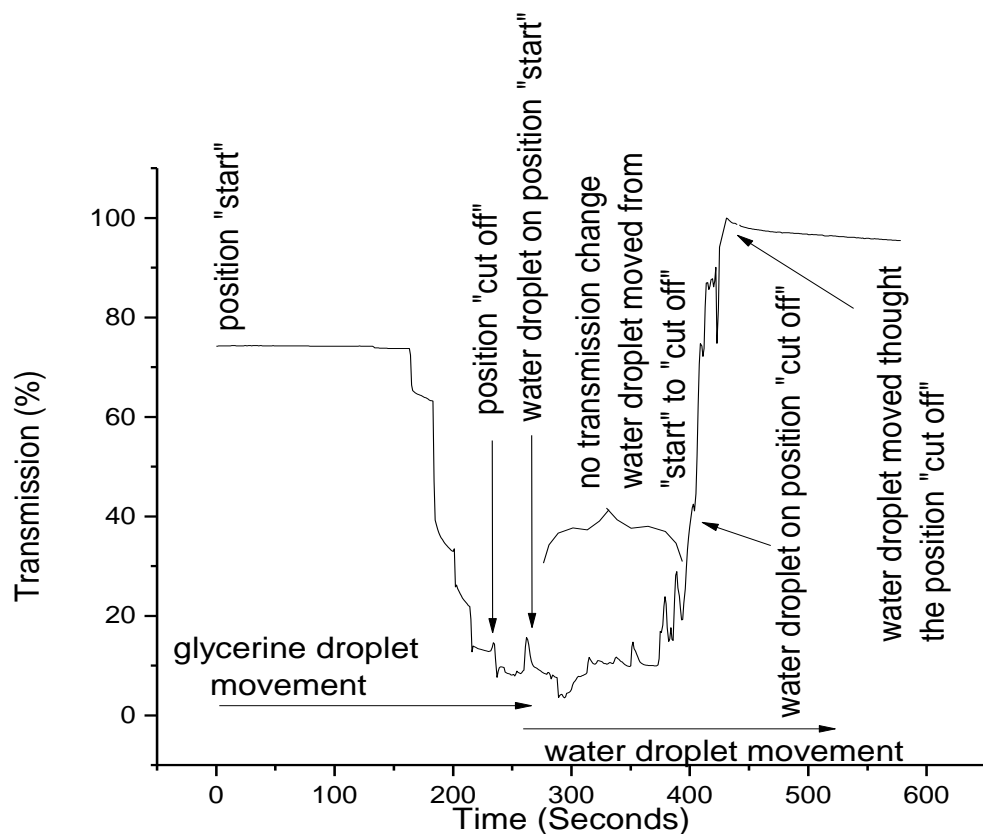

Fig. 4.34 Fibre attenuation change during glycerine droplet translation and then a pure water droplet cleaning movement

After each glycerine droplet had travelled along the polished region the fibre requires to be cleaned with a pure water droplet. When the glycerine droplet was removed from the

interaction region, the optical transmission did not change and remained at its lowest value. Then the water droplet was introduced and moved from the start of the polished region towards the middle. In doing so, the transmission did not increase in a stepped manner (Fig. 4.34), as occurred with the glycerine droplet when the transmission decreased stepwise. This is because the glycerine residue has the strongest impact on the transmission when the cladding thickness is lowest. Therefore the largest increment of the transmission occurs when the water droplet moves along the fibre and cleans the region of the lowest cladding thickness. The transmission increases to the 100% level as the water droplet is wetting the fibre surface. Transmission recovers completely to the level seen before application of the glycerine droplet, once the fibre is allowed to dry.

Another possible solution to glycerine residue is replacing the glycerine – water droplet with different liquid that will fulfil the basic requirements for the VOA device: such as possessing an applicable refractive index and comprising a water-based solution that can be translated with the electrowetting phenomenon. A sodium dichromate – water solution[17] is one such option. Appropriate concentration of sodium dichromate in water creates a solution that can reach the necessary refractive index (1.46). Tests were performed with 54% wt. sodium dichromate ($Na_2Cr_2O_7$) solution[8] (measured 1.46 refractive index with Atago Master-RI refractometer), ensuring the droplet had the round shape when placed on the hydrophobic surface of the EWOD platform. However, when voltage was applied to the electrode array to cause the droplet to move, the sodium dichromate – water solution did not move and electrolysis occurred. Different voltages and frequencies were tested to find the suitable values, but these combinations did not result in preventing electrolysis or translate the droplet.

The sodium dichromate droplet was moved manually along the fibre to determine whether the VOA transmission would decrease and the droplet adhesion would be less than in the case of the more viscous glycerine solution. (54% wt. sodium dichromate water solution has viscosity of 0.003 kg/ms[8] whereas 93% wt. glycerine-water solution has viscosity of 0.367 kg/ms[10]). Throughout the experiment the fibre (acquired from Phoenix Fibres Ltd) was connected to the EDFA light source and OSA to measure the broadband band performance of the attenuation change.

The results obtained (Fig. 4.35) show that the attenuation increases when the sodium dichromate droplet moves towards the centre of the polished region, then reaches the

maximum attenuation of around -26 dB, and then decreases when the droplet leaves the region of smallest cladding thickness. The increases of the transmission when the droplet moves towards second end of the interaction region provides that the fibre diameter slopes of both side of the polishing region, and also the droplet does not leave a residue as was happening with the glycerine – water droplet.
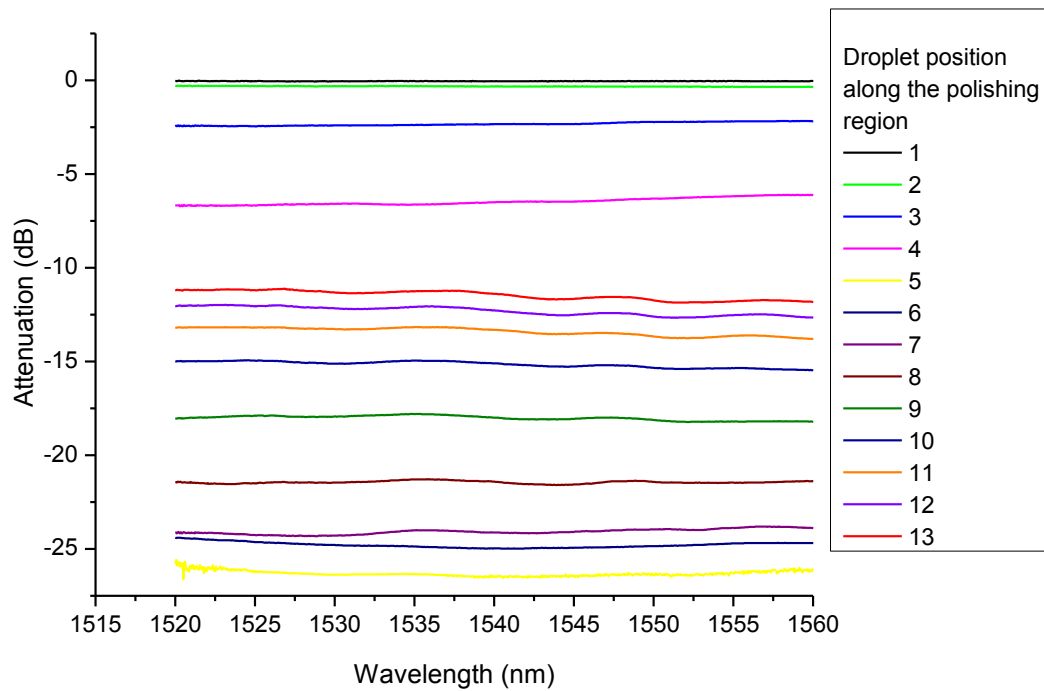
Fig. 4.35 Wavelength dependent loss of EWOD-VOA for the sodium dichromate – water droplet of the refractive index of 1.46

However, a significant disadvantage of the sodium dichromate-water solution is the toxic character of the liquid. Experiments with the solution needed to be performed in a fume cupboard with strict safety procedures preventing breathing the fumes or spilling the liquid. Above all, sodium dichromate-water droplets have not fulfilled the device requirements, and cannot be used as the liquid actuator.

One other liquid that had some potential due to its appropriate refractive index was a glucose-water solution. Unfortunately to reach the required 1.46 refractive index, the concentration of glucose was too high to create a liquid droplet on the hydrophobic surface that can be moved using the electrowetting phenomenon. To this point, a liquid that can replace the glycerine-water solution has not been found.

4.8 Summary

In summary, an optical side polished fibre that allowed external access to the optical evanescent field was chosen for VOA development due to its robust nature and longer interaction length (several millimetres) compared to for example taper fibres (of around 0.5 mm interaction length)[18]. The subsequent performance of the fabricated EWOD-VOA agrees well with results predicted from the theoretical analysis of the components of the VOA. The results obtained have shown that the refractive index of the droplet and size have a strong impact on the device performance and the shape of polished fibre region that is the main part of the device determines the behaviour of the VOA. It was also shown that even a small change of the fibre slope profile can significantly change the obtained steps in attenuation. A fibre fabrication issue that has some influence on the results is the fibre polishing depth, where the thickness of the remaining cladding can prevent a device from attaining the highest potential attenuation values. As was discussed, the maximum attenuation obtained for a VOA employing commercially obtained fibre was -22 dB; which suggests that a 0.3 μm cladding thickness remains covering core of the fibre. Attenuation for the VOA using side polished fibre fabricated in-house reached -25 dB; suggesting that 0.13 μm of cladding remained.

The experiments conducted also show that the size of the droplet is one of the important parameters of the VOA design. The interaction length between droplet and fibre can improve the performance of the device, as was shown for 0.6 mm and 1.2 mm droplets. However there is an optimum size of droplet which achieves the highest attenuation for a given fibre. The theoretical analysis predicts that longer interaction lengths should yield higher attenuation values but, for the presented fibre, droplets bigger than 1.2 mm did not achieve their predicted values. The geometry of polished region of the fibre affects the achievable attenuation and modification of this profile during manufacture could provide a means to reach higher attenuations than the achieved -30 dB, as predicted by the theoretical calculation. The effects of droplet size were confirmed by experiments performed with two different fibres (one acquired from Phoenix Fibres Ltd and one that was manufactured in our laboratory) and two different refractive indices.

A further conclusion is that it is possible to manipulate the resolution of the VOA device. Smaller droplets (used in conjunction with suitable electrode configurations) can be used to provide higher resolution (more attenuation steps) along a polished region of fibre. However, this high resolution comes at the expense of lower achievable levels of attenuation.

4.9   References:

[1]   R. Bergh, G. Kotler, and H. Shaw, "Single-mode fibre optic directional coupler," *Electron. Lett.*, vol. 16, no. 7, pp. 260–261, 1980.

[2]   O. Leminger and R. Zengerle, "Determination of the variable core-to-surface spacing of single-mode fiber-coupler blocks," *Opt. Lett.*, vol. 12, no. 3, pp. 211–213, 1987.

[3]   C. Hussey and J. Minelly, "Optical fibre polishing with a motor-driven polishing wheel," *Electron. Lett.*, vol. 24, no. 13, p. 805, 1988.

[4]   Z. Chen and C. Bai, "Effect of overlaid material on optical transmission of side-polished fiber made by wheel side polishing," *2008 1st Asia-Pacific Opt. Fiber Sensors Conf.*, vol. 6, no. 4, pp. 1–4, Aug. 2008.

[5]   U.-C. Yi and C.-J. Kim, "Characterization of electrowetting actuation on addressable single-side coplanar electrodes," *J. Micromechanics Microengineering*, vol. 16, no. 10, pp. 2053–2059, Oct. 2006.

[6]   S. Aghdaei, N. G. Green, T. B. Jones, and H. Morgan, "Droplet mixer based on electrowetting," *J. Phys. Conf. Ser.*, vol. 142, p. 012071, Dec. 2008.

[7]   S.-K. Fan, H. Yang, T.-T. Wang, and W. Hsu, "Asymmetric electrowetting--moving droplets by a square wave." *Lab Chip*, vol. 7, no. 10, pp. 1330–5, Oct. 2007.

[8]   R. C. Weast, M. J. Astle, and W. H. Beyer, "Handbook of chemistry and physics," CRC Press, Inc., 1985, pp. 234–235, 259.

[9]   J. B. Richard E. Mark, "Handbook of Physical Testing of Paper," in *Handbook of Physical Testing of Paper, Vol. 1*, C. Habeger, M. Bruce Lyne, R. Mark, and J. Borch, Eds. CRC Press, 2002, p. 152.

[10]   *Physical properties of glycerol and its solutions*. New York : Glycerine Producers' Association, 1963, p. 27.

[11]   A. Al-Azzawi, "Fibre optics, Principle and Practices," in *Fibre optics, Principle and Practices*, CRC Press, 2007, pp. 315–316.

[12]   C. Lee, "A MEMS VOA Using Electrothermal Actuators," *J. Light. Technol.*, vol. 25, no. 2, pp. 490–498, Feb. 2007.

[13]   H. Cai, X. Zhang, C. Lu, A. Q. Liu, and E. H. Khoo, "Linear MEMS variable optical attenuator using reflective elliptical mirror," *IEEE Photonics Technol. Lett.*, vol. 17, no. 2, pp. 402–404, Feb. 2005.

[14]   A. Liu, "Photonic MEMS devices: design, fabrication and control," in *Photonic MEMS devices: design, fabrication and control*, CRC Press, 2010, pp. 186–190.

[15]   A. Dudus, R. Blue, M. Zagnoni, and D. Uttamchandani, "Side-polished fiber optofluidic attenuator based on electrowetting-on-dielectric actuation," in *2013 International Conference on Optical MEMS and Nanophotonics (OMN)*, 2013, no. August, pp. 95–96.

[16]   B. Arkles, "Hydrophobicity, hydrophilicity and silanes," *Paint Coatings Ind. Mag.*, no. October, 2006.

[17]   J. Hsieh, P. Mach, F. Cattaneo, S. Yang, T. Krupenkine, K. Baldwin, and J. a. Rogers, "Tunable microfluidic optical-fiber devices based on electrowetting pumps and plastic microchannels," *IEEE Photonics Technol. Lett.*, vol. 15, no. 1, pp. 81–83, Jan. 2003.

[18]   A. Dudus, R. Blue, and D. Uttamchandani, "Comparative Study of Microfiber and Side-Polished Optical Fiber Sensors for Refractometry in Microfluidics," *IEEE Sens. J.*, vol. 13, no. 5, pp. 1594–1601, May 2013.

Chapter 5

Ferrofluid Variable Optical Attenuator

5.1   Introduction

This chapter presents an optofluidic implementation of a single mode fibre optic variable optical attenuator using magnetic field actuation with "fibre gap" configuration.

A ferrofluid is a magnetic fluid that consists of a colloidal suspension of nano-size ferromagnetic particles suspended in a liquid medium[1]. Application of an externally applied magnetic field causes the randomly orientated magnetic moments to align initiating the fluid as a whole to move towards the region of highest flux. When the magnetic field is removed the ferromagnetic particles inside the ferrofluid lose the induced orientation[1]. Interest in employing ferrofluids in a range of the applications has been growing in recent times.

5.2   Ferrofluid-based optical fibre devices

The magnetic properties of a ferrofluid opens new possibilities in optofluidic fibre optical device development. A ferrofluid not only can be translated by a magnetic field but also can change its refractive index when the applied magnetic field changes[2].

An optical fibre whose transmission properties were tuned via a magnetically actuated ferrofluid was demonstrated in 2011 by Konstantaki et al.[3] This system employed a ferrofluid in combination with a fibre long period grating (LPG). The ferrofluid acted as an outcladding overlayer for tuning of the LPG transmission. Two approaches were implemented to change the optical transmission of the LPG using a ferrofluid. First was tuning the LPG transmission by translating a water-based ferrofluid along the external surface of the fibre adjacent to the internal gratings (Fig. 5.1 a). A change of 7.5 nm and 6.5

dB in the wavelength and strength of the grating's attenuation band was observed. The second approach focused on the refractive index change of a stationary oil-based ferrofluid. The ferrofluid surrounding the LPG again acted as the additional cladding surface (Fig. 5.1 b) and then by applying a magnetic field up to 400 G the refractive index (n) of the fluid changed by up to $\Delta n = 0.205$ and the transmission of LPG attenuation band (at 1540.7 nm) modified by 0.5 dB (~10%).
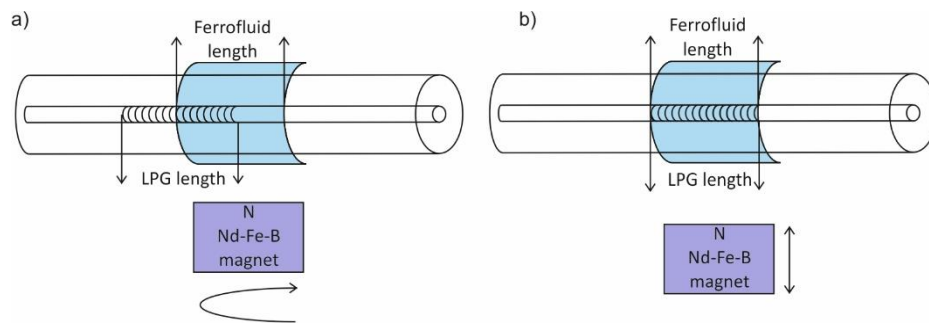
Fig. 5.1 Schematic of a) ferrofluid actuator approach, b) magnetic field sensor

Subsequently the same authors demonstrated a magnetometer based upon a ferrofluid located within a microstructured optical fibre containing a Bragg grating[4]. Application of a magnetic field changed the position of the ferrofluid along the grating and thus modified the reflection spectrum of the grating (Fig. 5.2). The magnetometer was able to measure a magnetic field range from 317 to 2500 G.
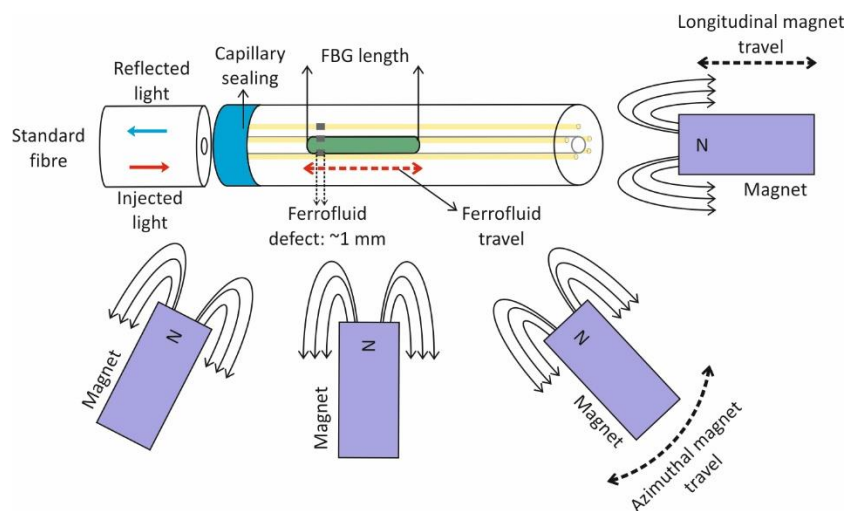
Fig. 5.2 Illustration of the MOF Bragg grating magnetometer[4]

Another example of an application that uses the ferrofluid for sensing a magnetic field was demonstrated by Miao et al.[5]. Their device was constructed from a tapered optical microfiber in combination with a ferrofluid. The fibre was surrounded by the ferrofluid and by applying a magnetic field the refractive index of the liquid was tuned (refractive index of the liquid was not given by Miao et al.), which modified the transmission of the fibre. The microfiber was aligned in an S shape geometry which resulted in an interferometer configuration, where part of the light travelled through the core and the rest was coupled into and then out from the cladding into the core again (Fig. 5.3 a). During the device operation the interferometric fringes were measured (Fig. 5.3 b). The magnetic field was changed from 25 to 200 Oe and the sensitivity was measured was 0.13056 dB/Oe and 0.056 nm/Oe.
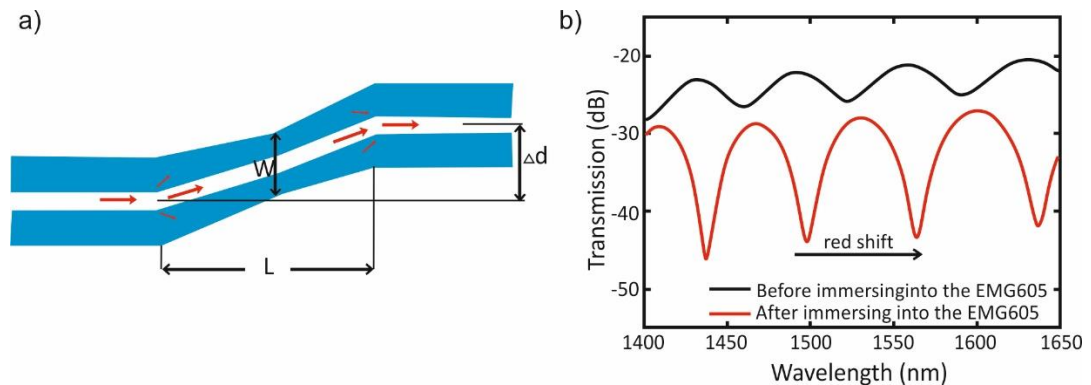
Fig. 5.3 a) Illustration of the S tapered fibre mode interference, b) transmission spectra of the microfiber

As described above, only liquid ferrofluids have been used to form optical attenuators using LPG fibres. In contrast, S. de Pedro et al.[6] reported in 2013 the use of a ferrofluid-doped solid PDMS cantilever-based VOA between two multimode fibers, which produced an optical attenuation of up to 3.5 dB as a magnetic field deflected the cantilever (Fig. 5.4).
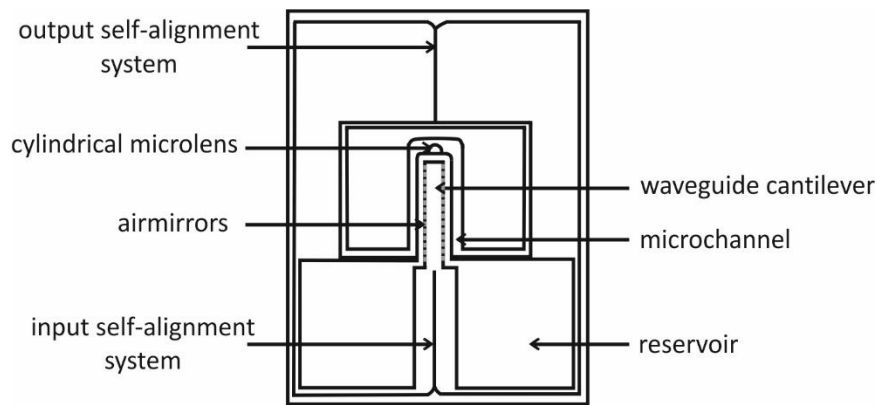
Fig. 5.4 Schematic of PDMS cantilever-based VOA

An optical switch operating at the telecommunication wavelength 1.55 µm and controlled by another optical light beam was shown by Dai et al.[7]. The device was built using two single mode fibres as the input light source and output light collector for a broadband band source operating across 1.525 to 1.565 µm. A capillary tube was positioned between the fibres and was filled with ferrofluid to form a reversible shutter (Fig. 5.5). The wavelength (µm) of the infrared light is higher than the average size (µm) of Fe_3O_4 particles in the capillary tube and scattering is weak and thus light transmission is at a maximum. Upon application of laser light (0.532 µm) focussed into the capillary tube causes the formation of magnetic clusters and increased scattering.
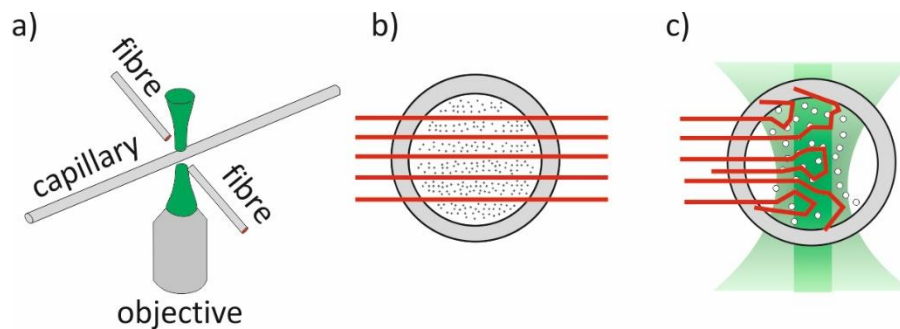
Fig. 5.5 Illustration of a) optofluidic switch, b) random position of the magnetic particles and maximum light transmission, c) magnetic clustering formation under control light and backscattering of infrared light

Another device that employs optofluidic technology to create a reconfigurable switch was reported by Yu Gu et al[8]. They demonstrated a device that consists of single and multi-mode waveguides inserted into a PDMS base with a microfluidic channel crossing the light path between the input and output waveguides. The switch was turned "ON" and "OFF" by the movement of the opaque liquid inside the microchannel (Fig. 5.6). The fluid used in the switch configuration was a water-based ferrofluid. The movement of the ferrofluid plug was actuated by a magnetic field. The device had a contrast ratio higher than 23 dB with switching time on the order of milliseconds and had only 7% degradation in repeatability over 72 h.
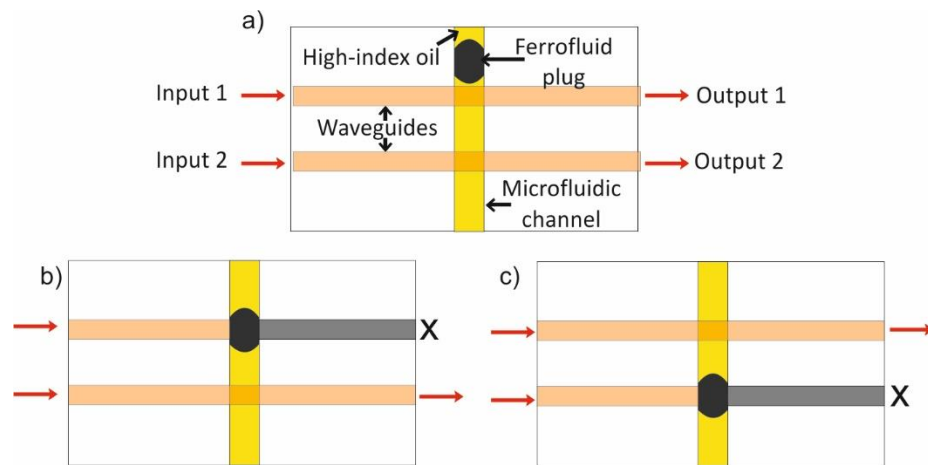
Fig. 5.6 a) Illustration of the optofluidic switch, b) First output OFF, c) Second output OFF

By applying a magnetic field not only will the position of ferrofluid change but the refractive index of the fluid can also change. For our research, the important point was the possibility of using the fluid as an attenuator. The last example above, where a moving ferrofluid plug between two optical waveguides can work as a switch, lends itself to creating a variable optical attenuator with single mode fibres.

5.3   Ferrofluidic VOA description

The optical attenuator that is presented in this chapter is a novel shutter-type single mode fibre VOA. The proposed VOA is a "fibre gap device" where the change in the

magnetic field can change the position of a liquid shutter. The main part of the device is a mobile opaque shutter crossing the light path and changing the transmission between two fibres. The shutter is an "all-fluidic" shutter that is moved by a magnetic fluid (ferrofluid) actuation. The shutter is created by an opaque liquid plug in direct contact with a transparent fluid. The ferrofluid is driven either by a permanent magnet located on a microstage or a fixed position variable electromagnet. The shutter is placed inside a rectangular glass channel with transparent walls. The transparent channel is located between the two GRIN lensed single-mode optical fibres. The fibres are aligned so that the light can leave the input fibre, cross the gap within the channel and be coupled into the output fibre aligned on the opposite side of the channel (Fig. 5.7). Depending on the opaque shutter position and the opacity of the shutter, the transmission will vary from 100 % to 0 %. In this way, a fibre optic-based fluidic variable optical attenuator is realized.

Fig. 5.7 Illustration of the fibre gap device configuration containing fluidic shutter

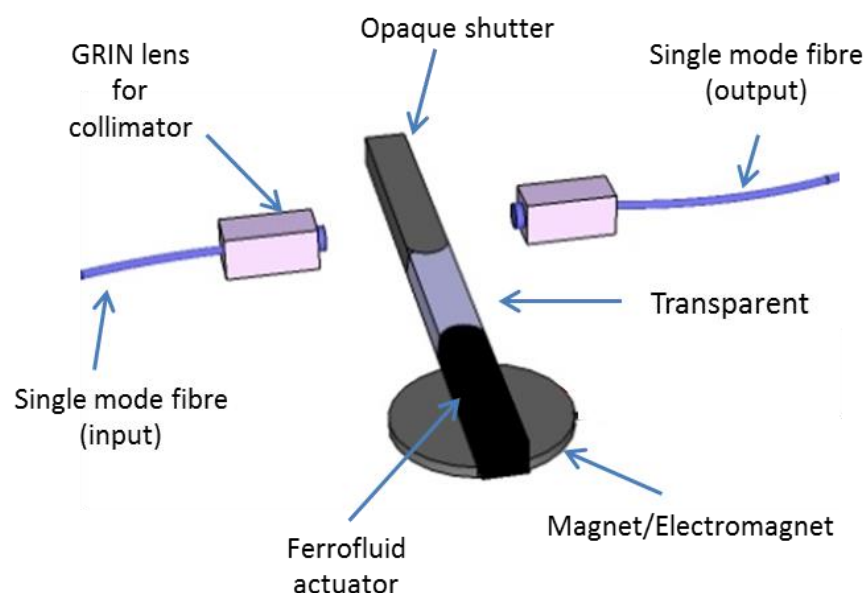Two different configurations of fluidic VOAs have been investigated. One fluidic/actuator was created using an oil-based ferrofluid actuator and a second using a water-based ferrofluid actuator.

5.4 Simple theoretical model of ferrofluid VOA

The behaviour of the VOA shutter is described by a simple one dimensional optical model. The opaque plug moves between two GRIN lenses, interrupting the light traveling between them and therefore attenuating the power received by the output fibre. A one-dimensional Gaussian function can be used to model the power distribution of the light travelling between the input light source through the channel to the output receiver.

In statistics the Gaussian function appears as the normal distribution function that defines the probability density and can be written as[9]:

$$A(x_1) = \frac{1}{\sigma\sqrt{2\pi}} exp\left(-\frac{(x-\mu)^2}{2\sigma^2}\right) \tag{5.1}$$

where $x \in R$, μ (mean) $\in R$ and σ (standard deviation) $\in R^+$.

The function value can be calculated when the x and standard deviation is known. The probability density is the symmetric function according to the value $x = \mu$. Function rises from $-\infty$ to μ, where in $x = \mu$ reaches maximum equals to $\frac{1}{\sigma\sqrt{2\pi}}$, and then decreases from μ to ∞. The maximum of the function in $x = \mu$ increases when σ decreases and then the shape of the probability density function is narrower, however when σ increases the shape of the function flattens.

The power distribution of the light in our system can be presented via a Gaussian function that adopts the form[9]:

$$A(x_1) = \int_{3\sigma}^{x_1} \frac{1}{\sigma\sqrt{2\pi}} exp\left(-\frac{x^2}{2\sigma^2}\right) dx \tag{5.2}$$

where $A(x_1)$ is the attenuation when the opaque shutter blocks the light from position 3σ to position $x = x_1$. Taking the diameter of the GRIN lens face to be 6σ and equal to 1.2 mm yields a value of $3\sigma = 0.6$ mm while $x_1 \in (-3\sigma, 3\sigma)$.
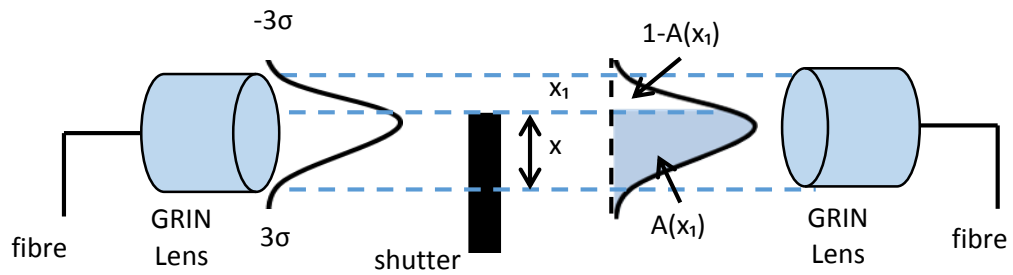
Fig. 5.8 Model of the Gaussian light distribution in shutter system

In Figure 5.8, it is assumed that the 100% of the light travels from input GRIN lens to the output GRIN lens. This statement is only true when the optical beam adopts a parallel form and diffraction is not taken into consideration in the model. Therefore there is no light loss on the travel path between the GRIN lenses. Such an assumption is reasonable using GRIN lenses to produce a parallel beam of the light. The light beam on the GRIN lens output maintains a circular shape in cross section and diameter of the beam equal to the GRIN lens size, which in our system is 1.2 mm. The shutter that moves between two GRIN lenses can move a maximum of $x = 6\sigma$. When the shutter translates to the maximum position the light transmission is blocked and the output GRIN lens does not receive any light.

The light transmission between GRIN lenses will change according to the position of the shutter on the light path. Table 5.1 below shows examples of the shutter displacement and corresponding optical power transmission.

Table 5.1 Shutter position versus VOA light transmission:

x_1 - Displacement (mm)	$1-A(x_1)$ - Transmission (%)
1.2	0.27
1.12	0.6
1.04	1.53
0.96	3.73
0.88	8.21
0.8	16
0.72	27.56

0.64	42.21
0.56	58.06
0.48	72.71
0.4	84.27
0.32	92.06
0.24	96.54
0.16	98.74
0.08	99.67
0	100

From the graph above (Fig. 5.9) we can see that when opaque shutter increasingly covers more of the light path, less light reaches the receiver lens but according to the Gauss function never reaches 0 %. Therefore when shutter translates 1.2 mm which is the diameter of the light beam the transmission decreases to 0.27%.

Fig. 5.9 Variation of optical transmission depending on the shutter position between two GRIN lenses
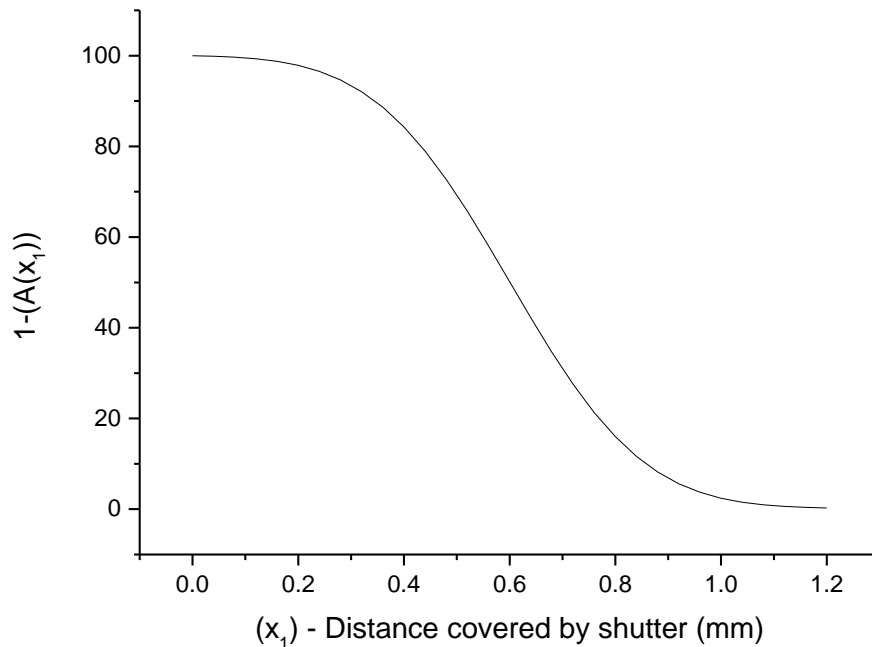
5.5   Oil-based Ferrofluid Actuator

5.5.1 VOA shutter (1:30 ferrofluid and water plugs)

The first type of ferrofluid VOA that was experimentally investigated was built from an opaque shutter made from an oil-based ferrofluid plug. The ferrofluid that was used to create the shutter was a solution of CHE006 type ferrofluid mixed with mineral oil in the ratio 1:30. The shutter moved inside a rectangular glass capillary channel acquired from Vitrotubes™. The glass capillary had an inside diameter of 1 mm and the thickness of glass walls are 0.2 mm. The 1:30 dilution ratio was chosen due to the problems that arose during the experiments using 100% ferrofluid. During plug motion inside the channel, the 100% ferrofluid left a residue on the channel walls. The transparency of the walls decreased with each translation of the plug, and therefore the transmission did not reverse when the shutter left the light path. On choosing the correct ratio there was a balance between the shutter being dark enough to substantially decrease the optical transmission and at the same time leaving no residue on the channel wall. Experimentally, the 1:30 solution was found not to deposit residue on the glass walls and at the same time was opaque enough to achieve a high attenuation.

The magnetic actuator that subsequently translates this liquid shutter system comprised a plug of undiluted oil-based ferrofluid (CHE006). That actuator was driven by either a permanent magnet or variable electromagnet depending on the experiment type. The challenge was to design the shutter system in a way that both undiluted and diluted ferrofluid would not mix with each other and only the 100 % ferrofluid would push the diluted ferrofluid shutter. To achieve this aim, the two ferrofluids were separated with a plug of water. The water had the task not only to divide both ferrofluids but also to help with preventing the diluted ferrofluid from leaving a residue on the channel walls. The overall layout is shown in Figure 5.10. When a magnetic field applied to the actuator is moved the position of the actuator will also move, and in turn changes the position of the opaque shutter. The movement of the shutter along the channel varied the optical power that was transmitted between the GRIN lenses.
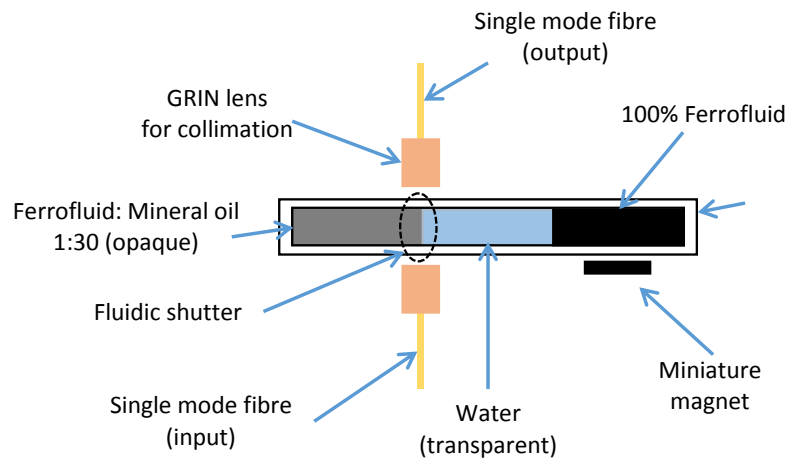
Fig. 5.10 Configuration of single mode fibre VOA containing oil-based ferrofluid actuator and shutter

The light that was launched into the single mode fibre input is produced in an erbium doped fibre amplifier (EDFA). That light propagates from input GRIN lens through the VOA and is coupled into the output single mode fibre via the second GRIN lens. The output fibre is connected to the photodetector/amplifier (LNP-2, Optosci Ltd, UK) that detects the optical signal. Next, that signal is converted into electric form that is recorded in real time by PicoScope data logger (Pico Technology Ltd, UK). The PicoScope sent the information to a computer that displayed and recorded the output from VOA (Fig. 5.11).
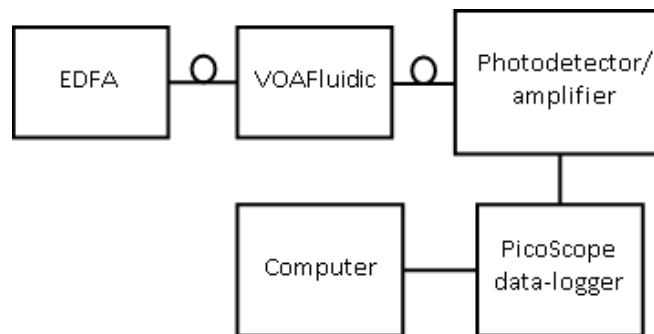
Fig. 5.11 Experimental setup testing optical properties of VOA

Initially, the VOA was tested with a permanent magnet mounted on a micro translation stage situated below the microfluidic glass channel in a position beneath the ferrofluid actuator as shown on Figure 5.10. However, before assembling and operating the

VOA, the magnetic field of the permanent magnet was measured with a gaussmeter (GM07/GM08, Hirst magnetic instruments LTD). The strength of the magnetic field is dependent on the distance between the magnet and the position of the gaussmeter probe. Figure 5.12 illustrates the characterisation of the magnetic field change for different distance between the magnet and the probe. It can be seen that the magnetic field of the permanent magnet exponential decreases with the increase of the distance between the magnet and the gaussmeter probe from 1100 Oe to almost 0 Oe. It has to be noted that the probe chip in the position 0 do not touch the magnet but there is 3 mm gap due to the probe chip plastic cover. After characterisation of the magnetic field of the permanent magnet, the distance between the magnet and the fluidic channel of the VOA was chosen to be 3 mm as the magnetic field is the strongest and the control of the ferrofluid position will be more precise.
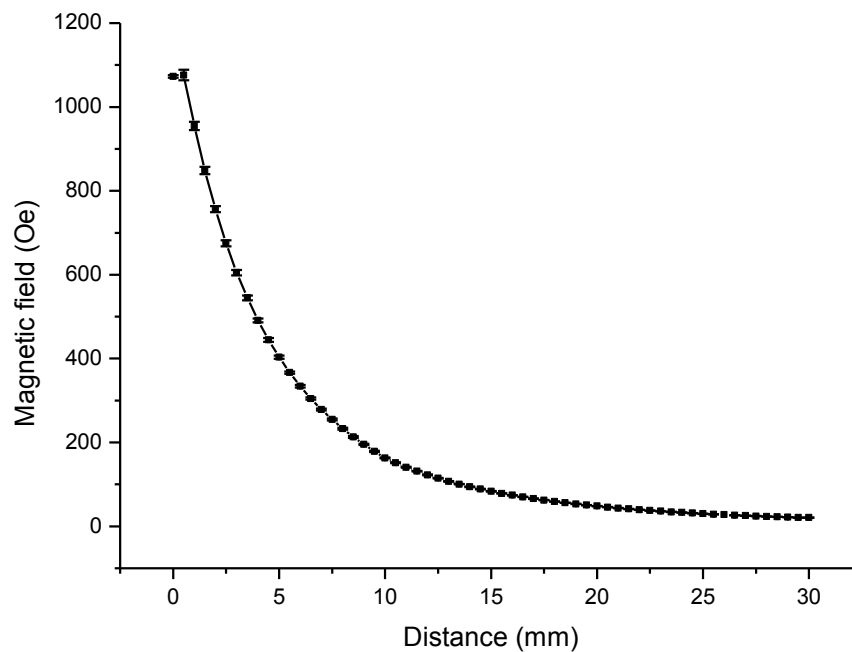
Fig. 5.12 Magnetic field change versus the distance between the permanent magnet and gaussmeter probe

The first part of the experiment was to transfer the light via the microfluidic channel with the water section in place between the GRIN lenses. The optical transmission

through the water indicates the highest value. The insertion loss measured at the output fibre with a powermeter (FiberHome Technologies Group) was 5 dB. The insertion loss of the system was caused due to misalignment between input and output GRIN lenses and from the reflection from the channel 0.2 mm thick walls.

The magnet under the undiluted ferrofluid was translated in steps of 100 μm and therefore it can be assumed that the ferrofluid actuator pushed the shutter 100 μm in each step. The permanent magnet was moved in two directions, firstly translating ferrofluid shutter into the light path, decreasing the light transmission and secondly magnet was moved into opposite direction increasing the optical transmission. Figure 5.13 presents the measured transmission between GRIN lenses according to the translated position of the ferrofluid shutter. The transmission decreased step wise to approximately 0 % when the shutter covered completely the light path (Fig. 5.13). The ferrofluid shutter was translated a distance of 1.4 mm to achieve the optical transmission of ~0 % between input GRIN lens and output GRIN lens.
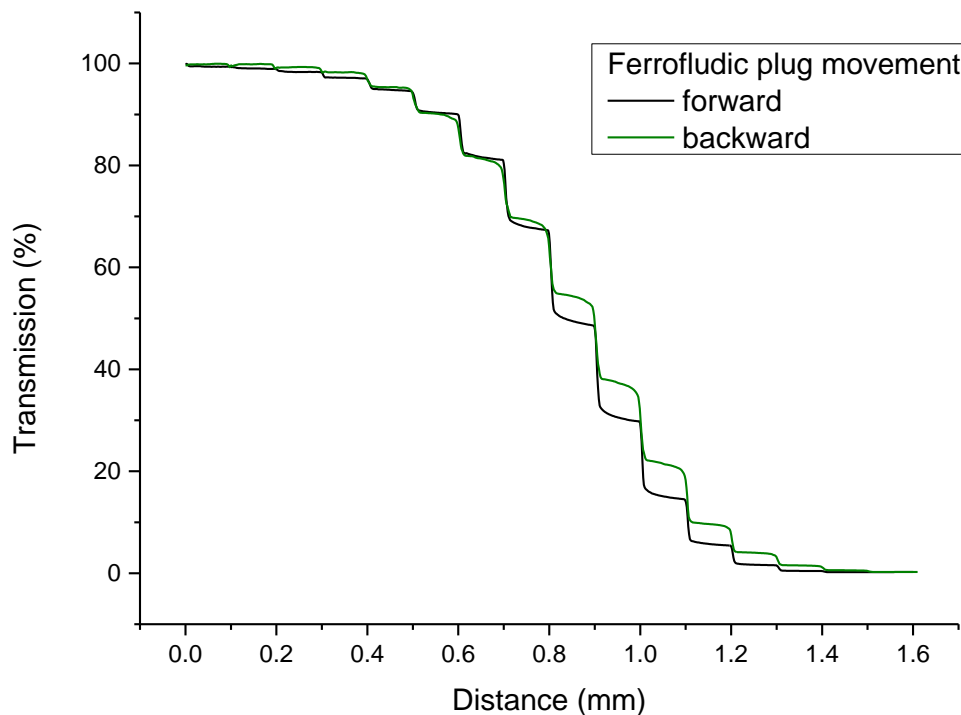
Fig. 5.13 Decrement and increment of optical transmission between the GRIN lenses during the shutter movement through the light path

The process of the transmission change was fully reversible and the ferrofluid shutter was moved in the opposite direction increasing the light transmission. The permanent magnet moved in the same step distance (100 µm) as before so the light power increases in the same step magnitude as can be seen on the graph above (Fig. 5.13).

5.5.2 Ferrofluid VOA broadband operation

After creating a viable ferrofluid-based VOA, the next step was to investigate if the device could operate broadband. The EDFA was used as the broadband light source and an Agilent 86140B optical spectrum analyser (OSA) employed to monitor the optical output of the receiver GRIN lens of the VOA (Fig. 5.14). The OSA was connected to a computer that recorded broadband spectrum from 1525 nm to 1560 nm, a common wavelength range used in the optical communication systems.
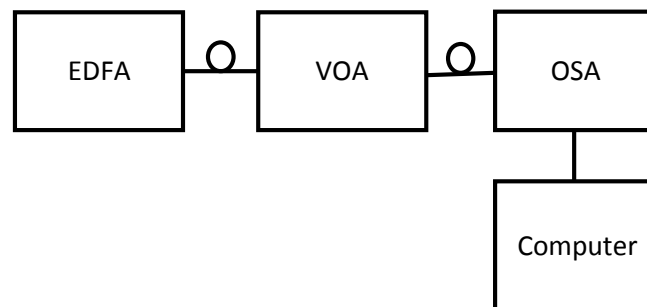
Fig. 5.14 Experiment setup to monitor the broadband performance of the VOA

Figure 5.15 shows the wavelength dependent loss (WDL) of the developed VOA at the different values of the attenuation over the 35 nm wavelength range (1525 to 1560 nm). Each attenuation line on the graph represents a position of the fluidic shutter as it moved across the light path in 100 µm steps as described previously.
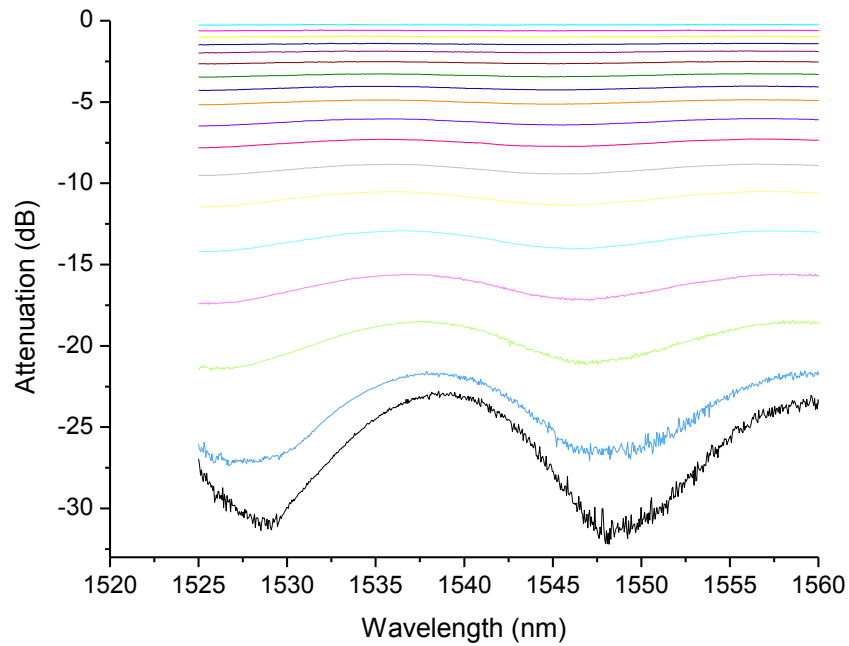
Fig. 5.15 Broadband optical behaviour of the variable optical attenuator

Figure 5.15 reveals that for high levels of attenuation (up to -32 dB) the WDL increases to 10 dB. It was observed that this increase in the value of WDL was a result of fringes that appeared on the transmission spectrum. It was speculated that optical interference was taking place. The optical interference could be a product of light that was partially passing through the 1:30 ferrofluid plug and partially the water plug (Fig. 5.16) that formed the shutter. Both light paths were different according to their refractive index of the liquid mediums and therefore the interference fringes could appear on the transmission spectrum.
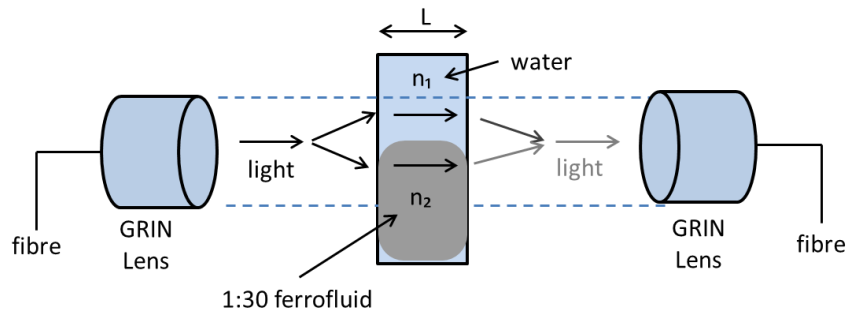
Fig. 5.16 Illustration of the interferometer that was created in the fluidic channel in the shutter system

The results shown on Figure 5.15 can be used to calculate the refractive index of the diluted ferrofluid. The system presented on the picture above (Fig. 5.16) is similar to the standard Mach-Zehnder interferometer. The function of such device is defined by wave interference theory, where part of the light beam is travelling through the 1:30 ferrofluid path and second part is travelling through the water plug. The input light is split to two beams of I_1 and I_2 intensity. When these two light beams reach the receiver GRIN lens they recombine into one beam but any phase difference between two beams will generate interference in output beam (I_{out}). Such a situation can be represented by[10]' [11]:

$$I_{out} = I_1 + I_2 + 2(I_1 I_2)^{1/2}\cos(\Delta\phi) \tag{5.3}$$

where ϕ_1 and ϕ_2 are the phase of the light beam that travels through the ferrofluid (1) and water (2).

The refractive index of a medium that light travels through has an impact on the phase velocity which can change phase of the light beam. The change of phase of the light that travelled through the medium can be described as[11]:

$$\Delta\phi = \frac{2\pi L}{\lambda}(n_2 - n_1) \tag{5.4}$$

where λ is a wavelength, n_1 and n_2 are refractive indices of materials, L is the length of the light path (1mm).

The refractive index of the 1:30 ferrofluid can be calculated from:

$$n_2 = \frac{\lambda_1 \lambda_2}{\lambda_1 - \lambda_2} \cdot \frac{1}{L} + n_1 \tag{5.5}$$

where n_1 is the water refractive index, n_2 is refractive index of the 1:30 ferrofluid, λ_1, λ_2 are the wavelength peaks (1538 nm and 1560 nm). The extended explanation of the optical interference is provided in the Appendix 3.

From the above Equation 5.4 and results obtained from the Figure 5.15, it is possible to calculate the 1:30 ferrofluid refractive index. The calculated value of the refractive index was 1.44. To verify if the value was realistic, the refractive index of the 1:30

ferrofluid was measured with a refractometer (60/70 Abbe refractometer). The value that was obtained from these measurements was 1.468. The difference between the calculated and measured value can be an effect of the very dark colour of the liquid which reduced the precision of the measurement of the refractive index.

The purpose of the ferrofluid refractive index calculation was to replace the water plug with a liquid that will have refractive index closer to the ferrofluid refractive index. When both refractive indices of transparent plug and opaque plug are close to each other then it will more equalise the speed of the light travelling through both mediums. When the speed of the light through mediums is similar then the interferometric fringes should reduce and reduce the WDL magnitude recorded from broadband operation. An investigation of a liquid of closer refractive index led to a glycerine-water solution. Such a solution is also transparent and it will not mix with both the ferrofluid shutter and the ferrofluid actuator. The most important thing is that it is possible to control the refractive index of the medium by varying the concentration of the glycerine in the water solution. A glycerine-water solution of 1.45 refractive index (measured with 60/70 Abbe refractometer) was prepared. The prepared mixture was placed between the ferrofluid actuator and shutter, replacing water in the microfluidic channel.

5.5.3 VOA shutter (1:30 ferrofluid and glycerine/water plugs)

The new type of VOA built from the 1:30 ferrofluid and the glycerine-water plugs was tested to investigate if the interferometric fringes decreased when the refractive indices on both side of the shutter (1:30 ferrofluid plug and glycerine-water plug) are closer to each other. Before measuring WDL, the microfluidic channel was placed between the two GRIN lenses and the insertion loss using this glycerine-water plug was measured. The measured insertion loss was now 12 dB rather than 5 dB with water only.

The input single mode fibre of the VOA was connected to the broadband EDFA source and the output signal from VOA was monitored by the OSA. Initially the light was passing through the glycerine-water plug and then the shutter was moved across the light path. The performance of the VOA was the same regardless of the direction that shutter was moved.
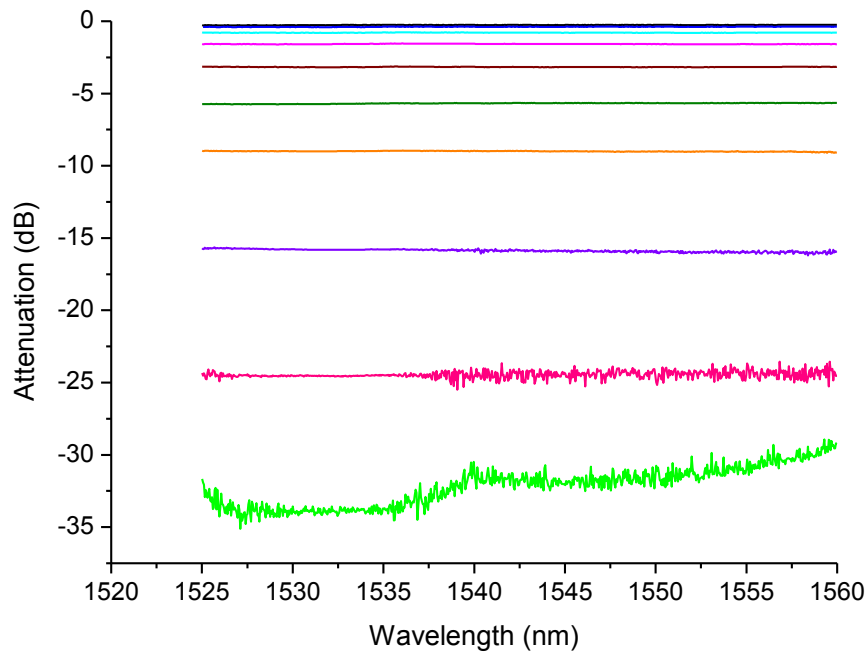
Fig. 5.17 Broadband optical performance of the index matching variable optical attenuator

Figure 5.17 illustrates the broadband optical operation of the VOA in which shutter plug and the transparent plug have closer matching refractive indices. It can be seen that the interferometric fringes had been significantly reduced compared to the previous presented results (Fig. 5.15). The only disadvantage of using glycerine-water plug that arose was that some artefact appears at the highest attenuation of around -30 dB. For that attenuation, wavelength dependent loss reaches 4 dB. Such an artefact was due to the weakness of the signal that arrived at the receiver. The signal was weak because the light was highly attenuated after travelling through the opaque shutter and from higher insertion loss. The artefact appears only for the highest attenuation and it cannot be seen for the lower attenuation, where for example WDL for -25 dB attenuation reaches 1 dB.

The new results indicates that the replacing water plug with the glycerine-water plug was appropriate to create a VOA with good performance -25 dB attenuation along with a WDL around 1 dB. For that VOA design the polarisation dependent loss (PDL) was measured likewise and the PDL reaches 0.25 dB.

5.5.4 Oil-based ferrofluid actuator – electromagnet actuation

Until now we have used a permanent magnet moved upon a microstage to actuate the VOA. In this subchapter the VOA will be controlled using a stationary electromagnet rather than a mobile permanent magnet. The VOA layout is shown in Figure 5.18. Inside the microfluidic channel the three liquid media in order are the 1:30 oil-based ferrofluid, the glycerine-water solution, and the 100% oil-based ferrofluid.
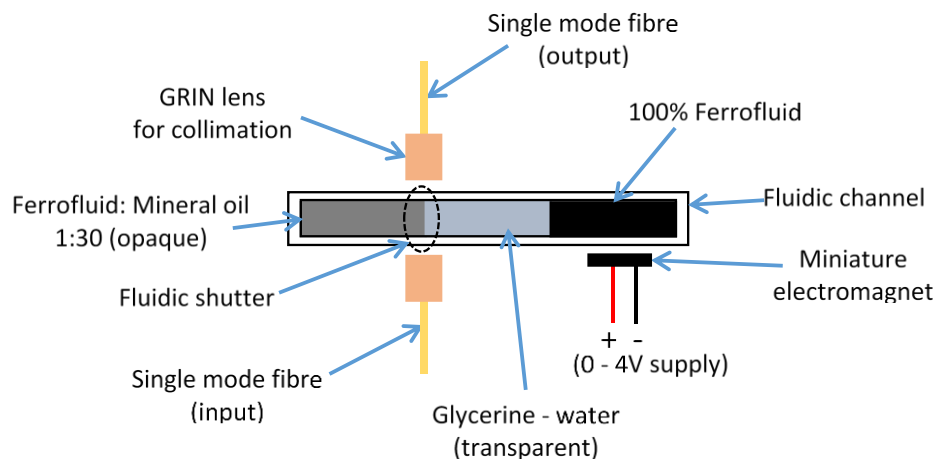
Fig. 5.18 Configuration of single mode fibre VOA using electromagnet

The electromagnet can produce a magnetic field of variable strength when a voltage is applied to it. By increasing voltage over the range 0 to 10 V the magnetic field increases. Firstly, the magnitude of the magnetic field that the electromagnet can produce was measured. The electromagnet was connected to a voltage supply (ET 20/2 Farnell instruments Ltd.) and the voltage was subsequently increased from 0 to 10 V in steps of 0.5 V. The magnetic field of the electromagnet was measured by a gaussmeter (GM07/GM08, Hirst magnetic instruments LTD). The gaussmeter probe was located in the middle of the electromagnet and probe chip was positioned 3 mm above the electromagnet.

As can be seen in Figure 5.19, the magnetic field increased linearly with the increment of the voltage applied to the electromagnet. The magnetic field increased from around 0 to around 220 Oe. Magnetic field of the electromagnet is lower than what permanent magnet is producing (1100 Oe), raising an initial concern as to whether the magnetic field would be strong enough to adequately control the ferrofluid actuator.
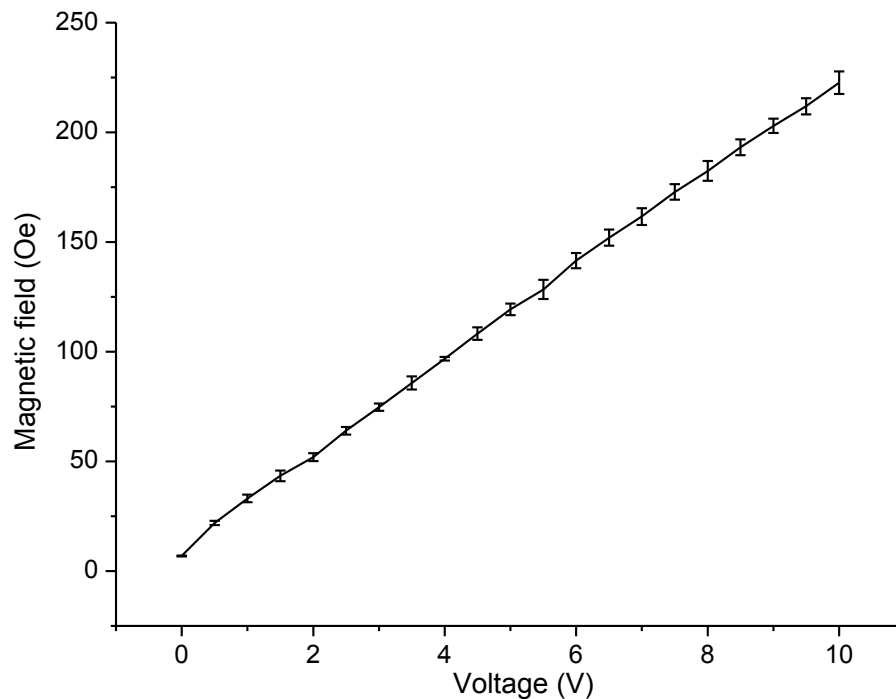
Fig. 5.19 Change of magnetic field of electromagnet when the voltage increase
from 0 to 10 V

The electromagnet was positioned into the VOA device as shown in Figure 5.18 and the microfluidic channel was fixed to the electromagnet. The first issue that was faced was how to reversibly control the ferrofluid actuator. It was shown that the ferrofluid was moving towards the magnetic field when the voltage was increasing. When the voltage was decreasing the ferrofluid actuator did not move and stayed in the same position. A solution was found whereby the microfluidic channel was positioned at an angle which allowed gravitational force to bring the ferrofluid back to the starting position in the channel. It was found that the channel positioned at an angle of 10° allowed the gravitational force to pull the ferrofluid actuator to its original position under a decreasing magnetic field. At the starting point, to keep the three liquid mediums in position fixed inside the channel, 0.25 V was applied to the electromagnet. 0.25 V corresponded to an electromagnetic field level of less than 25 Oe (Fig. 5.19). After that the voltage was increased incrementally in steps of 0.25 V which resulted in the ferrofluid actuator up the microchannel towards the electromagnet, and at the same time the shutter moved across the light path, increasing the light attenuation. It was found that to reach the highest attenuation (when the shutter

covers completely the light path) the voltage needed to increase to only 4 V which corresponded to 96 Oe. After the shutter covered completely the light path, the voltage was lowered to the 0.25 V and the gravitational force pulled down all three liquid components, and the shutter was removed from the light path.
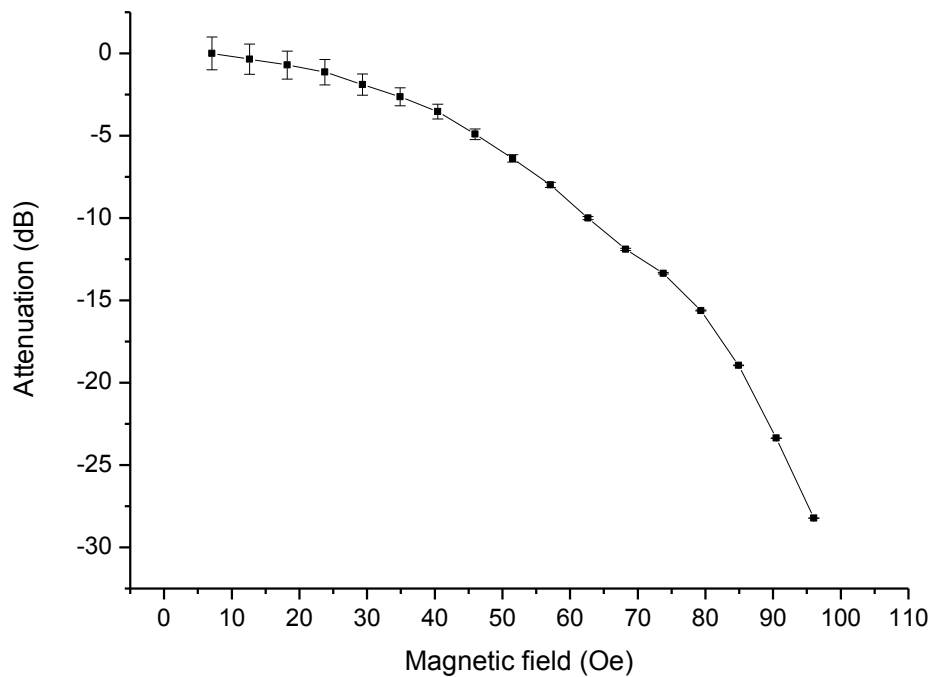
Fig. 5.20 Optical attenuation change when the magnetic field of electromagnet change

As can be seen in Figure 5.20, the attenuation of the VOA increased when the magnetic field increased. The attenuation increased in steps according to the step increment of the magnetic field. The maximum attenuation that was achieved was -28 dB which corresponded to the 96 Oe magnetic field of the electromagnet (4 V applied to the electromagnet) and thus this electromagnet easily supplied the actuation force necessary to form the VOA.

The presented results can be compared with the theoretical results that were obtained from the model of Gaussian function (Table. 5.1). The theoretical model allowed the calculation of how much light can travel from input fibre GRIN lens to the output fibre GRIN lens with respect to the position of the shutter in the light path. The Table 5.2 below presents a few examples of the obtained attenuation, the corresponding magnetic field and theoretically calculated shutter position for each of attenuation example.

Table. 5.2 Attenuation results corresponding to the theoretical calculated shutter position:

Attenuation (dB)	Magnetic field (Oe)	Shutter position (mm)
0	7.07	0
-1.14	23.75	0.46
-4.91	45.99	0.70
-9.99	62.66	0.86
-15.62	79.33	0.98
-28.23	96.01	1.20

5.6 Water-based ferrofluid actuator

For a complete investigation of a ferrofluid type VOA, one more type of the fluidic VOA was designed. The new format of VOA that was investigated had one key difference and it was the type of ferrofluid that was used as the shutter. The main reason to study this new type of the device was to reduce number of different liquids required to create the already demonstrated VOA.

The new idea was to reduce from three liquids mediums to two or (if it is possible) to one medium. In the beginning, the idea of having only one liquid (and air) was rejected due to the discussed problem of the interference that arises when light travels through mediums of largely different refractive indices. The second idea of having two mediums working as the shutter was chosen as the final design. The device consisted of a water-based ferrofluid (EMG 605, Ferrotec Corp.) as the opaque shutter and the second medium working as the transparent side of the shutter. The second medium was a mineral oil (Sigma Aldrich M3516), the mineral oil was chosen due to the refractive index (of 1.467) that closely matches the water-based ferrofluid and that the oil and the water-based ferrofluid would not mix with each other. Both liquids were inserted into the square glass microfluidic channel. The glass was pre-treated with the Aquapel (Aquapel Glass Treatemnet) that coated the glass with a thin hydrophobic layer that repels the water and prevents ferrofluid residue attaching to the walls. Due to the small amount of the water-

based ferrofluid that was available, it was possible only to characterise the VOA with the permanent magnet. The permanent magnet (magnetic field 1100 Oe measured with gaussmeter) was located under the microfluidic channel where the water-based ferrofluid was placed. The magnet was attached to the micro stage and translated in steps of 100 μm over a distance of 1.1 mm. During magnet translation the water-based ferrofluid moved across the light path, blocking the light transmission from input GRIN lens into the output GRIN lens (Fig. 5.21).
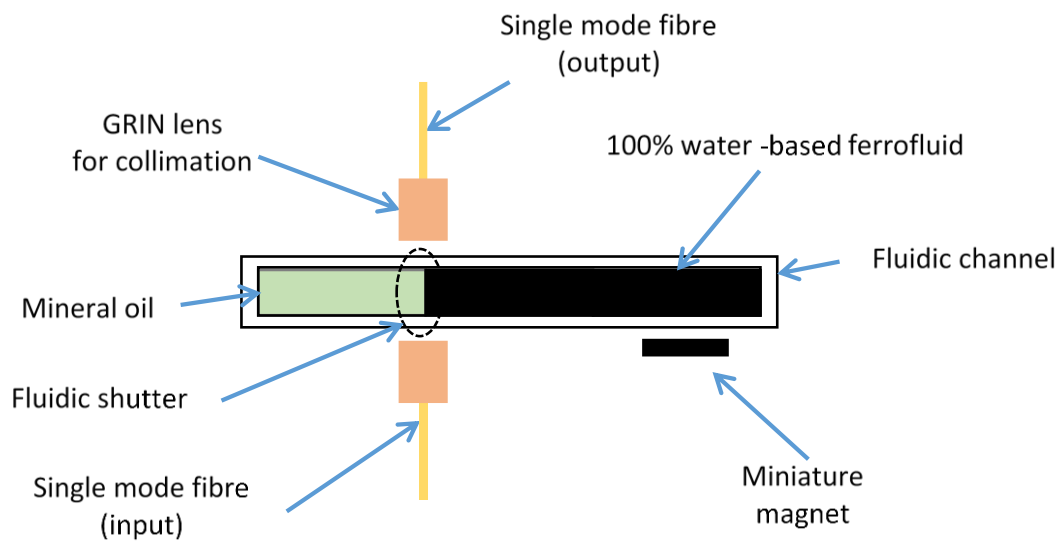
Fig. 5.21 Schematic of the water-based ferrofluid VOA

As was discussed above the use of the two liquids to create the VOA was necessary to reduce the possibility of generation previously recorded interferometric fringes when an oil-based ferrofluid VOA was used. The refractive index of the mineral oil was measured to be 1.467 (measured by 60/70 Abbe refractometer). A problem arose when measuring the refractive index of the water-based ferrofluid due to its dark colour. The liquid was subsequently diluted to the point that it was possible to measure the refractive index. The concentration that allowed the measurement was 1:30 and the measured refractive index was 1.46. The measured value leads to the assumption that the refractive index of undiluted water-based ferrofluid will be similar or higher than 1.46.
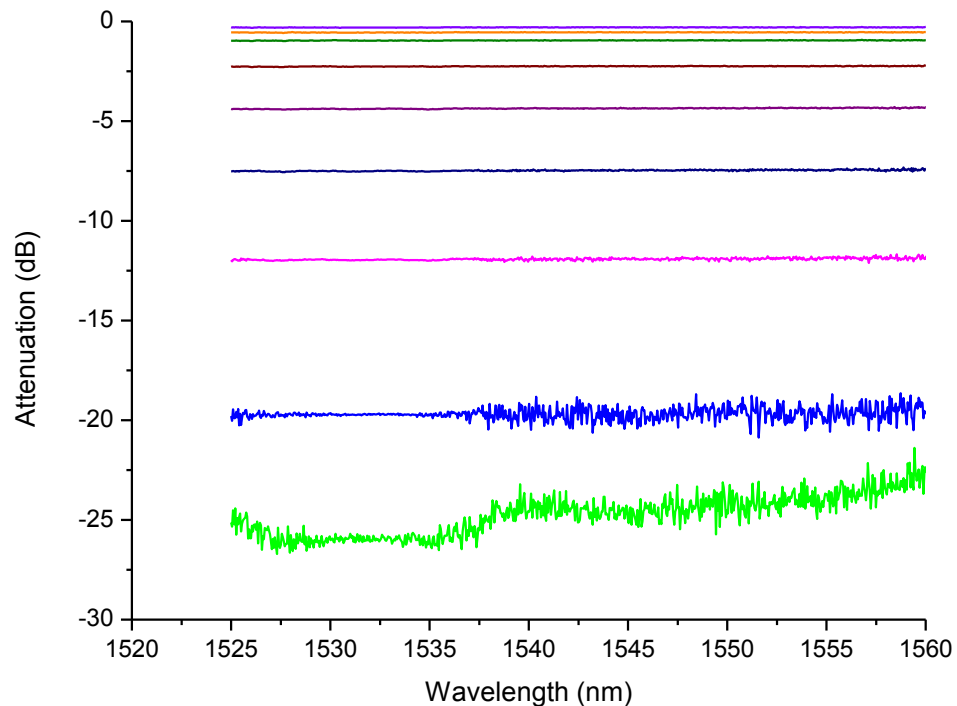
Fig. 5.22 Broadband optical performance of the water-based VOA

The testing of the VOA began with optical broadband testing as the shutter was moved in steps across the light path. The obtained results (Fig. 5.22) indicate that the refractive index of both liquids used to create the shutter are similar due to lack of the interferometric fringes. The highest attenuation that was achieved was approximately -25 dB with 3 dB WDL. The 3 dB WDL is the artefact that appeared only for the highest attenuation. As mentioned, the artefact can be an effect of the weak signal that arrived on the receiver fibre after light travel through the opaque shutter.

5.7 Conclusion

In this chapter have been presented two types of the fluidic VOAs with ferrofluid/magnetic actuation. Both VOAs are created using fluidic shutters but one is an oil-based ferrofluid and the second on a water-based ferrofluid. The problems that occurred during the oil-based VOA operation were resolved and these conclusions were

used to design the second type of VOA based on the water-based ferrofluid. Both VOAs achieved comparable attenuation of approximately -28 dB (for the oil-based ferrofluid) and -25 dB (for the water-based ferrofluid). The proposed VOAs have broadband performance and operate between 1525 nm and 1560 nm, which is a standard wavelength range that is used in optical communications. An advanced prototype of an oil-based VOA was described, that was based on the voltage control via an electromagnet. The voltage that was needed to operate the VOA is relatively low and did not exceed 4 V. The achieved optical attenuation range of these devices meets typical application requirements.

5.8   Reference:

[1]   N. A. Clark, "Ferromagnetic ferrofluids," *Nature*, vol. 504, pp. 229–230, 2013.

[2]   H. E. Horng, C.-Y. Hong, S. Y. Yang, and H. C. Yang, "Designing the refractive indices by using magnetic fluids," *Appl. Phys. Lett.*, vol. 82, no. 15, p. 2434, 2003.

[3]   M. Konstantaki, a. Candiani, and S. Pissadakis, "Optical fibre long period grating spectral actuators utilizing ferrofluids as outclading overlayers," *J. Eur. Opt. Soc. Rapid Publ.*, vol. 6, p. 11007, Mar. 2011.

[4]   A. Candiani, M. Konstantaki, W. Margulis, and S. Pissadakis, "Optofluidic magnetometer developed in a microstructured optical fiber," vol. 37, no. 21, pp. 4467–4469, 2012.

[5]   Y. Miao, J. Wu, W. Lin, K. Zhang, Y. Yuan, B. Song, H. Zhang, B. Liu, and J. Yao, "Magnetic field tunability of optical microfiber taper integrated with ferrofluid," vol. 21, no. 24, pp. 210–213, 2013.

[6]   S. de Pedro, V. J. Cadarso, X. Munoz-Berbel, J.A. Plaza, J. Sort, J. Brugger, S. Buttgenbach, A. Llobera, "Magnetically-actuated variable optical attenuators using ferrofluid-doped elastomer implemented by combination of soft lithography and inkjet printing technologies," in *2013 IEEE 26th International Conference on Micro Electro Mechanical Systems (MEMS)*, 2013, pp. 548–551.

[7]   Q.-F. Dai, H.-D. Deng, W.-R. Zhao, J. Liu, L.-J. Wu, S. Lan, and A. V. Gopal, "All-optical switching mediated by magnetic nanoparticles.," *Opt. Lett.*, vol. 35, no. 2, pp. 97–9, Jan. 2010.

[8]   Y. Gu, G. Valentino, and E. Mongeau, "Ferrofluid-based reconfigurable optofluidic switches for integrated sensing and digital data storage," *Appl. Opt.*, vol. 53, no. 4, pp. 537–543, 2014.

[9]   R. Walpole, R. Myers, S. Myers, and K. Ye, "Probability and statistics for engineers and scientists," in in *Probability and statistics for engineers and scientists*, Ninth., Prentice Hall, 2012, pp. 171–185.

[10]   J. Wilson and J. Hawkes, *Optoelectronics-an introduction*, 2nd ed. Prentice Hall, 1989, pp. 11–16.

[11]   M. I. Lapsley, I.-K. Chiang, Y. B. Zheng, X. Ding, X. Mao, and T. J. Huang, "A single-layer, planar, optofluidic Mach-Zehnder interferometer for label-free detection.," *Lab Chip*, vol. 11, no. 10, pp. 1795–800, May 2011.

Chapter 6

Summary

6.1   Conclusion

This thesis presented the research work on designing, fabricating, and characterisation of two optofluidic variable optical attenuators: a continuous fibre device and a fibre gap device.

Chapter 1 introduced the field of optofluidics and reviewed the state-of-the-art types of VOAs from MEMS to optofluidic types. Two formats of the device where briefly described (fibre gap device and continuous fibre device).

Chapter 2 described the electrowetting phenomenon and electrowetting on dielectric platform. The design of the electrowetting platform included the different mask design, choice of materials and the fabrication process. Several different designs of the platform were fabricated, and the configuration of the electrodes and the gap width varied. The manufactured platforms of 0.6 mm electrodes width and 0.07 mm gap between electrodes were chosen to be the standard size for our device. The standard platform was evaluated. From the obtained results some calculation was performed to characterise the platform. Characterisation concerned the change of the contact angle of the droplet and the electrowetting force that acts on the droplet so that droplet can be translated across electrodes.

In Chapter 3 the theoretical model of the light propagation through the side polished fibre was discussed. The model considered a scenario of different refractive indices of the external mediums influence on the light propagation through the fibre. Another scenario focused on the different contact length between the fibre and external medium and its impact on the light transmission. The theoretical analysis showed that the light attenuation will change depending on the refractive index and can be varied from a few dB to -35 dB for

contact length of 1.2 mm between the fibre and external medium (droplet). The theoretical model also studied if the achieved attenuation was wavelength dependent. The difference of the attenuation for three different wavelengths (1520, 1540 and 1560 nm) was approximately 0.5% and thus the device is not significantly wavelength dependent.

It was similarly shown that the change in contact length between the fibre and a droplet has a great influence on the light attenuation. The attenuation for different contact length can vary from few dB (0.2 mm contact length) to -70 dB (2.4 mm contact length) theoretically for a refractive index of 1.4600.

The variable optical attenuator device description, fibre manufacture process and device operation was discussed in Chapter 4. The complete device combined with the side polished fibre and EWOD platform was tested for different droplet refractive indices and sizes. The experimental results were presented and compared to the theoretical results obtained from the theoretical analysis in the previous chapter. It was shown that the fibre fabrication has an impact on the performance of the device and the polishing depth can affect the maximum attenuation that can be achieved. The fibre cladding thickness and the shape of the cladding slope has a great impact on the VOA performance. The droplet position upon the different spots along the polishing length of the fibre affects differently the light attenuation. It was observed that when droplet approaches the fibre core the attenuation increased and in the middle section of the polishing length the attenuation reaches maximum level.

The refractive index of the droplet influences the light attenuation, and it was found that when the refractive index of the droplet is close to the refractive index of the fibre core a maximum attenuation is reached, which was confirmed by theoretical analysis and also by the experimental results. The measured attenuation value (for 1.2 mm interaction length between droplet and fibre) changes from -9 dB (refractive index 1.4596) to -22 dB (refractive index 1.4602).

A second factor that affects the attenuation level is the droplet size and here also the experimental and theoretical results (for refractive index of 1.4602) agree. For a contact length between the droplet and the fibre the attenuation varied from -16 dB (0.8 mm contact length) to -30 dB (1.6 mm contact length). However, when the contact length exceeds 1.2 mm, there was no attenuation increase as was predicted with the theoretical model. That can be explained by the fibre shape of the polishing region. The droplet covers a longer length

of the fibre slope but the cladding in such a position is not constant but is getting thicker which does not result in higher attenuation. The device was tested over a wavelength range to confirm the operation of a broadband device from 1520 nm to 1560 nm.

For completeness, in Chapter 5 a fibre gap device was fabricated that worked as a VOA. Both devices (continuous VOA and fibre gap VOA) represents the field of optofluidics, but the fibre gap device differs with respect to the design structure, operation principle and liquid that attenuates the light. The device uses two fibres and a liquid shutter that moves between them. The operation principle of moving liquid is not based on an electrowetting but in this case on the magnetic field that actuates a ferrofluid (magnetic fluid).

There are two types of ferrofluids available, oil-based and water-based. Based on this availability two prototypes of VOA were designed, constructed and tested. In both prototypes ferrofluid moves with a magnetic field and moves across the light path that travels from input to the output fibre. The liquid is opaque and when it crosses the light path, attenuation of the light occurs.

The oil-based VOA was tested with two different magnets, in one case with permanent magnet moved on the micro stage and in second case with an electromagnet. The shutter was constructed with three liquids parts, a ferrofluid actuator, 1:30 ferrofluid shutter and liquid part that separates both the ferrofluids. The diluted mineral oil ferrofluid was used to reduce the staining left on the glass channels walls when ferrofluid is moved back from the light path.

Firstly, the VOA was tested when the liquid that separates ferrofluids was water. This liquid combination caused trouble with broadband wavelength operation causing an elevated WDL. It was found that an interferometry phenomenon occurred due to the difference in refractive index between the water and ferrofluid that formed the shutter. A resolution to this problem was found by using a glycerine-water solution that replaced the water plug. The glycerine-water plug had a refractive index closer to the refractive index of the ferrofluid. Retesting showed broadband operation with a much reduced WDL. The operation resolution of the device was 0.1 mm and the optical attenuation varied from 0 dB to -30 dB. The device was tested also with a variable electromagnet where the magnetic field changed from 25 Oe (0.25 V) to 96 Oe (4 V) and the optical attenuation reaches -28 dB.

The principle of operation of the water-based ferrofluid VOA was tested only with a permanent magnet. That device was a combination of only two parts: water-based ferrofluid

and a mineral oil. To avoid the interferometry phenomenon, the mineral oil was chosen due to the matching refractive index to the refractive index of water-based ferrofluid. The device had a resolution of 0.1 mm and an optical attenuation that varied from 0 dB up to -25 dB over broadband wavelength range from 1525 nm to 1560 nm.

These devices fulfil the basic requirements of optical attenuation range and broadband operation. These devices have some disadvantage due to the fibre gap device format. The main disadvantage is the fibres alignment process. The fibres need to be aligned carefully to reduce the insertion loss. Another disadvantage of the present device is the lack of a compact size. The channel size was of the 1 mm diameter and the liquid amount was several times bigger than the volume of the droplet that was used in the continuous fibre VOA. Additionally the electromagnet that was used to produce the magnetic field that moves the ferrofluid actuator produced some heat during the operation. Such a heat could warm up the ferrofluid and with the time dry the liquid which can affect the movement process of the actuator.

In contrast in the continuous fibre VOA there is no problem of the fibre alignment therefore there is no additional insertion loss. The device is not sensitive to the vibrations, although the device is not fully portable because that device is an open type system. Further design of the device encapsulation will need to be done to create fully transportable VOA. The continuous fibre VOA uses lower volume of liquid and does not heat up the system. Despite the disadvantages of the optofluidic VOA based on the electrowetting droplet actuation along a side polished fibre, it is a novel type of the optofluidic device. The device has future potential of creating completely sealed and portable device.

The two types of VOAs presented in this research have performance parameters comparable to the other optofluidic VOAs and MEMS VOAs (Table 6.1). The fibre gap VOA achieved the attenuation level of approximately of -28 dB which is an attenuation level that is lower than the attenuation range (32 dB – 40 dB) of other optofluidic fibre gap VOAs presented below. In contrast, the attenuation that was reached by the continuous fibre VOA is on the level of 28 dB but is higher than the attenuation range (10 – 20 dB) achieved by the listed continuous fibre VOAs. Another advantage of our device is the broadband operation where the VOAs presented below have narrowband operation.

Table 6.1 Comparison between research presented here with published research from other groups:

Optofluidic VOAs			
Fibre gap device			
Type of attenuator	**Method of attenuation**	**Wavelength operation range**	**Maximum attenuation**
Ferrofluid shutter	Ferrofluid actuations – voltage up to 4 V	Broadband operation – 1525 – 1560 nm	28 dB (oil-based ferrofluid actuator); 25 dB (water-based ferrofluid actuator)
Fluid/PDMS interface[1]	Fluid flow - refractive index change	Narrowband operation – 532 nm laser light	35 dB
Droplet stretching[2]	Dielectric droplet stretching - voltage up to 80 V_{rms}	Broadband operation – 1530 – 1560 nm	32 dB
Liquid lens[3]	EWOD controlled variable focus liquid lens – voltage up to 46 V_{rms}	Broadband operation – 1530 – 1700 nm	40 dB
Continuous fibre device			
Droplet (refractive index) transport along the side polished fibre[4]	EWOD actuation of the droplet – voltage up to 180 V	Broadband operation – 1520 – 1560 nm	28 dB
Plug (refractive index) transport along the LPG fibre[5]	EWOD plug transport (toxic liquid)	Narrowband – 1538 nm	20 dB

Plug (refractive index) transport along the LPG fibre[6]	EWOD plug transport (toxic liquid)	Narrowband – 1530 nm	20 dB
Plugs (refractive index) displacement across the LPG fibre[7]	EWOD multiple plug displacement	Narrowband – 1530 nm	10 dB
MEMS VOAs			
Shutter[8]	Displacement of the shutter – voltage up to 34 V	Broadband operation	29 dB
Mirror[9]	Displacement of the mirror	Broadband operation – 1520 – 1620 nm	44 dB
Fibre misalignment[10]	Displacement of the fibres	Broadband operation	20 dB

6.2   Future design of the VOAs

The continuous fibre variable optical attenuator presented in Chapters 2-4 is an open platform device where both the fibre and liquid droplet are exposed to outside environment. A future device can be redesigned to be a sealed device, where the liquid will not evaporate and any dust will not settle on the platform and fibre surface. This will require the device not only need to be sealed to but further research concerning liquid and fibre coatings will be required. As mentioned in previous chapters, the liquid that is used in the device is a glycerine-water solution. Such a liquid has some disadvantages like the requirement of a high voltage (180 V) to move the liquid droplet by EWOD. More importantly the droplet was leaving some residue behind that impaired the performance of the device (the optical

transmission did not fully increase when droplet left the fibre region of the thinner cladding thickness and thus the fibre needed to be clean with a water droplet). Some search for a liquid of desirable parameters was undertaken but as yet such a liquid was not found, and glycerine-water solution was the best option at that time. The main requirements for the liquid were a refractive index (at least 1.46) and possibility of using electrowetting to move the droplet. Alternative liquids that could be potentially used in the device were tested included sodium dichromate – water solution, glucose solution, but both of them did not fully fulfil the requirements to be used in the device (results of the tests were presented in Chapter 4.7).

Another option to solve the problem of glycerine sticking to the fibre might be a better fibre coating. At the moment fibre was coated with hydrophobic layer of Aquapel. That layer did not fully prevent glycerine adhering to the fibre surface. An alternative to the Aquapel was a layer of Silane. However, tests performed did not give successive results, as the optical transmission did not adequately decrease when the droplet moved along the interaction region of the fibre. The possible reason of that was thickness of that hydrophobic layer which acted as an additional cladding layer and the droplet did not interact fully with the evanescent field of the fibre and could not affect the optical transmission. An alternative to Silane is required, or an improved technique to deposit a Silane layer of nanometres thickness.

The continuous fibre VOA can be further improved for instance by redesigning the electrodes on EWOD platform. Such a new platform may allow the production of a droplet from a liquid reservoir on the platform (or electrodes can reconfigured to create a close loop), so that one droplet of glycerine can be followed by a cleaning water droplet.

The second VOA presented in this thesis (Chapter 5) was a fibre gap device that used a ferrofluid as an optical attenuator. Future work that might improve the device could design an integrated device where two GRIN lensed single-mode optical fibres are inbuilt onto the same platform where a ferrofluid moves in a channel across the light path. A miniature magnet could be also inbuilt to the platform so that an external magnetic source would not be needed to operate the VOA. The overall challenge for this project is to decrease the device in size and integrate every part of the VOA in one sealed platform.

6.3 References:

[1]   M. I. Lapsley, S.-C. S. Lin, X. Mao, and T. J. Huang, "An in-plane, variable optical attenuator using a fluid-based tunable reflective interface," *Appl. Phys. Lett.*, vol. 95, no. 8, p. 083507, 2009.

[2]   S. Xu, H. Ren, J. Sun, and S.-T. Wu, "Polarization independent VOA based on dielectrically stretched liquid crystal droplet," *Opt. Express*, vol. 20, no. 15, p. 17059, Jul. 2012.

[3]   S. A. Reza and N. a. Riza, "A liquid lens-based broadband variable fiber optical attenuator," *Opt. Commun.*, vol. 282, no. 7, pp. 1298–1303, Apr. 2009.

[4]   A. Duduś, R. Blue, M. Zagnoni, G. Stewart, and D. Uttamchandani, "In-line single-mode fiber variable optical attenuator based on electrically addressable microdroplets," *Appl. Phys. Lett.*, vol. 105, no. 2, Jul. 2014.

[5]   J. Hsieh, P. Mach, F. Cattaneo, S. Yang, T. Krupenkine, K. Baldwin, and J. a. Rogers, "Tunable microfluidic optical-fiber devices based on electrowetting pumps and plastic microchannels," *IEEE Photonics Technol. Lett.*, vol. 15, no. 1, pp. 81–83, Jan. 2003.

[6]   B. R. Acharya, T. Krupenkin, S. Ramachandran, Z. Wang, C. C. Huang, and J. a. Rogers, "Tunable optical fiber devices based on broadband long-period gratings and pumped microfluidics," *Appl. Phys. Lett.*, vol. 83, no. 24, p. 4912, 2003.

[7]   P. Müller, A. Kloss, P. Liebetraut, W. Mönch, and H. Zappe, "A fully integrated optofluidic attenuator," *J. Micromechanics Microengineering*, vol. 21, no. 12, p. 125027, Dec. 2011.

[8]   L. Li and D. Uttamchandani, "Design and evaluation of a MEMS optical chopper for fibre optic applications," *Sci. Meas. …*, vol. 151, pp. 77–84, 2004.

[9]   H. Cai, X. Zhang, C. Lu, A. Q. Liu, and E. H. Khoo, "Linear MEMS variable optical attenuator using reflective elliptical mirror," *IEEE Photonics Technol. Lett.*, vol. 17, no. 2, pp. 402–404, Feb. 2005.

[10]   A. Llobera, G. Villanueva, V. J. Cadarso, S. Battgenbach, and J. A. Plaza, "Polymeric MOEMS Variable Optical Attenuator," *IEEE Photonics Technol. Lett.*, vol. 18, no. 22, pp. 2425–2427, Nov. 2006.

Appendix 1 – Reflectivity for frustrated TIR

Summary

First of all, we summarise the ray theoretical results describing the reflectivity for the situation when a discrete droplet comes in contact with the reduced cladding region and the evanescent field, hence exerting an influence on it.
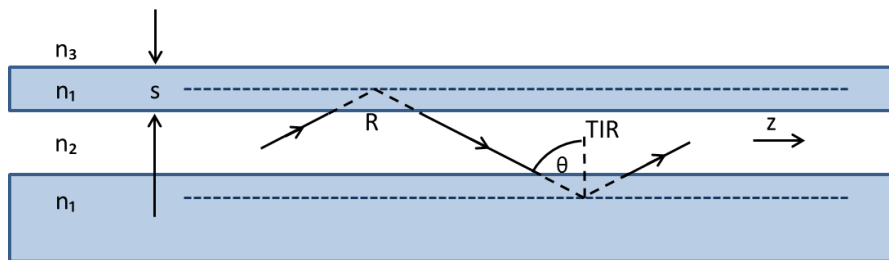

Fig. 1 Schematic of the ray optics approach applied to a side-polished optical fibre.

The reflectivity for frustrated total internal reflection when the medium 3 (liquid) is either loss-less or lossy can be calculated from[1]:

$$R = \frac{e^{2\gamma s} + a^2 e^{-2\gamma s} + 2a\cos(\varphi_{21} - \varphi_{13})}{e^{2\gamma s} + a^2 e^{-2\gamma s} + 2a\cos(\varphi_{21} + \varphi_{13})} \tag{1}$$

where s is the remaining cladding thickness, a is related to the absorption loss, and can be calculated from:

$$a = \sqrt{\frac{1 - \Delta}{1 + \Delta}} \tag{2}$$

$$\Delta = \frac{2k\rho\gamma}{n_3\left(\rho^2 + \gamma^2 + \dfrac{k^2\rho^2}{n_3{}^2}\right)} \tag{3}$$

where k is the imaginary part of the index for medium 3 (k=0 and a=1 for a loss-less medium) and ϕ_{21} and ϕ_{13} are the phase shifts for the reflection coefficients at the n_2/n_1 boundary and the n_1/n_3 boundary respectively, given by:

$$\varphi_{21} = -2tan^{-1}\left(\frac{\gamma}{\alpha}\right) \tag{4}$$

$$\varphi_{13} = \pi - tan^{-1}\left(\frac{\gamma - \dfrac{k\rho}{n_3}}{\rho}\right) - tan^{-1}\left(\frac{\gamma + \dfrac{k\rho}{n_3}}{\rho}\right) \tag{5}$$

where $\alpha = k_0\sqrt{n_2{}^2 - n_e{}^2}$, $\gamma = k_0\sqrt{n_e{}^2 - n_1{}^2}$, $\rho = k_0\sqrt{n_3{}^2 - n_e{}^2}$, n_1, n_2, n_3 are the refractive indices of the fibre cladding, fibre core, and the external medium respectively, n_e is the effective index of the guided mode and $k_0 = \frac{2\pi}{\lambda}$. The effective index of the mode is described by $n_e = \frac{\beta_m}{k_0}$, where β_m is the propagation constant.

For a guided mode with effective index, n_e, the waveguiding condition is:

$$2dk_0\sqrt{n_2{}^2 - n_e{}^2} = 2m\pi + \varphi_{21} + \varphi_{21} \Rightarrow \tan\left(\frac{1}{2}\alpha d\right) = \left(\frac{\gamma}{d}\right) \tag{6}$$

for m=0 for TE modes in a symmetric waveguide of thickness d and index n_2 bounded on either side by a medium of index n_1.

Derivation of the Reflectivity Equation:

When a wave is incident on the boundary of two media of different optical properties, it separates into a transmitted (into second medium) and a reflected (back into first medium) wave (Fig. 2).
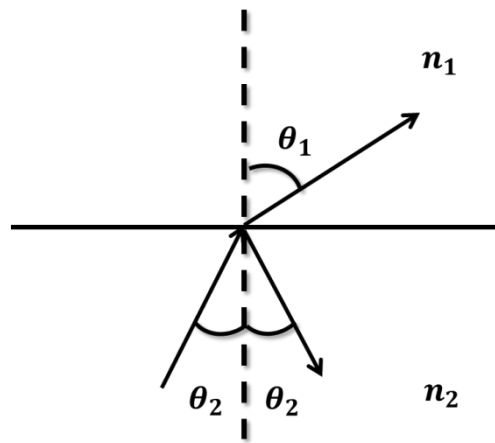
Fig. 2 Light reflection on the n_1 and n_2 media boundary

According to the Fresnel formula the reflected wave for s-polarisation wave can be expressed by:

$$r_{21} = \frac{n_2 cos\theta_2 - n_1 cos\theta_1}{n_2 cos\theta_2 + n_1 cos\theta_1} \tag{7}$$

When θ_1 when exceeds the critical angle, all the light is reflected from the boundary and does not cross into the second medium. Such a situation where all light is reflected is called "total reflection". An electromagnetic field in second medium still exists, but there is no energy flow through boundary.

For this case we can write by Snell's Law:

$$n_2 sin\theta_2 = n_1 sin\theta_1 \tag{8}$$

$$cos\theta_1 = \sqrt{1 - sin^2\theta_1} = \sqrt{1 - \frac{n_2{}^2 sin^2\theta_2}{n_1{}^2}} \tag{9}$$

Hence

$$n_1 cos\theta_1 = \sqrt{n_1{}^2 - n_2{}^2 sin^2\theta_2} = \pm i\sqrt{n_2{}^2 sin^2\theta_2 - n_1{}^2} \tag{10}$$

where the imaginary term arises since $n_2^2 sin^2\theta_2 > n_1^2$ for TIR

Hence

$$r_{21} = \frac{n_2\sqrt{1 - sin^2\theta_2} - i\sqrt{n_2{}^2 sin^2\theta_2 - n_1{}^2}}{n_2\sqrt{1 - sin^2\theta_2} + i\sqrt{n_2{}^2 sin^2\theta_2 - n_1{}^2}} \tag{11}$$

Defining $n_e = n_2 sin\theta_2$

$$r_{21} = \frac{\sqrt{n_2{}^2 - n_e{}^2} - i\sqrt{n_e{}^2 - n_1{}^2}}{\sqrt{n_2{}^2 - n_e{}^2} + i\sqrt{n_e{}^2 - n_1{}^2}} \tag{12}$$

With the definitions:

$$k_0\sqrt{n_2{}^2 - n_e{}^2} = \alpha \tag{13}$$

$$k_0\sqrt{n_e{}^2 - n_1{}^2} = \gamma \tag{14}$$

we can write:

$$r_{21} = \frac{\alpha - i\gamma}{\alpha + i\gamma} \tag{15}$$

From equation 15 the phase for reflection coefficients at the boundary between second medium and first medium is describe by:

$$\varphi_{21} = -2tan^{-1}(\frac{\gamma}{\alpha}) \tag{16}$$

Hence we can write

$$r_{21} = e^{j\varphi_{21}} \tag{17}$$

since from equation 15

$$|r_{21}| = 1 \tag{18}$$

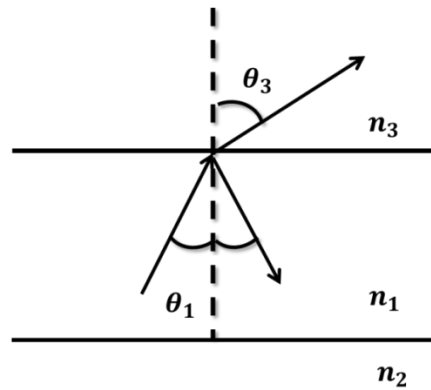For a second boundary as shown in figure below (Fig. 3):

Fig. 3 Light reflection on the n_1 and n_3 media boundary

the same procedure can be applied to r_{13}

$$r_{13} = \frac{n_1 cos\theta_1 - n_3 cos\theta_3}{n_1 cos\theta_1 + n_3 cos\theta_3} \tag{19}$$

to give

$$r_{13} = \frac{i\sqrt{n_2 sin^2\theta_2 - n_1{}^2} - n_3 cos\theta_3}{i\sqrt{n_2 sin^2\theta_2 - n_1{}^2} + n_3 cos\theta_3} \tag{20}$$

$$r_{13} = \frac{i\sqrt{n_e{}^2 - n_1{}^2} - \sqrt{n_3{}^2 - n_e{}^2}}{i\sqrt{n_e{}^2 - n_1{}^2} + \sqrt{n_3{}^2 - n_e{}^2}} \tag{21}$$

$$r_{13} = \frac{i\gamma - \rho}{i\gamma + \rho} \tag{22}$$

where

$$\rho = k_0\sqrt{n_3{}^2 - n_e{}^2} \tag{23}$$

Since from equation 22

$$|r_{13}| = 1 \tag{24}$$

Hence

$$r_{13} = e^{j\varphi_{13}} \tag{25}$$

and the phase for reflection coefficients is:

$$\varphi_{13} = \pi - 2\tan^{-1}\left(\frac{\gamma}{\rho}\right) \tag{26}$$

When medium n_3 is lossy then n_3 is replaced by $n_3 + jk$

$$\rho = k_0\sqrt{{n_3}^2 - {n_e}^2} = k_0 n_3 \cos\theta_3 \Rightarrow k_0(n_3 + jk)\cos\theta_3 \tag{27}$$

$$k_0\sqrt{{n_3}^2 - {n_e}^2} = \rho + j\frac{\rho}{n_3}k \tag{28}$$

Hence

$$r_{13} = \frac{i\gamma - \rho}{i\gamma + \rho} \Rightarrow \frac{i\gamma - (\rho + j\frac{\rho}{n_3}k)}{i\gamma + (\rho + j\frac{\rho}{n_3}k)} \tag{29}$$

$$r_{13} = \frac{i\left(\gamma - \frac{\rho}{n_3}k\right) - \rho}{i\left(\gamma + \frac{\rho}{n_3}k\right) + \rho} \tag{30}$$

We can write:

$$r_{13} = ae^{j\varphi_{13}} \tag{31}$$

Where

$$|r_{13}|^2 = \frac{\rho^2 + \left(\gamma - \frac{\rho}{n_3}k\right)^2}{\rho^2 + \left(\gamma + \frac{\rho}{n_3}k\right)^2} = \frac{\rho^2 + \gamma^2 + (\frac{\rho}{n_3}k)^2 - 2\frac{\rho\gamma}{n_3}k}{\rho^2 + \gamma^2 + (\frac{\rho}{n_3}k)^2 + 2\frac{\rho\gamma}{n_3}k} \tag{32}$$

And

$$a = |r_{13}| = \sqrt{\frac{1 - \Delta}{1 + \Delta}} \tag{33}$$

Where

$$\Delta = \frac{2k\rho\gamma}{n_3(\rho^2 + \gamma^2 + \frac{k^2\rho^2}{n_3{}^2})} \tag{34}$$

Also

$$\varphi_{13} = \pi - tan^{-1}\left(\frac{\gamma - \frac{\rho}{n_3}k}{\rho}\right) - tan^{-1}\left(\frac{\gamma + \frac{\rho}{n_3}k}{\rho}\right) \tag{35}$$
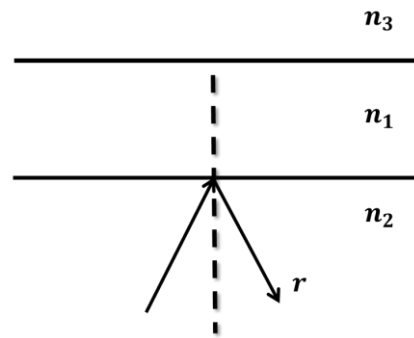

Fig. 4 Light reflection from the 3-layer structure

The overall reflection coefficient for the 3-layer structure (Fig. 4) is given by[1]:

$$r = \frac{r_{21} \mp r_{13}e^{-2\gamma s}}{1 + r_{21}r_{13}e^{-2\gamma s}} = \frac{e^{j\varphi_{21}} + ae^{j\varphi_{13}}e^{-2\gamma s}}{1 + ae^{j(\varphi_{21}+\varphi_{13})}e^{-2\gamma s}} \tag{36}$$

The reflectivity is given by:

$$R = |r|^2 = \frac{(cos\varphi_{21} + ae^{-2\gamma s}cos\varphi_{13})^2 + (sin\varphi_{21} + ae^{-2\gamma s}sin\varphi_{13})^2}{(1 + e^{-2\gamma s}(\cos(\varphi_{21} + \varphi_{13}))^2 + (ae^{-2\gamma s}\sin(\varphi_{21} + \varphi_{13}))^2} \qquad (37)$$

$$R = |r|^2 = \frac{1 + a^2 e^{-4\gamma s} + 2ae^{-2\gamma s}\cos(\varphi_{21} - \varphi_{13})}{1 + a^2 e^{-4\gamma s} + 2ae^{-2\gamma s}\cos(\varphi_{21} + \varphi_{13})} \qquad (38)$$

$$R = |r|^2 = \frac{(e^{2\gamma s} + a^2 e^{-2\gamma s} + 2a\cos(\varphi_{21} - \varphi_{13})}{(e^{2\gamma s} + a^2 e^{-2\gamma s} + 2a\cos(\varphi_{21} + \varphi_{13})} \qquad (39)$$

Reference:

[1]   M. Born and E. Wolf, "Principles of optics: electromagnetic theory of propagation, interference and diffraction of light," in *Principles of optics: electromagnetic theory of propagation, interference and diffraction of light*, 7th ed., NY: Cambridge University Press, 1999, p. Chapter 1.

Appendix 2 – Series of pictures of polished region of the fibre

In Chapter 4 (Section 4.1.2) fibre geometry was analysed with the focus on the profile of polished region of the in-house fabricated fibre. Series of pictures below presents full section of the polished region of the fibre with the use of a microscope. Pictures section of the in-house fabricated fibre were taken to investigate if the profile of this fibre matched the predicted shape of the slope profile. The diameter of the fibre decreased towards the centre of the fibre as was predicted. Pictures (Fig. 1) present following section of the polished region of the fibre from full diameter via the smallest diameter towards again to full diameter of the fibre. Figure 2 presents a plot of the measured polishing depth versus the distance along fibre (from the smallest diameter – middle of the fibre to the full diameter of the fibre) taken from these photographs.

125 μm

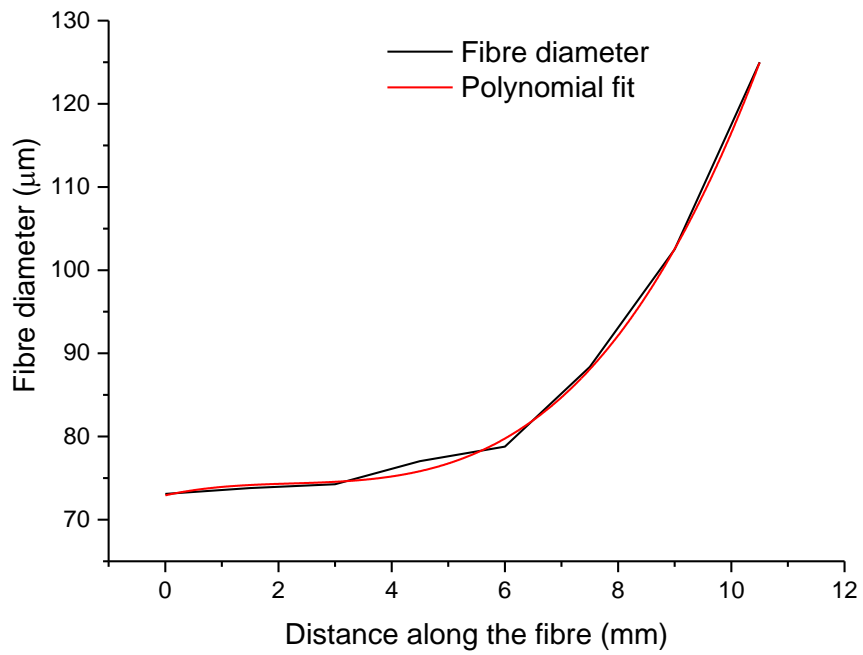Fig. 1 Series of pictures of the polsihed region of the fibre

Fig. 2 Effect of polishing on the fibre diameter measured directly using an optical microscope (third order of polynomial)

Appendix 3 – Optical interference

During the ferrofluid VOA operation, it was observed that the value of WDL increased and it was a result of fringes that appeared on the transmission spectrum (Fig. 5.15, Chapter 5). The optical interference that was taking place was an explanation of the phenomenon that occurs during device operation. The optical interference could be a product of light that was partially passing through the 1:30 ferrofluid plug and partially the water plug (Fig. 1) that formed the shutter. Difference in both paths was a product of different refractive index of the liquid mediums and therefore the interference fringes could appear on the transmission spectrum.
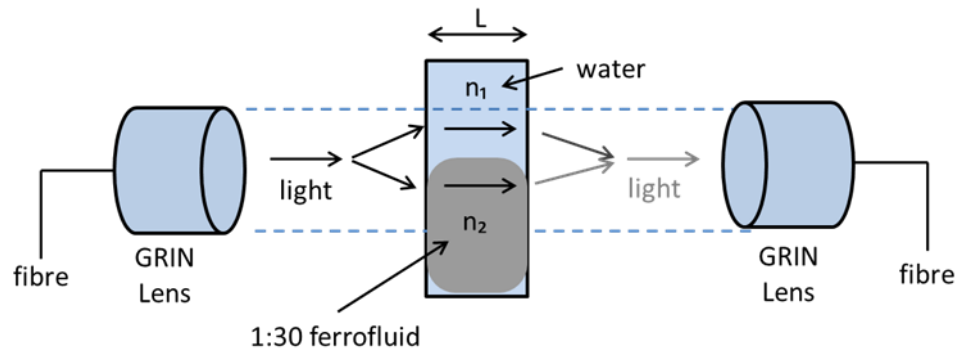

Fig. 1 Illustration of the interferometer that was created in the fluidic channel in the shutter system.

The standard Mach-Zehnder interferometer can be a representation of the situation that took part when the light was traveling from source light to the receiver. The input light is split to two beams of I_1 and I_2 intensity, with I1 travelling through the water and I2 travelling through the diluted ferrofluid. When these two light beams reach the receiver they recombine into one beam but any phase difference between two beams will generate interference in the output beam (I_{out}). Such a situation can be represented by[1]:

$$I_{out} = I_1 + I_2 + 2(I_1 I_2)^{1/2} \cos(\Delta\phi) \qquad (1)$$

where

$$\Delta\phi = \frac{2\pi L}{\lambda}(n_2 - n_1) \qquad (2)$$

is the phase difference between the two beams, where λ is a wavelength, n_1 and n_2 are refractive indices of materials, L is the length of the light path (1mm).

Transmission peaks will occur at wavelengths defined by[2]:

$$\Delta\phi = 2m\pi \qquad (3)$$

Therefore for neighbouring peaks at λ_1 and λ_2 we have:

$$\frac{2\pi L}{\lambda_1}(n_2 - n_1) = 2m\pi \qquad (4)$$

$$\frac{2\pi L}{\lambda_2}(n_2 - n_1) = 2m\pi + 2\pi \qquad (5)$$

where m is the order of the Mach-Zehnder interference

Taking the difference between equation (4) and equation (5) yields the following:

$$(n_2 - n_1)L(\frac{1}{\lambda_2} - \frac{1}{\lambda_1}) = 1 \qquad (6)$$

The refractive index of the 1:30 ferrofluid can be calculated from equation (6) above:

$$n_2 = \frac{\lambda_1 \lambda_2}{\lambda_1 - \lambda_2} \cdot \frac{1}{L} + n_1 \qquad (7)$$

where n_1 is the water refractive index, n_2 is refractive index of the 1:30 ferrofluid, λ_1, λ_2 are the wavelength peaks (1538 nm and 1560 nm).

From the above equation, it is possible to calculate the 1:30 ferrofluid refractive index. The calculated value of the refractive index was 1.44, for L = 1mm and n1 = 1.33.

References:

[1]   J. Wilson and J. Hawkes, *Optoelectronics-an introduction*, 2nd ed. Prentice Hall, 1989, pp. 11–16.

[2]   P. Lu, L. Men, K. Sooley, and Q. Chen, "Tapered fiber Mach–Zehnder interferometer for simultaneous measurement of refractive index and temperature," *Appl. Phys. Lett.*, vol. 94, no. 13, p. 131110, 2009.

List of publications of the author:

1. A. Duduś, R. Blue, D. Uttamchandani, "Single mode fiber variable optical attenuator based on a ferrofluid shutter", Applied Optics, 2015

2. A. Duduś, R. Blue, M. Zagnoni, G. Stewart, and D. Uttamchandani, "Modeling and characterization of an electrowetting based single mode fiber variable optical attenuator", Journal of Selected Topics in Quantum Electronics, 2014,

3. A. Duduś, R. Blue, M. Zagnoni, G. Stewart, and D. Uttamchandani, "Theoretical and experimental analysis of side-polished fiber optofluidic variable attenuator", Optical MEMS & Nanophotonics, Glasgow, UK, 17-21 Aug. 2014,

4. A. Duduś, R. Blue, D. Uttamchandani, "Miniaturized ferrofluid actuated single mode fiber variable optical attenuator (VOA)", Optical MEMS & Nanophotonics, Glasgow, UK, 17-21 Aug. 2014,

5. R. Blue, A. Duduś, M. Konstantaki, S. Pissadakis, D. Uttamchandani, "Characterisation of a double tilted fiber Bragg grating using an electrowetting platform", Optical MEMS & Nanophotonics, Glasgow, UK, 17-21 Aug. 2014,

6. A. Duduś, R. Blue, M. Zagnoni, G. Stewart, and D. Uttamchandani, "In-line single-mode fiber variable optical attenuator based on electrically addressable microdroplets", Appl. Phys. Lett., vol. 105, no. 2, 2014.

7. A. Duduś, R. Blue, M. Konstantaki, S. Pissadakis, and D. Uttamchandani, "Optical characterisation of long-period grating using liquid droplets on an electrowetting-on-dielectric platform," Micro Nano Lett., vol. 9, pp. 399–402, Jun. 2014.

8. A. Duduś, R. Blue, M. Zagnoni, D. Uttamchandani, "Side-polished fiber optofluidic attenuator based on electrowetting-on-dielectric actuation", Optical MEMS & Nanophotonics, Kanazawa, Japan, 18-22 August 2013

9. A. Duduś, R. Blue, and D. Uttamchandani, "Comparative study of microfiber and side-polished optical fiber sensors for refractometry in microfluidics", IEEE Sensors Journal, vol. 13, no. 5, pp. 1594-1601, Jan. 2013.

10. A. Duduś, R. Blue, D. Uttamchandani, "Comparison of fluidic refractive index sensing using microfibers and side-polished fibers", Optical MEMS & Nanophotonics, Banff, Canada, 6-9 August 2012.